

U  
S H  
E R S Y  
N D R O M E  
S P A G 5 C A C N A 1 D  
E P S 8 N I N L C L A R I N 1

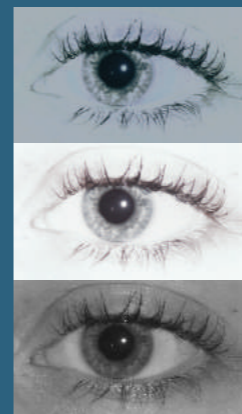


Keeping an eye on novel members of the Usher protein network Ferry F.J. Kersten

Keeping an eye on novel members  
of the Usher protein network



Ferry F.J. Kersten



**Keeping an eye on novel members of the Usher  
protein network**

**Ferry F.J. Kersten**

Ferry F.J. Kersten, 2011

Keeping an eye on novel members of the Usher protein network

Publication of this thesis was financially supported by the Departments of Human Genetics and Ophthalmology Radboud University Nijmegen Medical Centre, Nationale Hoorstichting/VriendenLoterij, Stichting Blindenhulp, Landelijke Stichting voor Blinden en Slechtzienden, Laméris Ootech B.V., Ergra Low Vision.

© 2011, Ferry F.J. Kersten, Nijmegen, The Netherlands

All rights reserved. No part of this publication may be reproduced or transmitted in any form or by any means electronic or mechanical, by print or otherwise without prior permission in writing from the author.

**Cover design en layout:** Ferry F.J. Kersten

**Cover photo:** L'Hemisfèric, Ciudad de las Artes y las Ciencias (City of Arts and Sciences), Valencia, Spain (may 2010)

**Printed by:** Ipskamp Drukkers B.V., Enschede

**ISBN:** 978-90-9026178-2

# **Keeping an eye on novel members of the Usher protein network**

Een wetenschappelijke proeve op het gebied van de  
Medische Wetenschappen

## **PROEFSCHRIFT**

ter verkrijging van de graad van doctor  
aan de Radboud Universiteit Nijmegen  
op gezag van de rector magnificus prof. mr. S.C.J.J. Kortmann,  
volgens besluit van het college van decanen  
in het openbaar te verdedigen  
op maandag 24 oktober 2011  
om 13.30 uur precies

door

**Ferry Fredericus Johannes Kersten**

geboren op 03 november 1979  
te Arnhem

**Promotoren:**

Prof. dr. H. Kremer

Prof. dr. J.E.E. Keunen

**Copromotor:**

Dr. ir. R. Roepman

**Manuscriptcommissie:**

Prof. dr. J.G.J. Hoenderop (voorzitter)

Prof. dr. L.P.W.J. van den Heuvel

Dr. H.J. Bolz (Ingelheim, Duitsland)



## **Table of contents**

<b>Abbreviations</b>	8
<b>Chapter 1</b>	11
General introduction	
1. Introduction	13
2. Usher syndrome	13
3. USH proteins co-function in a protein network	15
4. The affected organs in Usher syndrome	18
4.1. The ear	18
4.1.1. The structure and function of the inner ear	18
4.2. The eye	20
4.2.1. The structure and function of the retina	21
5. Architecture of the cilium	22
6. Ciliogenesis and intraflagellar transport	24
7. Localization of USH proteins in the inner ear and retina	25
7.1. USH proteins in inner ear hair bundles	26
7.2. USH proteins in neurons of the inner ear	29
7.3. USH proteins in the synaptic regions of hair cells and photoreceptor cells	29
7.4. USH proteins at the outer limiting membrane, outer segments and RPE in the retina	30
7.5. USH proteins in the periciliary region of photoreceptor cells	31
8. Insights in pathogenesis - animal models	32
8.1. Hearing loss: the hair bundle	32
8.2. Hearing loss and Retinitis pigmentosa: the synapse	35
8.3. Retinitis pigmentosa: the photoreceptor cells	35
9. The outline of this thesis	38
10. References	39
<b>Chapter 2</b>	51
Association of whirlin with Ca <sub>v</sub> 1.3 ( $\alpha_{1D}$ ) channels in photoreceptors, defining a novel member of the Usher protein network	
<b>Chapter 3</b>	77
A hypofunctional EPS8 variant predisposes to ototoxicity	
<b>Chapter 4</b>	101
Usher syndrome and Leber congenital amaurosis are molecularly linked via a novel isoform of the centrosomal ninein-like protein	

<b>Chapter 5</b>	135
The mitotic spindle protein SPAG5/Astrin connects to the Usher protein network postmitotically	
<b>Chapter 6</b>	159
<i>CLRN1</i> mutations cause non-syndromic retinitis pigmentosa	
<b>Chapter 7</b>	177
General discussion	
1. The expanding USH protein network	179
1.1. Identification of novel members of the USH protein network	180
1.2. Biological relevance of the interactions with novel members	180
2. Functions of the USH protein network: what do novel members tell?	181
2.1. Organization of ion channels	182
2.2. Planar cell polarity	182
2.3. Stereocilia formation and elongation	183
2.4. Vesicle transport	184
3. Disease association of genes encoding USH proteins and novel members of the protein network	185
3.1. Clinical variability	186
3.2. Disease association of genes encoding novel members of the USH protein network	187
4. Prospects on future research	189
4.1. Extending the knowledge on the function of the USH protein network	189
4.2. Dynamics of the USH protein complex	190
4.3. Therapeutic interventions	190
5. References	191
<b>Summary / Samenvatting</b>	199
<b>Dankwoord</b>	209
<b>Curriculum vitae / List of publications</b>	215



## Abbreviations

aa	: amino acid
AAV	: adeno-associated virus
ALA	: ankle link antigen
ANK	: ankyrin
arRP	: autosomal recessive retinitis pigmentosa
BB	: basal body
BBS	: Bardet-Biedl syndrome
Calx	: Ca <sup>2+</sup> -binding calcium exchanger $\beta$
CASK	: calcium/calmodulin-dependent serine protein kinase
Ca <sub>v</sub> 1.3	: L-type calcium channel pore-forming subunit ( $\alpha$ 1D)
CC	: connecting cilium
CDH23	: cadherin-23
cDNA	: copy / complement deoxyribonucleic acid
CE	: collar-like extension of the apical inner segment
CLRN1	: clarin-1
cM	: centimorgan
CNS	: central nervous system
DFNA	: autosomal dominant deafness
DFNB	: autosomal recessive deafness
DIG	: digoxigenin
DTT	: 1,4-dithiothreitol
E	: embryonic day
eCFP	: enhanced cyan fluorescent protein
EM	: electronmicroscopy
EPS8	: epidermal growth factor receptor substrate 8
ERG	: electroretinography
FN3	: fibronectin type III
GCL	: ganglion cell layer
GFP	: green fluorescent protein
GPR98	: G-protein coupled receptor 98 kDa
GST	: glutathion-S-transferase
HA	: hemagglutinin
HCA	: hair cell antigen
Hz	: hertz
IB	: immune blot
IFT	: intra flagellar transport
IHC	: inner hair cell
INL	: inner nuclear layer

IP	: immune precipitation
IPL	: inner plexiform layer
IS	: inner segment
ISH	: <i>in situ</i> hybridization
IsoB	: isoform B
kDa	: kilodalton
LamG	: laminin G-like
LamNT	: laminin N-terminal
LCA	: Leber congenital amaurosis
LOD	: log of odds
mRFP	: monomeric red fluorescent protein
MYO7A	: myosin VIIa
MYO15A	: myosin XVa
NBC3	: sodium bicarbonate transporter 3
NINL	: ninein-like protein
OHC	: outer hair cell
OLM	: outer limiting membrane
ONL	: outer nuclear layer
OPL	: outer plexiform layer
OS	: outer segment
P	: postnatal day
PBM	: PDZ-binding motif
PBS	: phosphate buffered saline
PCDH15	: protocadherin-15
PCP	: planar cell polarity
PDZ	: postsynaptic density 95, PSD-95; discs large, Dlg; zonula occludens-1, ZO-1
PST	: proline-, serine-, threonine-rich
PTX	: pentaxin
RP	: retinitis pigmentosa
RPE	: retinal pigment epithelium
SAM	: sterile-alpha motif
SDS-PAGE	: sodium dodecyl sulfate polyacrylamide gel electrophoresis
SNP	: single-nucleotide polymorphisms
SPAG5	: sperm associated antigen 5
TAP	: tandem affinity purification
TLA	: tip link antigen
TM	: transmembrane
TspN	: thrombospondin
TUNEL	: terminal deoxynucleotidyl transferase dUTP nick end labeling
USH	: Usher
WHRN	: whirlin



# Chapter



# 1

## General introduction





## **1. Introduction**

Hearing and vision are essential for communication and the loss of those senses often leads to a loss of independence. Moreover, life nowadays requires intense use of communication skills and information technologies which is a major disadvantage for individuals suffering from Usher syndrome. Usher syndrome is the most common cause of inherited deaf-blindness <sup>1</sup> with a prevalence ranging from 3.5 to 6.2 per 100,000 in different populations <sup>2-6</sup> and currently there is no cure for this disease.

Many diseases including Usher syndrome are heterogeneous. Initially, it was unclear how mutations in genes encoding proteins from different protein families could lead to a similar phenotype. Proteins do not function in isolation, but rather interact with other proteins in a network and thereby play a major role in different cellular processes. Deciphering protein networks contributes to the understanding of the structure, function and dynamics of a cell. Thousands of protein-protein interactions have been studied and for the human proteome almost 40,000 protein interactions are summarized in the Human Protein Reference Database (<http://www.hprd.org>) <sup>7-9</sup>. The knowledge of network members and their involvement in different pathways contributes to the understanding of the pathogenic mechanisms underlying human diseases. Proteins encoded by genes associated with the same disease often interact with one another, they are present in the same tissues and have coherent functions <sup>10</sup>. A gene encoding an interaction partner of a protein encoded by a disease causing gene can therefore be expected to cause the same or a similar disease <sup>10,11</sup> and the proteins could have similar or coherent functions. Therefore protein-protein interaction studies can be very useful for the indirect identification of candidate disease genes and/or contribute to the elucidation of the molecular pathology of a disease, such as Usher syndrome, to pave the way for the ultimate goal of therapeutic intervention.

## **2. Usher syndrome**

Patients suffering from both deafness and blindness were first described by Albrecht von Graefe in 1858 <sup>12</sup>, but Usher syndrome was finally eponymously named after the ophthalmologist Charles H. Usher in 1935 <sup>13</sup>. The syndrome exhibits a recessive pattern of inheritance <sup>1</sup>. The vision loss is caused by retinitis pigmentosa (RP), a progressive retinal

dystrophy, characterized by intraretinal bone spicule-shaped pigmentation as a result of pigment release by the degenerating retinal pigment epithelium (RPE). The first symptoms of RP are nyctalopia (night blindness) that precedes reduction of the peripheral visual field (tunnel vision). Eventually, the central vision become affected as well, which often leads to blindness<sup>14</sup>. Bell<sup>15</sup> already reported differences in the severity of hearing loss among patients with Usher syndrome, and the current classification of three clinical types<sup>16</sup> type I (USH1), type II (USH2) and type III (USH3) is based on these findings. Congenital, stable severe to profound hearing loss is characteristic of USH1 as is the absence of vestibular function which leads to delayed motor milestones. Diagnosis of RP is generally before puberty in USH1. The genes associated with USH1 are *MYO7A* (USH1b), *USH1C* (USH1c), *CDH23* (USH1d), *PCDH15* (USH1f), and *USH1G* (USH1g)<sup>17-21</sup>. Two additional loci have been identified, USH1e and USH1h, but the corresponding genes have not yet been identified<sup>22,23</sup>.

For USH2, congenital moderate to severe stable hearing loss is typical. However, hearing loss may exhibit some progression<sup>24</sup>. High frequency hearing is most severely affected. Vestibular function is within the normal range as are motor milestones of the patients. RP is usually diagnosed later than in USH1, around or after puberty. *USH2A*, *GPR98*, and *DFNB31* are the genes involved in the three known genetic subtypes USH2a, USH2c and USH2d, respectively<sup>25-27</sup>. For USH2 there is at least one additional locus for which the gene remains to be identified<sup>28</sup>. *CLRN1* (USH3a)<sup>29</sup> is associated with USH3 which is characterized by progressive hearing loss with onset at variable age. Also the onset of RP is variable and can precede that of hearing loss. Vestibular function can be normal, absent or partially impaired. In a subset of patients, the disease cannot be classified as one of the three types USH1-3 and is, therefore, called atypical<sup>30-32</sup>. Congenital severe to profound hearing loss has for example been described to be associated with late onset or subclinical RP caused by mutations in *CDH23* or *USH1G*<sup>18,30,33</sup> and the symptoms associated with mutations in USH genes can vary from nonsyndromic hearing loss to nonsyndromic RP<sup>33</sup>.

USH proteins (Fig. 1) belong to protein families with very diverse functions<sup>34-37</sup>. Myosin VIIa is an actin based motor protein. Harmonin and whirlin are homologous PDZ domain-containing proteins and are scaffold proteins as is SANS. Cadherin-23 and protocadherin-15 are members of the cadherin superfamily of cell adhesion molecules. Also USH2A and

GPR98, a G-protein coupled receptor, are transmembrane proteins with large extracellular regions that consist of domains suggesting a role in outside-in signaling. Clarin-1 is predicted to be a protein with four-transmembrane domains and is part of the vertebrate-specific clarin protein family. For most of the known USH genes alternative transcripts are known that are predicted to encode several protein isoforms (Fig. 1). Recently, five novel Clarin-1 splice variants have been identified<sup>38</sup>. Alternative splicing is most extensively studied for murine *Pcdh15* for which 24 different transcripts have been described<sup>39</sup>.

### **3. USH proteins co-function in a protein network**

Proteins do not function in isolation, but interact with other proteins. USH1 and USH2 proteins are part of an USH protein network (Fig. 2) and directly interact with at least one other USH protein. The USH3 protein clarin-1, in line with USH1 and USH2 proteins, is expected to belong to the USH protein network<sup>40</sup>, but so far no direct interaction between clarin-1 and one of the other USH proteins have been demonstrated although several indirect links have been suggested. Clarin-1 is thought to regulate the actin cytoskeleton and thereby an indirect link was suggested between clarin-1 and the actin binding USH proteins harmonin and myosin VIIa<sup>41</sup>. Another link was suggested by the interaction between clarin-1 and protein 4.1 which indirectly binds to whirlin via p55<sup>41</sup>. Both USH2A and clarin-1 bind to integrin subunits<sup>41,42</sup> which might be a further indirect connection to the USH protein network. Harmonin and whirlin are the main organizers of this network based on the interaction of their PDZ domains with PDZ-binding motifs in several of the other USH proteins<sup>40,43-47</sup>. Also myosin VIIa interacts with several USH1 and USH2 proteins.

The USH protein network is dynamic since different combinations of USH proteins, or even different combinations of USH isoforms during development, vary at different subcellular locations (see below). This spatiotemporal dynamics is further supported by the fact that several USH proteins were found to interact with the same domain of another USH protein. PDZ1 and PDZ2 of whirlin, for example, can bind both USH2A and GPR98<sup>47</sup>. The majority of the direct interactions within the USH protein network have been determined by using *in vitro* assays and/or *in vivo* assays based on over expression of the proteins of interest. The



biological relevance has been proven for only a subset of these interactions *e.g.* mislocalization of harmonin-b in mice defective for SANS or myosin VIIa<sup>48</sup>.

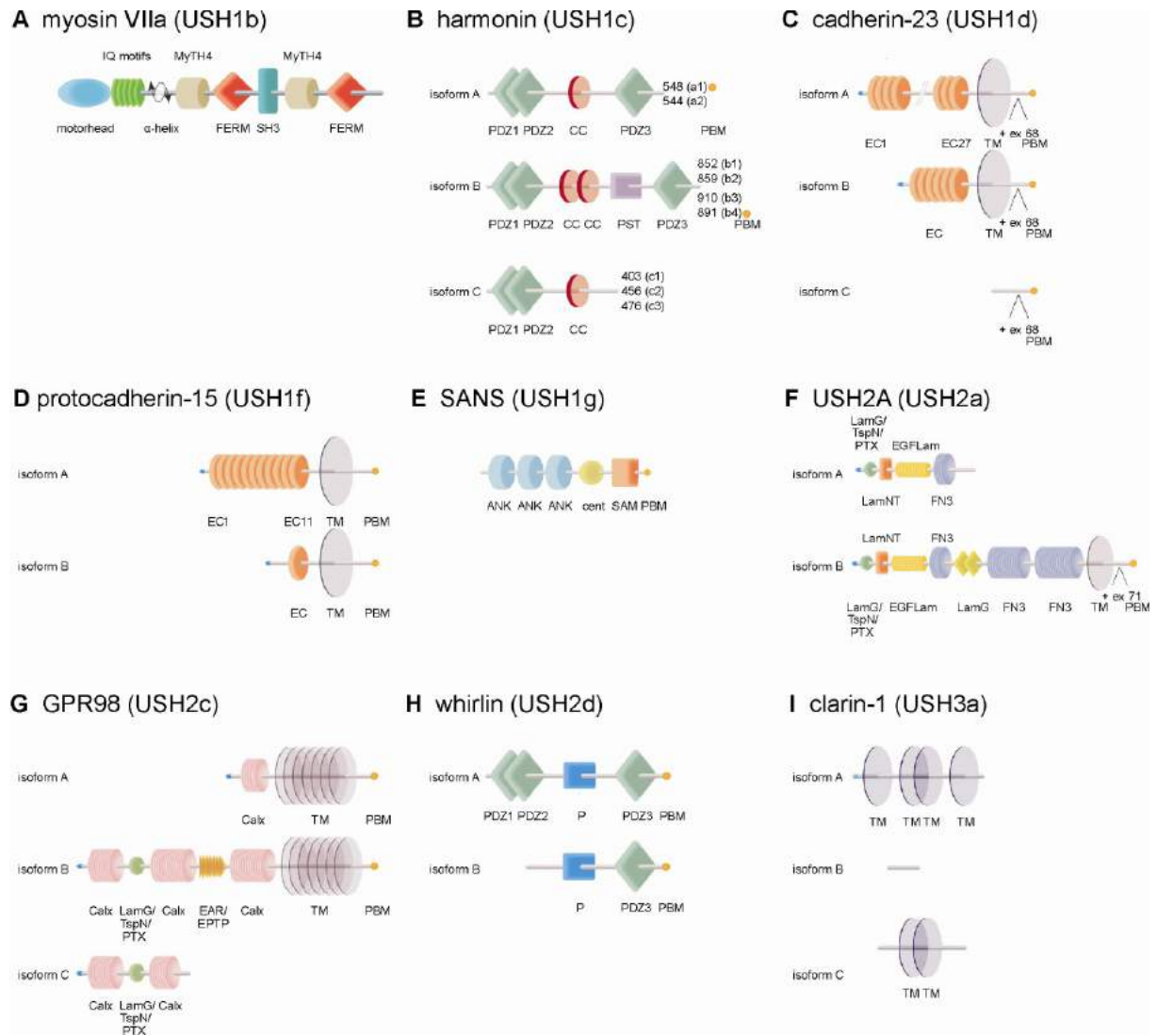


**Figure 1.** Schematic representation of the architecture of the Usher type I, type II and type III proteins and their different isoforms. **(A)** The USH1b protein, myosin VIIa, is composed of a motor head domain, five calmodulin-binding IQ motifs, two FERM domains, two MyTH4 domains and a Src homology 3 (SH3) domain. **(B)** Three different classes of isoforms of the USH1c protein, harmonin, are identified. All three isoforms consist of two PDZ (*PSD95*, *discs large*, *ZO-1*) domains (PDZ1 and 2), and one coiled-coil (CC) domain. In addition, class A isoforms contain an additional PDZ domain (PDZ3). The class B isoforms contain also this third PDZ domain, a *proline, serine, threonine*-rich region (PST). Isoforms A1 and B4 contain a C-terminal class I PDZ-binding motif (PBM). **(C)** Representation of the three different isoforms of cadherin-23 (USH1d). Isoform A is composed of 27  $\text{Ca}^{2+}$ -binding extracellular cadherin domains (EC1-27), a transmembrane domain (TM) and a short intracellular region with a C-terminal class I PBM. Isoform B is similar to isoform A, but lacks the first 21 EC domains. Isoform C only consists of the intracellular region and C-terminal PBM.

(D) Like cadherin-23, the non-classical cadherin protocadherin-15 (USH1f) consists of either eleven (isoform A) or one (isoform B) EC domain(s), a transmembrane domain and a C-terminal class I PBM. (E) The scaffold protein SANS (USH1g) consists of three ankyrin domains (ANK), a central region (cent), a sterile *alpha motif* (SAM) and a C-terminal class I PBM. Schematic representation of the architecture of the Usher type II and Usher type III proteins and their different isoforms. (F) Isoform A of USH2A (USH2a) contains a thrombospondin/pentaxin/laminin G-like domain, a laminin N-terminal (LamNT) domain, ten laminin-type EGF-like (EGF Lam) and four fibronectin type III (FN3) domains. In addition to the domain structure of isoform A, isoform B contains two laminin G (LamG) domains, 28 FN3 domains, a transmembrane domain (TM) and an intracellular region with a C-terminal class I PBM. (G) Three isoforms of the G-protein coupled Receptor 98 kDa, GPR98 (USH2c), are identified. The longest isoform, isoform B, consists of a thrombospondin/pentaxin/laminin G-like domain, 35 Ca<sup>2+</sup>-binding *calcium exchanger*  $\beta$  (Calx) domains, seven EAR/EPTP repeats, a seven-transmembrane region and an intracellular region containing a C-terminal class I PBM. Isoform A is composed of the last 6 C-terminal Calx domains, the seven-transmembrane region and the intracellular region with the C-terminal class I PBM. The predicted extracellular isoform C only contains the first 16 N-terminal Calx domains and the thrombospondin/pentaxin/laminin G-like domain. (H) Isoform A of whirlin, the USH2d protein, contains three PDZ domains and a proline-rich region (P). Isoform B lacks the two N-terminal PDZ domains. Both isoforms contain a C-terminal class II PBM. (I) Clarin-1, the USH3a protein, only contains four (isoform A) or two transmembrane (isoform C) domains. For isoform B, no domains are predicted. Adapted from <sup>36</sup>.

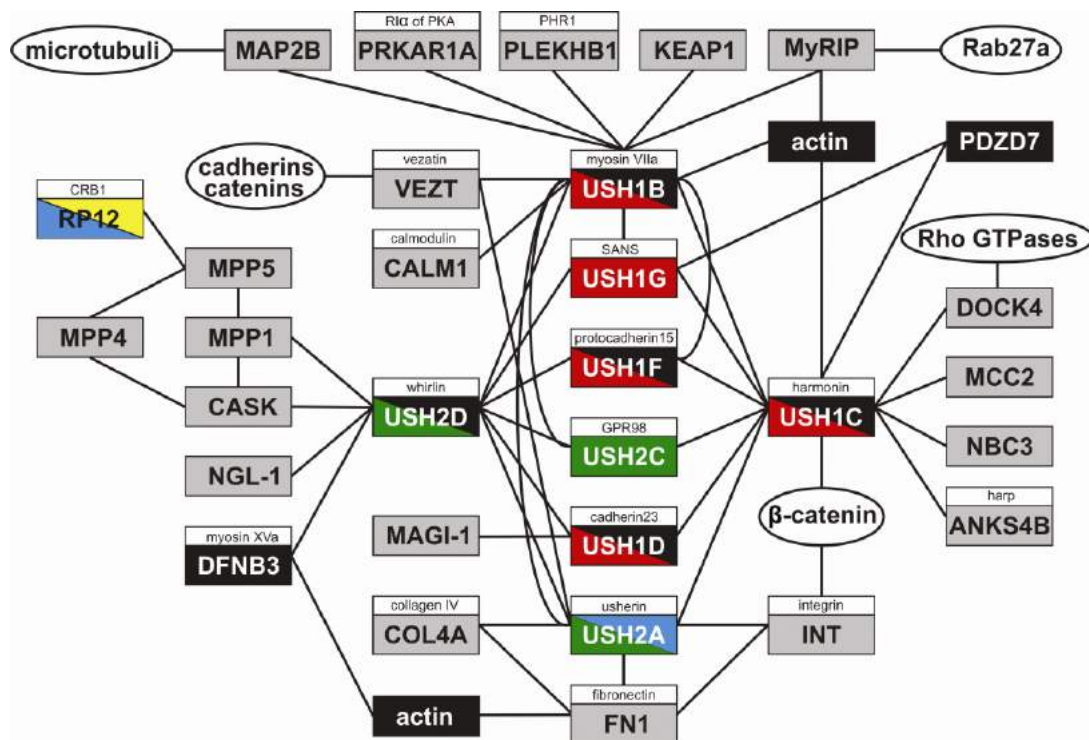


**Figure 2.** The USH protein network. Protein-protein interactions are indicated by lines. Red indicates association with Usher syndrome type I (USH1), green indicates association with Usher syndrome type II (USH2), blue indicates association with isolated retinitis pigmentosa (RP), black indicates association with isolated deafness. The binding of cadherin-23 and protocadherin-15 to whirlin has been identified in a yeast two-hybrid assay (van Wijk *et al.*, unpublished data).

## **4. The affected organs in Usher syndrome**

The hallmark of Usher syndrome is the dysfunction of the inner ear and retina. Insight in the subcellular localization, spatiotemporal dynamics and the interaction partners of the USH proteins contribute to the knowledge of the function, development and the molecular disease pathology of the inner ear and retina. To unravel the complexities of the degeneration of the sensory cells in the inner ear and retina, the normal structure and function of these sensory organs need to be understood.

### **4.1 The ear**

The ear captures sound waves from the environment, with frequencies between 20 and 20.000 Hertz and a wide range of amplitudes<sup>48,49</sup>. In the ear, these sound impulses are converted into neuronal impulses which are subsequently transmitted to the brain, where the actual sound perception takes place<sup>34</sup>. The ear contains three anatomical compartments: the outer, the middle, and the inner ear (Fig. 3A). In the outer ear, sound waves are captured by the pinna (auricle) and conducted via the ear canal to the tympanic membrane (eardrum) which is set in motion and thereby, the sound pressure wave is converted into a mechanical wave. Loud sounds can be toned down by relaxation of the tympanic membrane which is controlled by muscles. The vibration of the tympanic membrane causes the subsequent movement of the three ossicles, malleus, incus and stapes in the middle ear which can amplify quiet sounds (Fig. 3A). The sound waves are transmitted to the scala vestibuli of the cochlea by movement of the stapes footplate into the oval window. The Eustachian tube can equalize the pressure between the middle ear and the atmosphere (Fig. 3A).

#### ***4.1.1 The structure and function of the inner ear***

The sensitive inner ear is protected by being embedded into in the hardest bone of the human body, the temporal bone. The inner ear contains the sensory cochlea for hearing and the vestibulum for balance, coordination and orientation<sup>50</sup>. The cochlear duct is divided in three compartments by the Reissner's membrane and the basilar membrane (Figs. 3B and C). Two of these compartments, the scala vestibuli and the scala tympani, are filled with perilymph containing high levels of sodium and low levels of potassium. The third compartment, the scala media, contains the organ of Corti and is filled with endolymph containing low levels of sodium and high levels of potassium (Figs. 3B and C)<sup>51</sup>. The spiral ligament connects the

basilar membrane to the outer cochlear wall and the stria vascularis functions in the maintenance of the potassium concentration in the endolymph. The organ of Corti is the sensory epithelium of the auditory system and contains supporting cells, three rows of outer hair cells (OHCs), and one row of inner hair cells (IHCs) (Fig. 3C) <sup>51</sup>. Hair cells (mainly IHCs) have highly organized ribbon synapses at their base which connect them to the afferent fibers of the cochlear nerve. At their apical surface they have actin-based protrusions, the stereocilia, in a “V”-shaped staircase-like arrangement. Stereocilia are anchored in the cuticular plate and mutually connected via fibrous links. Only during development the microtubule based kinocilium is present and its position defines the orientation of the hair bundle (see below). The stereocilia of the IHCs may touch the tectorial membrane, a gelatinous structure which is anchored at the spiral limbus, but the OHCs stereocilia are attached to it (Fig. 3C). When sound waves enter the cochlea the basilar membrane with the organ of Corti vibrates against the tectorial membrane resulting in deflection of the stereocilia. As a consequence, ion channels in the tips of the stereocilia are mechanically opened by the so called fibrous tip links, that connect the tips of shorter stereocilia to the sides of the neighboring taller stereocilia. This leads to an influx of potassium and calcium ions from the endolymph and subsequently to hair cell depolarization, neurotransmitter release, and signaling via the cochlear nerve to the brain <sup>52</sup>. The auditory information is transmitted to the brain by the IHCs, whereas the OHCs are important in both sensing and tuning the frequency of the vibrations and to amplify the mechanical signal, which is then transduced by the IHCs <sup>50,53</sup>. Hair cells at the base of the cochlea respond to high frequencies and those at the apex to low frequencies <sup>54</sup>.

The vestibular system comprises the semicircular canals that respond to rotational movements of the head, and the otolithic organs, utricle and saccule, which indicate linear accelerations. Rotation of the head results in the displacement of the endolymph in the semicircular canals which subsequently causes displacement of the cupula, a hair cell-containing gelatinous structure <sup>55</sup>. The movement of the cupula leads to the deflection of the stereocilia and eventually to a neurotransmitter release <sup>56</sup>. The signal is transmitted via the vestibular nerve to the brain. The sensory patches of the utricle and saccule contain hair cells and calcium carbonate crystals, otoconia (ear stones), embedded in a gelatinous membrane that covers the sensory epithelium of the saccule and the utricle. Forces due to gravity and linear acceleration

act through otoconia to deflect the stereocilia of the hair cells resulting in neurotransmitter release onto the vestibular nerve <sup>57</sup>. The hair cells of the otolithic organs and semicircular canals send signals to the neural structures that control eye movements, and to the muscles to keep in balance <sup>58</sup>.

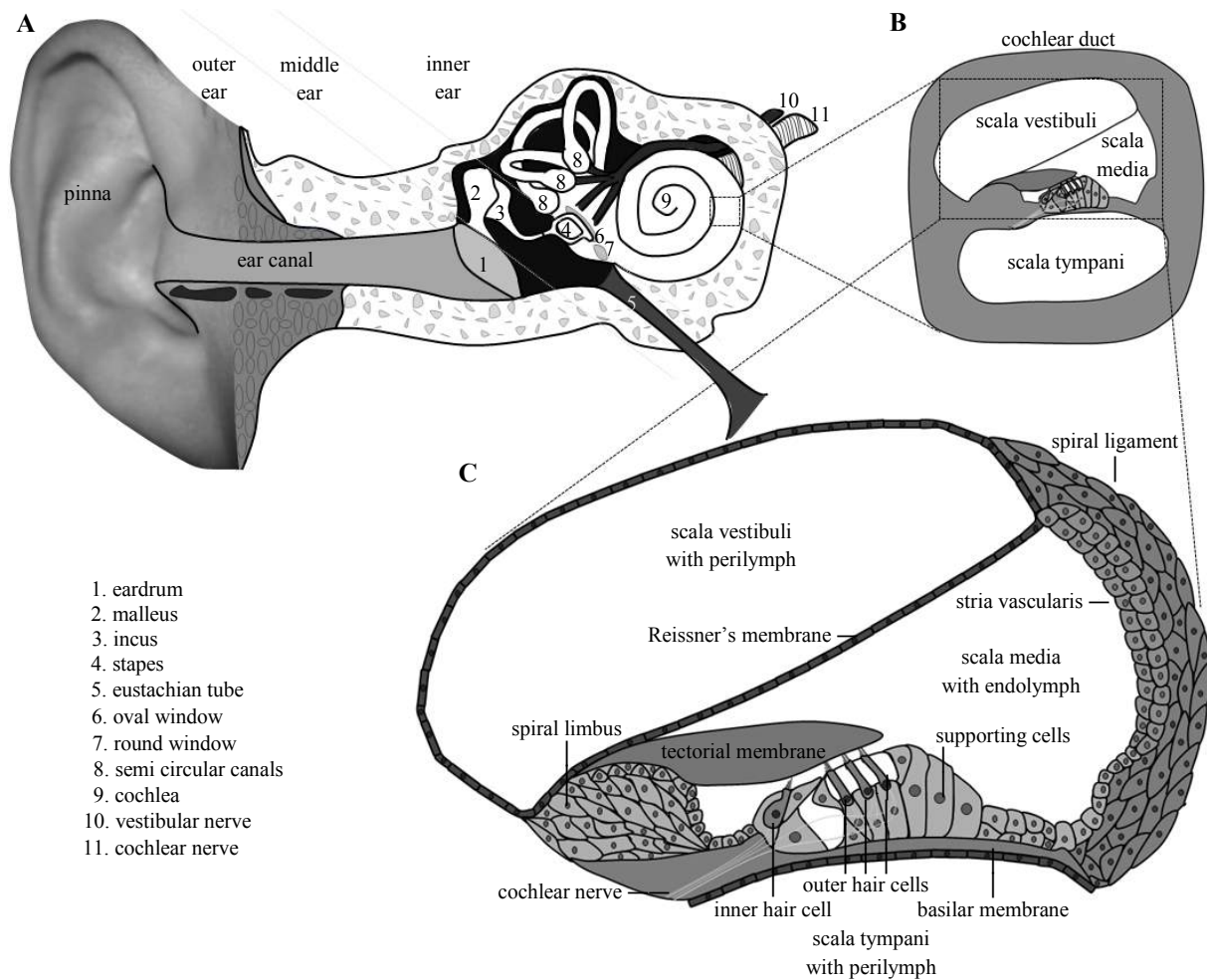


**Figure 3.** Schematic representation of the human ear. (A) The ear consist of the outer, the middle and the inner ear. (B) A section trough the cochlea shows the three fluid-filled compartments of the inner ear. (C) The organ of Corti comprises numerous of cells types including inner- and outer hair cells.

## 4.2 The eye

Light enters the eye via the cornea that refracts the light and contributes to most of the eye's focusing capabilities (Fig. 4) <sup>59</sup>. Subsequently, the light passes through the aqueous humour that maintains the eye pressure in the anterior compartment after which the light passes through the pupil and the lens. By changing its shape with the use of the ciliary body, the lens

refracts the light to focus on objects. Focal adjustment of closer objects is a role of the iris that also regulates the amount of light entering the eye<sup>60</sup>. The amount and type of pigmentation in the iris determines the eye color<sup>61</sup> and protects the underlying tissues from ultraviolet radiation<sup>62</sup>. The interior of the eye is protected by the sclera, a white dense fibrous dynamic connective tissue that can regulate the ocular size and refraction by altering extracellular matrix composition and biomechanical properties<sup>63</sup>. To maintain the shape of the eye, a constant pressure is needed in the space between the lens and the retina which is provided by a viscous liquid, the vitreous humour. Scattered light is absorbed by the pigment of the choroid, a vascular layer that provides the outer layers of the retina with oxygen and nourishment<sup>64</sup>. The retina contains the light sensitive photoreceptor cells which convert light into neuronal signals during the phototransduction cascade after which the neuronal signals are processed during the visual cycle into electrical signals that are transmitted via the optic nerve to the visual cortex of the brain (Fig. 4)<sup>65</sup>.

#### ***4.2.1 The structure and function of the retina***

The retina is a multi-layered tissue of about 0.5 millimeters thick and lines the back of the eye (Fig. 4). Light reaches the retina at the side of the inner limiting membrane and the nerve fiber layer. Subsequently it passes the five neuronal layers i.e. the ganglion cells, the amacrine cells, the bipolar cells, the horizontal cells and the photoreceptor cells before it reaches the retinal pigment epithelium (RPE) (Fig. 4B). The RPE contains granules of the pigment melanin that absorb scattered and excessive light. Furthermore, it is the blood-retinal barrier and selectively transports nutrients to the retina. Thereby, it prevents access of harmful molecules to the retina. In addition, the RPE is involved in the renewal of the photoreceptor outer segments by phagocytosis of outer segment discs. Müller glial cells are stretched across the entire retina and contact all other cell bodies, adherence junctions and blood vessels<sup>66</sup>. Müller cells play an active role in retinal function<sup>67</sup> by the maintenance of retinal homeostasis<sup>68</sup>. They also provide retinal neurons with nutrients and remove metabolic waste products<sup>69</sup>. Importantly, they play a role in retinol metabolism<sup>70</sup>. The light-sensitive photoreceptor cells convert light into electrical signals and the bipolar cells, the horizontal cells, the amacrine cells and the ganglion cells transmit these signals from the photoreceptors to the brain (Fig. 4B). There are two major types of photoreceptor cells, rods and cones. In humans, the rods

predominate and constitute 95% (an average of 92 million) of the photoreceptor cells of which only 5% (an average of 4.6 million) are cones <sup>71</sup>. The latter are concentrated in the central retina (fovea) where they are responsible for daytime vision and the perception of color. Rods are more sensitive to light and enable night vision. They are mainly located in the peripheral retina and the region around the fovea <sup>72</sup>.

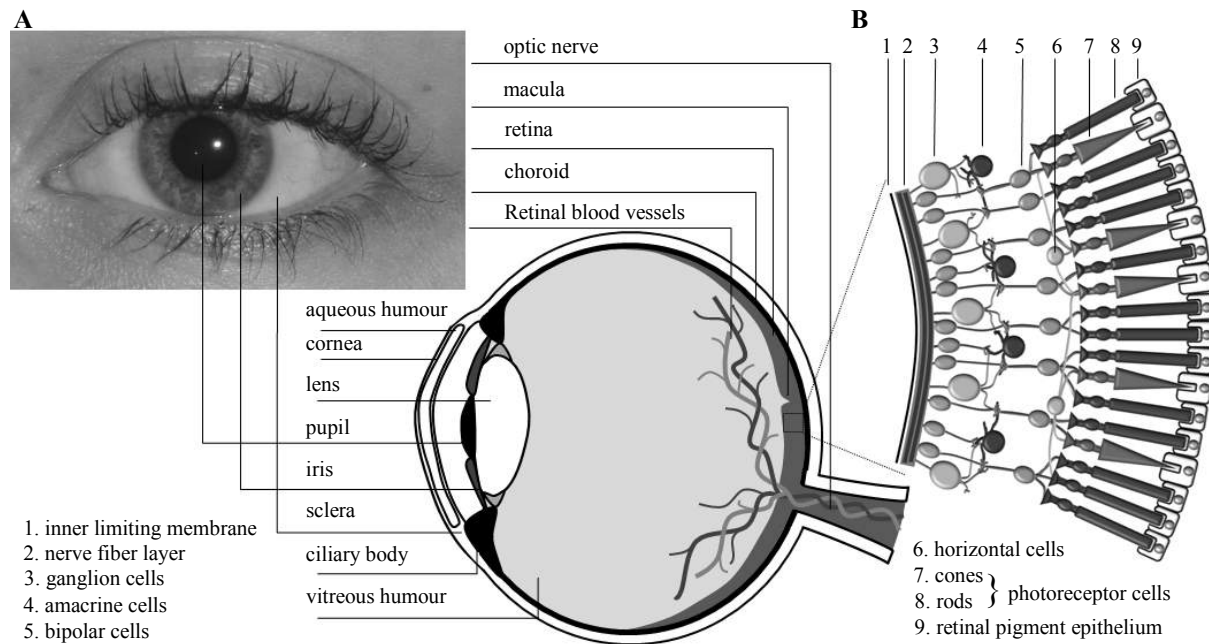


**Figure 4.** The human eye. (A) Anatomy of the eye. (B) Cellular structure of the retina.

## 5. Architecture of the cilium

To date, over 200 genetic loci have been associated with retinal diseases <sup>73</sup>. Many of the identified genes encode proteins that localize to the connecting cilium of photoreceptor cells. This structure connects the photoreceptor inner segments with the outer segments. Interestingly, mutations in the genes encoding these proteins are often not only causing retinal degeneration, but can lead to complex disorders with phenotypes including deafness, renal failure, obesity, and cognitive disabilities <sup>74</sup>. The similarity between those diseases is a dysfunctional cilium and these disorders are collectively called ‘retinal ciliopathies’. Usher syndrome can also be considered a retinal ciliopathy <sup>74</sup>, as symptoms indicating the involvement of several other (ciliated) tissues in addition to inner ear and retina have been reported in patients with Usher syndrome including anosmia, ataxia and sperm abnormalities

(for review see <sup>37</sup>). However, the underlying genetic defects in patients with these symptoms have not yet been elucidated.

Cilia are microtubule-based antenna-like protrusions of the cell surface that are present on most eukaryotic cells at some timepoint in their cell cycle <sup>75</sup>. Depending on the cell type, they can be involved in a wide variety of important functions, such as chemical sensation, signal transduction, and the control of cell growth <sup>76,77</sup>. The base of a cilium consists of a barrel-shaped structure comprising nine microtubule triplets, the basal body, which serves as the nucleation site of cilium growth. Basal bodies are attached to the plasma membrane by transition fibers at their apex, forming the basal part of the transition zone. At its base, the basal body is connected to a ciliary rootlet. These rootlets are thought to organize basal body position/orientation, to provide structural support and to have a protein scaffolding function (Fig. 5) <sup>79-82</sup>. The ciliary transition zone is important for the nucleation of ciliary microtubules, and may also play a role as a docking site for protein transport (Fig. 5) <sup>78</sup>. Cilia can be classified in two main types according to their microtubule composition within the axoneme: motile cilia (often called flagella), and immotile cilia (often called primary cilia). The axonemes of all cilia contain nine microtubule doublets in a ring-shape, “9+0” arrangement instead of the nine microtubule triplets in the basal body <sup>83</sup>. Only the motile cilia have an additional pair of microtubule bundles in the centre, a “9+2” configuration (Fig. 5). They also contain radial spokes that are thought to transmit signals from the centre microtubule pair to dynein arms which are present on the other microtubule doublets, thereby contributing to ciliary motility <sup>84,85</sup>. Some specific cilia escape this classification in two types: the motile “9+0” cilia on the embryonic node and the immotile “9+2” cilia of olfactory sensory neurons and kinocilia in the inner ear <sup>86-88</sup>.

In mammals, the kinocilium of the hair cell is only present during development. In contrast to the actin-based stereocilia, it is a true microtubule-based cilium (Figs. 5, 6). In the retina, the photoreceptor outer segment is also a specialized sensory cilium, with the same structural core as a primary cilium (Fig. 5) <sup>89</sup>. It contains all proteins of the phototransduction cascade that are synthesized in the photoreceptor inner segments, and subsequently actively transported through the microtubule tracks of the connecting cilium. This structure corresponds to the



transition zone, the short junction between the basal body and the axoneme of a prototypic primary cilium (Figs. 5, 6) <sup>90</sup>.

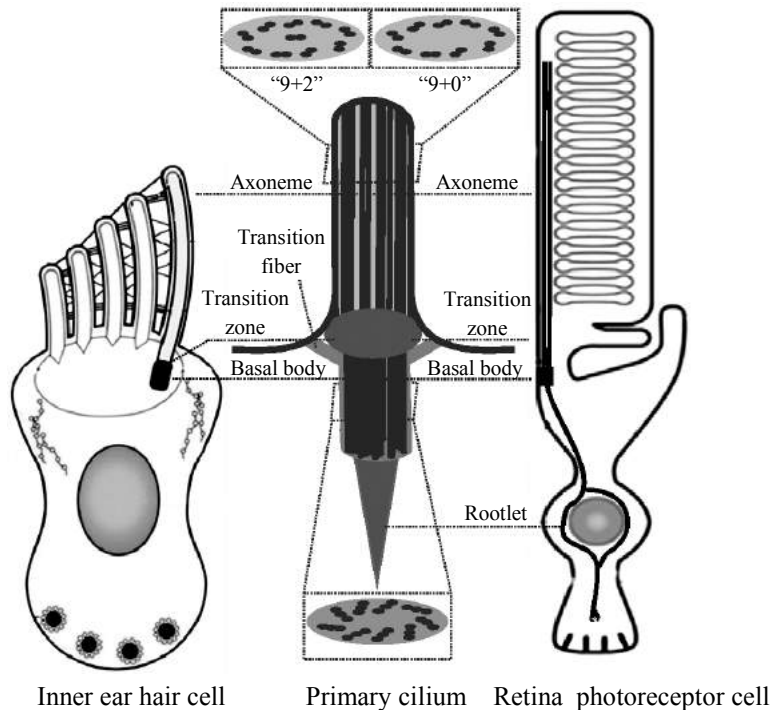


**Figure 5.** Similar core structure of primary cilia, inner ear hair cell kinocilia, and retinal photoreceptor cilia. All cilia contain an axoneme and a basal body. The basal body contains nine microtubule triplets and the axoneme contains nine microtubule doublets in a “9+0”, or a “9+2” arrangement. Ciliary rootlets provide stability, while transition fibers attach the basal body to the plasma membrane.

## 6. Ciliogenesis and intraflagellar transport

In many non-dividing (quiescent) cells during the interphase, a Golgi-derived vesicle localizes to the oldest of the two centrioles, the mother centriole, and invaginates this nascent axoneme <sup>91</sup>. The invaginated mother centriole migrates to the cell surface, where it docks with its distal- and subdistal appendages to the cell membrane to form a basal body <sup>92,93</sup>. Once the basal body has docked, assembly of the cilium and its maintenance is mediated via bi-directional intraflagellar transport (IFT). Structural and signaling components are transported as large IFT particles along the microtubules <sup>94</sup>. The IFT particles were found to consist of two multisubunit protein complexes, IFT-A and IFT-B <sup>95</sup>. The latter is thought to function in transport from cytoplasm towards tip (anterograde transport) by using kinesin-II motor proteins and the IFT-A complex is involved in the opposite retrograde transport by using the dynein motor complex <sup>94,96-98</sup>.

A similar transport mechanism is necessary in the photoreceptor sensory cilium to transport proteins from the inner segment, through the connecting cilium to the outer segment. The

outer segments mainly contain stacks of hundreds of membrane discs that are packed with photopigments and the other components of the phototransduction cascade. These discs are continuously renewed throughout the cell's lifetime. It is expected that the outer segments of a 80 years old person have been completely renewed approximately 3000 times <sup>99</sup>. These discs are formed at the base of the outer segment by repeated infolding of the existing outer membrane which then envelops the stack of discs, and the newly formed discs replace the older ones. The old discs are separated from the remaining stack by infolding of the membrane near the tip of the outer segment and phagocytosed by the RPE <sup>99</sup>. This continuous turnover of outer segments is enabled by the rapid, IFT-associated delivery of the required proteins and membrane components across the connecting cilium, as illustrated by the recent localization of many IFT proteins in the photoreceptor <sup>100</sup>. Therefore, the IFT proteins play an key role in the assembly and maintenance of photoreceptor outer segments <sup>101,102</sup>.

## **7. Localization of USH proteins in the inner ear and retina**

Hair cells and photoreceptor cells are the cell types that are found to be primarily affected in Usher syndrome as was concluded from studies in animal models and supported by the localization of USH proteins in these sensory cells (Fig. 6). In the hair cells USH proteins are mainly present in the stereocilia and the synaptic region (Fig. 6A). In photoreceptor cells USH proteins are mainly located at the periciliary region i.e. the apical inner segment, basal body and connecting cilium and at the synapse of the retina photoreceptor (Fig. 6B). These are sites where photoreceptor cells and hair cells display structural similarities. The structurally and functionally unique “ribbon” synapses are involved in high rates of sustained neurotransmitter release <sup>103</sup>. A basal body and a microtubule-based axoneme are present in both the photoreceptor and the hair cell namely the outer segment and kinocilium, respectively (Figs. 5, 6). Stereocilia which are microvilli with an actin core show similarity with the calycal processes of the photoreceptor cell. Calycal processes are microvilli-like extensions that project from the apical inner segment and extend alongside the basal outer segment <sup>36,104,105</sup>. In the following paragraphs, the localization of USH proteins in inner ear and retina will be described in more detail and subsequently the insights into pathogenesis of Usher syndrome as obtained by the analysis of animal models with defects in USH genes.

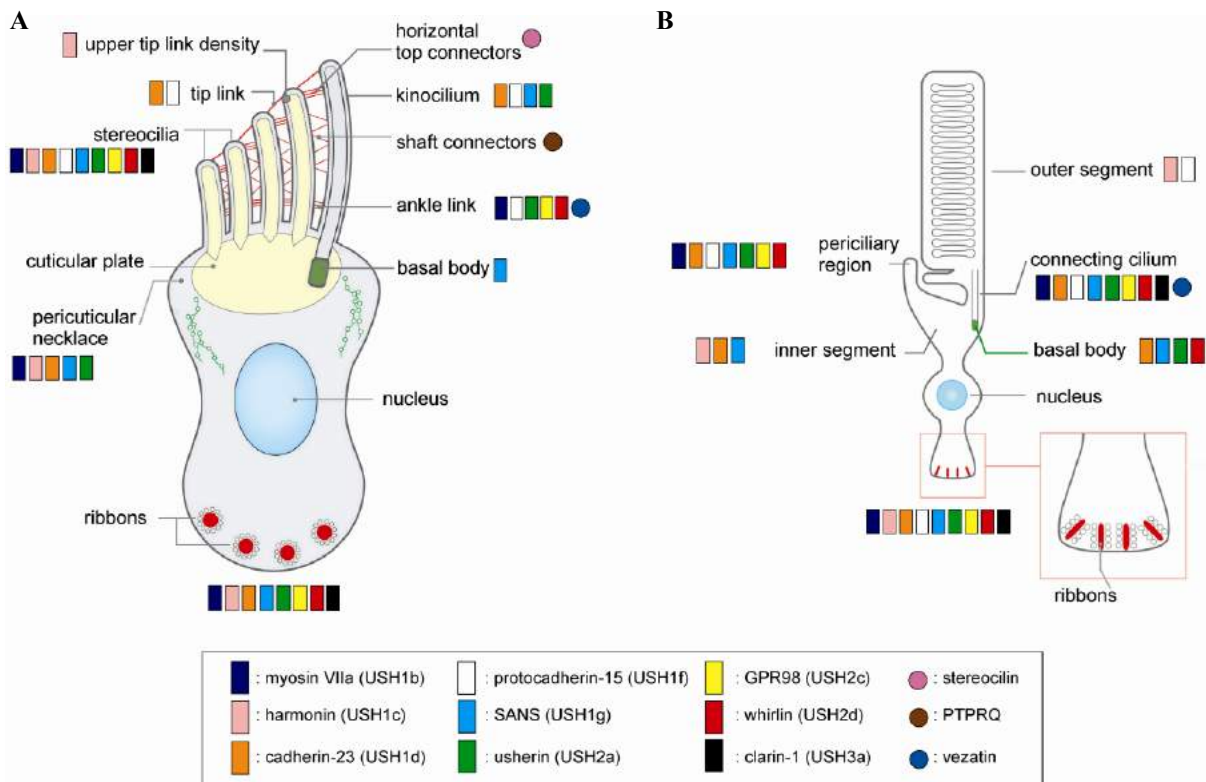


**Figure 6.** Schematic representation of the sensory cells in the inner ear and retina which are affected in Usher syndrome patients. The boxes represent USH proteins and the circles represent USH interaction partners. **(A)** The apical side of the inner ear hair cell carries the highly organized, actin-filled stereocilia, in which the echanotransduction takes place. Stereocilia are anchored in the actin-rich cuticular plate and are kept together by fibrous links. Lateral from the largest stereocilium the kinocilium is present which is a true cilium. The basal side of the hair cell, the synaptic junction between hair cell, efferent and afferent neurons, contains the ribbons. **(B)** The photoreceptor cells can be divided in rods (shown) and cones and consist of an outer segment, where the primary signal transduction takes place, which is separated from the inner segment by the connecting cilium. The periciliary region is a collar-like extension of the apical inner segment and surrounds the connecting cilium. The nuclei of the photoreceptor cells are situated in the outer nuclear layer of the retina. The synaptic terminals, containing the ribbons, connect the photoreceptors with horizontal cells and bipolar cells.

### 7.1 USH proteins in inner ear hair bundles

In the mouse, postmitotic cells in the sensory epithelium of the cochlea differentiate into hair cells in medial-to-lateral and basal-to-apical gradients along the cochlear duct from embryonic day 12.5 (E12.5) onwards<sup>48,106</sup>. Shortly thereafter, actin based protrusions emerge from the apical surface of these hair cells that ultimately form the stereocilia<sup>107,108</sup>. These microvilli of similar size surround the kinocilium which is positioned centrally on the apical surface of the developing hair cells. From early stages of development, E13 to E16 onwards, transient lateral

links are present between adjacent stereocilia and between stereo- and kinocilia. Immunohistochemical analyses revealed that these links contain hair cell antigen (HCA), ankle link antigen (ALA), and tip link antigen (TLA) which are also present in other types of links later in development or in the mature hair bundle<sup>109-111</sup>. At E17.5-18.5 the kinocilium migrates to the peripheral edge of the hair cell, thus determining the orientation of the hair bundle and thereby defining the planar cell polarity axis of the sensory epithelium.

From postnatal day 1 (P1) to P5 stereocilia begin to elongate differentially, according to their position in the hair bundle and present a staircase like pattern. During this elongation step the motor protein myosin XVa transports whirlin, and perhaps other molecules that are essential for the programmed stereocilia elongation to the tips of the stereocilia<sup>112,113</sup>. Myosin VIIa was recently shown to associate directly with the actin polymerization inhibitor twinfilin-2<sup>114</sup>. It was hypothesized that this protein complex, present in the tips of shorter stereocilia at levels proportional to their length, is responsible for slower rates of actin turnover in shorter stereocilia and that the interplay between the myosin XVa-whirlin complex and the myosin VIIa-twinfilin-2 complex is essential for the staircase like patterning of the hair bundle.

During the growth and maturation process of mouse cochlear hair bundles, different types of interstereociliar links emerge and disappear to maintain the cohesion between the stereocilia and kinocilium<sup>111</sup>. From P1 onwards, transient lateral links diminish and ankle links appear that persist until approximately P12. It has been postulated that ankle links play a role in signaling during hair bundle differentiation, rather than fulfilling a structural function<sup>111</sup>. The molecular composition of ankle links and other types of inter-stereociliar fibrous links has been elucidated based on spatiotemporal expression, immunohistochemistry, and immunoelectronmicroscopy. Based on this, the transmembrane proteins GPR98, USH2A, and vezatin are indicated to be part of the ankle link complex (Fig. 6A)<sup>43,45,115-117</sup>. Whirlin is likely to scaffold this complex by a direct association with USH2A and GPR98<sup>43,47</sup>. Also protocadherin-15 has been indicated to be part of the ankle links, although not essential for their presence<sup>118</sup>. Myosin VIIa, which directly interacts with all these ankle link components *in vitro*, is thought to function as a motor protein that delivers proteins of the ankle link complex to the stereocilia and to anchor this complex to their actin core (Fig. 6A)<sup>45</sup>.

Shaft connectors are transiently present (from E17.5 to P15) in the bundle of basal turn outer hair cells, but persist into maturity in other hair cells of the cochlea and the vestibular organ. Goodyear and coworkers<sup>119</sup> determined that the HCA, which was later identified as the receptor-like inositol lipid phosphatase Q (PTPRQ)<sup>110</sup>, is a component of these links (Fig. 6A) and is required for the complete maturation of cochlear hair bundles and long term maintenance of high frequency hair cells. Recently, clarin-1 was detected along the shaft of stereocilia exclusively at P0<sup>120</sup>. It is unclear whether clarin-1 is a component of transient fibrous links or whether it is involved in their anchoring. By P1, clarin-1 is only detected at low levels in hair cell bodies.

After disappearance of the ankle links, the horizontal top connectors develop (from P9 onwards) which are maintained throughout adulthood in outer hair cells. These top connectors are built by stereocilin molecules (Fig. 6A)<sup>121</sup>. Tip links are present from E17.5 onwards<sup>122</sup> and are structurally similar to kinociliary links<sup>123</sup>. Both share common epitopes<sup>110,124</sup>, and are insensitive to the treatment with proteinase subtilisin but sensitive to the calcium ions chelators BAPTA and EGTA<sup>110</sup>. Tip links are formed by asymmetric protein complexes consisting of cadherin-23 at the upper side and two intertwined protocadherin-15 molecules at the lower part of the link<sup>125</sup> and are thought to be essential for hair bundle integrity and mechanotransduction. To date, the molecular composition of the tip links is still under debate since hair bundles of mice with predicted *Cdh23* null alleles contain tip link like filaments<sup>126</sup>. Cadherin-23 is anchored at the upper tip link density (UTLD) by harmonin-b<sup>127</sup>, which in turn is dependent on the presence of SANS for its localization at the stereocilia tip<sup>128</sup>. Absence of harmonin-b prohibits UTLD formation and leads to altered mechanotransduction, resembling that of immature cochlear hair cells. Tip links, however, are still intact. Protocadherin-15 is anchored at the lower tip link density (LTLT), which is still intact in absence of harmonin-b. Beurg and coworkers have shown that the lower end of the tip link is most probably directly or indirectly associated with two mechanotransduction channels and that these channels are absent from the row with tallest stereocilia<sup>129</sup>. Also MAGI-1, an interaction partner of cadherin-23 was suggested to be an adapter protein in the tip link complex, thereby providing a connection to the actin core of stereocilia and other components of the mechanotransduction complex<sup>130</sup>.

Also in the hair bundle of vestibular hair cells interstereociliary links and fibrous links that connect stereocilia and kinocilia are present and essential for hair bundle morphogenesis and survival. However, this has been studied in less detail as compared to the cochlear hair cells.

## 7.2 USH proteins in neurons of the inner ear

To date, whirlin, USH2A, clarin-1, GPR98, and protocadherin-15 have been demonstrated in the cell bodies of the spiral ganglion neurons of the inner ear and whirlin is also present in the nerve fibers<sup>47,131</sup>. Since no abnormalities of spiral ganglion cells have been reported in these cells in mice with defects in the corresponding genes, there are no indications for a specific function of USH proteins in these cells.

## 7.3 USH proteins in the synaptic regions of hair cells and photoreceptor cells

All nine USH proteins have been detected in the outer plexiform layer of the retina, where the synapses of photoreceptor cells are localized (Fig. 6B)<sup>46,47,132-139</sup>. In the inner ear, only protocadherin-15 has not been reported to be present at the synaptic terminals of the inner and outer hair cells and whirlin was demonstrated in the synaptic region of outer hair cells only (Fig. 6A)<sup>40,46,47,132,133,140</sup>. Interestingly, clarin-1 was detected at the base of inner and outer hair cells and in type I afferent terminals from E18 to P6 which overlaps with the reduction of afferent and increase of efferent synaptic terminals at the outer hair cells during development<sup>141</sup>. Except for clarin-1, it is not known yet whether USH proteins are present pre- and/or postsynaptically in photoreceptor cells and hair cells, and in addition whether these proteins are located in the afferent or efferent nerve terminals in the inner ear. Both photoreceptor cells and hair cells have synaptic ribbons to which synaptic vesicles are tethered. Ribbon synapses have unique features such as fast and sustained release of neurotransmitters and a response to graded changes of membrane potential<sup>103</sup>. So far there are no indications that USH proteins are associated with the ribbons.

Several functions have already been suggested for USH proteins in the synaptic regions. The transmembranous USH proteins anchored by harmonin and whirlin may have a role in keeping the synaptic membranes closely apposed and the Calx $\beta$  domains of GPR98 might in addition function in the Ca<sup>2+</sup> homeostasis in the synaptic cleft<sup>46</sup>. For the scaffold proteins harmonin and whirlin, a role in the organization of ion channels or transporters had already

been proposed based on the direct interaction of harmonin with NBC3<sup>46</sup>. The latter is a sodium bicarbonate co-transporter that regulates the pH of cellular compartments, especially at the synapses and defects in the corresponding gene lead to deaf-blindness in mice<sup>142</sup>. Also, signal transduction at the synapses of hair cells in *Clrn1*<sup>-/-</sup> mice may be affected as indicated by prolonged peak latencies in auditory brain stem response measurements<sup>143</sup>. A function in synapses of sensory cells had already been proposed, based on the homology of clarin-1 with stargazin, a synapse protein in the cerebellum<sup>144</sup>. A possible role in microtubule associated vesicle transport in the synapses of photoreceptor and hair cells and in synaptic development and maintenance has been suggested by Zalocchi and coworkers<sup>141</sup>. However, it should be noted that the expression of *Clrn1* in photoreceptors is disputed<sup>138,145</sup>. The actin based motor protein myosin VIIa has been hypothesized to function in transporting synaptic molecules<sup>36,134</sup> and SANS is suggested to have a function in handing over molecules from the long range microtubule based transport to actin based transport at the synaptic terminal. The direct association of SANS and myosin VIIa might function in this process<sup>134</sup>.

#### **7.4 USH proteins at the outer limiting membrane, outer segments and RPE in the retina**

The identification of protocadherin-15, harmonin, USH2A, GPR98, SANS, whirlin at the outer limiting membrane and the association of whirlin with MPP1, a member of the Crumbs protein complex and also present at this location, suggest that the USH protein complex may have a role in cell-cell adhesion at the site of photoreceptor-Müller glia cell junctions with a central role for whirlin<sup>46,47,146-148</sup>.

So far only protocadherin-15 and harmonin-b have been identified in photoreceptor outer segments (Fig. 6B)<sup>46,135</sup> although the presence of harmonin-b in the photoreceptor is under debate<sup>19,149</sup>. Protocadherin-15 was detected at the plasma membrane of the outer segment base and at the disc membranes, whereas harmonin-b was only detected at the disc membranes. Protocadherin-15 and harmonin-b directly interact and thereby may connect the outer segment membranes to the actin cytoskeleton, which is known to play a role in the biogenesis of outer segment discs<sup>46,135</sup>.

Myosin VIIa appears to be the only USH protein in the RPE and its suggested role is the transport of melanosomes and phagosomes<sup>140,150-152</sup>.

## 7.5 USH proteins in the periciliary region of photoreceptor cells

Besides the synapse, the (peri)ciliary region (apical inner segment, basal body and connecting cilium) is a main location of USH proteins in the photoreceptor. The exact localization of proteins in the (peri)ciliary region cannot be determined by light- and fluorescence microscopy, but only by immuno-electron microscopy. All USH proteins are present in this periciliary region except harmonin and clarin-1 (Fig. 6B). This is mainly determined in mouse, rat and in *Xenopus*. The *Xenopus* photoreceptor is a good model since the periciliary region is underdeveloped in mice as compared to human and frog<sup>153</sup>. USH2A, GPR98, whirlin and SANS were detected in the periciliary region in mouse photoreceptor cells and in the ridges of the periciliary ridge complex in frog photoreceptor cells<sup>115,117,148</sup>. Also protocadherin-15 was reported to be located at the apical inner segment membrane<sup>154</sup> and although not mentioned by the authors, cadherin-23 was detected by immuno-electron microscopy in the periciliary region of mouse photoreceptors as well<sup>133</sup>. SANS has been shown to be already present at the apical tip of the neuroblast layer during development (P0 and P7) suggesting that the function of SANS is not limited to a role in photoreceptor functioning and/or maintenance<sup>134</sup>.

Fibrous links connect the membrane of the apical inner segment to the membrane of the connecting cilium. GPR98 was found to be essential for the formation of these links because they were absent in *Gpr98*-deficient (*Vlgr1/del7TM*) mice<sup>148</sup>. Since USH2A and whirlin are also present in this apical inner segment the fibrous links are thought to be the analogs of the ankle links in the hair bundle of cochlear hair cells. The fibrous links may be formed by homo- and/or heteromeric binding of the extracellular domains of USH2A and GPR98 which are intracellularly tethered by whirlin. SANS and whirlin directly interact and SANS thereby may provide the molecular link to the microtubule transport machinery<sup>40,47,148</sup>. The fibrous links may function as structural support of the apical inner segment and the connecting cilium<sup>36</sup> and analogous to the function of the links in the hair bundle, they may play a role in development of this region of the photoreceptor although there are no indications for aberrations due to mutations in the USH genes. In addition to the structural role, the proteins may play a role in defining the membranous regions and thereby contribute to the control of vesicle docking and cargo transfer from the inner segment transport system to that of the cilium<sup>148</sup>.



In the basal body, cadherin-23, SANS, USH2A, and whirlin have been detected and these proteins are also present in the accessory centriole<sup>133,148</sup>. By immunostaining, clarin-1 is found at the base of the connecting cilium, probably the basal body<sup>141</sup>. In the connecting cilium, all USH proteins are detected with the exception of harmonin, and clarin-1 only very weakly (Fig. 6B)<sup>133,141,148</sup>. The role of USH proteins in the basal body and connecting cilium remains largely elusive. The presence of USH2A, GPR98, whirlin, and SANS in the connecting cilium is likely to be explained by their role in the formation of the fibrous links<sup>148</sup>. The fact that they are present in the connecting cilium may already explain their association with the transport system. But in addition to that, some of the USH proteins are suggested to be involved in the control of protein transport from the inner segment through the connecting cilium to the outer segment. The motor protein myosin VIIa was the first USH protein found to function in protein transport through the connecting cilium<sup>155,156</sup>. Subfractionation of bovine epithelial tracheal cells also indicates an association of USH proteins with transport vesicles<sup>157</sup>.

## **8. Insights in pathogenesis – animal models**

Our insights in the pathogenesis of Usher syndrome originate from the analysis of animal models, mainly mice with defects in the orthologs of USH genes but also rat, zebrafish and *Drosophila* (Table 1). Only very few studies have been performed on postmortem tissues of humans with Usher syndrome and structural abnormalities of microtubules in the connecting cilium have been described<sup>158,159</sup>. However, these were suggested to be acquired rather than inherited<sup>160</sup> and so far, studies in animal models are not in line with such defects.

### **8.1 Hearing loss: the hair bundle**

In the mouse inner ear, USH proteins have been shown to be either components of the fibrous interstereociliary links and links between stereocilia and the kinocilium or are likely to be involved in the anchoring of these links to the actin core of the stereocilia or kinocilium. Only for clarin-1 such a function has so far not been indicated although the disorganization of outer hair cell stereocilia from P2 onwards in *Clarin-1*<sup>-/-</sup> mice suggests such a role which may also be indirect<sup>143</sup>. Studies in mice and rats with mutations regarded to be severe or null alleles in the orthologs of USH1 genes demonstrate that all USH1 proteins are essential for normal

development of the hair bundle. In these mice and rats stereocilia of both inner and outer hair cells are splayed and their differential growth is disturbed (Fig. 7).

USH subtype	Gene	Protein	Mouse (Rat) models	Other animal models: zebrafish (drosophila)
USH1b	<i>MYO7A</i>	myosin VIIa	<i>Shaker-1</i> , <i>Polka</i> , <i>Myo7a</i> <sup>4626SB</sup> , <i>Myo7a</i> <sup>816SB</sup> , <i>Myo7a</i> <sup>7J</sup> , <i>Myo7a</i> <sup>8J</sup> , and <i>Myo7a</i> <sup>9J</sup> , <i>Myo7a</i> <sup>6J</sup> ( <i>Myo7a</i> <sup>tnd-1Hubr/tnd-1Hubr</sup> )	<i>Mariner (crinkled)</i>
USH1c	<i>USH1C</i>	harmonin	<i>Deaf circler</i> , <i>Deaf circler2</i> Jackson, <i>Ush1c</i> <sup>-/-</sup> , <i>Ush1c</i> <sup>216AA</sup>	(CG5921)*
USH1d	<i>CDH23</i>	cadherin-23	<i>Waltzer</i> , <i>Salsa</i> , <i>Erlong</i>	<i>Sputnik (Cad88C)</i> *
USH1f	<i>PCDH15</i>	protocadherin-15	<i>Ames waltzer</i> ( <i>Kyoto circling</i> )	<i>Orbiter</i> <sup>PCDH15a</sup> ( <i>Cad99C</i> )
USH1g	<i>USH1G</i>	SANS	<i>Jackson shaker</i>	( <i>Sans</i> )
USH2a	<i>USH2A</i>	USH2A	<i>Ush2a</i> <sup>-/-</sup>	
USH2c	<i>GPR98</i>	GPR98	<i>USh2c</i> <sup>-/-</sup> , <i>Vlgr1del7TM</i> , <i>Mass1</i> <sup>Frings</sup>	
USH2d	<i>DFNB31</i>	whirlin	<i>Whirler</i> , <i>Whirlin</i> <sup>-/-</sup>	
USH3a	<i>CLRN1</i>	clarin-1	<i>Clarin-1</i> <sup>-/-</sup>	

**Table 1.** Animal models for Usher syndrome. \*These animal models are uncharacterized

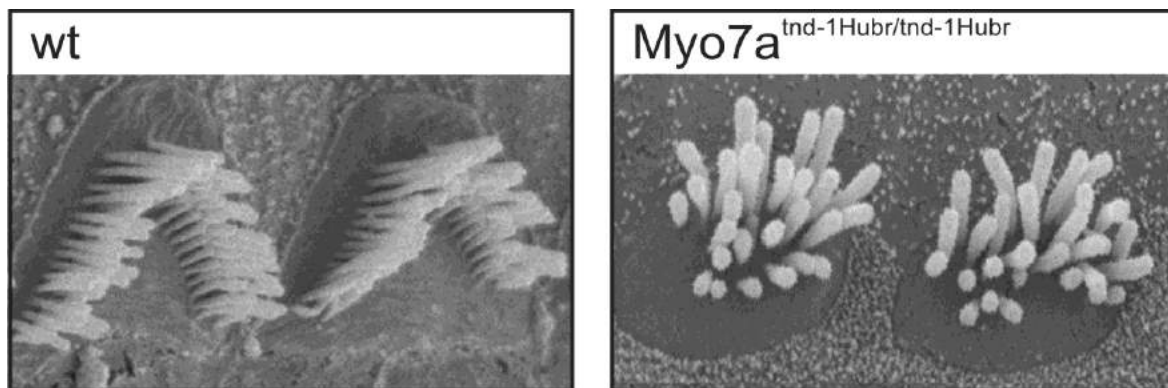


**Figure 7.** Scanning electron microscope images of cochlear outer hair cells of postnatal day 30 (P30) *Myo7a*<sup>tnd-1Hubr/tnd-1Hubr</sup> rats with a nonsense mutation in *Myo7a* display elongated, degenerated, disorganized and fused stereocilia with respect to those of age-matched wild type (wt) animals<sup>161</sup>.

The cohesion in the hair bundle is lost and the kinocilium is displaced which is associated with abnormal orientation of the hair bundle <sup>48</sup>. It has been suggested that tension forces applied to the early lateral links and tip links are essential for the cohesion and orientation of the hair bundle and for stereocilia elongation, respectively, and for hair cell survival. Less severe mutations in USH genes will certainly reveal more distinct effects on hair cell structure and function as is nicely demonstrated by the progressive loss of tip links in the *salsa* mouse with a missense mutation in *Cdh23* predicted to affect  $\text{Ca}^{2+}$  chelation of a cadherin repeat <sup>162</sup>. Development and maintenance of a normal hair bundle and the presence of tip links are essential for mechanotransduction and thus for hearing. Also, myosin VIIa is required for the normal gating of transducer channels <sup>163</sup> and harmonin-b is involved in the process of adaptation <sup>164</sup>.

The hearing loss associated with USH2 is congenital as is that in USH1 but it is less severe and most prominent in the lower frequencies. This is also seen in *Ush2a*<sup>-/-</sup> mice <sup>165</sup> and mice with a targeted deletion of exon 1 of the *Whrn* gene encoding whirlin <sup>166</sup>. Mutations in the 5' part of the *DFNB31/Whrn* gene cause both vision and hearing impairment in humans and mice <sup>25,166</sup>. Mutations in the 3' region of the gene however are associated with more severe deafness in all frequencies but not with retinal degeneration neither in humans nor in *whirler* mice <sup>167,168</sup>. The more severe hearing loss reflects the function of whirlin in the elongation of stereocilia which is severely impaired in *whirler* mice <sup>167,169</sup> and which is mainly attributed to the short isoform of whirlin. The inner hair cell stereocilia in the *Whrn* knockout mice appear normal <sup>166</sup>. USH2A and GPR98 as part of the ankle links are likely to be anchored by whirlin via an interaction with the PDZ domains in the N-terminal region of whirlin. Degeneration of outer hair cells in *Ush2a*<sup>-/-</sup> mice is restricted to the basal part of the cochlea suggesting the importance of USH2A for maintenance of the outer hair cells only in that region of the cochlea. Inner hair cells appear to be normal <sup>165</sup>. In mice with defects in *Gpr98*, inner hair cell abnormalities vary in different mutants but can be milder than those in outer hair cells and less severe at the apex of the cochlea than in the base. This is comparable to what is seen in mice with defects in *Ush2a* <sup>117,170,171</sup>. The hearing loss can be more severe in mice with defects in *Gpr98* than in *Ush2a*<sup>-/-</sup> mice depending on the mutation and thus on the affected isoforms of *Gpr98* and in addition on the genetic background <sup>117,170-172</sup>. This is not apparent yet in humans.

## 8.2 Hearing loss and Retinitis pigmentosa: the synapse

In patients with Usher syndrome, there are no such indications for synaptic dysfunction as in patients with retinopathies specifically affecting the photoreceptor synapses<sup>173</sup>. However, disturbed exocytosis at the synapse has been indicated in hair cells of *dfer* mice<sup>174</sup> which show a normal synaptic ultrastructure in the retina and normal electroretinograms (ERGs)<sup>149</sup>. In zebrafish, downregulation of *Ush2a* and *Gpr98* does not cause pronounced aberrations in photoreceptor morphology but leads to mislocalization of the synaptic proteins GluR2/3 and SV2<sup>175</sup>. Also a decreased b-wave amplitude in ERG recordings in zebrafish after downregulation of *Pcdh15* may suggest disturbed synaptic transmission<sup>176</sup>. Hearing, balance and vision defects are observed in the *Ush1c* zebrafish mutant and after downregulation of *Ush1c*. The mutation or knockdown results in the formation of fewer stereocilia, moreover, these are bent and splayed. The USH proteins Ush2a and Cip98a are mislocalized in the *Ush1c* mutant and morphant, suggesting that Ush1c is required for their correct subcellular localization<sup>177,178</sup>. Photoreceptor ribbon synapses of *Ush1c* mutants and morphants are disorganized and synaptic transmission is disrupted<sup>178</sup>. In *Clrn1*<sup>-/-</sup> mice, signal transduction at the synapses of hair cells may be affected as indicated by prolonged peak latencies in auditory brain stem response measurements<sup>143</sup>.

## 8.3 Retinitis pigmentosa: the photoreceptor cells

The pathogenesis of RP associated with Usher syndrome remains largely elusive. Previously available mice with defects in the orthologs of USH1 genes did not exhibit retinal degeneration. However, mild functional abnormalities in photoreceptor cells and secondary neurons are indicated by reduced ERG amplitudes of both the a- and b-waves in several mutant alleles of *Myo7a*, *Cdh23*, and *Pcdh15*<sup>179-181</sup>. These abnormalities are already present at young age. A reduced b-wave was also seen after downregulation of *Pcdh15b*, the *PCHD15* ortholog expressed in the zebrafish retina and this was an early effect<sup>182</sup>. Very recently, a knock-in mouse for *Ush1c* with a cryptic splice site mutation as found in USH1c patients has been described which demonstrates a progressive loss of photoreceptor cells from 6.5 months onwards. The first ERG measurements at one month of age already demonstrated retinal dysfunction by a reduced amplitude of the a- and b-waves and in addition a faster implicit time was measured<sup>183</sup>. The latter was also indicated for several of the other *Ush1*

mutant mice <sup>180,181</sup> and in patients with USH2 <sup>184</sup>. Further studies on this *Ush1c* knock-in mouse to elucidate more details on structural or functional abnormalities in photoreceptor cells or other retinal cell types will certainly provide more insight into pathogenic mechanisms of retinal degeneration in these mice. The same holds true for the analysis of *Ush2a*<sup>-/-</sup> mice with normal ERG and photoreceptor morphology up to 10 months but with signs of photoreceptor degeneration such as shortening of outer and inner segments of the photoreceptors followed by a gradual thinning of the outer nuclear layer <sup>165</sup>. That photoreceptor cells were under stress was already indicated at 2 months of age by an upregulation of glial fibrillary acidic protein (GFAP) in Müller cells <sup>165</sup>. Mice with a targeted deletion of exon 1 of *Whrn* show reduced ERG amplitudes and outer nuclear layer thickness and shortened photoreceptor outer segments at 28-33 months of age <sup>166</sup>. No significant functional or structural abnormalities were described in mice defective for the longest isoform of Gpr98 and in the *Vlgl1/del7TM* mice. However, retinal function is mildly impaired at the age of 15 months which is significant only for light-adapted cone-only responses <sup>117,171</sup>.

The most prominent localization of USH proteins in photoreceptor cells is in the region of the connecting cilium which suggests a direct or indirect role in the bidirectional transport processes that are taking place in this region. In the inner ear, the fibrous links are essential for development and maintenance of the hair bundle and for mechanotransduction. The fibrous links that connect the membranes of the apical inner segment and the connecting cilium are not essential for normal development of the photoreceptor outer segments and also not for maintenance of photoreceptor cells in mice as is indicated by the *Gpr98* defective mice which lack these links. They are suggested to provide structural support and thereby may be important for long term maintenance of the photoreceptor cells in humans and possibly also zebrafish as suggested by increased TUNEL labeling (terminal deoxynucleotidyl transferase dUTP nick end labeling) in the retina in the first week of development after injection of *Ush2a* and *Ush2c* morpholinos <sup>175</sup>. A contribution to transport in this region by targeting post-Golgi vesicles to the periciliary membrane may in particular be the case for SANS that is indicated to associate with microtubules <sup>148</sup> and as such may cooperate with the IFT20 and IFT52 which are found to be associated with transport vesicles in this region <sup>102</sup>. Therefore, a more detailed analysis, both at the electron microscopic and the biochemical level especially in the *Jackson shaker* mice might provide further clues on this role in

transport and/or vesicle docking. Myosin VIIa is indicated to participate in transport through the connecting cilium by using actin filaments in the cilium. One of the molecules that are thought to be transported by myosin VIIa is opsin. In the connecting cilium, myosin VIIa colocalizes with opsin which accumulates in the cilium of *Shaker-1* mice resulting in a retarded renewal of the outer segment discs<sup>155,156</sup>. However, this could also be due to impaired phagocytosis of the outer segment discs by the RPE cells. Myosin VIIa is highly expressed in these cells<sup>140,151</sup> and associated with the motility of melanosomes<sup>152,185</sup> and lysosomes<sup>186</sup> and thereby in phagocytosis of outer segment discs. Defects in renewal of discs in the outer segments or in phagocytosis cause photoreceptor death and progressive retinal degeneration in humans<sup>155,185</sup>.

Besides detailed studies on those mouse models for Usher syndrome that indeed exhibit photoreceptor degeneration, characterization of zebrafish with mutations in USH genes or after knockdown of genes with morpholinos will provide further clues. The zebrafish *mariner* mutant (*Myo7a*) has been reported to exhibit mild abnormalities in the photoreceptor outer segments in transmission electron microscopy and a slight increase in cell death in the outer nuclear layer<sup>187</sup>. In the same mutant Biehlmaier and coworkers showed abnormal pigment migration during light adaptation and they suggested that this may lead to photoreceptor degeneration<sup>188</sup>. The outer segment defects and reduced amplitude of the b-wave as reported for zebrafish with defects in *Pcdh15b* have been ascribed to an impaired adhesive contact between the outer segment of photoreceptor cells and the RPE<sup>182</sup>. Downregulation of *Cip98a* (*whrn*) in zebrafish blocks the light dependent ciliary transport of Opsin in photoreceptors. This knockdown further results in vision, hearing and balance defects<sup>178</sup>. Downregulation of *Clrn1* results in slower optokinetic response and in balance problems<sup>189</sup>. Studies on the Drosophila orthologs of *USH1G*, *MYO7A*, and *PCDH15* indicate a conserved role in the organization of actin filament bundles as present in microvilli and stereocilia<sup>190-192</sup> and for the SANS homolog a role in vesicle transport may be conserved as well<sup>191</sup>. A function of USH proteins in the organization of actin filaments in the photoreceptor cells has not yet been demonstrated although actin filaments are prominently present at the subcellular locations of USH proteins namely at the outer limiting membrane, the periciliary region, the calycal processes, the distal end of the connecting cilium/base of the outer segment and the synapse<sup>104,193,194</sup>.

## 9. The outline of this thesis

Elucidation of the molecular pathogenesis of Usher syndrome and related disorders is essential for the development of safe targeted molecular interventions. The identification of novel members of the USH protein complex, as described in this thesis, and understanding the function of this complex will finally contribute to treatment.

**Chapter 2** reports on the connection of a voltage-gated calcium channel subunit,  $Ca_v1.3$  to the USH protein network via whirlin in photoreceptors. Therefore, we hypothesized that whirlin contributes to the organization of this channel and possibly other channels in the photoreceptor cells, where both proteins may be involved in membrane fusions. **Chapter 3** describes a family with antibiotic induced deafness caused by a homozygous mutation in *EPS8*. The EPS8 protein interacts with whirlin and this binding is reduced by the mutation. The EPS8-whirlin association is biologically relevant as demonstrated by the aberrant localization of EPS8 and whirlin in *whirler* mice and EPS8 knockout mice, respectively. **Chapter 4** reports the link between Usher syndrome and Leber congenital amaurosis by the identification of a novel isoform of the centrosomal ninein-like protein that interacts with both USH2A<sup>isoB</sup> and lebercillin. **Chapter 5** describes the identification of the centrosomal and microtubule-associated protein SPAG5 as an interaction partner of both USH2A<sup>isoB</sup> and NINL<sup>isoB</sup> in photoreceptors cells. It is hypothesized that SPAG5, USH2A<sup>isoB</sup> and NINL<sup>isoB</sup> function in microtubule-based cytoplasmic protein trafficking, ciliary transport and structural maintenance of the cilium. **Chapter 6** reports that two different mutations in *CLRN1*, the gene involved in USH3, cause non-syndromic arRP in two families. The mutated protein is retained in the endoplasmic reticulum, whereas the wild type protein is transported to the plasma membrane. A general discussion and future prospects are given in **Chapter 7**.

## 10. References

1. Marazita ML, Ploughman LM, Rawlings B, et al. Genetic epidemiological studies of early-onset deafness in the U.S. school-age population. *Am J Med Genet.* 1993;46:486-491.
2. Grondahl J. Estimation of prognosis and prevalence of retinitis pigmentosa and Usher syndrome in Norway. *Clin Genet.* 1987;31:255-264.
3. Hope CI, Bunday S, Proops D, et al. Usher syndrome in the city of Birmingham--prevalence and clinical classification. *Br J Ophthalmol.* 1997;81:46-53.
4. Nuutila A. Dystrophia retinae pigmentosa--dysacusis syndrome (DRD): a study of the Usher- or Hallgren syndrome. *J Genet Hum.* 1970;18:57-88.
5. Rosenberg T, Haim M, Hauch AM, et al. The prevalence of Usher syndrome and other retinal dystrophy-hearing impairment associations. *Clin Genet.* 1997;51:314-321.
6. Spandau UH, Rohrschneider K. Prevalence and geographical distribution of Usher syndrome in Germany. *Graefes Arch Clin Exp Ophthalmol.* 2002;240:495-498.
7. Rual JF, Venkatesan K, Hao T, et al. Towards a proteome-scale map of the human protein-protein interaction network. *Nature.* 2005;437:1173-1178.
8. Stelzl U, Worm U, Lalowski M, et al. A human protein-protein interaction network: a resource for annotating the proteome. *Cell.* 2005;122:957-968.
9. Prasad TS, Kandasamy K, Pandey A. Human Protein Reference Database and Human Proteinpedia as discovery tools for systems biology. *Methods Mol Biol.* 2009;577:67-79.
10. Goh KI, Cusick ME, Valle D, et al. The human disease network. *Proc Natl Acad Sci U S A.* 2007;104:8685-8690.
11. Oti M, Brunner HG. The modular nature of genetic diseases. *Clin Genet.* 2007;71:1-11.
12. Von Graefe A. Exceptionelles Verhalten des Gesichtsfeldes bei Pigmententartung der Netzhaut. *Archiv für Ophthalmologie.* 1858;4:250-253.
13. Usher CH. Bowman Lecture: On a few hereditary eye affections. *Trans Ophthalmol Soc UK.* 1935;164-245.
14. Pagon RA. Retinitis pigmentosa. *Surv Ophthalmol.* 1988;33:137-177.
15. Bell J. Retinitis pigmentosa and allied diseases. In: Pearson K (ed), *The Treasury of Human Inheritance.* London Cambridge Press. 1922;1-29.
16. Smith RJ, Berlin CI, Hejtmancik JF, et al. Clinical diagnosis of the Usher syndromes. Usher Syndrome Consortium. *Am J Med Genet.* 1994;50:32-38.
17. Ahmed ZM, Riazuddin S, Bernstein SL, et al. Mutations of the protocadherin gene PCDH15 cause Usher syndrome type 1F. *Am J Hum Genet.* 2001;69:25-34.
18. Bolz H, von Brederlow B, Ramirez A, et al. Mutation of CDH23, encoding a new member of the cadherin gene family, causes Usher syndrome type 1D. *Nat Genet.* 2001;27:108-112.



19. Verpy E, Leibovici M, Zwaenepoel I, et al. A defect in harmonin, a PDZ domain-containing protein expressed in the inner ear sensory hair cells, underlies Usher syndrome type 1C. *Nat Genet.* 2000;26:51-55.
20. Weil D, Blanchard S, Kaplan J, et al. Defective myosin VIIA gene responsible for Usher syndrome type 1B. *Nature.* 1995;374:60-61.
21. Weil D, El Amraoui A, Masmoudi S, et al. Usher syndrome type I G (USH1G) is caused by mutations in the gene encoding SANS, a protein that associates with the USH1C protein, harmonin. *Hum Mol Genet.* 2003;12:463-471.
22. Ahmed Z, Riazuddin S, Khan S, et al. USH1H, a novel locus for type I Usher syndrome, maps to chromosome 15q22-23. *Clin Genet.* 2008;75:86-91
23. Chaib H, Kaplan J, Gerber S, et al. A newly identified locus for Usher syndrome type I, USH1E, maps to chromosome 21q21. *Hum Mol Genet.* 1997;6:27-31.
24. Pennings RJ, Huygen PL, Cremers WR. Hearing impairment in Usher syndrome type II. *Ann Otol Rhinol Laryngol.* 2003;112:825
25. Ebermann I, Scholl HP, Charbel IP, et al. A novel gene for Usher syndrome type 2: mutations in the long isoform of whirlin are associated with retinitis pigmentosa and sensorineural hearing loss. *Hum Genet.* 2007;121:203-211.
26. Eudy JD, Weston MD, Yao S, et al. Mutation of a gene encoding a protein with extracellular matrix motifs in Usher syndrome type IIa. *Science.* 1998;280:1753-1757.
27. Weston MD, Luijendijk MW, Humphrey KD, et al. Mutations in the VLGR1 gene implicate G-protein signaling in the pathogenesis of Usher syndrome type II. *Am J Hum Genet.* 2004;74:357-366.
28. Ben-Rebeh, I, Benzina Z, Dhoub H, et al. Identification of candidate regions for a novel Usher syndrome type II locus. *Mol Vis.* 2008;14:1719-1726.
29. Joensuu T, Hamalainen R, Yuan B, et al. Mutations in a novel gene with transmembrane domains underlie Usher syndrome type 3. *Am J Hum Genet.* 2001;69:673-684.
30. Kalay E, de Brouwer AP, Caylan R, et al. A novel D458V mutation in the SANS PDZ binding motif causes atypical Usher syndrome. *J Mol Med.* 2005;83:1025-1032.
31. Liu X, Ondek B, Williams DS. Mutant myosin VIIa causes defective melanosome distribution in the RPE of shaker-1 mice. *Nat Genet.* 1998;19:117-118.
32. Bashir R, Fatima A, Naz S. A frameshift mutation in SANS results in atypical Usher syndrome. *Clin Genet.* 2010;78:601-603.
33. Cohen M, Bitner-Glindzicz M, Luxon L. The changing face of Usher syndrome: clinical implications. *Int J Audiol.* 2007;46:82-93.
34. Brown SD, Hardisty-Hughes RE, Mburu P. Quiet as a mouse: dissecting the molecular and genetic basis of hearing. *Nat Rev Genet.* 2008;9:277-290.
35. El Amraoui A, Petit C. Usher I syndrome: unravelling the mechanisms that underlie the cohesion of the growing hair bundle in inner ear sensory cells. *J Cell Sci.* 2005;118:4593-4603.

36. Kremer H, van Wijk E, Marker T, et al. Usher syndrome: molecular links of pathogenesis, proteins and pathways. *Hum Mol Genet.* 2006;15:262-270.
37. Reiners J, Nagel-Wolfrum K, Jurgens K, et al. Molecular basis of human Usher syndrome: deciphering the meshes of the Usher protein network provides insights into the pathomechanisms of the Usher disease. *Exp Eye Res.* 2006;83:97-119.
38. Vastinsalo H, Jalkanen R, Dinculescu A, et al. Alternative splice variants of the USH3A gene Clarin 1 (CLRN1). *Eur J Hum Genet.* 2010.
39. Ahmed ZM, Goodyear R, Riazuddin S, et al. The tip-link antigen, a protein associated with the transduction complex of sensory hair cells, is protocadherin-15. *J Neurosci.* 2006;26:7022-7034.
40. Adato A, Michel V, Kikkawa Y, et al. Interactions in the network of Usher syndrome type 1 proteins. *Hum Mol Genet.* 2005;14:347-356.
41. Tian G, Zhou Y, Hajkova D, et al. Clarin-1, encoded by the Usher Syndrome III causative gene, forms a membranous microdomain: possible role of clarin-1 in organizing the actin cytoskeleton. *J Biol Chem.* 2009;284:18980-18993.
42. Cosgrove DE, Bhattacharya G, Meehan D et al. Usherin binds integrins on RPE cells and may mediate adhesion and cellular homeostasis. *Invest Ophthalmol Vis Sci.* 2004;abstract 2483.
43. Adato A, Lefevre G, Delprat B, et al. Usherin, the defective protein in Usher syndrome type IIA, is likely to be a component of interstereocilia ankle links in the inner ear sensory cells. *Hum Mol Genet.* 2005;14:3921-3932.
44. Boeda B, El Amraoui A, Bahloul A, et al. Myosin VIIa, harmonin and cadherin 23, three Usher I gene products that cooperate to shape the sensory hair cell bundle. *EMBO J.* 2002;21:6689-6699.
45. Michalski N, Michel V, Bahloul A, et al. Molecular characterization of the ankle-link complex in cochlear hair cells and its role in the hair bundle functioning. *J Neurosci.* 2007;27:6478-6488.
46. Reiners J, van Wijk E, Maerker T, et al. Scaffold protein harmonin (USH1C) provides molecular links between Usher syndrome type 1 and type 2. *Hum Mol Genet.* 2005;14:3933-3943.
47. van Wijk E, van der Zwaag B, Peters TA, et al. The DFNB31 gene product whirlin connects to the Usher protein network in the cochlea and retina by direct association with USH2A and VLGR1. *Hum Mol Genet.* 2006;15:751-765.
48. Lefevre G, Michel V, Weil D, et al. A core cochlear phenotype in USH1 mouse mutants implicates fibrous links of the hair bundle in its cohesion, orientation and differential growth. *Development.* 2008;135:1427-1437.
49. Cutnell JD, Johnson KW. *Physics.* New York Wiley. 1998
50. Dror AA, Avraham KB. Hearing loss: mechanisms revealed by genetics and cell biology. *Annu Rev Genet.* 2009;43:411-437.
51. Raphael Y, Altschuler RA. Structure and innervation of the cochlea. *Brain Res Bull.* 2003;60:397-422.
52. Hudspeth AJ. How hearing happens. *Neuron.* 1997;19:947-950.
53. He DZ, Jia S, Dallos P. Mechano-electrical transduction of adult outer hair cells studied in a gerbil hemicochlea. *Nature.* 2004;429:766-770.

54. Muller M. Frequency representation in the rat cochlea. *Hear Res.* 1991;51:247-254.
55. Rabbitt RD, Breneman KD, King C, et al. Dynamic displacement of normal and detached semicircular canal cupula. *J Assoc Res Otolaryngol.* 2009;10:497-509.
56. Rusch A, Thurm U. Cupula displacement, hair bundle deflection, and physiological responses in the transparent semicircular canal of young eel. *Pflugers Arch.* 1989;413:533-545.
57. Highstein SM, Fay RR, Popper AN. *The vestibular system.* Springer-verlag. 2004
58. Cullen K and Sadeghi S. Vestibular system. *Scholarpedia.* 2008;3:3013
59. Cassin B, Solomon SA, Rubin ML. *Dictionary of Eye Terminology.* Triad publishing company. 1990.
60. vis-Silberman N, shery-Padan R. Iris development in vertebrates; genetic and molecular considerations. *Brain Res.* 2008;1192:17-28.
61. Wielgus AR, Sarna T. Melanin in human irides of different color and age of donors. *Pigment Cell Res.* 2005;18:454-464.
62. Saornil MA. Iris colour and uveal melanoma. *Can J Ophthalmol.* 2004;39:448-452.
63. Rada JA, Shelton S, Norton TT. The sclera and myopia. *Exp Eye Res.* 2006;82:185-200.
64. Hayreh SS. Segmental nature of the choroidal vasculature. *Br J Ophthalmol.* 1975;59:631-648.
65. Rodieck RW. *First steps in seeing.* Sinauer Associates. 1998.
66. Sarthy V, Ripps H. *The Retinal Muller Cell: Structure and Function.* Plenum Publishing Co. 2001.
67. Newman E, Reichenbach A. The Muller cell: a functional element of the retina. *Trends Neurosci.* 1996;19:307-312.
68. Bringmann A, Pannicke T, Grosche J, et al. Muller cells in the healthy and diseased retina. *Prog Retin Eye Res.* 2006;25:397-424.
69. Tsacopoulos M, Magistretti PJ. Metabolic coupling between glia and neurons. *J Neurosci.* 1996;16:877-885.
70. Hao W, Fong HK. Blue and ultraviolet light-absorbing opsin from the retinal pigment epithelium. *Biochemistry.* 1996;35:6251-6256.
71. Curcio CA, Sloan KR, Kalina RE, et al. Human photoreceptor topography. *J Comp Neurol.* 1990;292:497-523.
72. Kandel ER, Schwartz JH, Jessell TM. *Principles of Neural Science.* In. 4th ed ed.: McGraw-Hill, New York; 2000:507-513.
73. Daiger SD, Sullivan SL, Bowne SJ. Retinal Information Network: <http://www.sph.uth.tmc.edu/Retnet>.
74. Adams NA, Awadein A, Toma HS. The retinal ciliopathies. *Ophthalmic Genet.* 2007;28:113-125.
75. Pazour GJ, Witman GB. The vertebrate primary cilium is a sensory organelle. *Curr Opin Cell Biol.* 2003;15:105-110.
76. Christensen ST, Pedersen LB, Schneider L, et al. Sensory cilia and integration of signal transduction in human health and disease. *Traffic.* 2007;8:97-109.
77. Singla V, Reiter JF. The primary cilium as the cell's antenna: signaling at a sensory organelle. *Science.* 2006;313:629-633.

78. Dutcher SK. Dissecting of basal body and centriole function in unicellular green alga *Chlamydomonas reinhardtii*. In: Nigg EA (ed), *Centrosomes in Development and Disease*. Wiley-VCH Weinheim Germany. 2004.
79. Bornens M. Organelle positioning and cell polarity. *Nat Rev Mol Cell Biol*. 2008;9:874-886.
80. Hagiwara H, Aoki T, Ohwada N, et al. Development of striated rootlets during ciliogenesis in the human oviduct epithelium. *Cell Tissue Res*. 1997;290:39-42.
81. Hagiwara H, Ohwada N, Aoki T, et al. Ciliogenesis and ciliary abnormalities. *Med Electron Microsc*. 2000;33:109-114.
82. Yang J, Gao J, Adamian M, et al. The ciliary rootlet maintains long-term stability of sensory cilia. *Mol Cell Biol*. 2005;25:4129-4137.
83. Rohlich P. The sensory cilium of retinal rods is analogous to the transitional zone of motile cilia. *Cell Tissue Res*. 1975;161:421-430.
84. Smith EF, Yang P. The radial spokes and central apparatus: mechano-chemical transducers that regulate flagellar motility. *Cell Motil Cytoskeleton*. 2004;57:8-17.
85. Yang P, Diener DR, Yang C, et al. Radial spoke proteins of *Chlamydomonas* flagella. *J Cell Sci*. 2006;119:1165-1174.
86. Berbari NF, O'Connor AK, Haycraft CJ, et al. The primary cilium as a complex signaling center. *Curr Biol*. 2009;19:526-535.
87. Dabdoub A, Kelley MW. Planar cell polarity and a potential role for a Wnt morphogen gradient in stereociliary bundle orientation in the mammalian inner ear. *J Neurobiol*. 2005;64:446-457.
88. Nonaka S, Tanaka Y, Okada Y, et al. Randomization of left-right asymmetry due to loss of nodal cilia generating leftward flow of extraembryonic fluid in mice lacking KIF3B motor protein. *Cell*. 1998;95:829-837.
89. Liu Q, Tan G, Levenkova N, et al. The proteome of the mouse photoreceptor sensory cilium complex. *Mol Cell Proteomics*. 2007;6:1299-1317.
90. Roepman R, Wolfrum U. Protein networks and complexes in photoreceptor cilia. *Subcell Biochem*. 2007;43:209-235.
91. Satir P, Christensen ST. Overview of structure and function of mammalian cilia. *Annu Rev Physiol*. 2007;69:377-400.
92. Graser S, Stierhof YD, Lavoie SB, et al. Cep164, a novel centriole appendage protein required for primary cilium formation. *J Cell Biol*. 2007;179:321-330.
93. Marshall WF. Basal bodies platforms for building cilia. *curr top dev biol*. 2008;85:1-22.
94. Rosenbaum JL, Witman GB. Intraflagellar transport. *Nat Rev Mol Cell Biol*. 2002;3:813-825.
95. Pedersen LB, Veland IR, Schroder JM, et al. Assembly of primary cilia. *Dev Dyn*. 2008;237:1993-2006.
96. Orozco JT, Wedaman KP, Signor D, et al. Movement of motor and cargo along cilia. *Nature*. 1999;398:674.
97. Scholey JM. Kinesin-II, a membrane traffic motor in axons, axonemes, and spindles. *J Cell Biol*. 1996;133:1-4.

98. Signor D, Wedaman KP, Orozco JT, et al. Role of a class DHC1b dynein in retrograde transport of IFT motors and IFT raft particles along cilia, but not dendrites, in chemosensory neurons of living *Caenorhabditis elegans*. *J Cell Biol.* 1999;147:519-530.
99. Young RW. Visual cells and the concept of renewal. *Invest Ophthalmol Vis Sci.* 1976;15.
100. Sedmak T, Wolfrum U. Intraflagellar transport molecules in ciliary and nonciliary cells of the retina. *J Cell Biol.* 2010;189:171-186.
101. Pazour GJ, Baker SA, Deane JA, et al. The intraflagellar transport protein, IFT88, is essential for vertebrate photoreceptor assembly and maintenance. *J Cell Biol.* 2002;157:103-113.
102. Krock BL, Perkins BD. The intraflagellar transport protein IFT57 is required for cilia maintenance and regulates IFT-particle-kinesin-II dissociation in vertebrate photoreceptors. *J Cell Sci.* 2008;121:1907-1915.
103. Sterling P, Matthews G. Structure and function of ribbon synapses. *Trends Neurosci.* 2005;28:20-29.
104. Chaitin MH, Schneider BG, Hall MO, et al. Actin in the photoreceptor connecting cilium: immunocytochemical localization to the site of outer segment disk formation. *J Cell Biol.* 1984;99:239-247.
105. Nagle BW, Okamoto C, Taggart B, et al. The teleost cone cytoskeleton. Localization of actin, microtubules, and intermediate filaments. *Invest Ophthalmol Vis Sci.* 1986;27:689-701.
106. Chen L, Chetkovich DM, Petralia RS, et al. Stargazin regulates synaptic targeting of AMPA receptors by two distinct mechanisms. *Nature.* 2000;408:936-943.
107. Lim DJ, Anniko M. Developmental morphology of the mouse inner ear. A scanning electron microscopic observation. *Acta Otolaryngol Suppl.* 1985;422:1-69.
108. Sher AE. The embryonic and postnatal development of the inner ear of the mouse. *Acta Otolaryngol Suppl.* 1971;285:1-77.
109. Bartolami S, Goodyear R, Richardson G. Appearance and distribution of the 275 kD hair-cell antigen during development of the avian inner ear. *J Comp Neurol.* 1991;314:777-788.
110. Goodyear RJ, Richardson GP. A novel antigen sensitive to calcium chelation that is associated with the tip links and kinociliary links of sensory hair bundles. *J Neurosci.* 2003;23:4878-4887.
111. Goodyear RJ, Marcotti W, Kros CJ, et al. Development and properties of stereociliary link types in hair cells of the mouse cochlea. *J Comp Neurol.* 2005;485:75-85.
112. Belyantseva IA, Boger ET, Naz S, et al. Myosin-XVa is required for tip localization of whirlin and differential elongation of hair-cell stereocilia. *Nat Cell Biol.* 2005;7:148-156.
113. Stepanyan R, Belyantseva IA, Griffith AJ, et al. Auditory mechanotransduction in the absence of functional myosin-XVa. *J Physiol.* 2006;576:801-808.
114. Rzadzinska AK, Nevalainen EM, Prosser HM, et al. MyosinVIIa interacts with Twinfilin-2 at the tips of mechanosensory stereocilia in the inner ear. *PLoS One.* 2009;4:e7097.
115. Goodyear R, Richardson G. The ankle-link antigen: an epitope sensitive to calcium chelation associated with the hair-cell surface and the calycal processes of photoreceptors. *J Neurosci.* 1999;19:3761-3772.

116. Kussel-Andermann P, El-Amraoui A, Safieddine S, et al. Vezatin, a novel transmembrane protein, bridges myosin VIIA to the cadherin-catenins complex. *EMBO J.* 2000;19:6020-6029.
117. McGee J, Goodyear RJ, McMillan DR, et al. The very large G-protein-coupled receptor VLGR1: a component of the ankle link complex required for the normal development of auditory hair bundles. *J Neurosci.* 2006;26:6543-6553.
118. Senften M, Schwander M, Kazmierczak P, et al. Physical and functional interaction between protocadherin 15 and myosin VIIa in mechanosensory hair cells. *J Neurosci.* 2006;26:2060-2071.
119. Goodyear R, Richardson G. Distribution of the 275 kD hair cell antigen and cell surface specialisations on auditory and vestibular hair bundles in the chicken inner ear. *J Comp Neurol.* 1992;325:243-256.
120. Zallocchi M, Meehan DT, Delimont D, et al. Localization and expression of clarin-1, the Cln1 gene product, in auditory hair cells and photoreceptors. *Hear Res.* 2009;255:109-120.
121. Verpy E, Weil D, Leibovici M, et al. Stereocilin-deficient mice reveal the origin of cochlear waveform distortions. *Nature.* 2008;456:255-258.
122. Zine A, Romand R. Development of the auditory receptors of the rat: a SEM study. *Brain Res.* 1996;721:49-58.
123. Tsuprun V, Goodyear RJ, Richardson GP. The structure of tip links and kinocilial links in avian sensory hair bundles. *Biophys J.* 2004;87:4106-4112.
124. Siemens J, Lillo C, Dumont RA, et al. Cadherin 23 is a component of the tip link in hair-cell stereocilia. *Nature.* 2004;428:950-955.
125. Kazmierczak P, Sakaguchi H, Tokita J, et al. Cadherin 23 and protocadherin 15 interact to form tip-link filaments in sensory hair cells. *Nature.* 2007;449:87-91.
126. Rzadzinska AK, Steel KP. Presence of interstereocilial links in waltzer mutants suggests Cdh23 is not essential for tip link formation. *Neuroscience.* 2009;158:365-368.
127. Grillet N, Xiong W, Reynolds A, et al. Harmonin mutations cause mechanotransduction defects in cochlear hair cells. *Neuron.* 2009;62:375-387.
128. Caberlotto E, Foucher I, Michel V et al. Mechano-electrical transduction current characteristics and morphogenetic phenotype in USH1 mouse mutants. *Molecular Biology of Hearing and Deafness.* 2009;abstract 111.
129. Beurg M, Fettiplace R, Nam JH, et al. Localization of inner hair cell mechanotransducer channels using high-speed calcium imaging. *Nat Neurosci.* 2009;12:553-558.
130. Xu Z, Peng AW, Oshima K, et al. MAGI-1, a candidate stereociliary scaffolding protein, associates with the tip-link component cadherin 23. *J Neurosci.* 2008;28:11269-11276.
131. Alagramam KN, Murcia CL, Kwon HY, et al. The mouse Ames waltzer hearing-loss mutant is caused by mutation of Pcdh15, a novel protocadherin gene. *Nat Genet.* 2001;27:99-102.
132. El Amraoui A, Sahly I, Picaud S, et al. Human Usher 1B/mouse shaker-1: the retinal phenotype discrepancy explained by the presence/absence of myosin VIIA in the photoreceptor cells. *Hum Mol Genet.* 1996;5:1171-1178.

133. Lagziel A, Overlack N, Bernstein SL, et al. Expression of cadherin 23 isoforms is not conserved: implications for a mouse model of Usher syndrome type 1D. *Mol Vis.* 2009;15:1843-1857.
134. Overlack N, Maerker T, Latz M, et al. SANS (USH1G) expression in developing and mature mammalian retina. *Vision Res.* 2008;48:400-412.
135. Reiners J, Reidel B, El Amraoui A, et al. Differential distribution of harmonin isoforms and their possible role in Usher-1 protein complexes in mammalian photoreceptor cells. *Invest Ophthalmol Vis Sci.* 2003;44:5006-5015.
136. Reiners J, Marker T, Jurgens K, et al. Photoreceptor expression of the Usher syndrome type 1 protein protocadherin 15 (USH1F) and its interaction with the scaffold protein harmonin (USH1C). *Mol Vis.* 2005;11:347-355.
137. Zallocchi M, Sisson JH, Cosgrove D. Biochemical characterization of native Usher protein complexes from a vesicular subfraction of tracheal epithelial cells. *Biochemistry.* 2010;49:1236-1247.
138. Cosgrove D, Zallocchi M. Clarin-1 protein expression in photoreceptors. *Hear Res.* 2010;259:117.
139. Williams DS. Usher syndrome: animal models, retinal function of Usher proteins, and prospects for gene therapy. *Vision Res.* 2008;48:433-441.
140. Hasson T, Heintzelman MB, Santos-Sacchi J, et al. Expression in cochlea and retina of myosin VIIa, the gene product defective in Usher syndrome type 1B. *Proc Natl Acad Sci U S A.* 1995;92:9815-9819.
141. Zallocchi M, Meehan DT, Delimont D, et al. Localization and expression of clarin-1, the *Clrn1* gene product, in auditory hair cells and photoreceptors. *Hear Res.* 2009;255:109-120.
142. Bok D, Galbraith G, Lopez I, et al. Blindness and auditory impairment caused by loss of the sodium bicarbonate cotransporter NBC3. *Nat Genet.* 2003;34:313-319.
143. Geng R, Geller SF, Hayashi T, et al. Usher syndrome IIIA gene clarin-1 is essential for hair cell function and associated neural activation. *Hum Mol Genet.* 2009;18:2748-2760.
144. Adato A, Vreugde S, Joensuu T, et al. USH3A transcripts encode clarin-1, a four-transmembrane-domain protein with a possible role in sensory synapses. *Eur J Hum Genet.* 2002;10:339-350.
145. Geller SF, Guerin KI, Visel M, et al. CLRN1 is nonessential in the mouse retina but is required for cochlear hair cell development. *PLoS Genet.* 2009;5:e1000607.
146. Gosens I, van Wijk E, Kersten FFJ, et al. MPP1 links the Usher protein network and the Crumbs protein complex in the retina. *Hum Mol Genet.* 2007;16:1993-2003.
147. Lillo C, Siemens J, Kazmierczak P, et al. Roles and interactions of three USH1 proteins in the retina and inner ear. *Invest Ophthalmol Vis Sci.* 2005;abstract 5176.
148. Maerker T, van Wijk E, Overlack N, et al. A novel Usher protein network at the periciliary reloading point between molecular transport machineries in vertebrate photoreceptor cells. *Hum Mol Genet.* 2008;17:71-86.
149. Williams DS, Aleman TS, Lillo C, et al. Harmonin in the murine retina and the retinal phenotypes of *Ush1c*-mutant mice and human USH1C. *Invest Ophthalmol Vis Sci.* 2009;50:3881-3889.
150. Gibbs D, Azarian SM, Lillo C, et al. Role of myosin VIIa and Rab27a in the motility and localization of RPE melanosomes. *J Cell Sci.* 2004;117:6473-6483.

151. Wolfrum U, Liu X, Schmitt A, et al. Myosin VIIa as a common component of cilia and microvilli. *Cell Motil Cytoskeleton*. 1998;40:261-271.
152. Gibbs D, Kitamoto J, Williams DS. Abnormal phagocytosis by retinal pigmented epithelium that lacks myosin VIIa, the Usher syndrome 1B protein. *Proc Natl Acad Sci U S A*. 2003;100:6481-6486.
153. Petit C. Usher syndrome: from genetics to pathogenesis. *Annu Rev Genomics Hum Genet*. 2001;2:271-297.
154. Sun X, Pawlyk B, Adamian M, et al. Functional and structural deficits of cone photoreceptors in mice lacking PCDH15, a protein encoded by the Ush1F gene. *Invest Ophthalmol Vis Sci*. 2006;abstract 5770.
155. Liu X, Udovichenko IP, Brown SD, et al. Myosin VIIa participates in opsin transport through the photoreceptor cilium. *J Neurosci*. 1999;19:6267-6274.
156. Wolfrum U, Schmitt A. Rhodopsin transport in the membrane of the connecting cilium of mammalian photoreceptor cells. *Cell Motil Cytoskeleton*. 2000;46:95-107.
157. Zallocchi M, Sisson JH, Cosgrove D. Biochemical characterization of native Usher protein complexes from a vesicular subfraction of tracheal epithelial cells. *Biochemistry*. 2010;49:1236-1247.
158. Barrong SD, Chaitin MH, Fliesler SJ, et al. Ultrastructure of connecting cilia in different forms of retinitis pigmentosa. *Arch Ophthalmol*. 1992;110:706-710.
159. Hunter DG, Fishman GA, Mehta RS, et al. Abnormal sperm and photoreceptor axonemes in Usher's syndrome. *Arch Ophthalmol*. 1986;104:385-389.
160. Szczeny PJ. Retinitis pigmentosa and the question of photoreceptor connecting cilium defects. *Graefes Arch Clin Exp Ophthalmol*. 1995;233:275-283.
161. Smits BM, Peters TA, Mul JD, et al. Identification of a rat model for usher syndrome type 1B by N-ethyl-N-nitrosourea mutagenesis-driven forward genetics. *Genetics*. 2005;170:1887-1896.
162. Schwander M, Xiong W, Tokita J, et al. A mouse model for nonsyndromic deafness (DFNB12) links hearing loss to defects in tip links of mechanosensory hair cells. *Proc Natl Acad Sci U S A*. 2009;106:5252-5257.
163. Kros CJ, Marcotti W, van Netten SM, et al. Reduced climbing and increased slipping adaptation in cochlear hair cells of mice with Myo7a mutations. *Nat Neurosci*. 2002;5:41-47.
164. Michalski N, Michel V, Caberlotto E, et al. Harmonin-b, an actin-binding scaffold protein, is involved in the adaptation of mechano-electrical transduction by sensory hair cells. *Pflugers Arch*. 2009;459:115-130.
165. Liu X, Bulgakov OV, Darrow KN, et al. Usherin is required for maintenance of retinal photoreceptors and normal development of cochlear hair cells. *Proc Natl Acad Sci U S A*. 2007;104:4413-4418.
166. Yang J, Liu X, Zhao Y, et al. Ablation of whirlin long isoform disrupts the USH2 protein complex and causes vision and hearing loss. *PLoS Genet*. 2010;6:e1000955.
167. Mburu P, Mustapha M, Varela A, et al. Defects in whirlin, a PDZ domain molecule involved in stereocilia elongation, cause deafness in the whirler mouse and families with DFNB31. *Nat Genet*. 2003;34:421-428.



168. Tlili A, Charfedine I, Lahmar I, et al. Identification of a novel frameshift mutation in the DFNB31/WHRN gene in a Tunisian consanguineous family with hereditary non-syndromic recessive hearing loss. *Hum Mutat.* 2005;25:503.
169. Holme RH, Kiernan BW, Brown SD, et al. Elongation of hair cell stereocilia is defective in the mouse mutant whirler. *J Comp Neurol.* 2002;450:94-102.
170. Johnson KR, Zheng QY, Weston MD, et al. The Mass1frings mutation underlies early onset hearing impairment in BUB/BnJ mice, a model for the auditory pathology of Usher syndrome IIC. *Genomics.* 2005;85:582-590.
171. Yagi H, Tokano H, Maeda M, et al. Vlgr1 is required for proper stereocilia maturation of cochlear hair cells. *Genes Cells.* 2007;12:235-250.
172. Yagi H, Takamura Y, Yoneda T, et al. Vlgr1 knockout mice show audiogenic seizure susceptibility. *J Neurochem.* 2005;92:191-202.
173. Jacobson SG, Cideciyan AV, Aleman TS, et al. Usher syndromes due to MYO7A, PCDH15, USH2A or GPR98 mutations share retinal disease mechanism. *Hum Mol Genet.* 2008;17:2405-2415.
174. Gregory F, Couchoux H, Pangrsic T, et al. A presynaptic role for harmonin in regulating Cav1.3 channels in mouse inner hair cells. *ARO 2010 abstract*;587.
175. Phillips JB, Easley CN, Chiem JL, et al. Zebrafish Usher genes are necessary for retinal cell function and survival. *International symposium on Usher syndrome and related disorder 2006 abstract.*
176. Westerfield M. Zebrafish models of Usher syndrome reveal early developmental defects. *International symposium on Usher syndrome and related disorder 2006 abstract.*
177. Blanco B, Philips JB, Wegner J, et al. The role of USH1C during hair bundle development in the zebrafish. *International symposium on Usher syndrome and related disorder 2010 abstract 10.*
178. Philips JB, Blanco B, Toro S, et al. Usher scaffold proteins provide complementary functions in retina and inner ear. *International symposium on Usher syndrome and related disorder 2010 abstract.*
179. Haywood-Watson RJ, Ahmed ZM, Kjellstrom S, et al. Ames Waltzer deaf mice have reduced electroretinogram amplitudes and complex alternative splicing of Pcdh15 transcripts. *Invest Ophthalmol Vis Sci.* 2006;47:3074-3084.
180. Libby RT, Steel KP. Electroretinographic anomalies in mice with mutations in Myo7a, the gene involved in human Usher syndrome type 1B. *Invest Ophthalmol Vis Sci.* 2001;42:770-778.
181. Libby RT, Kitamoto J, Holme RH, et al. Cdh23 mutations in the mouse are associated with retinal dysfunction but not retinal degeneration. *Exp Eye Res.* 2003;77:731-739.
182. Seiler C, Finger-Baier KC, Rinner O, et al. Duplicated genes with split functions: independent roles of protocadherin15 orthologues in zebrafish hearing and vision. *Development.* 2005;132:615-623.
183. Lentz JJ, Gordon WC, Farris HE, et al. Deafness and retinal degeneration in a novel USH1C knock-in mouse model. *Dev Neurobiol.* 2010;70:253-267.
184. Seeliger MW, Zrenner E, pfelstedt-Sylla E, et al. Identification of Usher syndrome subtypes by ERG implicit time. *Invest Ophthalmol Vis Sci.* 2001;42:3066-3071.

185. Schwander M, Lopes V, Sczaniecka A, et al. A novel allele of myosin VIIa reveals a critical function for the C-terminal FERM domain for melanosome transport in retinal pigment epithelial cells. *J Neurosci.* 2009;29:15810-15818.
186. Soni LE, Warren CM, Bucci C, et al. The unconventional myosin-VIIa associates with lysosomes. *Cell Motil Cytoskeleton.* 2005;62:13-26.
187. Perkins BD, Matsui JI, Murphy MK, et al. Histological and physiological abnormalities in myosin VIIA mutant zebrafish. *Invest Ophthalmol Vis Sci.* 2004;abstract 3591.
188. Biehlmaier O, Hodel C, Neuhauss SC. The visual mutant zebrafish Mariner: A model system for human Usher syndrome 1B. *Invest Ophthalmol Vis Sci.* 2005;abstract 1673.
189. Västinsalo H, Philips JB, Sankila, J, et al. Expression of the Usher syndrome type3 gene (CLRN1) in zebrafish sensory cells. *International symposium on Usher syndrome and related disorder 2010* abstract 11.
190. D'Alterio C, Tran DD, Yeung MW, et al. Drosophila melanogaster Cad99C, the orthologue of human Usher cadherin PCDH15, regulates the length of microvilli. *J Cell Biol.* 2005;171:549-558.
191. Demontis F, Dahmann C. Characterization of the Drosophila ortholog of the human Usher Syndrome type 1G protein sans. *PLoS One.* 2009;4:e4753.
192. Todi SV, Franke JD, Kiehart DP, et al. Myosin VIIA defects, which underlie the Usher 1B syndrome in humans, lead to deafness in Drosophila. *Curr Biol.* 2005;15:862-868.
193. Chaitin MH, Carlsen RB, Samara GJ. Immunogold localization of actin in developing photoreceptor cilia of normal and rds mutant mice. *Exp Eye Res.* 1988;47:437-446.
194. Deretic D, Huber LA, Ransom N, et al. Rab8 in retinal photoreceptors may participate in rhodopsin transport and in rod outer segment disk morphogenesis. *J Cell Sci.* 1995;108:215-224.



# Chapter 2

## **Association of whirlin with Ca<sub>v</sub>1.3 ( $\alpha_{1D}$ ) channels in photoreceptors, defining a novel member of the Usher protein network**

Ferry F.J. Kersten<sup>1-5</sup>, Erwin van Wijk<sup>1,2,4,5</sup>, Jeroen van Reeuwijk<sup>1,4</sup>, Bert van der Zwaag<sup>6</sup>, Tina Märker<sup>7</sup>, Theo A. Peters<sup>2,4,5</sup>, Nicholas Katsanis<sup>8</sup>, Uwe Wolfrum<sup>7</sup>, Jan E.E. Keunen<sup>3</sup>, Ronald Roepman<sup>1,4,#</sup> and Hannie Kremer<sup>2,4,5,#</sup>

#These authors contributed equally to this work

<sup>1</sup>Department of Human Genetics, <sup>2</sup>Department of Otorhinolaryngology, Head and Neck Surgery and <sup>3</sup>Department of Ophthalmology, Radboud University Nijmegen Medical Centre, Nijmegen, The Netherlands, <sup>4</sup>Nijmegen Centre for Molecular Life Sciences, and <sup>5</sup>Donders Institute for Brain, Cognition and Behaviour, Radboud University Nijmegen, Nijmegen, The Netherlands, <sup>6</sup>Department of Neuroscience and Pharmacology, Rudolf Magnus Institute of Neuroscience, University Medical Centre Utrecht, Utrecht, The Netherlands, <sup>7</sup>Department of Cell and Matrix Biology, Institute of Zoology, Johannes Gutenberg University of Mainz, Mainz, Germany, <sup>8</sup>McKusick-Nathans Institute of Genetic Medicine and Departments of Ophthalmology and Molecular Biology and Genetics, Johns Hopkins University, Baltimore, Maryland, 210205 USA.

*Investigative Ophthalmology & Visual Science* 2010; 51 (5): 2338-2346





## **Abstract**

Usher syndrome is the most common form of hereditary deaf-blindness. It is both clinically and genetically heterogeneous. The USH2D protein whirlin interacts via its PDZ domains with other Usher-associated proteins containing a C-terminal type I PDZ binding motif. These proteins co-localize with whirlin at the region of the connecting cilium and at the synapse of photoreceptor cells. This study was undertaken to identify novel, Usher syndrome associated, interacting partners of whirlin and thereby obtain more insights into the function of whirlin. The database of ciliary proteins was searched for proteins that are present in both retina and inner ear and contain a PDZ-binding motif. Interactions with whirlin were evaluated by yeast two-hybrid analyses, and validated by glutathione *S*-transferase pull-down assays, co-immunoprecipitations and co-localization in the retina with immunofluorescence and immunoelectron microscopy. The L-type calcium channel subunit Ca<sub>v</sub>1.3 ( $\alpha_{1D}$ ) specifically interacts with whirlin. In adult photoreceptors, Ca<sub>v</sub>1.3 ( $\alpha_{1D}$ ) and whirlin co-localize in the region of the connecting cilium and at the synapse. During murine embryonic development, the expression patterns of the *Whrn* and *Cacna1d* genes show significant overlap and include expression in the eye, the inner ear and the central nervous system. The findings indicate that Ca<sub>v</sub>1.3 ( $\alpha_{1D}$ ) is connected to the Usher protein network. This conclusion leads the hypothesis that, in the retina whirlin scaffolds Ca<sub>v</sub>1.3 ( $\alpha_{1D}$ ) and therefore contributes to the organization of calcium channels in the photoreceptor cells, where both proteins may be involved in membrane fusions.

## Introduction

Usher syndrome is the most common form of human hereditary deaf-blindness and has an autosomal recessive pattern of inheritance. Three clinical types, USH1, -2, and 3, are distinguished based on the progression and severity of the hearing loss and the presence or absence of vestibular dysfunction, with visual loss due to retinitis pigmentosa (RP) in all three types<sup>1</sup>. To date, the affected genes have been identified for 9 out of the 12 described Usher loci<sup>2-10</sup>. Besides being causative for Usher syndrome, mutations in the Usher genes *MYO7A*, *USH1C*, *CDH23*, *PCDH15* and *DFNB31* are also associated with nonsyndromic hearing loss<sup>2,6-10</sup>. In addition, mutations in the *USH2A* gene can lead to nonsyndromic autosomal recessive RP<sup>2,8,11,12</sup>. All USH1 and -2 proteins are integrated in an Usher protein network in both the inner ear and the retina, with a central scaffolding role for the proteins whirlin and harmonin<sup>6,13-15</sup>. These proteins contain multiple PDZ domains, homologous to domains identified in postsynaptic density protein 95 (PSD-95), disc large (Dlg) and zonula occludens-1 (ZO-1), which link them to the intracellular moieties of transmembrane Usher proteins with a C-terminal PDZ-binding motif (PBM). The USH1 and -2 proteins are prominently located in the ciliary transition zone (connecting cilium) and periciliary region of the photoreceptor cells, rendering Usher syndrome a ciliopathy. In addition, most of the proteins localize to the synapse of photoreceptor cells<sup>6-8,14-16</sup>. At these specific sites, the Usher proteins are suggested to function in protein transport, structural support and organization of ion channels<sup>6,8,14,17,18</sup>. To identify novel members of the Usher protein complex and thereby obtain more clues on the function of whirlin and harmonin, we employed a bioinformatic approach. This approach revealed the L-type calcium channel pore forming subunit Ca<sub>v</sub>1.3 ( $\alpha_{1D}$ ) as a potential new member of the Usher protein complex. It is a transmembrane protein that is predicted to contain four transmembrane and four ion transport domains<sup>19</sup>. Ca<sub>v</sub>1.3 ( $\alpha_{1D}$ )-deficient mice are deaf due to the complete absence of L-type currents in cochlear inner hair cells and degeneration of both the inner and outer hair cells. The mice do not show any signs of vestibular dysfunction or retinal degeneration<sup>20</sup>. The zebrafish Ca<sub>v</sub>1.3a ( $\alpha_{1D}$ ) mutant does exhibit, besides hearing loss, a vestibular (circling) phenotype, but no retinal degeneration has been described although the latter may be explained by the presence of a second copy of the gene which is differentially expressed in the retina<sup>21</sup>.

In this study, we sought to identify a specific PDZ – PBM based interaction between whirlin and Ca<sub>v</sub>1.3 ( $\alpha_{1D}$ ) and their co-localization in different layers of the retina, including the outer limiting membrane (OLM), the outer plexiform layer (OPL), and the region of the connecting cilium. We suggest that in the retina, the interaction of whirlin with Ca<sub>v</sub>1.3 ( $\alpha_{1D}$ ) contributes to the organization of voltage-gated L-type calcium channels.

## Results

### Identification of Candidate Members of the Usher Proteome Complex

To obtain more clues to the function of whirlin and harmonin, we used a bioinformatic approach to identify novel members of the Usher protein complex. We developed a script to select for human proteins from the Swiss-Prot database ([www.uniprot.org](http://www.uniprot.org)) that match the class I PBM, as many of the interactions in the Usher protein network are PDZ – PBM based<sup>6,15</sup>. Out of the resulting 955 proteins, 147 are present in the ciliary proteome database<sup>22</sup>. As our candidate Usher genes should be expressed in the eye or inner ear, a filter for expression in eye or ear ([www.ncbi.nlm.nih.gov/UniGene/](http://www.ncbi.nlm.nih.gov/UniGene/)) yielded 117 genes. We then used the Mouse Genome Informatics (MGI) database ([www.informatics.jax.org](http://www.informatics.jax.org)) to restrict our selection of candidate Usher genes to genes which are associated with vision/eye (MP:0005391) or hearing/vestibular/ear phenotypes (MP:0005377) in mice. This query yielded 18 genes including the three of the known Usher genes *CDH23*, *PCDH15* and *USH2A*, which validates our approach. Of these 18 genes, we selected the gene encoding the L-type calcium channel pore forming subunit Ca<sub>v</sub>1.3 ( $\alpha_{1D}$ ) as a very promising candidate Usher gene for further analysis, since the phenotype of early hair cell degeneration in the cognate mouse mutant<sup>20</sup> is most similar to the phenotypes of the known Usher mouse mutants<sup>23</sup>.

### Interaction of Ca<sub>v</sub>1.3 ( $\alpha_{1D}$ ) and Whirlin

A yeast two-hybrid assay was used to assess whether the PDZ domains of whirlin and harmonin associate with part (aa 1938-2181) of the intracellular C-terminal tail of Ca<sub>v</sub>1.3 ( $\alpha_{1D}$ ), which contains a class I PBM (aa 2178-2181). We identified an interaction between the cytoplasmic region of Ca<sub>v</sub>1.3 ( $\alpha_{1D}$ ) and the N-terminal two PDZ domains of whirlin (Fig. 1A). Weak associations of Ca<sub>v</sub>1.3 ( $\alpha_{1D}$ ) with PDZ1 and -3 of harmonin were suggested by



limited growth of the yeast colonies. No interaction between the  $\text{Ca}_v1.3$  ( $\alpha_{1D}$ ) C-terminus and whirlin PDZ3 or harmonin PDZ2 could be detected (Fig. 1A).

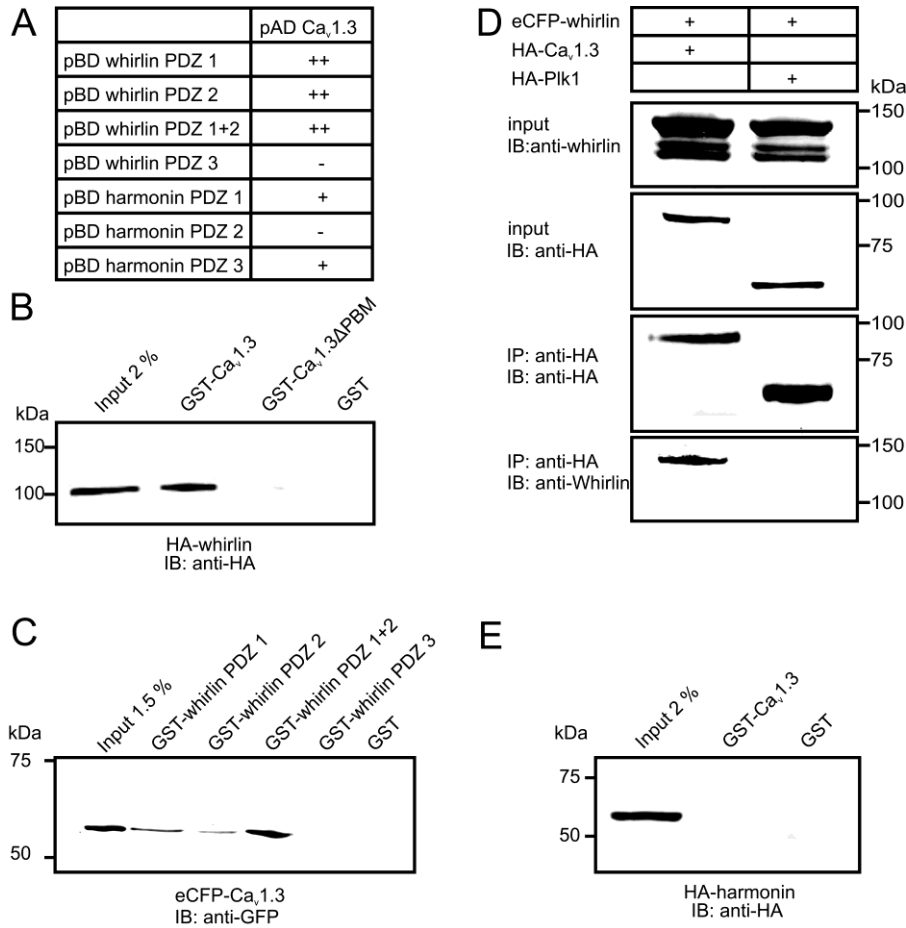


**Figure 1.** Validation of  $\text{Ca}_v1.3$  ( $\alpha_{1D}$ ) - whirlin interaction. **(A)** Yeast two-hybrid assays were performed with a part of the  $\text{Ca}_v1.3$  ( $\alpha_{1D}$ ) C-terminus fused to the activation domain (AD) and whirlin PDZ1, PDZ2, PDZ1+2 and PDZ3 or harmonin PDZ1, PDZ2 and PDZ3 fused to the DNA binding domain (BD) of the GAL4 reporter gene, respectively.  $\text{Ca}_v1.3$  ( $\alpha_{1D}$ ) interacts with the PDZ1 and/or PDZ2 domains, but not with the PDZ3 domain of whirlin.  $\text{Ca}_v1.3$  ( $\alpha_{1D}$ ) interacts with the PDZ1 and PDZ3, but not with the PDZ2 domain of harmonin, but this interaction was weak (+) compared to the  $\text{Ca}_v1.3$  ( $\alpha_{1D}$ )-whirlin (++) interaction. **(B)** GST pull-down assays showing that HA-tagged whirlin was efficiently pulled down by GST- $\text{Ca}_v1.3$  ( $\alpha_{1D}$ ) C-terminus, but not by  $\text{Ca}_v1.3$  ( $\alpha_{1D}$ ) $\Delta$ PBM or GST alone, as detected by an anti-HA antibody. The first lane shows 2% of the input of COS-1 cell lysate. **(C)** GST pull-down assays, showing that eCFP-tagged  $\text{Ca}_v1.3$  ( $\alpha_{1D}$ ), detected by an anti-GFP antibody, was efficiently pulled down by GST-whirlin PDZ1, PDZ2 and PDZ1+2, but not by GST-whirlin PDZ3 or GST alone. The first lane shows 1.5% of the input eCFP- $\text{Ca}_v1.3$  ( $\alpha_{1D}$ ) protein lysate. **(D)** Co-immunoprecipitation assay from COS-1 cell lysates, showing that eCFP-whirlin co-immunoprecipitated with the HA-tagged C-terminal region of  $\text{Ca}_v1.3$  ( $\alpha_{1D}$ ), but not with the HA-tagged protein Plk1. **(E)** GST pull-down assay, showing that HA-tagged harmonin not was pulled down by GST- $\text{Ca}_v1.3$  ( $\alpha_{1D}$ ) C-terminus with the PBM or GST alone, as detected by an anti-HA antibody. The first lane shows 2% of the input of COS-1 cell lysate.

The association of whirlin and Ca<sub>v</sub>1.3 ( $\alpha_{1D}$ ) was confirmed by using a glutathione *S*-transferase (GST) pull-down assay. Full-length HA-tagged whirlin was efficiently pulled down from COS-1 cell lysates by the GST-fused C-terminal part of Ca<sub>v</sub>1.3 ( $\alpha_{1D}$ ), but not by GST alone (Fig. 1B). Deletion of the predicted C-terminal class I PBM in Ca<sub>v</sub>1.3 ( $\alpha_{1D}$ ) disrupts the binding, indicating that this interaction is indeed based on a PDZ–PBM association (Fig. 1B).

To confirm that specifically the PDZ domains 1 and 2 of whirlin are involved in this interaction, we expressed the domains separately as GST fusion proteins to pull down the enhanced cyan fluorescent protein (eCFP)-tagged cytoplasmic tail of Ca<sub>v</sub>1.3 ( $\alpha_{1D}$ ). As shown in Figure 1C, whirlin PDZ1, PDZ2 and a peptide containing both PDZ domains are able to bind to the C-terminal part of Ca<sub>v</sub>1.3 ( $\alpha_{1D}$ ), but not PDZ3 or GST alone.

As a further validation of the interaction *in vivo*, a co-immunoprecipitation assay from COS-1 cells was performed, which showed that full length eCFP-tagged whirlin specifically co-immunoprecipitates with the HA-tagged C-terminus of Ca<sub>v</sub>1.3 ( $\alpha_{1D}$ ), but not with the unrelated HA-tagged protein Plk1 (Fig. 1D). In contrast, HA-tagged harmonin was not pulled down from COS-1 cell lysates with the GST-fused C-terminal part of Ca<sub>v</sub>1.3 ( $\alpha_{1D}$ ) (Fig. 1E). Therefore, the interaction between harmonin and Ca<sub>v</sub>1.3 ( $\alpha_{1D}$ ) was not further investigated.

### **Ca<sub>v</sub>1.3 ( $\alpha_{1D}$ ) and Whirlin Co-localize in the Retina**

To investigate whether Ca<sub>v</sub>1.3 ( $\alpha_{1D}$ ) and whirlin co-localize in the retina, we co-immunostained retinal cryosections with antibodies against whirlin (green; Fig. 2A) and Ca<sub>v</sub>1.3 ( $\alpha_{1D}$ ) (red; Fig. 2B), revealing expression and co-localization of these proteins (Fig. 2C) at the region of the connecting cilium, the OLM and the OPL. Immunostaining of Ca<sub>v</sub>1.3 ( $\alpha_{1D}$ ) was also observed at the inner plexiform layer (IPL) (Figs. 2B, 2C). Double immunostaining of Ca<sub>v</sub>1.3 ( $\alpha_{1D}$ ) and centrin, markers for the accessory centriole, basal body and connecting cilium<sup>24</sup>, further confirmed the localization of Ca<sub>v</sub>1.3 ( $\alpha_{1D}$ ) in this region since a (partial) co-localization was observed (Figs. 2D-F).

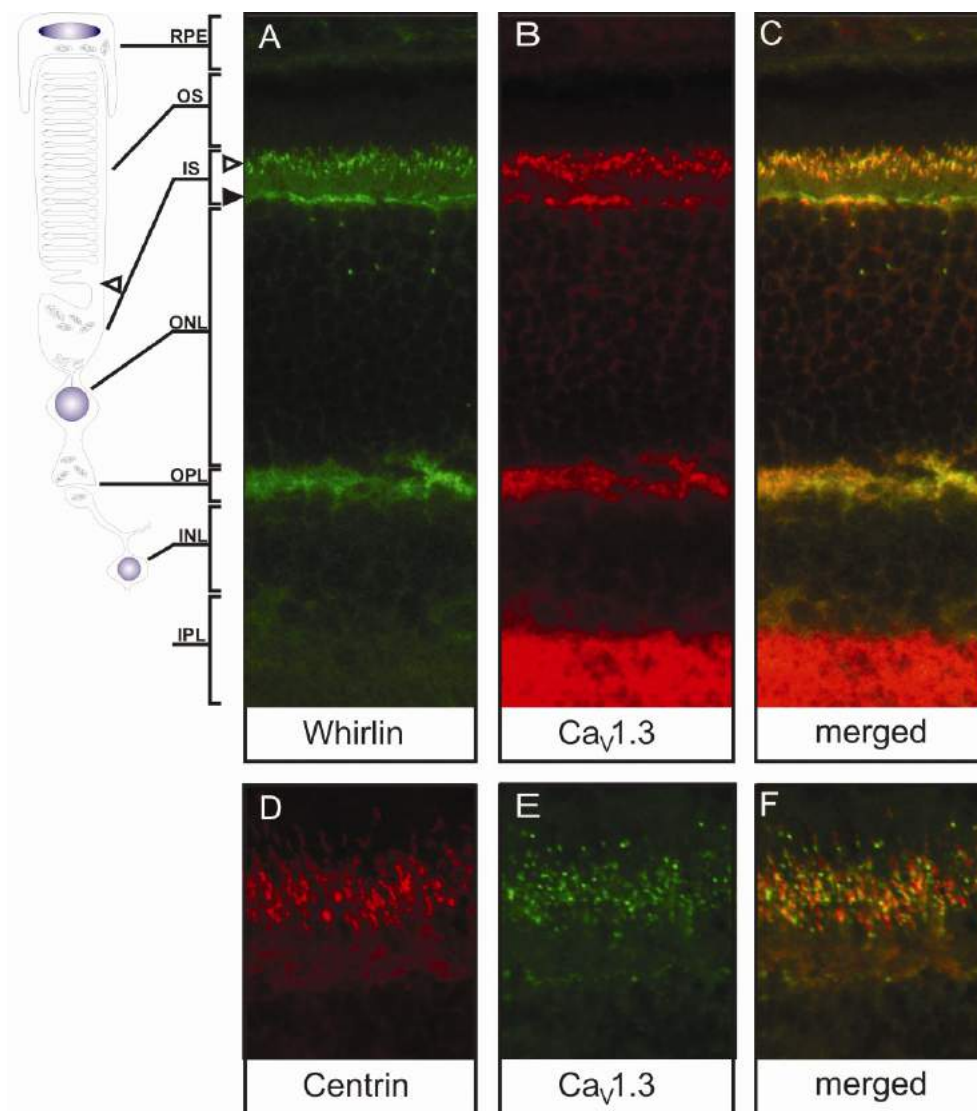


**Figure 2.** Whirlin and Ca<sub>v</sub>1.3 ( $\alpha_{1D}$ ) co-localize in rat photoreceptor cells. Subcellular localization of whirlin and Ca<sub>v</sub>1.3 ( $\alpha_{1D}$ ) in retina cryosections of adult (P20) rat. Immunostaining with (A) anti-whirlin (*green*), (B) anti-Ca<sub>v</sub>1.3 ( $\alpha_{1D}$ ) (*red*) and (C) an overlay (*yellow*) indicate co-localization at the region of the connecting cilium (CC; *open arrow heads*), the outer limiting membrane (OLM; *filled arrow heads*) and the outer plexiform layer (OPL). (D-F) Immunofluorescence with anti-Ca<sub>v</sub>1.3 ( $\alpha_{1D}$ ) (*green*) and anti-*pan* centrin (*red*) as a marker for the connecting cilium, centriole and basal body confirmed the localization in this region since partial co-localization (*yellow*) was observed.

Recently, the subcellular localization of whirlin in the mouse photoreceptor was determined using immunoelectron microscopy<sup>6,17</sup>. Here, we present the results for Ca<sub>v</sub>1.3 ( $\alpha_{1D}$ ). Pre-embedding labelling with an antibody directed against Ca<sub>v</sub>1.3 ( $\alpha_{1D}$ ) revealed its localization in the collar-like extension of the apical inner segment (Figs. 3A, 3B), at the basal body

complex (Fig. 3B, 3C), in the connecting cilium (Figs. 3B-D), in the basal region of the outer segments (Figs. 3A-C), and at the synapse (Figs. 3E, 3F) of mouse photoreceptor cells. As whirlin was also detected at these exact subcellular sites, with the exception of the outer segments and the synapse<sup>6,17</sup>, these results confirm the co-localization of Ca<sub>v</sub>1.3 ( $\alpha_{1D}$ ) and whirlin.

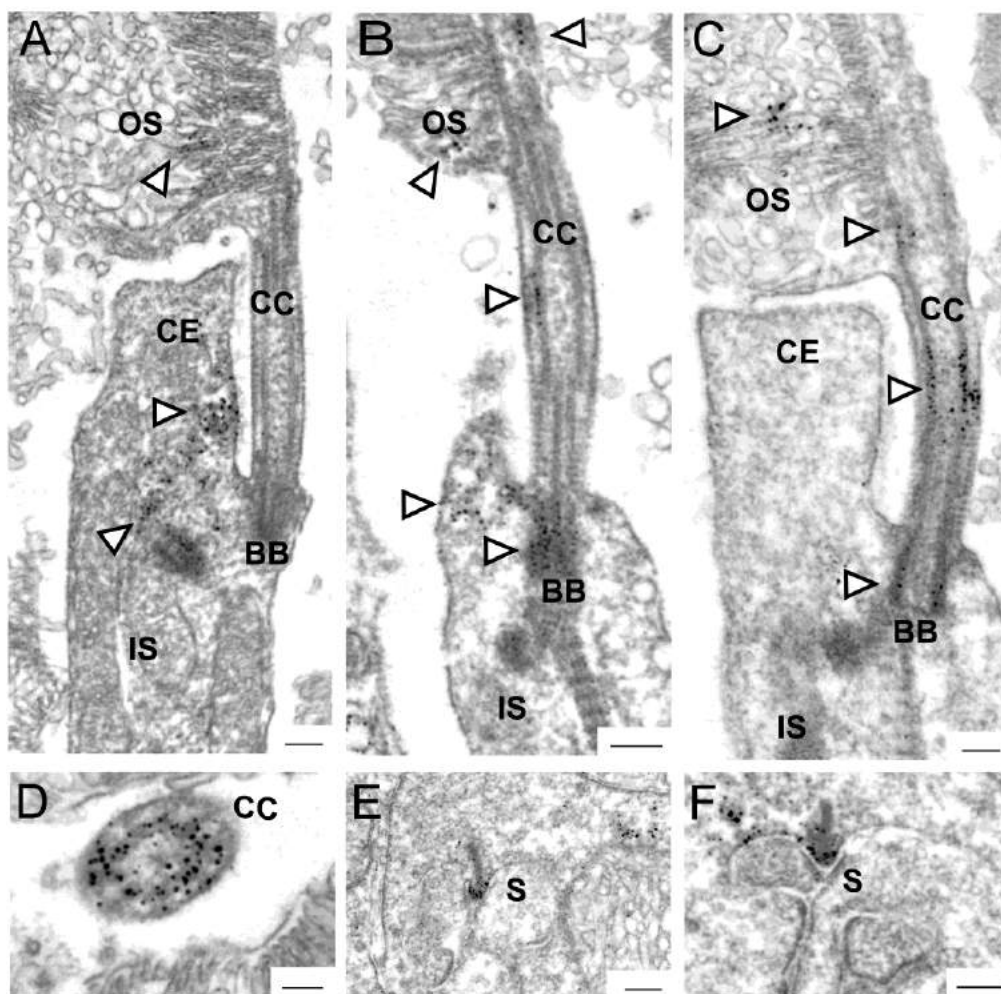


**Figure 3.** Localization of Ca<sub>v</sub>1.3 ( $\alpha_{1D}$ ) by immunoelectron microscopy. Micrographs of anti-Ca<sub>v</sub>1.3 ( $\alpha_{1D}$ ) labeling in longitudinal (A-C, E-F) and cross (D) sections of rod mouse photoreceptor cells. Ca<sub>v</sub>1.3 ( $\alpha_{1D}$ ) was detected in the collar-like extension of the apical inner segment (CE; A, B), at the basal body complex (BB; B, C) and in the connecting cilium (CC; B-D). Ca<sub>v</sub>1.3 ( $\alpha_{1D}$ ) was also detected in the base of the outer segment (OS; A-C) and at the synapses (S) of mouse photoreceptor (E, F). IS, inner segment. Scale bars: (A-C) 0.25  $\mu$ m; (D, F) 0.1  $\mu$ m; (E) 0.5  $\mu$ m.

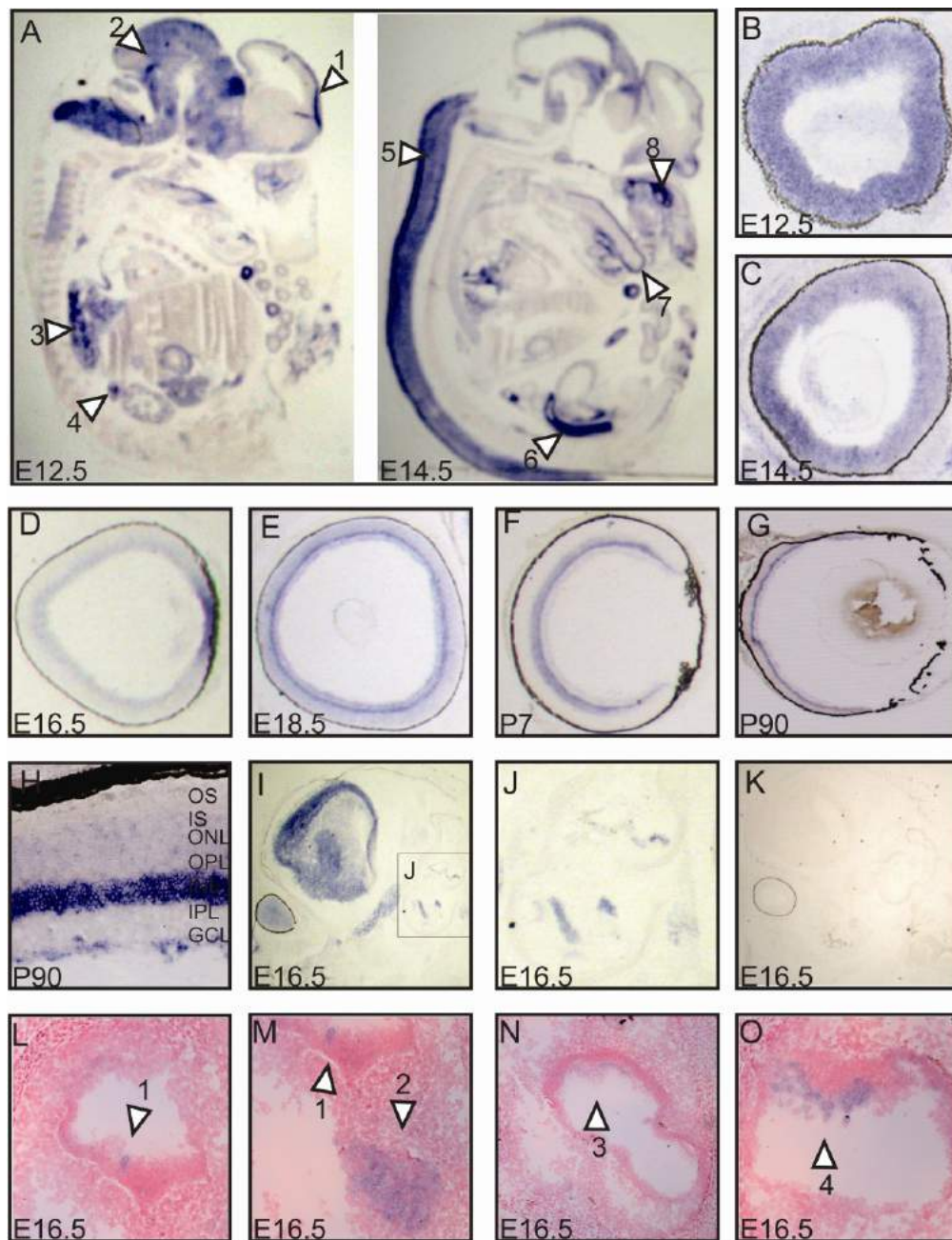


**Figure 4.** RNA in situ hybridization of *Cacna1d* mRNA in embryonic and adult mouse. *Cacna1d* was widely expressed during development (E12.5-E16.5), with most intense signals in the following structures (indicated by numbers and *arrowheads*). (A) neopallial cortex (1), midbrain (2), lung (3), adrenal gland (4), spinal cord (5), stomach wall (6), tongue (7), olfactory epithelium (8). Expression was also observed in the kidney, choroid plexus of the fourth ventricle, the lower and upper jaws, olfactory bulb, trigeminal (V) ganglion, duodenum, thalamus, umbilical cord, and venous heart region (data not shown). (B-H) A strong signal for *Cacna1d* was observed in the eye. Embryonic development of the eye at E12.5 (B) and E14.5 (C), in which expression was observed in the whole neuroblastic layer of the retina. At E16.5 (D), *Cacna1d* was expressed in the inner neuroblastic layer of the retina, and at E18.5 (E) expression was observed in a subset of the cells and the inner nuclear layer (INL). Expression of *Cacna1d* was maintained at postnatal day 7 (F) and 90 (G, H).

A strong signal, indicative of a high level of expression, was observed in the INL, and a subset of the GCL. Furthermore, expression was seen in the ONL and inner segments (IS; **H**). From E14.5 on, *Cacna1d* expression in the developing inner ear was observed and became more pronounced at E16.5 (**I, J, L-O**). Sections of the developing inner ear at E16.5 with *Cacna1d* expression in the inner hair cell (**L, 1; M, 1**), the spiral ganglion cells (**M, 2**), developing sensory cells of the macula of the utricle (**N, 3**), and in the crista ampullaris of the semicircular canals (**O, 4**). To increase structural detail, several sections were counterstained with nuclear Fast red (**L-O**). (**K**) Sections hybridized with the sense *Cacna1d* cRNA probe revealed no staining, indicating the specificity of antisense cRNA probe used in these experiments.

### ***Cacna1d* Expression during Murine Development**

The expression of *Cacna1d* in development was assessed by RNA *in situ* hybridization using mouse embryos of gestational days E12.5 to E18.5 and eyes of mice at P7 and P90. *Cacna1d* was widely expressed during murine embryonic development. From E12.5 to E16.5, expression was observed in the eye, inner ear, thalamus, neopallial cortex, midbrain, choroid plexus of the fourth ventricle, spinal cord, jaw, olfactory bulb, olfactory epithelium, lung, tongue, trigeminal (V) ganglion, duodenum, umbilical cord, venous heart region, kidney, adrenal gland and the stomach wall (Fig. 4A, and data not shown). At E18.5, the expression became more restricted and was detected in the lung, kidney, spinal cord, olfactory epithelium and intense staining was observed in the brain, inner ear (data not shown) and eye (Fig. 4E). In the developing retina, *Cacna1d* was transcribed from E12.5 onward (Figs. 4B-H). At E12.5, there was a strong signal in the complete neuroblastic layer (Fig. 4B). The signal at E14.5 was comparable with that at E12.5, but no staining was detected at the outermost cells. At E16.5, expression was detected in the inner neuroblastic layer of the retina, with the highest signal intensity in the area around the developing lens (Fig. 4D). At E18.5, the *Cacna1d* expression could be clearly distinguished in a subset of the ganglion cells, the inner nuclear layer (INL), and low-intensity staining was present in the neuroepithelium surrounding these layers (Fig. 4E). In juvenile P7 and P90 eyes, *Cacna1d* transcripts were detected in the INL, the outer nuclear layer (ONL), and in the inner segments. A high-intensity signal, suggestive of a high level of *Cacna1d* expression, was seen in a subset of the ganglion cells and in INL (Figs. 4F-H). In the developing inner ear, distinct expression was observed from E14.5 onward, which became more pronounced at E16.5 (Fig. 4I). At higher magnification, we show the expression of *Cacna1d* in the vestibular system and cochlea of the E16.5 inner ear (Fig. 4J). To obtain more structural detail for the inner ear, we

counterstained several sections of an E16.5 embryo with nuclear Fast red, revealing that *Cacna1d* expression was situated in the inner hair cells (IHCs) of the cochlea and in the spiral ganglion cells (Figs. 4L, 4M). Also, expression in the developing sensory cells of the macula of the utricle and the cristae ampullaris of the semicircular canals was detected (Figs. 4N, 4O). Hybridizations with a sense cRNA probe revealed no signals, indicating the specificity of the antisense cRNA probe used in these experiments (Fig. 4K).

## Discussion

In this study, we demonstrated that the C-terminus of the calcium channel subunit Ca<sub>v</sub>1.3 ( $\alpha_{1D}$ ) interacts with PDZ1 and -2 of whirlin and that these proteins co-localize at distinct sites in photoreceptor cells. A functional calcium channel is a heteromultimeric protein complex, composed of a pore-forming  $\alpha_1$  subunit, such as Ca<sub>v</sub>1.3 ( $\alpha_{1D}$ ), and the auxiliary subunits  $\beta$ ,  $\gamma$ , and  $\alpha_2\delta$ . Ten  $\alpha_1$ -subunit pore-forming isoforms ( $\alpha_{1a}$ - $\alpha_{1I}$  and  $\alpha_{1S}$ ) of voltage-activated calcium channels are described<sup>25</sup>. The  $\alpha_1$  subunit imparts most of the conductive properties of the channel, whereas the accessory subunits modulate calcium currents and channel activation/inactivation kinetics<sup>26-28</sup>.

Ca<sub>v</sub>1.3 ( $\alpha_{1D}$ ), encoded by the *CACNA1D* gene, is the most abundant isoform in hair cells and fulfills distinct physiological roles in the inner ear<sup>20,29</sup>. In the retina of mouse, rat and zebrafish, Ca<sub>v</sub>1.3 ( $\alpha_{1D}$ ) mRNA has been observed in the ONL, the INL, and in the ganglion cell layer (GCL)<sup>21,30-32</sup>. At the protein level, Ca<sub>v</sub>1.3 ( $\alpha_{1D}$ ) has been detected in the Müller cells, the OPL and photoreceptor cell bodies of the rat retina<sup>32</sup>. In the salamander retina, immunoreactivity is observed in the GCL, Müller cells, the IPL, the OPL, and the photoreceptor inner segment<sup>33,34</sup>.

During development, the murine *Cacna1d* gene is widely expressed (*e.g.* in the eye, the inner ear and in the CNS). Of note, *Whrn* expression has also been detected in these tissues<sup>15</sup>. We and others have shown that whirlin is connected to the dynamic Usher protein interactome, and we suggested that whirlin mediates multiple biological processes in the inner ear and the retina<sup>6,15</sup>. Our findings indicate that through whirlin, Ca<sub>v</sub>1.3 ( $\alpha_{1D}$ ), a voltage gated calcium channel subunit, is connected to the Usher protein network, underlining the molecular diversity of this interactome.

### ***Cacna1d* Expression During Murine Development**

At early embryonic stages (E12.5-E14.5) *Cacna1d* expression was detected in the eye, the inner ear, the midbrain, spinal cord, tongue, lung, choroid plexus of the fourth ventricle and kidney, in which *Whrn* RNA was also shown to be present<sup>15</sup>. This overlap in expression may indicate a function of both proteins in the same complex, even at these early embryonic stages in several tissues. In the developing inner ear *Cacna1d* expression was observed in the



cochlear IHCs, the spiral ganglion cells and the sensory cells of the vestibular part. Also, *Whrn* is expressed in these cells, although in the sensory epithelium of the cochlea only detectable from E18.5 onward<sup>15</sup>. In a recent study, RNA *in situ* hybridization was performed on whole-mount preparations of mature mouse organs of Corti, and *Cacnald* mRNA was detected in both IHCs and outer hair cells (OHC), but mainly in the OHCs<sup>35</sup>. We were able to show *Cacnald* expression only in the IHCs. This discrepancy may be explained by the difference in age of the animals-embryonic stages in our study versus P19 in the study of Knirsch et al.<sup>35</sup>.

At early developmental stages of the retina, both *Cacnald* (present data) and *Whrn* (described by van Wijk et al.<sup>15</sup>) are expressed, although *Whrn* transcripts are mainly present in the innermost layers, whereas *Cacnald* transcripts are detected in the entire developing retina. From E16.5 on, the retinal expression patterns of *Cacnald* and *Whrn* have a higher similarity. *Cacnald* expression in the adult mouse retina was observed in all three nuclear layers (GCL, INL, ONL), which is consistent with the findings in a previous study<sup>31</sup>. The difference in relative signal strength between the study of Xiao et al.<sup>31</sup> and the data we present may be due to a difference in antibody concentration and colorimetric reaction time. In postnatal stages of retinal development and in adult retina, *Cacnald* expression was most prominent in the INL, whereas *Whrn* expression is highest in the ONL. The overlap in *Cacnald* and *Whrn* expression at several stages of mouse development and in several organs, although at an apparently different quantitative distribution, together with the interaction at the protein level, indicates that Ca<sub>v</sub>1.3 ( $\alpha_{1D}$ ) and whirlin serve in the same processes of neuronal differentiation.

### **Ca<sub>v</sub>1.3 ( $\alpha_{1D}$ ) Localization and Function in the Photoreceptor**

In mature photoreceptor cells, Ca<sub>v</sub>1.3 ( $\alpha_{1D}$ ) and whirlin co-localize at regions where also Usher syndrome-associated proteins such as USH2A, SANS and GPR98 (VLRG1) co-localize with whirlin<sup>14,15,17</sup>. We previously suggested that whirlin may contribute to the organization of ion channels in the pre- and/or postsynaptic membranes of hair cells and photoreceptor cells<sup>6,14,15</sup>. Our present data indicate that Ca<sub>v</sub>1.3 ( $\alpha_{1D}$ ) is one of these ion channels at the OPL of the photoreceptor. In contrast to Ca<sub>v</sub>1.3 ( $\alpha_{1D}$ ), whirlin was not observed in the IPL by immunohistochemistry, which indicates that whirlin does not play a

role in Ca<sub>v</sub>1.3 ( $\alpha_{1D}$ ) organization in the synapses of this layer. Expression of whirlin, synonymously named CIP98, was detected, not only in the synaptic region of the photoreceptor cells, but also in the synaptic regions of the cochlear sensory cells<sup>15</sup> and possibly in neurons in the brain. Whirlin interacts with calmodulin-dependent serine kinase (CASK), and both proteins are co-immunoprecipitated from brain extracts. The whirlin-CASK complex has been suggested to play a role in trafficking of synaptic vesicles for transmission<sup>36</sup>. Of note, CASK is also detected at the OPL of the retina,<sup>37</sup> and therefore whirlin may serve as an adaptor protein linking CASK and Ca<sub>v</sub>1.3 ( $\alpha_{1D}$ ) in the synaptic regions of the retinal sensory cells. The complex may participate in the regulation of neurotransmission via the organization of Ca<sub>v</sub>1.3 ( $\alpha_{1D}$ ) channels in the photoreceptor cell synapses. Also, in the inner ear, Ca<sub>v</sub>1.3 ( $\alpha_{1D}$ ) channels are involved in the regulation of exocytosis of synaptic vesicles in IHCs and probably also in OHCs<sup>35,38-40</sup>. Although whirlin was not detected in the synaptic region of IHCs, it was found to be present in the synaptic region of OHCs,<sup>15</sup> and therefore the whirlin-Ca<sub>v</sub>1.3 ( $\alpha_{1D}$ ) interaction may play a role in synaptic transmission in these cells as well. However, to confirm this hypothesis, the localization of whirlin and its co-localization with Ca<sub>v</sub>1.3 ( $\alpha_{1D}$ ) in the synaptic region of OHCs should be studied in more detail.

The role of Ca<sub>v</sub>1.3 ( $\alpha_{1D}$ ) and its possible interaction with whirlin at the basal body and in the connecting cilium remains elusive. It is thought that the basal body functions in the organization of transport of cytoplasmic and transmembrane proteins into and through the connecting cilium. Therefore, the presence of whirlin and Ca<sub>v</sub>1.3 ( $\alpha_{1D}$ ) in the basal body may be explained by the fact that they are transported from there into the connecting cilium, where both proteins have been detected. In the connecting cilium, the whirlin-Ca<sub>v</sub>1.3 ( $\alpha_{1D}$ ) interaction may function in the organization of the channels and thereby in the Ca<sup>2+</sup> homeostasis in this region and the regulation of the Ca<sup>2+</sup>-dependent interaction of centrin and the visual G-protein transducin<sup>24</sup>. The centrin-transducin interaction is thought to regulate the light dependent translocation of transducin through the connecting cilium<sup>24</sup>.

Recently, our group and others described the molecular and ultrastructural homology between the periciliary structures in mammalian and amphibian photoreceptor cells. In mammals, the membrane domain of the apical inner segment collar corresponds to the periciliary ridge

complex (PRC) of the amphibian photoreceptor<sup>17,41</sup>. Besides providing structural support of the connecting cilium, this region is thought to function in docking trans-Golgi derived cargo vesicles containing proteins that are essential for outer segment formation and renewal and phototransduction<sup>6,17,42,43</sup>. We previously identified whirlin as one of the major molecules of the PRC<sup>17</sup> and subsequently Mazelova et al.<sup>44</sup> used an antibody against whirlin as a marker for the PRC, demonstrating the association of the SNARE proteins syntaxin 3 and SNAP25 with this region<sup>44</sup>. Also, the interaction of whirlin and Ca<sub>v</sub>1.3 ( $\alpha_{1D}$ ) may have a role in the transport to or organization of the calcium channel at the plasma membrane. The role of the Ca<sub>v</sub>1.3 ( $\alpha_{1D}$ ) channel at these subcellular sites may be the regulation of docking and fusion of cargo vesicles, involving SNARE proteins, through mediation of the Ca<sup>2+</sup> concentration, and Ca<sub>v</sub>1.3 ( $\alpha_{1D}$ ) was shown to be in a complex with SNARE proteins<sup>45,46</sup>. As is shown for synaptic vesicle fusion and exocytosis, the increase in Ca<sup>2+</sup> concentration via Ca<sup>2+</sup> influx through voltage-gated calcium channels initiates these processes<sup>27,47</sup>. Of note, Ca<sub>v</sub>1.3 ( $\alpha_{1D}$ ) was also detected in the pericuticular region of hair cells in the inner ear,<sup>38</sup> and in this region also SNARE proteins were detected<sup>48</sup>. This region is thought to be the site of vesicular trafficking, endocytosis, exocytosis, and membrane recycling for stereocilia repair<sup>49</sup> and therefore may have functional similarities to the periciliary region of photoreceptor cells.

We detected Ca<sub>v</sub>1.3 ( $\alpha_{1D}$ ) also at the base of the outer segments. At this site, the process of outer segment disc morphogenesis occurs. Rab and SNARE proteins, present in this region are suggested to contribute to this process by mediating membrane fusion of vesicles containing outer segment proteins<sup>50,51</sup>. For vesicles loaded with rhodopsin the targeting and fusion was indicated to be regulated by the protein SARA through its direct interaction with rhodopsin, syntaxin 3 and PI3P<sup>50</sup>. The Ca<sup>2+</sup>-dependence of the process of membrane fusion,<sup>52-54</sup> as discussed in the previous paragraph, may explain the presence of Ca<sub>v</sub>1.3 ( $\alpha_{1D}$ ) in this region.

### ***CACNA1D* in Disease**

Voltage-gated L-type calcium channels contribute to retinal signal transmission<sup>55</sup>. Recently, it has been shown that a mutation in the *CACNA2D4* gene, which encodes one of the auxiliary subunits ( $\alpha_2\delta$ ) of the L-type calcium channels, causes autosomal recessive progressive cone

dystrophy<sup>56</sup>. The gene encoding the L-type calcium channel  $\alpha_1$ -subunit named *CACNA1F* is associated with other types of retinal dysfunction—namely, incomplete X-linked congenital stationary night blindness (CSNB2)<sup>57,58</sup> and X-linked cone-rod dystrophy (CORDX3)<sup>59</sup>. The main cellular function of Ca<sub>v</sub>1.4 ( $\alpha_{1F}$ ) is thought to be mediation of neurotransmitter release from photoreceptor and bipolar cells<sup>60</sup>, a function that could be assumed for Ca<sub>v</sub>1.3 ( $\alpha_{1D}$ ) as well. Therefore, and because of the Ca<sub>v</sub>1.3 ( $\alpha_{1D}$ ) expression in the developing retina, *CACNA1D* is a candidate gene for retinal dysfunction in humans. However, no mutations have been described in patients with retinal disorders, and animal models with defects in *Cacna1d* do not exhibit a retinal phenotype. Despite the absence of an obvious retinal phenotype in a Ca<sub>v</sub>1.3<sup>-/-</sup> mouse model, there is a reduced electroretinogram (ERG) light peak (LP) amplitude<sup>61</sup>. The LP of the ERG reflects the depolarization of the basolateral plasma membrane of the retinal pigment epithelium (RPE), resulting from changes in the activity of one or more calcium-sensitive chloride channels<sup>62</sup>. However, we did not observe immunostaining of Ca<sub>v</sub>1.3 ( $\alpha_{1D}$ ) in the RPE (Fig. 2B). The lack of retinal phenotypes in the animal models may be due to compensation by other  $\alpha$ -subunits. In zebrafish, Ca<sub>v</sub>1.3b is one of the obvious candidates<sup>21</sup> and, in mouse, it could be Ca<sub>v</sub>1.4 ( $\alpha_{1F}$ )<sup>57-59</sup>. The absence of a retinal dysfunction of the Ca<sub>v</sub>1.3<sup>-/-</sup>-defective mice does not rule out a retinal dysfunction in humans with defects in the orthologous gene, since several mouse mutants with defects in genes involved in Usher syndrome do not exhibit retinal degeneration, but only mild ERG abnormalities in some of them<sup>63-66</sup>. For the whirler mouse with defects in the *Whrn* gene, no retinal phenotype has been reported. However, progressive retinal degeneration has been described in a *Whrn*-knockout mouse<sup>67</sup>. Whether the Ca<sub>v</sub>1.3 ( $\alpha_{1D}$ ) localization or function is disturbed in this mouse mutant remains to be determined. To the authors' knowledge, no locus for syndromic or nonsyndromic retinal dysfunction or deafness has been reported for the *CACNA1D* locus. The locus for Usher syndrome type 2b, which harbored the *CACNA1D* gene, has recently been withdrawn<sup>68,69</sup>.

## **Acknowledgements**

This research was supported by the Radboud University Nijmegen Medical Centre, Nijmegen, The Netherlands, The British Retinitis Pigmentosa Society (GR552), and by the Heinsius Houbolt Foundation.

## **Material and methods**

### **Bioinformatics**

Swiss-Prot protein sequences were downloaded from UniProt ([www.uniprot.org/](http://www.uniprot.org/)<sup>70</sup>) in FASTA format, and proteins matching the C-terminal class I PDZ binding motif (PBM; [ST].[VIL]\$) ([http://elm.eu.org/elmPages/LIG\\_PDZ\\_1.html/](http://elm.eu.org/elmPages/LIG_PDZ_1.html/) ELM [Eukaryotic Linear Motif] Functional Sites in Protein, provided in the public domain by a consortium funded by the European Union) were extracted. The resulting dataset was filtered for proteins associated with ciliary function, by using the Ciliary Proteome database ver. 3.0 ([www.ciliaproteome.org/](http://www.ciliaproteome.org/)<sup>22</sup>), study selection: all except for Liu et al. 2007, database type: all; cutoff *E*-value: 30. Subsequently, a filter for proteins that are encoded by genes expressed in eye or ear (UniGene; <http://www.ncbi.nlm.nih.gov/Unigene/>; provided in the public domain by the National Center for Biotechnology Information, Bethesda, MD) was applied. A final selection of candidate Usher proteins was made by selecting for homologues of mouse mutant proteins that are associated with vision/eye (MP:0005391) or hearing/vestibular/ear (MP:0005377) phenotype, as contained in the Mouse Genome Informatics database ([www.informatics.jax.org/](http://www.informatics.jax.org/) provided in the public domain by The Jackson Laboratory, Bar Harbor, ME)

### **Animals**

Wistar rats and C57BL6 JOLaHsd mice (Harlan, Horst, The Netherlands) used in this study were housed in standard cages and received water and food ad libitum. All experiments were conducted according to the ARVO Statement for the Use of Animals in Ophthalmic and Vision Research and international and institutional guidelines.

### **Cloning**

Human brain cDNA (Marathon; Clontech, Palo Alto, CA) was used as a template to amplify the cDNA encoding part of the C-terminal intracellular domain of CACNA1D (amino acids [aa] 1938-2181). The aa numbers are according to the following GenBank entries: Ca<sub>v</sub>1.3 ( $\alpha_{1D}$ ) NP\_000711, whirlin NP\_056219, harmonin NP\_710142, Plk1 NP\_005021 (<http://www.ncbi.nlm.nih.gov/Genbank/>; provided in the public domain by the National Center for Biotechnology Information, Bethesda, MD). All constructs were generated with commercial cloning technology (Gateway; Invitrogen, Carlsbad, CA), according to the manufacturer's instructions.

### **Yeast Two-Hybrid Analysis**

To test whether there is an interaction between Ca<sub>v</sub>1.3 ( $\alpha_{1D}$ ) and whirlin, a Gal4-based yeast two-hybrid system (HybriZAP; Stratagene, La Jolla, CA) was used according to methods previously described<sup>15, 71</sup>.

### **Antibodies**

The antibodies against whirlin and centrins have been described<sup>14,15,24</sup>. Anti-HA and anti-Ca<sub>v</sub>1.3 were derived from Sigma-Aldrich (Munich, Germany). Anti-GFP (Roche, Mannheim, Germany) was used to detect eCFP tagged proteins. As secondary antibodies, goat-anti-guinea pig Alexa 488, goat-anti-rat Alexa 568, IRDye800 goat-anti-guinea pig IgG, and IRDye800 goat-anti-mouse were used (all from Molecular Probes-Invitrogen, Carlsbad, CA).

### **GST Pull-Down**

The GST-fusion proteins were produced by transforming *Escherichia coli* BL21-DE3 with plasmids pDEST15-whirlin PDZ1 (aa 138-233), PDZ2 (aa 279-360), PDZ1+2 (aa 138-360), PDZ3 (aa 819-907), pDEST15-Ca<sub>v</sub>1.3 (aa 1938-2181), or pDEST15-Ca<sub>v</sub>1.3ΔPBM (aa 1938-2175), according to methods previously described<sup>15</sup>. HA-tagged whirlin full length (aa 1-907), eCFP-Ca<sub>v</sub>1.3 (aa 1938-2181), and eCFP-Ca<sub>v</sub>1.3ΔPBM (aa 1938-2175) were produced by transfecting COS-1 cells with pcDNA3-HA-Whirlin fl, pDEST501-Ca<sub>v</sub>1.3, and pDEST501-Ca<sub>v</sub>1.3ΔPBM, respectively, using a transfection reagent (Effectene; QIAGEN, Hildene, Germany), according the manufacturer's instruction. The follow-up of the experiment is described elsewhere<sup>15</sup>.

### **Co-Immunoprecipitation in COS-1 Cells**

Full length eCFP-tagged whirlin (aa 1-907) was expressed by using the expression vector pDest501. HA-tagged Ca<sub>v</sub>1.3 (aa 1938-2181) and Plk1 (aa 1-603) were expressed by using the pcDNA3-HA/Dest expression vector. COS-1 cells were transfected (Effectene; QIAGEN) according to the manufacturer's instruction. Twenty-four hours after transfection, the cells were washed with phosphate-buffered saline (PBS) and subsequently lysed on ice in IP lysis buffer<sup>15</sup>. eCFP-tagged whirlin was immunoprecipitated from cleared lysates overnight at 4 °C by using the anti-whirlin antibody<sup>15</sup>. HA-tagged Ca<sub>v</sub>1.3 and Plk1 were immunoprecipitated by using anti-HA monoclonal antibody (Sigma-Aldrich) and protein A/G PLUS-Sepharose beads (Santa Cruz Biotechnology, Santa Cruz, USA). The protein complexes were washed four times with IP lysis buffer and subsequently analyzed by Western blots analysis (Odyssey Infrared Imaging System; LI-COR, Lincoln, NE).

### **Immunohistochemistry in Rat Retina**

Unfixed eyes of 20-day-old (P20) Wistar rats were isolated and frozen in melting isopentane. Seven-micrometer-thick cryosections were treated and immunolabeled as described previously<sup>15</sup>.

### **Digoxigenin Labelling of cRNA In Situ Hybridization Probes**

A probe corresponding to nucleotides 556-1673 (GenBank NM\_001083616), which recognizes mouse *Cacna1d* transcripts was generated from mouse retina cDNA (Marathon; Clontech), with 5'- gccaacgaggcaactatg -3' used as a forward primer and 5'- ccaaggatgatcagactaac -3' used as a reversed primer. The labeling was performed as previously described<sup>15</sup>.

### **RNA In Situ Hybridization**

C57Bl6 Jlc0 mouse embryos were collected at various embryonic stages (E12.5-E18.5), as well as postnatal day (P)7 (P7) and P90 mouse eyes. RNA in situ hybridization was performed as previously described<sup>15</sup>. To increase

structural detail, several slides were incubated in nuclear Fast red (Sigma-Aldrich) for 10 seconds before embedding in rapid mounting media (Entellan; ProSciTech, Kirwan, QLD, Australia). Images were recorded with a microscope (Axioskop2; Carl Zeiss Meditec, Inc., Oberkochen, Germany) equipped with a 3CCD color video camera (HAD DXC-950P; Sony, Tokyo, Japan).

### **Pre-Embedding Immunoelectron Microscopy**

Vibratome sections of mouse retina were stained by a 100x diluted antibody against Ca<sub>v</sub>1.3 ( $\alpha_{1D}$ ) and visualized by a secondary antibody (Vectastain ABC-Kit; Vector Laboratories, Peterborough, UK). After fixation with 0.5% OsO<sub>4</sub>, the specimens were embedded in araldite, and ultrathin sections were analyzed with a transmission electron microscope (Tecnai 12; FEI, Hillsboro, OR). The procedure is described in detail elsewhere<sup>17</sup>.

## References

1. Smith RJ, Berlin CI, Hejtmancik JF, et al. Clinical diagnosis of the Usher syndromes. Usher Syndrome Consortium. *Am J Med Genet.* 1994;50:32-38.
2. Ahmed ZM, Riazuddin S, Riazuddin S, et al. The molecular genetics of Usher syndrome. *Clin Genet.* 2003;63:431-444.
3. Ahmed ZM, Riazuddin S, Khan SN, et al. USH1H, a novel locus for type I Usher syndrome, maps to chromosome 15q22-23. *Clin Genet.* 2009;75:86-91.
4. Chaib H, Kaplan J, Gerber S, et al. A newly identified locus for Usher syndrome type I, USH1E, maps to chromosome 21q21. *Hum Mol Genet.* 1997;6:27-31.
5. Ebermann I, Scholl HP, Charbel IP, et al. A novel gene for Usher syndrome type 2: mutations in the long isoform of whirlin are associated with retinitis pigmentosa and sensorineural hearing loss. *Hum Genet.* 2007;121:203-211.
6. Kremer H, van Wijk E, Marker T, et al. Usher syndrome: molecular links of pathogenesis, proteins and pathways. *Hum Mol Genet.* 2006;15 Suppl 2:R262-R270.
7. Petit C. Usher syndrome: from genetics to pathogenesis. *Annu Rev Genomics Hum Genet.* 2001;2:271-297.
8. Reiners J, Nagel-Wolfrum K, Jurgens K, et al. Molecular basis of human Usher syndrome: deciphering the meshes of the Usher protein network provides insights into the pathomechanisms of the Usher disease. *Exp Eye Res.* 2006;83:97-119.
9. Weil D, El Amraoui A, Masmoudi S, et al. Usher syndrome type I G (USH1G) is caused by mutations in the gene encoding SANS, a protein that associates with the USH1C protein, harmonin. *Hum Mol Genet.* 2003;12:463-471.
10. Weston MD, Lujendijk MW, Humphrey KD, et al. Mutations in the VLGR1 gene implicate G-protein signaling in the pathogenesis of Usher syndrome type II. *Am J Hum Genet.* 2004;74:357-366.
11. Rivolta C, Sweklo EA, Berson EL, et al. Missense mutation in the USH2A gene: association with recessive retinitis pigmentosa without hearing loss. *Am J Hum Genet.* 2000;66:1975-1978.
12. Seyedahmadi BJ, Rivolta C, Keene JA, et al. Comprehensive screening of the USH2A gene in Usher syndrome type II and non-syndromic recessive retinitis pigmentosa. *Exp Eye Res.* 2004;79:167-173.
13. Adato A, Michel V, Kikkawa Y, et al. Interactions in the network of Usher syndrome type 1 proteins. *Hum Mol Genet.* 2005;14:347-356.
14. Reiners J, van Wijk E, Marker T, et al. Scaffold protein harmonin (USH1C) provides molecular links between Usher syndrome type 1 and type 2. *Hum Mol Genet.* 2005;14:3933-3943.
15. van Wijk E, van der Zwaag B, Peters T, et al. The DFNB31 gene product whirlin connects to the Usher protein network in the cochlea and retina by direct association with USH2A and VLGR1. *Hum Mol Genet.* 2006;15:751-765.
16. Reiners J, Marker T, Jurgens K, et al. Photoreceptor expression of the Usher syndrome type 1 protein protocadherin 15 (USH1F) and its interaction with the scaffold protein harmonin (USH1C). *Mol Vis.* 2005;11:347-355.



17. Maerker T, van Wijk E, Overlack N, et al. A novel Usher protein network at the periciliary reloading point between molecular transport machineries in vertebrate photoreceptor cells. *Hum Mol Genet.* 2008;17:71-86.
18. van Wijk E, Kersten FF, Kartono A, et al. Usher syndrome and Leber congenital amaurosis are molecularly linked via a novel isoform of the centrosomal ninein-like protein. *Hum Mol Genet.* 2009;18:51-64.
19. Bateman A, Coin L, Durbin R, et al. The Pfam protein families database. *Nucleic Acids Res.* 2004;32:D138-D141.
20. Platzer J, Engel J, Schrott-Fischer A, et al. Congenital deafness and sinoatrial node dysfunction in mice lacking class D L-type Ca<sup>2+</sup> channels. *Cell.* 2000;102:89-97.
21. Sidi S, Busch-Nentwich E, Friedrich R, et al. gemini encodes a zebrafish L-type calcium channel that localizes at sensory hair cell ribbon synapses. *J Neurosci.* 2004;24:4213-4223.
22. Gherman A, Davis EE, Katsanis N. The ciliary proteome database: an integrated community resource for the genetic and functional dissection of cilia. *Nat Genet.* 2006;38:961-962.
23. Williams DS. Usher syndrome: animal models, retinal function of Usher proteins, and prospects for gene therapy. *Vision Res.* 2008;48:433-441.
24. Trojan P, Krauss N, Choe HW, et al. Centrins in retinal photoreceptor cells: regulators in the connecting cilium. *Prog Retin Eye Res.* 2008;27:237-259.
25. Dolphin AC. Calcium channel diversity: multiple roles of calcium channel subunits. *Curr Opin Neurobiol.* 2009;19:237-244.
26. Arikath J, Campbell KP. Auxiliary subunits: essential components of the voltage-gated calcium channel complex. *Curr Opin Neurobiol.* 2003;13:298-307.
27. Catterall WA. Structure and regulation of voltage-gated Ca<sup>2+</sup> channels. *Annu Rev Cell Dev Biol.* 2000;16:521-555.
28. Song H, Nie L, Rodriguez-Contreras A, et al. Functional interaction of auxiliary subunits and synaptic proteins with Ca(v)1.3 may impart hair cell Ca<sup>2+</sup> current properties. *J Neurophysiol.* 2003;89:1143-1149.
29. Dou H, Vazquez AE, Namkung Y, et al. Null mutation of alpha1D Ca<sup>2+</sup> channel gene results in deafness but no vestibular defect in mice. *J Assoc Res Otolaryngol.* 2004;5:215-226.
30. Kamphuis W, Hendriksen H. Expression patterns of voltage-dependent calcium channel alpha 1 subunits (alpha 1A-alpha 1E) mRNA in rat retina. *Brain Res Mol Brain Res.* 1998;55:209-220.
31. Xiao H, Chen X, Steele EC, Jr. Abundant L-type calcium channel Ca(v)1.3 (alpha1D) subunit mRNA is detected in rod photoreceptors of the mouse retina via in situ hybridization. *Mol Vis.* 2007;13:764-771.
32. Xu HP, Zhao JW, Yang XL. Expression of voltage-dependent calcium channel subunits in the rat retina. *Neurosci Lett.* 2002;329:297-300.
33. Henderson D, Doerr TA, Gottesman J, et al. Calcium channel immunoreactivity in the salamander retina. *Neuroreport.* 2001;12:1493-1499.

34. Welch NC, Wood S, Jollimore C, et al. High-voltage-activated calcium channels in Muller cells acutely isolated from tiger salamander retina. *Glia*. 2005;49:259-274.
35. Knirsch M, Brandt N, Braig C, et al. Persistence of Ca(v)1.3 Ca<sup>2+</sup> channels in mature outer hair cells supports outer hair cell afferent signaling. *J Neurosci*. 2007;27:6442-6451.
36. Yap CC, Liang F, Yamazaki Y, et al. CIP98, a novel PDZ domain protein, is expressed in the central nervous system and interacts with calmodulin-dependent serine kinase. *J Neurochem*. 2003;85:123-134.
37. Aartsen WM, Kantardzhieva A, Klooster J, et al. Mpp4 recruits Psd95 and Veli3 towards the photoreceptor synapse. *Hum Mol Genet*. 2006;15:1291-1302.
38. Brandt A, Striessnig J, Moser T. CaV1.3 channels are essential for development and presynaptic activity of cochlear inner hair cells. *J Neurosci*. 2003;23:10832-10840.
39. Brandt A, Khimich D, Moser T. Few CaV1.3 channels regulate the exocytosis of a synaptic vesicle at the hair cell ribbon synapse. *J Neurosci*. 2005;25:11577-11585.
40. Hafidi A, Dulon D. Developmental expression of Ca(v)1.3 (alpha1d) calcium channels in the mouse inner ear. *Brain Res Dev Brain Res*. 2004;150:167-175.
41. Papermaster DS, Schneider BG, DeFoe D, et al. Biosynthesis and vectorial transport of opsin on vesicles in retinal rod photoreceptors. *J Histochem Cytochem*. 1986;34:5-16.
42. Roepman R, Wolfrum U. Protein networks and complexes in photoreceptor cilia. *Subcell Biochem*. 2007;43:209-235.
43. Deretic D, Papermaster DS. Polarized sorting of rhodopsin on post-Golgi membranes in frog retinal photoreceptor cells. *J Cell Biol*. 1991;113:1281-1293.
44. Mazelova J, Ransom N, Stuto-Gribble L, et al. Syntaxin 3 and SNAP-25 pairing, regulated by omega-3 docosahexaenoic acid, controls the delivery of rhodopsin for the biogenesis of cilia-derived sensory organelles, the rod outer segments. *J Cell Sci*. 2009;122:2003-2013.
45. Hibino H, Pironkova R, Onwumere O, et al. RIM binding proteins (RBPs) couple Rab3-interacting molecules (RIMs) to voltage-gated Ca(2+) channels. *Neuron*. 2002;34:411-423.
46. Ramakrishnan NA, Drescher MJ, Drescher DG. Direct interaction of otoferlin with syntaxin 1A, SNAP-25, and the L-type voltage-gated calcium channel Cav1.3. *J Biol Chem*. 2009;284:1364-1372.
47. Lin RC, Scheller RH. Mechanisms of synaptic vesicle exocytosis. *Annu Rev Cell Dev Biol*. 2000;16:19-49.
48. Safieddine S, Wenthold RJ. SNARE complex at the ribbon synapses of cochlear hair cells: analysis of synaptic vesicle- and synaptic membrane-associated proteins. *Eur J Neurosci*. 1999;11:803-812.
49. Kachar B, Battaglia A, Fex J. Compartmentalized vesicular traffic around the hair cell cuticular plate. *Hear Res*. 1997;107:102-112.
50. Chuang JZ, Zhao Y, Sung CH. SARA-regulated vesicular targeting underlies formation of the light-sensing organelle in mammalian rods. *Cell*. 2007;130:535-547.
51. Kwok MC, Holopainen JM, Molday LL, et al. Proteomics of photoreceptor outer segments identifies a subset of SNARE and Rab proteins implicated in membrane vesicle trafficking and fusion. *Mol Cell Proteomics*. 2008;7:1053-1066.

52. Boesze-Battaglia K, Albert AD, Yeagle PL. Fusion between disk membranes and plasma membrane of bovine photoreceptor cells is calcium dependent. *Biochemistry*. 1992;31:3733-3738.
53. Jena BP. Membrane fusion: role of SNAREs and calcium. *Protein Pept Lett*. 2009;16:712-717.
54. Leabu M. Membrane fusion in cells: molecular machinery and mechanisms. *J Cell Mol Med*. 2006;10:423-427.
55. Baumann L, Gerstner A, Zong X, et al. Functional characterization of the L-type Ca<sup>2+</sup> channel Cav1.4alpha1 from mouse retina. *Invest Ophthalmol Vis Sci*. 2004;45:708-713.
56. Wycisk KA, Zeitz C, Feil S, et al. Mutation in the auxiliary calcium-channel subunit CACNA2D4 causes autosomal recessive cone dystrophy. *Am J Hum Genet*. 2006;79:973-977.
57. Bech-Hansen NT, Naylor MJ, Maybaum TA, et al. Loss-of-function mutations in a calcium-channel alpha1-subunit gene in Xp11.23 cause incomplete X-linked congenital stationary night blindness. *Nat Genet*. 1998;19:264-267.
58. Strom TM, Nyakatura G, pfelstedt-Sylla E, et al. An L-type calcium-channel gene mutated in incomplete X-linked congenital stationary night blindness. *Nat Genet*. 1998;19:260-263.
59. Jalkanen R, Mantyjarvi M, Tobias R, et al. X linked cone-rod dystrophy, CORDX3, is caused by a mutation in the CACNA1F gene. *J Med Genet*. 2006;43:699-704.
60. Berntson A, Taylor WR, Morgans CW. Molecular identity, synaptic localization, and physiology of calcium channels in retinal bipolar cells. *J Neurosci Res*. 2003;71:146-151.
61. Wu J, Marmorstein AD, Striessnig J, et al. Voltage-dependent calcium channel CaV1.3 subunits regulate the light peak of the electroretinogram. *J Neurophysiol*. 2007;97:3731-3735.
62. Gallemore RP, Steinberg RH. Light-evoked modulation of basolateral membrane Cl<sup>-</sup> conductance in chick retinal pigment epithelium: the light peak and fast oscillation. *J Neurophysiol*. 1993;70:1669-1680.
63. Haywood-Watson RJ, Ahmed ZM, Kjellstrom S, et al. Ames Waltzer deaf mice have reduced electroretinogram amplitudes and complex alternative splicing of Pcdh15 transcripts. *Invest Ophthalmol Vis Sci*. 2006;47:3074-3084.
64. Libby RT, Steel KP. Electroretinographic anomalies in mice with mutations in Myo7a, the gene involved in human Usher syndrome type 1B. *Invest Ophthalmol Vis Sci*. 2001;42:770-778.
65. Libby RT, Kitamoto J, Holme RH, et al. Cdh23 mutations in the mouse are associated with retinal dysfunction but not retinal degeneration. *Exp Eye Res*. 2003;77:731-739.
66. McGee J, Goodyear RJ, McMillan DR, et al. The very large G-protein-coupled receptor VLGR1: a component of the ankle link complex required for the normal development of auditory hair bundles. *J Neurosci*. 2006;26:6543-6553.
67. Yang J, Liu X, Adamian M, et al. N-terminal mutation of whirlin disrupts the Usher syndrome II (USH2) protein complex and causes retinal and inner ear defects in mice. *ARVO abstract*. 2008;49:4405.
68. Hmani-Aifa M, Benzina Z, Zulficar F, et al. Identification of two new mutations in the GPR98 and the PDE6B genes segregating in a Tunisian family. *Eur J Hum Genet*. 2008;17:474-482.

69. Hmani M, Ghorbel A, Boulila-Elgaied A, et al. A novel locus for Usher syndrome type II, USH2B, maps to chromosome 3 at p23-24.2. *Eur J Hum Genet.* 1999;7:363-367.
70. The UniProt Consortium. The Universal Protein Resource (UniProt). *Nucleic Acids Res.* 2009;37:169-174
71. Roepman R, Schick D, Ferreira PA. Isolation of retinal proteins that interact with retinitis pigmentosa GTPase regulator by interaction trap screen in yeast. *Methods Enzymol.* 2000;316:688-704.



# Chapter

# 3

## **A hypofunctional EPS8 variant predisposes to ototoxicity**

Abdullah Üzümcü<sup>1,#</sup>, Nina Offenhäuser<sup>2,#</sup>, Ferry F.J. Kersten<sup>3-6,#</sup>, Yun Li<sup>7,9,#</sup>, Agnieszka K. Rzadzinska<sup>8,#</sup>, Oya Uyguner<sup>1</sup>, Esther Pohl<sup>7,9</sup>, Charlotte Blanche Ekalle Soppo<sup>2</sup>, Nicola Strenzke<sup>10</sup>, Gökhan Yigit<sup>7,9</sup>, Gudrun Nürnberg<sup>7,11,12</sup>, Melike Emiroglu<sup>13</sup>, Gunther Hafiz<sup>13</sup>, Hülya Kayserili<sup>1</sup>, Christian Becker<sup>7,11</sup>, Birsen Karaman<sup>1</sup>, Ignacio del Castillo<sup>15</sup>, Seher Basaran<sup>1</sup>, Memnune Yüksel Apak<sup>1</sup>, Peter Nürnberg<sup>7,11,12,14</sup>, Tobias Moser<sup>10</sup>, Christian Kubisch<sup>7,9,12,14</sup>, Karen P. Steel<sup>8</sup>, Pier Paolo Di Fiore<sup>2,16,17</sup>, Hannie Kremer<sup>3,4,6</sup>, Bernd Wollnik<sup>1,7,9,14</sup>

# These authors contributed equally to this work

<sup>1</sup>Department of Medical Genetics, Istanbul Medical Faculty, Istanbul University, Istanbul, Turkey, <sup>2</sup>IFOM, Fondazione Istituto FIRC di Oncologia Molecolare, Milan, Italy, <sup>3</sup>Department of Human Genetics, <sup>4</sup>Department of Otorhinolaryngology, Head and Neck Surgery and <sup>5</sup>Department of Ophthalmology, Radboud University Nijmegen Medical Centre, Nijmegen, The Netherlands, <sup>6</sup>Nijmegen Centre for Molecular Life Sciences, and Donders Institute for Brain, Cognition and Behaviour, Radboud University Nijmegen, Nijmegen, The Netherlands, <sup>7</sup>Center for Molecular Medicine Cologne (CMMC), University of Cologne, Cologne, Germany, <sup>8</sup>Wellcome Trust Sanger Institute, Cambridge, Hinxton, UK, <sup>9</sup>Institute of Human Genetics, University Hospital Cologne, University of Cologne, Cologne, Germany, <sup>10</sup>InnerEarLab, Department of Otolaryngology, Göttingen University Medical School, Göttingen, Germany, <sup>11</sup>Cologne Centre for Genomics, University of Cologne, Cologne, Germany, <sup>12</sup>Institute of Genetics, University of Cologne, Cologne, Germany, <sup>13</sup>Department of Otolaryngology, Istanbul Medical Faculty, Istanbul University, Istanbul, Turkey, <sup>14</sup>Cologne Excellence Cluster on Cellular Stress Responses in Aging-Associated Diseases (CECAD), University of Cologne, Cologne, Germany, <sup>15</sup>Unidad de Genética Molecular, Hospital Ramón y Cajal, Madrid, Spain, <sup>16</sup>Dipartimento di Medicina, Chirurgia ed Odontoiatria, Università degli Studi di Milano, Milan, Italy, <sup>17</sup>Istituto Europeo di Oncologia, Via Ripamonti 435, 20141, Milan, Italy.

*Manuscript submitted to Nature Genetics.*





**Abstract**

Aminoglycosides are the most commonly used antibiotics worldwide<sup>1</sup>. Although highly effective, their use is restricted by side effects such as ototoxicity in a significant subset of patients<sup>2,3</sup>. Administration of therapeutic doses over a few days can cause permanent hearing impairment, especially in newborns and young children. However, underlying pathogenesis and pharmacogenetic risk variants are largely unknown<sup>4,5</sup>. Here we show that dysfunction of Epidermal Growth Factor Receptor 8 (EPS8) can result in a drug-inducible disturbance of actin dynamics and an irreversible hearing impairment in humans. By positional cloning, we identified a homozygous missense variant in *EPS8* as a cause of aminoglycoside-induced hearing impairment. *EPS8* encodes a known regulator of actin dynamics. We demonstrate that EPS8 is a component of the tip complex that regulates stereocilia length and that it interacts with whirlin. The mutation severely impairs this interaction *in vitro*. Complete loss of Eps8 function in *Eps8<sup>-/-</sup>* mice leads to a constitutive hearing loss associated with shortened stereocilia.



We have examined a large Turkish family with AIHI in four children from three branches of the family (Fig. 1A). All affected individuals were born to consanguineous parents suggesting an autosomal recessively inherited predisposition to aminoglycoside-induced ototoxicity. Affected children showed normal developmental milestones including speech acquisition. A hearing impairment was reported for affected individuals immediately after treatment of general infections with aminoglycosides (streptomycin and gentamicin) for several days (online methods). The induced hearing impairment occurred between five and nine years of age. It was moderate to severe, bilateral, permanent, and affected particularly high-frequency hearing (Fig. 1B). No progression of the clinical course has been observed yet. Compatible with the clinical phenotype, primary fibroblasts of individual V:7 responded with a significant and dose-dependent increase in the rate of cell death on kanamycin treatment when compared with homozygous wild-type cells (Fig. 1C). A similar effect was seen in V:7 patients' fibroblasts after hydrogen peroxide treatment (Supplementary Fig. 1A) suggesting a general increase of sensitivity to stress-inducing agents.

After exclusion of the mitochondrial m.1555A>G *MTRNR1* mutation (MIM 651000), we genotyped DNAs from participating family members using 10K SNP arrays. A single genomic region, located on chromosome 12p13, exhibited statistically significant linkage with a parametric LOD score of 4.83 (Supplementary Fig. 1B). This locus also showed significant linkage when only affected individuals were included in the analysis (data not shown). Subsequent genotyping of microsatellite markers confirmed the homozygous state of this region in affected individuals (Fig. 1A, Supplementary Fig. 1C) and defined a shared homozygous interval of approximately 7.44 Mb between single nucleotide polymorphisms (SNPs) rs2416669 and rs726391 (Supplementary Fig. 2). We sequenced all 77 annotated genes within the critical region (Supplementary Table 1) and identified one putatively pathogenic alteration, c.986T>C (p.L329P), in *EPS8*. All four affected individuals were homozygous for this variant, whereas parents were found to be heterozygous carriers (Fig. 1D). The c.986T>C mutation was not detected in 300 Turkish and 200 healthy Caucasian control individuals.

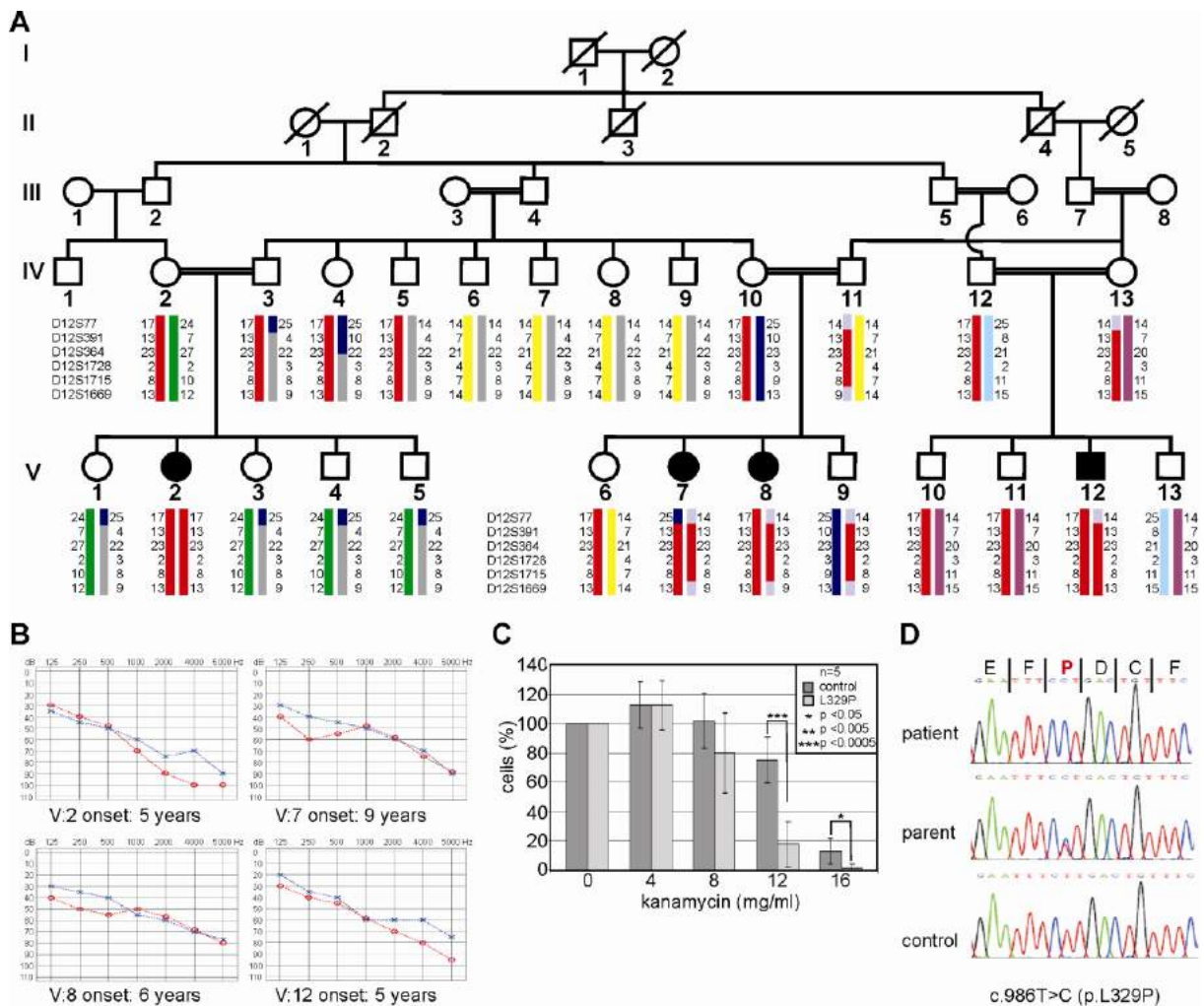


**Figure 1.** Identification of an *EPS8* mutation in a Turkish family with aminoglycoside-induced hearing impairment. **(A)** Pedigree of the family showing the homozygous haplotypes on chromosome 12p13 in the affected individuals V:2, 7, 8 and 12. **(B)** Audiograms of the affected individuals (left ear: red line, right ear: blue line) **(C)** The p.L329P variant causes increased cell death in aminoglycoside treated homozygous fibroblast cells of the patient V:7 (grey bars) compared to homozygous wt fibroblasts of a healthy control individual (black bars). **(D)** Identification of a homozygous 9 (p.L329P) *EPS8* variant in patient V:7. The parents are heterozygous for this variant shown for individual IV:10.

The 21 exons of the Epidermal Growth Factor Receptor Substrate 8 (*EPS8*) are transcribed into a 4088 bp transcript (NM\_004447.5), which encodes a protein of 822 amino acids (NP\_004438.3)<sup>6</sup>. *Eps8* is a key regulator of actin dynamics<sup>7,8,9,10</sup> and exerts both capping and bundling activities<sup>7,9,11</sup>. Like other proteins of the *EPS8L* family<sup>12</sup>, *EPS8* consists of a phosphotyrosine-binding domain (PTB), an SH3 domain, and a C-terminal actin-binding domain<sup>9,13</sup> (Supplementary Fig. 4A). The c.986T>C variant is predicted to substitute a proline

for the partially conserved leucine at position 329 (p.L329P), which is located in a region that has not yet been associated with a specific function of EPS8.

To address a function of Eps8 in hearing, we examined Eps8 knockout mice (*Eps8*<sup>-/-</sup>)<sup>9,12,14</sup>. Indeed, *Eps8*<sup>-/-</sup> mice did not exhibit Preyer reflexes as early as 14 days after birth indicating that complete loss of Eps8 leads to early postnatal hearing loss (Supplementary Fig. 3A). *Eps8*<sup>-/-</sup> mice lacked auditory brain stem responses up to 90 decibel sound pressure level, demonstrating a profound deafness (Supplementary Fig. 3B). In wildtype (wt) cochlea, we detected both Eps8 mRNA and protein at postnatal days (P) 5 and 7 (Supplementary Fig. 3C, D). Confocal microscopy of phalloidin stained whole mounts of auditory sensory epithelia of *Eps8*<sup>-/-</sup> mice showed morphological changes. The hair bundles of outer hair cells (OHCs) appeared smaller than in controls, and stereocilia of inner hair cells (IHCs) appeared more numerous and significantly shorter in length (Fig. 2A). The morphology of the hair bundle closely resembled that of the *whirler* mouse (*Whrn*<sup>wi/wi</sup>)<sup>15,16</sup>, and therefore, we hypothesized that Eps8 and whirlin co-function in stereocilia elongation by direct interaction.

Using a yeast two-hybrid assay, a binary interaction between EPS8 and whirlin was observed (Fig. 2B, Supplementary Figs. 4B, 4C), but not between EPS8 and harmonin. The latter has a high structural and functional similarity to whirlin. To confirm the EPS8-whirlin interaction we used an *in vitro* glutathione S-transferase (GST) pull-down assay. Hemagglutinin (HA)-tagged full-length whirlin was efficiently pulled down from COS-1 lysates by the GST-fused EPS8 wt, but not by GST alone (Fig. 2C). Several deletion constructs for EPS8 and whirlin were tested in additional yeast two-hybrid assays to identify the interaction surfaces. The region of EPS8 which associates with whirlin was mapped between amino acids 182 and 533, while the whirlin interaction surface encompasses the proline rich region (Supplementary Figs. 4A-C).

The novel *EPS8* mutation p.L329P we identified is located within the newly characterized whirlin-interacting domain of EPS8. Therefore, we evaluated the effect of the mutation on the EPS8-whirlin interaction. By *in vitro* GST pull-down assays, we demonstrated that only a minute amount of HA-tagged whirlin interacts with the GST-fused EPS8 L329P mutant, when compared to wt GST-EPS8 (Fig. 2C). A similar and significant reduction of whirlin binding affinity of the EPS8 mutant was shown in a yeast two-hybrid assay (Fig. 2B). When

expressed in COS-1 cells, whirlin was diffusely distributed and EPS8 wt, p.L329P mutant, and p.L329V (a control variant; valine is present at position 329 in some species; Supplementary Fig. 4D) were organized in filamentous structures presumably rich in actin<sup>10</sup> (Fig. 2D). Under conditions of co-expression, whirlin became enriched and co-localized along the filamentous structures in EPS8 wt or EPS8 p.L329V, but not in the whirlin-binding deficient EPS8 p.L329P mutant (Fig. 2D, supplementary Fig. 4E). Collectively, these data demonstrate that the amino acid at position 329 of EPS8 is critical for binding to whirlin and that the p.L329P mutation represents a hypofunctional allele.

The biological relevance of the Eps8-whirlin interaction was further assessed in the inner ear of wt mice and mice deficient for *Eps8*, *Whrn* and *Myo15a*. In wt or heterozygous mutant *Whrn*<sup>+/*wi*</sup> mice, Eps8 was enriched at the tip of the tallest row of stereocilia in hair bundles of both IHCs and OHCs early in postnatal development (P2). This distribution was obvious from base to apex of the cochlea and was maintained throughout development (P8) (Fig. 3A) until adulthood (P80) (Supplementary Fig. 4F). Weaker Eps8 immunofluorescence spots were also detected in the tips of stereocilia in the shorter rows and weak Eps8 immunostaining lined the length of stereocilia. This observation suggests that Eps8 enhancement at the tip of stereocilia is correlated to their length, as is known for myosin XVa<sup>17</sup>. At the tips of the tallest stereocilia, Eps8 co-localized with whirlin, but was not seen in the rows of shorter stereocilia or at the stereocilia base where whirlin is part of the ankle link complex<sup>18</sup> (Fig. 3B). At the stereocilia tip site, whirlin is thought to mediate the assembly of a protein complex that regulates differential stereocilia elongation in the hair bundle<sup>17</sup>. In the abnormally short hair bundles of *Whrn*<sup>*wi/wi*</sup> mice, Eps8 immunoreactivity was present along the stereocilia and at their tips but, in contrary to wt mice, it was not enriched at the tip of the tallest ones (Fig. 3C; Supplementary Fig. 4F) This staining pattern was maintained until adulthood. In *Eps8*<sup>-/-</sup> mice, whirlin immunostaining was seen in the distal part of the tallest stereocilia but it was strongly reduced and the enrichment at the distal tip was hardly visible (Fig. 3D). Interestingly, both IHCs and OHCs of *MyoXVa*<sup>*sh2/sh2*</sup> mice demonstrated uniform Eps8 staining along the length of their stereocilia but no enhancement at the tip (Fig. 3E). These mice also lack whirlin at the tip of their stereocilia and, like *whirler* and *Eps8*<sup>-/-</sup> mutants, have short stereocilia<sup>10,15,19</sup>. Our data demonstrate that myosinXVa is essential for Eps8 localization at the stereocilia tip, not only through its role in the localization of whirlin.

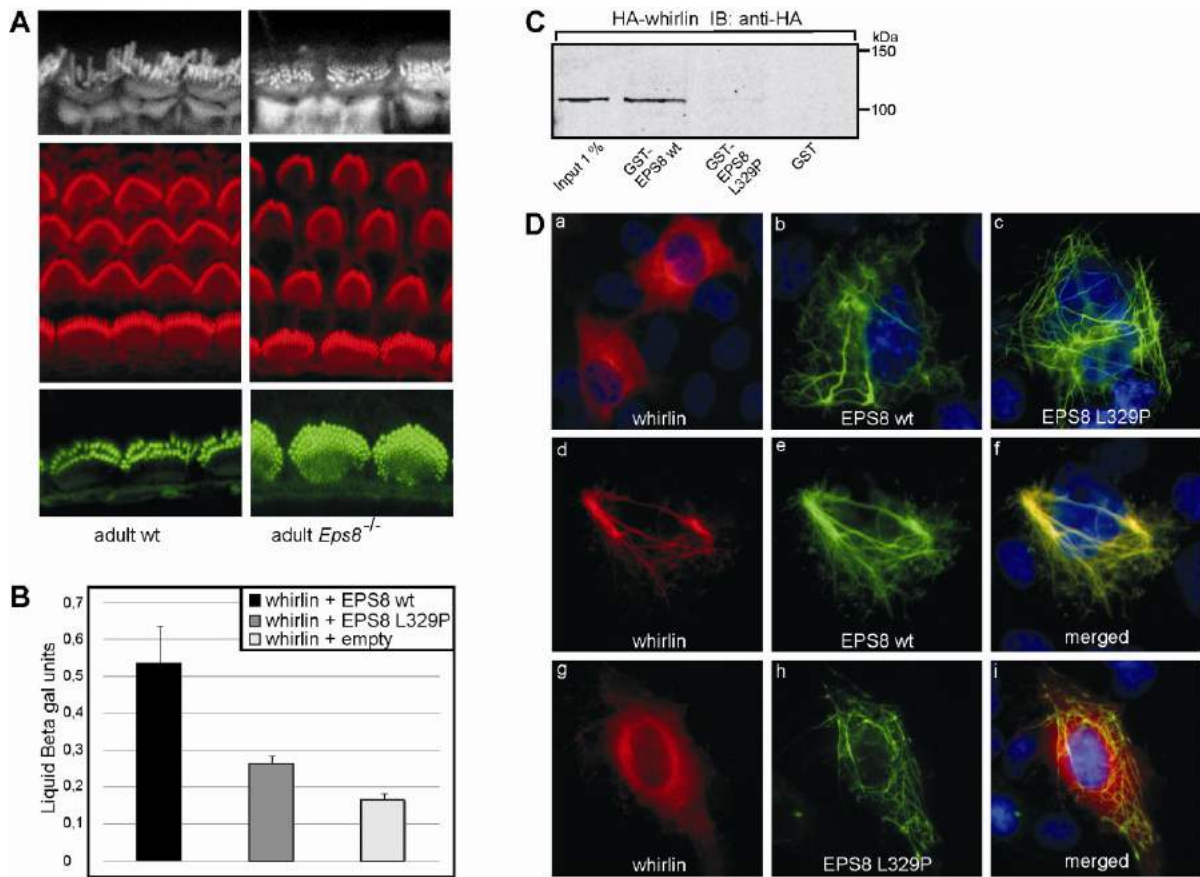


**Figure 2.** Phenotype of the *Eps8* KO mice and Eps8-whirlin interaction. (A) *Eps8*<sup>-/-</sup> mice display shorter and more numerous stereocilia compared to wt mice assessed by phalloidin immunostaining on whole mount cochleae from adult mice. (B) A quantitative liquid beta-galactosidase assay shows a specific interaction between EPS8 and whirlin (black bar). The p.L329P variant reduced the binding of these proteins (grey bar), but not completely to background level (white bar). (C) GST pull-down assays showing that HA-whirlin was efficiently pulled-down by GST-fused EPS8, but not by GST alone. The pull-down of HA-whirlin by GST-fused EPS8 p.L329P was less efficient compared with GST-fused EPS8 wt. The left lane shows 1% input of the protein lysate. (D) Single- and co-transfections of COS-1 cells with plasmids encoding mRFP-whirlin and eCFP-Eps8 wt or L329P. In single transfected cells, whirlin was mainly located in the cytoplasm (a), whereas Eps8 wt and L329P were located in actin-like structures (b, c). In cells expressing wt EPS8 and whirlin, the latter was recruited to the actin-like structures and co-localized with EPS8 (d-f). In cells expressing both whirlin and Eps8 L329P, whirlin was partially recruited to actin structures, but the protein was mainly localized in the cytoplasm (g-i).

We conclude from our studies that Eps8 is essential in hair cell development to achieve the characteristic pattern of stereocilia elongation in both IHCs and OHCs. The biological relevance of the whirlin-Eps8 interaction as demonstrated by aberrant distribution of Eps8 in mice with a defective *Whrn* gene (and *vice versa*) supports a causative role of the p.L329P in hearing impairment. In this context, Eps8, like gelsolin in shorter stereocilia<sup>20</sup>, may directly link the protein complex organized by whirlin primarily to actin in the tip of the longest stereocilia, thereby regulating actin dynamics in concert with other actin regulatory proteins.

While Eps8 and whirlin are both required for the proper development and organization of stereocilia and auditory function in mice, human individuals carrying the hypomorphic *EPS8* p.L329P mutation had normal speech acquisition and hearing prior to aminoglycoside treatment. Why, then, does a reduced EPS8-whirlin interaction predispose to auditory dysfunction upon exposure to aminoglycosides? One likely explanation is suggested by the observation that Eps8 and whirlin are critical components of a much larger protein complex at the stereocilia tips. Within such a complex, a weakened EPS8-whirlin interaction might well be compensated by other protein:protein interactions that stabilize the complex sufficiently in order to achieve proper development of stereocilia. Subsequent aminoglycoside treatment may worsen the already suboptimal function of an EPS8 p.L329P-containing tip complex, possibly impinging on other aspects of actin dynamics, ultimately leading to disruption of the patient's stereocilia. In support of this hypothesis, aminoglycoside treatment in mice<sup>21,22</sup> and of patients' fibroblasts (data not shown) resulted in altered F-/G-actin ratios.

Our finding that a homozygous variant in *EPS8* predisposes to ototoxicity after aminoglycoside treatment links this pathological drug response to actin dynamics and might help in devising strategies to counteract this severe side-effect of aminoglycosides.



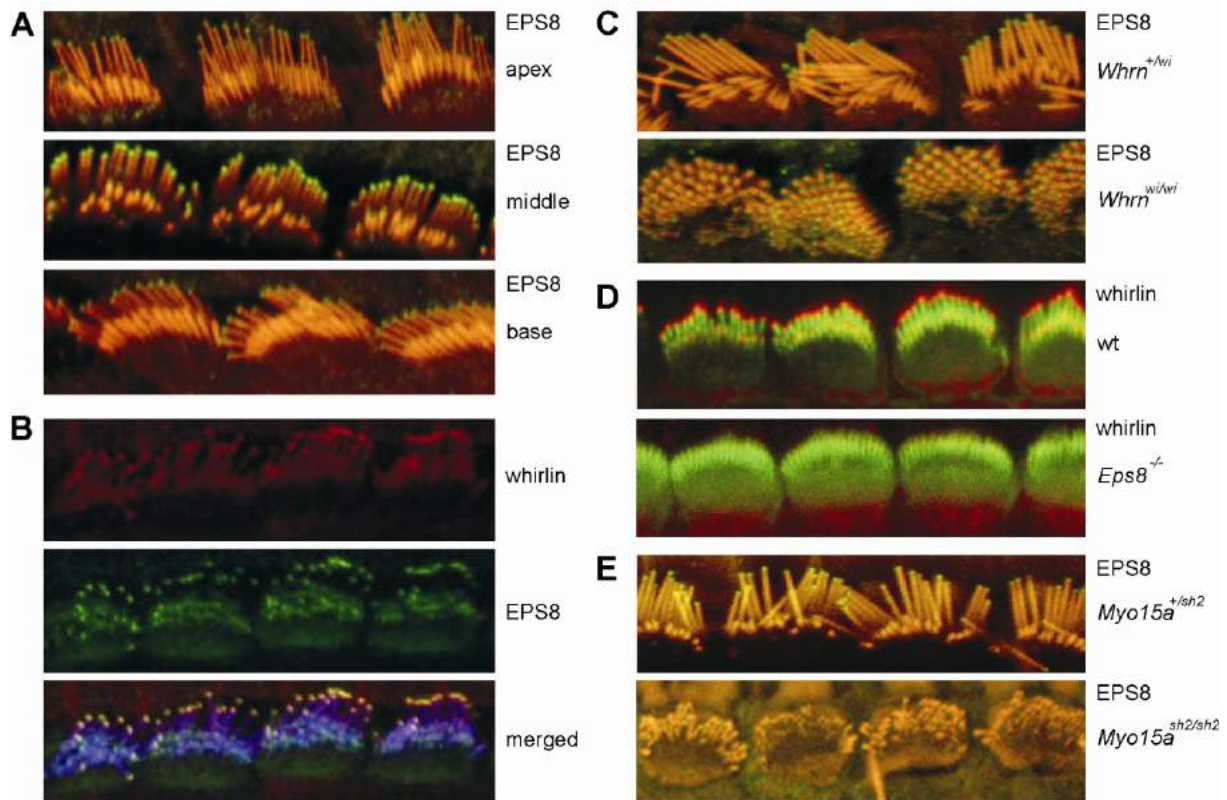


**Figure 3.** Eps8 and whirlin colocalize at the tips of the stereocilia and are mislocalized in *whirler* and *Eps8* KO mice, respectively. Eps8 is absent from the stereocilia tips in *Myo15a<sup>sh2/sh2</sup>* mice. (A) In stereocilia bundles of outer and inner hair cells (OHC; IHC) of wt mice at postnatal day 8 (P8), Eps8 (green) was localized along the stereocilia length (shown by rhodamine/phalloidin-red). Eps8 was also concentrated at the tips of the longest, most lateral stereocilia, and the staining intensity was comparable along the length of the cochlear duct. (B) Localization of Eps8 and whirlin was assessed by immunofluorescence on whole mount cochleae from P7 wt mice. Whirlin (red) and Eps8 (green) colocalize at the tips of the longest stereocilia (stained by rhodamine/phalloidin; blue), but not at the tips of stereocilia from the second and shorter rows. (C) Eps8 labeling (green), in both *Whrn<sup>+/wi</sup>* and *Whrn<sup>wi/wi</sup>* mice at P8, was observed along the length of all stereocilia (stained by rhodamine/phalloidin; red) and in the tips of the tallest stereocilia or in the tips of all stereocilia. This is shown for the IHC of the cochlea middle turn. (D) Localization of whirlin (red) was assessed by immunofluorescence on whole mount cochlea from P7 *Eps8<sup>-/-</sup>* and wt mice. The stereocilia were stained with AlexaFluor 488 /phalloidin (green). A displaced and reduced whirlin expression was observed in the IHC stereocilia of the *Eps8<sup>-/-</sup>* mice compared to wt. (E) Localization of Eps8 in hair bundles of *Myo15a<sup>sh2/sh2</sup>* mice, which lack whirlin and, as in *whirler* mutants, have short stereocilia. In the *Myo15a<sup>sh2/sh2</sup>* mice, Eps8 was present along the length of the OHC and IHC stereocilia (stained by rhodamine/phalloidin; red) in the same pattern as in the *Myo15a<sup>+/sh2</sup>* mice, but without the enhancement of Eps8 at the stereocilia tips. This is shown for the IHCs of the apical turn of the cochlea at P40.

## **Acknowledgements**

We are grateful to all family members that participated in this study, Esther Milz for excellent technical assistance, and Karen Brown and Karin Boss for critically reading the manuscript. This work was supported by the German Federal Ministry of Education and Research (BMBF) by grant number 01GM0801 (E-RARE network CRANIRARE) to B.W.; by the Turkish Academy of Sciences (BW/TUBA-GEBIP/2002-1-20) to B.W.; by the European Commission FP6 Integrated Project EUROHEAR (LSHG-CT-20054-512063 to C.K., H.K., K.P.S., and B.W.); Bernstein Focus for Neurotechnology to T.M.; by the Associazione Italiana per la Ricerca sul Cancro (AIRC) to P.P.D.F., G.C. and N.O.; by the CARIPO Foundations to P.P.D.F. and N.O.; by The Compagnia San Paolo to N.O.; by the European Community (FP6 and FP7), the European Research Council, the Italian Ministries of Education-University-Research (MIUR) and of Health, the Ferrari Foundation, the Monzino Foundation, to P.P.D.F., and the Wellcome Trust (077189 to K.P.S.).

## **Material and methods**

### **Subjects**

All subjects or their legal representatives gave written informed consent to the study. The study was performed in accordance to the Declaration of Helsinki protocols and approved by the local institutional review boards. 19 participating members of the DF48 families underwent general otological examinations, pure-tone audiometry with air and bone conduction at 250Hz, 500Hz, 1000Hz, 2000Hz, 4000Hz, and 8000Hz. All affected individuals in the DF48 family were born to consanguineous parents and have an autosomal recessive predisposition to aminoglycoside-induced hearing impairment. Vestibular evaluation in affected individuals did not display any symptoms of vestibular dysfunction. Developmental milestones were normal and the Romberg test was negative in all patients. DNA from participating family members was extracted from peripheral blood lymphocytes by standard extraction procedures.

### **Linkage analysis and mutation screening**

Genome-wide linkage analysis in available family members of the DF48 family was performed using the Affymetrix GeneChip® Human Mapping 10K SNP Array Xba142 (version 2.0). Genotypes were called by the GeneChip® DNA Analysis Software (GDAS v3.0, Affymetrix). We verified sample genders by counting heterozygous SNPs on the X chromosome. Relationship errors were evaluated with the help of the program Graphical Relationship Representation. The program PedCheck was applied to detect Mendelian errors and data for SNPs with such errors were removed from the data set. Non-Mendelian errors were identified by using the program MERLIN and unlikely genotypes for related samples were deleted. Multipoint LOD scores were calculated using the program ALLEGRO. Haplotypes were reconstructed with ALLEGRO and presented



graphically with HaploPainter. All data handling was performed using the graphical user interface ALOHOMORA. Database searches were done to identify all genes located within the critical region on chromosome 12p13 (NCBI: <http://www.ncbi.nlm.nih.gov/>, GeneDistiller: <http://www.genedistiller.org/>, Ensemble Genome Server: <http://www.ensembl.org/>, and UCSC Genome Bioinformatics: <http://www.genome.ucsc.edu/>). A total of 77 genes located in the shared homozygous interval of approximately 7.44 Mb were analyzed by direct sequencing (Table S1). Primers were designed according to the reference sequences to amplify the coding exons and adjacent splice sites of these candidate genes.

### **Control analysis using Taqman allelic discrimination**

The mutation was analysed in Turkish and German healthy control individuals using Taqman allelic discrimination assay. The primers and probes were designed and purchased from Applied Biosystems (EPS8\_E11: forward primer; GCAAAACCTCCACCTCCTGAT. reverse primer; ACTTACCAGAAGGTTAAATCCG-TGTT, and probe\_wt: 5'-VIC-AAACAGTCA~~A~~GAAATT-MGB-3; probe\_mut: 5'-FAM-AAACAGTCA~~G~~GAAATT-MGB-3). The Amplicon size was 75bp. Each reaction had 20 µl volume contained 10 µl 2 x universal master mix buffer, 700 nM of the primers, 400nM of both probes. 10 ng genomic DNAs were used as templates. Thermal cycling was performed with 10 min at 95°C, then 40 cycles for 15 s at 92°C and for 1 min at 60°C. The fluorescent signals for the individual genotypes were determined after amplification using allelic discrimination program on an ABI PRISM 7500 System (Applied Biosystems).

### **Human fibroblast cultures**

Primary human fibroblasts were maintained at 37°C under a 5% CO<sub>2</sub> atmosphere in DMEM medium (Gibco; Grand Island, NY, USA) supplemented with 10% fetal bovine serum, 100 units/ml of penicilline and 700 ng/ml of amphotericin B, and subcultured at a 1:2 to 1:4 ratio. To test cell viability, cells (passage 8-11) were cultured in 96-well plates (3 x 10<sup>3</sup> of control fibroblasts and 4 x 10<sup>3</sup> of L329P fibroblasts for same confluency). Hydrogen peroxide was purchased from Sigma (St. Louis, MO, USA) and dissolved at 10 mM in medium before starting each experiment. To assess cell damage after kanamycin treatment, cells (passage 7-13) were cultured in 6-well plates (0.7 x 10<sup>5</sup> of control fibroblasts and 1 x 10<sup>5</sup> of L329P fibroblasts). Kanamycin was purchased from AppliChem (Darmstadt, Germany) and dissolved at 100 mg/ml in PBS.

### **Cell viability after kanamycin treatment**

Cell viability was assessed by trypan blue exclusion (n = 5). Cells were incubated with the indicated concentrations of kanamycin in Ham's F-12 medium (Lonza; Verviers, Belgium) for 8 h. After the treatment, cells were washed with PBS and treated with 0.5% Trypsin-EDTA (Gibco, Grand Island, NY, USA). After centrifugation, cells were resuspended in 50 µl of PBS for trypan blue exclusion. Trypan blue was purchased from AppliChem (Darmstadt, Germany). Test of significance was determined by student's t test.

### **MTT assay for cell viability**

The viability of the fibroblasts was determined by measuring the level of 3-(4, 5-dimethylthiazol-2-yl)-2,5-diphenyltetrazolium bromide (MTT) reduction to formazan (n = 5). To induce oxidative stress, the fibroblasts

were incubated with the indicated concentrations of hydrogen peroxide for 2 h. After the treatment, the cells were washed twice with 100  $\mu$ l of PBS, and MTT (Sigma; St. Louis, MO, USA, 100  $\mu$ g/100  $\mu$ l of DMEM) was added to each well. The fibroblasts were then incubated at 37°C for 2.5 h. After removing the medium, 100  $\mu$ l of DMSO were added to each well to dissolve the formazan crystals. The absorbance was measured at 578 nm using a model Immuno Reader NJ-2000 (Nippon InterMed K.K.; Tokyo, Japan). Test of significance was determined by student's t test.

### **Cloning**

All constructs were generated to make use of the Gateway cloning technology (Invitrogen; Calsbad, USA)

### **Liquid $\beta$ -galactosidase assay**

PJ69-4 $\alpha$  yeast cells co-transformed with pAD-whirlin constructs and pBD-EPS8 constructs were cultured in selective medium lacking Trp and Leu (SD-WL). After two overnight incubation steps at 30 °C, the optical density of the cultures were determined at a wavelength of 600 nm. Cell lysis and subsequent staining reactions were performed by using the Yeast  $\beta$ -galactosidase assay kit (Pierce; Rockford, USA) according to manufacturer's instructions. Absorbance was measured at a wavelength of 420 nm.

### **GST pull-down**

The GST-fusion proteins were produced by transforming *E.coli* BL21-DE3 with pDEST15-EPS8 wild type or pDEST15-EPS8 L329P constructs. Cells were overnight induced at 30°C with 0.5 mM IPTG and subsequently lysed with STE buffer [1% Sarkosyl, 1% Triton X-100, 5 mM 1,4-dithiothreitol (DTT)] supplemented with complete protease inhibitor cocktail (Roche, Germany). Lysates were incubated with glutathione-Sepharose 4B beads (Amersham Biosciences, USA). The GST fusion proteins bound to the beads were washed with lysis buffer and TBSTD [TBS with 1% Triton X-100 and 2 mM DTT]. The amount of bound GST-fusion protein was verified on a NUPAGE Novex 4-12% Bis-Tris SDS-PAGE gel which was stained with SimplyBlue SafeStain (Invitrogen; Carlsbad, USA). HA-tagged whirlin full length (aa 1-907) were produced by transfecting COS-1 cells with pcDNA3-HA-Whirlin fl using Effectene transfection reagent (QIAGEN; Hilden, Germany) according the manufacturer's instruction. Twenty-four hours after transfection the cells were washed with phosphate-buffered saline (PBS) and subsequently lysed on ice in IP lysis buffer [50 mM Tris-HCL pH 7.5, 150 mM NaCl, 0.5% Nonidet-P40, 1 mM Sodium-orthovanadate orthovanadate supplemented with complete protease inhibitor cocktail (Roche, Germany). The lysate was incubated for 2 hours at 4°C with equal amounts of beads with GST or beads with GST-fusion proteins. The beads were washed several times with IP lysis buffer and further heated in 1 x SDS sample buffer. The proteins were analyzed on a NUPAGE Novex 4-12% Bis-Tris SDS-PAGE gel (Invitrogen; Carlsbad, USA) and detected by Western blot analysis using the Odyssey Infrared Imaging System (LI-COR, USA). The tagged proteins were detected by an anti-HA antibody. IRDye800 goat-anti-mouse was used as a secondary antibody (Molecular Probes, USA).

### **Co-localization in COS-1 cells**

To determine the cellular localization of human EPS8 wt, EPS8 L329P, EPS8 L329V and whirlin in COS-1 cells, we cloned the EPS8 cDNA's into pDest501, resulting in N-terminally fused eCFP-EPS8 fusion proteins. Whirlin was cloned into pDest733 resulting in N-terminally mRFP-whirlin fusion protein. COS-1 cells were co-transfected with mRFP-whirlin together with eCFP-EPS8 wt, eCFP-EPS8 L329P, eCFP-EPS8 L329V by using Lipofectamine (Invitrogen; Carlsbad, USA) according to the manufacturer's instructions. Twenty hours after transfection the cells were washed with PBS, fixed with 4% paraformaldehyde for 20 minutes, washed with PBS, permeabilized for 6 minutes with 0.2% Triton/PBS and mounted with Vectashield containing DAPI (Vector Laboratories, Inc, UK). Images were taken with an Axioplan2 Imaging fluorescence microscope (Zeiss) equipped with a DC350FX camera and processed using Adobe Photoshop (Adobe systems, USA)

### **Mice and housing conditions**

Mice were housed on a 12-hrs light/dark cycle and had *ad libitum* access to water and food. *Eps8<sup>-/-</sup>* mice were backcrossed for 18 generations into C57BL/6 mice and then used for the experiments. Behavioural experiments were performed on mice derived from heterozygous crosses, morphological analysis on second or third generation animals from wildtype or *Eps8<sup>-/-</sup>* colonies. All experiments were performed in accordance with the guidelines established in the IFOM-IEO Campus Principles of Laboratory Animal Care (directive 86/609/ECC).

### **Preyer's Reflex measurement**

Preyer's reflex was measured in *Eps8<sup>-/-</sup>* or wildtype mice at 14 days after birth and in adult mice. The observer was blind to the genotype. Mice were placed singly in a cage and backward movement of the pinna was scored after a loud handclap. Mice that showed backward movement of the ear's pinna were scored positive, mice that lacked backward movement were scored negative.

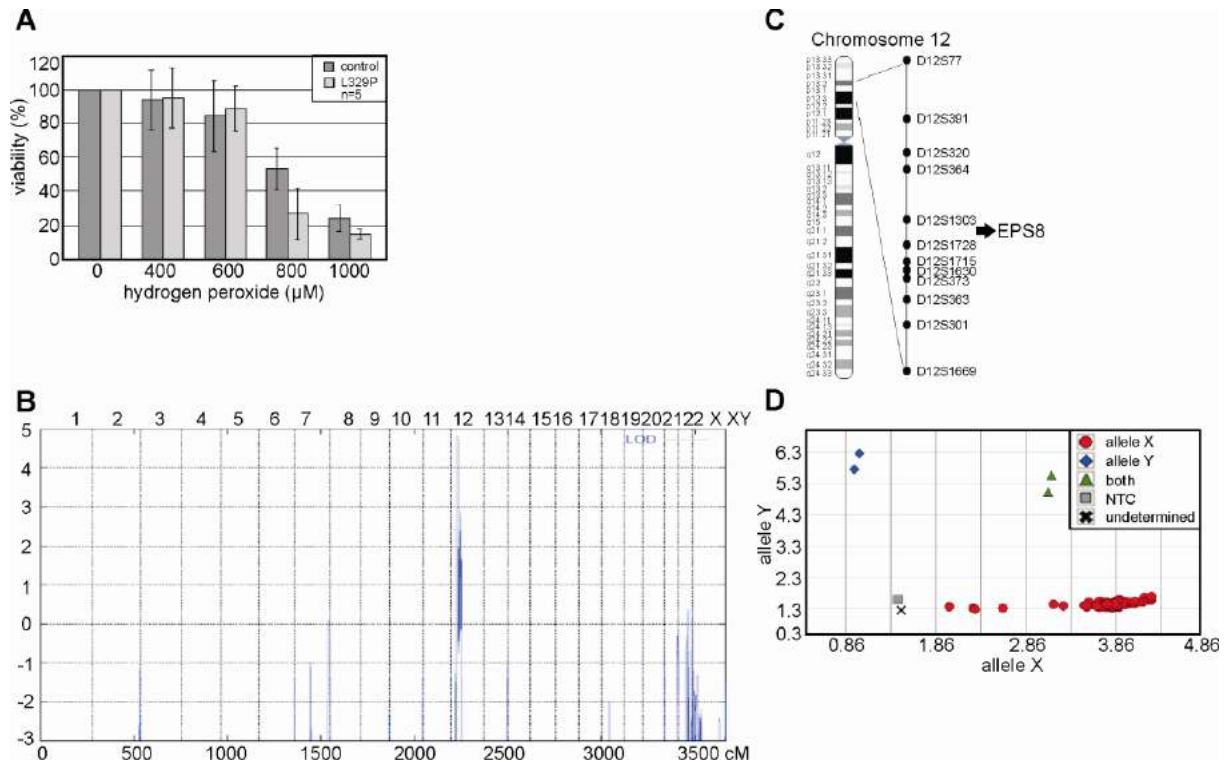
### **Immunofluorescence**

Freshly isolated inner ear tissues were fixed in 4% paraformaldehyde for 2 h at room temperature as previously described<sup>17</sup>. Immunolocalization was performed using the primary antibodies: 1:100 monoclonal anti-EPS8 (BD Biosciences, USA), 1:250 guinea pig affinity purified anti-whirlin, 1:400 rabbit polyclonal anti-whirlin antibodies (a kind gift from Dr T.B. Friedman, NIDCD, described<sup>19</sup>). Actin filaments were counterstained with rhodamine or Alexa Fluor 633 labelled phalloidin (Molecular Probes, USA). As secondary antibodies anti mouse Alexa Fluor 488, anti rabbit Alexa Fluor 555 (Molecular Probes, USA) or appropriate secondary fluorescently-labelled from Jackson laboratories, USA) were used. Samples were then mounted using glycerol-antifade or antifade Gold (Molecular Probes, USA) and analyzed at the Leica DM IRE2 HC Fluo TCS confocal microscope or at the LSM 510 Meta confocal microscope (Zeiss; Welwyn Garden City) using a 63x 1.4 n.a. objective. Postacquisition image analyses were performed using ImageJ (<http://rsbweb.nih.gov/ij/>) software or Adobe Photoshop CS2.

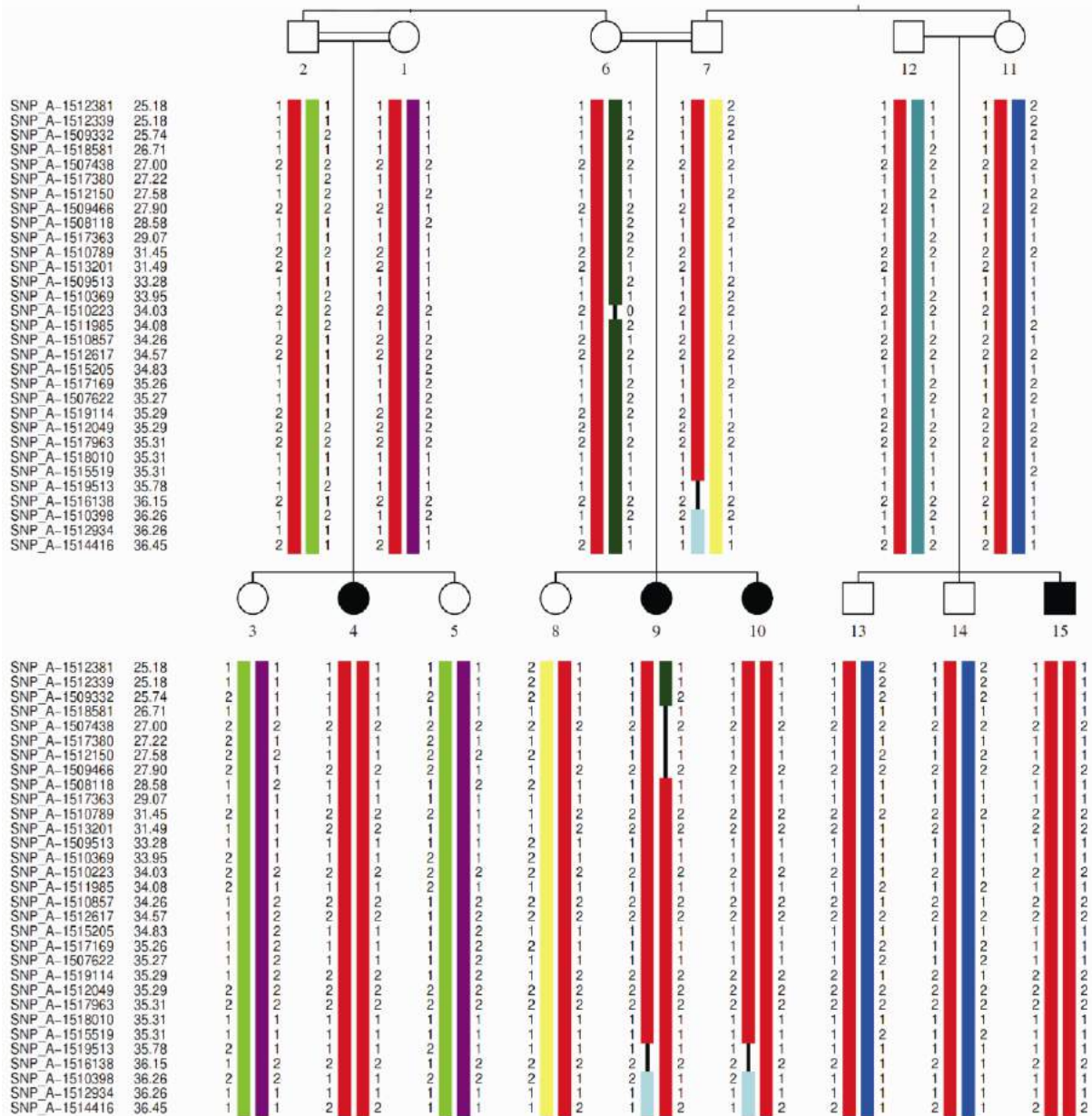
**Expression analysis by QPCR and Western Blot**

Cochlea from postnatal day 5 and 7 were dissected and immediately flash frozen in liquid nitrogen. For QPCR cochlear RNA was extracted with the TRIzol<sup>®</sup> reagent (Invitrogen; Carlsbad, USA), followed by DNase treatment. Two mg of RNA were reverse-transcribed using SuperScript First-Strand Synthesis System (Invitrogen; Carlsbad, USA). Expression levels were determined using Taqman chemistry on an ABI 7900HT sequence detection system (Applied Biosystems). For Western Blotting cochlea were homogenized in RIPA buffer and 20 µg protein was resolved by SDS-PAGE, transferred to a Nylon membrane and immunoblotted with an anti-EPS8 antibody.

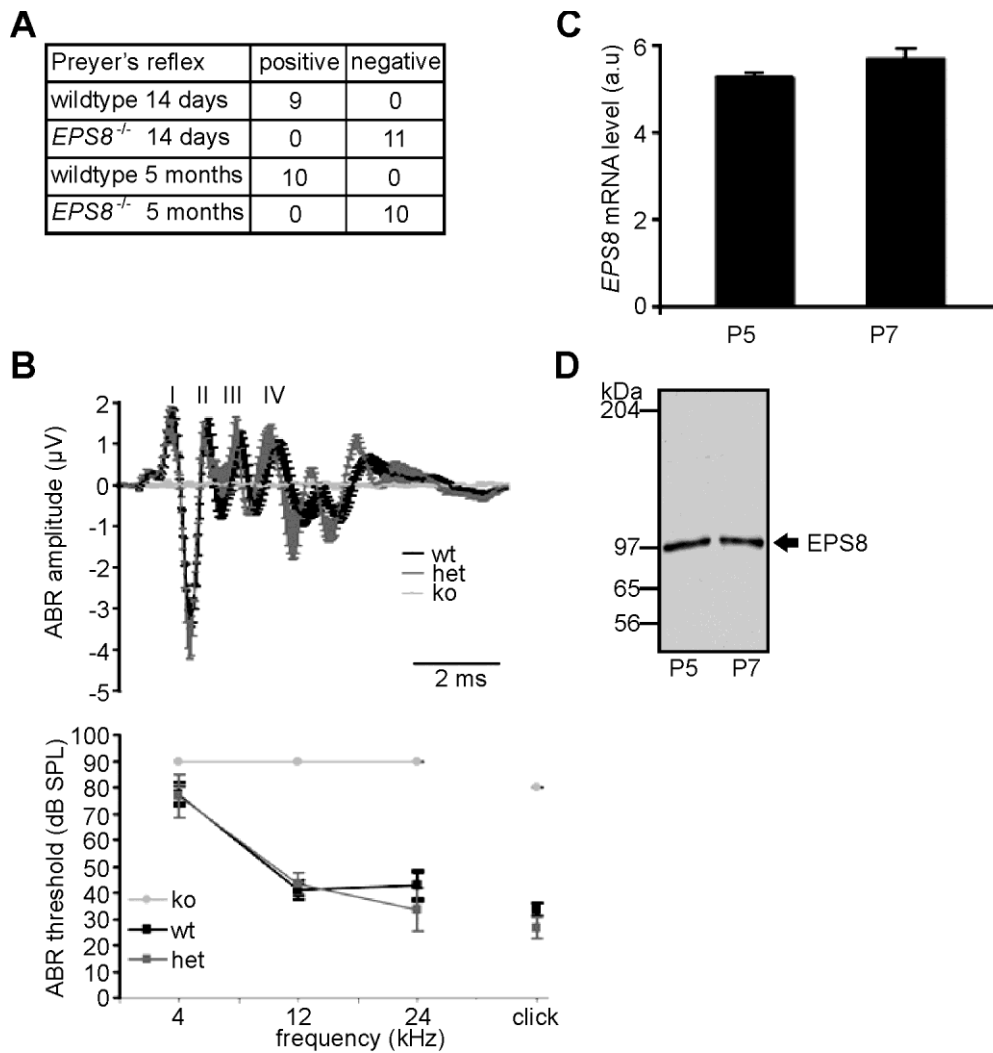
## Supplementary material



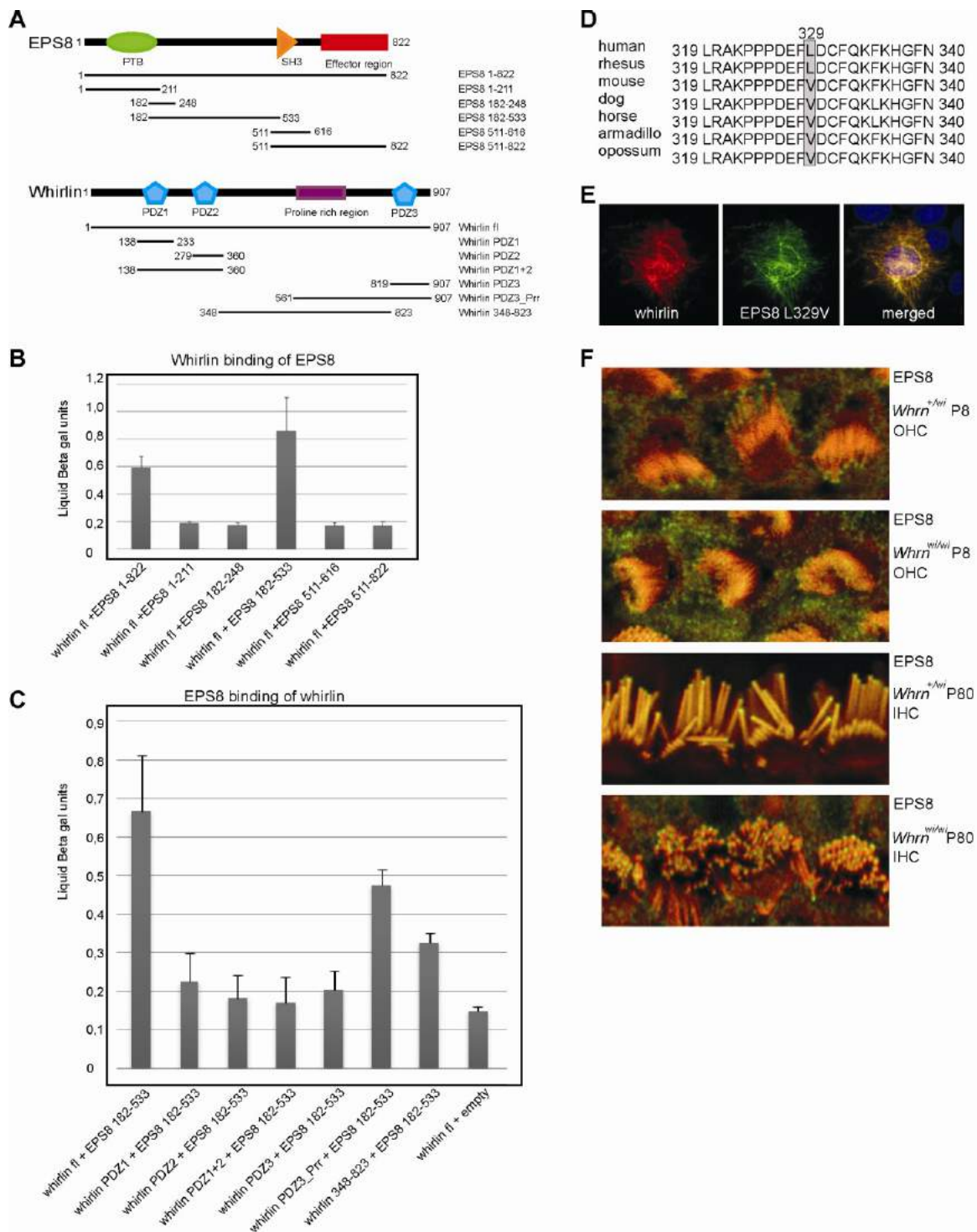
**Supplementary Figure 1.** Mapping and gene identification. **(A)** Hydrogen peroxide results in a cellular stress response. The p.L329P variant causes a decreased cell viability in hydrogen peroxide treated homozygous fibroblast cells of the patient V:7 (grey bars) compared to homozygous wt fibroblasts of a healthy control individual (black bars). **(B)** A genome scan of the family using a 10K SNP array resulted in a LOD score of 4.8 at chromosome 12. **(C)** Fine-mapping using microsatellite markers resulted in the critical region flanked by the markers D12S77 and D12S1669 at 12p12.3. Sequence analysis of all 77 genes located in the critical region identified a causative variation in *EPS8*. **(D)** The *EPS8* L329P mutation was not identified in 1,000 control chromosomes by a TaqMan assay.



**Supplementary Figure 2.** SNP haplotypes of the linked region on chromosome 12p12.3. All affected individuals are homozygous for the haplotype marked in red. The critical region is defined by recombinations observed in individual 9 and by SNP\_A-1509332 (rs2416669) and SNP\_A-1510398 (rs726391).



**Supplementary Figure 3.** *Eps8* is expressed in the cochlea and *Eps8*<sup>-/-</sup> mice are profoundly hearing impaired. (A) *Eps8*<sup>-/-</sup> and their wild type littermates were tested for the Preyer's reflex following a loud handclap. Backward movement of the pinna was counted as positive Preyer's reflex, no reaction was valued negative. All tested *Eps8*<sup>-/-</sup> mice at P14 and 5 months of age had a negative Preyer's reflex. (B) Lack of auditory brainstem responses (ABRs) to click stimuli of 80 dB (peak equivalent) in *Eps8*<sup>-/-</sup> mice (light gray; n=3). The ABRs for wt (black; n=4) and *Eps8*<sup>+/-</sup> (dark gray; n=3) mice are comparable. Hearing thresholds were obtained by ABR recordings. The average threshold of *Eps8*<sup>-/-</sup> mice (light gray; n=3) exceeds 80 dB (peak equivalent) for clicks and 90 dB (sound pressure level) for 4-24 kHz tone bursts. For comparison, the mean audiograms of wt (black; n=4) and *EPS8*<sup>+/-</sup> (dark gray; n=3), are shown. (C) *Eps8* mRNA levels in postnatal day 5 (P5) and P7 wt cochlea were accessed using quantitative PCR. Values (x10<sup>-3</sup>) are normalized to GAPDH levels and expressed in arbitrary units (a.u.) (D) *Eps8* protein expression was analyzed in P5 and P7 wt cochlea by Western blot analysis. The molecular weight of the marker is given in kiloDaltons (kDa). The specific *Eps8* protein band of 97kDa is indicated.



**Supplementary Figure 4.** Interaction domains of EPS8 and whirlin. The conservation around the mutation of *EPS8* and its localization in the young and adult *whirler* mice. (A) Schematic protein structure of EPS8 and whirlin and fragments encoded by deletion constructs with the corresponding amino acids (aa) are depicted. (B) Yeast two-hybrid analysis showed a specific interaction between full length whirlin and the EPS8 region containing aa 182-533. (C) Yeast two-hybrid analysis revealed a specific interaction between EPS8 aa 182-533



and whirlin aa 561-907 and aa 348-823 resulting in aa 561-823 of whirlin binding to Eps8. **(D)** The region (aa 319-340) surrounding the EPS8 L329P variation is highly conserved among species. In human and rhesus the aa at position 329 is a leucine, but in lower mammals it is a valine. **(E)** Cotransfections of COS-1 cells with plasmids encoding mRFP-whirlin and eCFP-EPS8 p.L329V. In cells expressing both EPS8 p.L329V and whirlin, the latter was recruited to the actin-like structures and colocalized with EPS8. This result is similar when using eCFP-EPS8 wt (Fig. 2D). **(F)** Localization of Eps8 in young and adult *whirler* mice. Eps8 labeling (green), in both *Whrn*<sup>+/wi</sup> and *Whrn*<sup>wi/wi</sup> mice at P8, was observed along the length and in the tips of the stereocilia (stained by rhodamine/phalloidin; red). This is shown for the OHCs of the cochlear middle turn. Eps8 labeling was also observed in the apical parts of supporting cells. The same labeling was observed in both *Whrn*<sup>+/wi</sup> and *Whrn*<sup>wi/wi</sup> mice at P80. This is shown for the IHC of the cochlea middle turn.

Gene name	No. of exons	SNPs found
GABARAPL1	4	rs7248
KLRD1	6	rs2302489
KLRK1	11	rs2617151, rs2255336, rs2255353
KLRC4	4	rs1841957
KLRC3	6	rs2741881, rs2682490, rs2682491, rs2741882, c.588-9C>T, c.678+128C>T
KLRC2	6	rs35175989, rs2981590, rs2981593, rs3003
KLRC1	8	rs2682472, rs2734441
KLRA1	7	rs2168749, rs2244387, rs2607890
FLJ10292	5	rs10845182, rs10845181, rs2125089, rs2125090, rs3947920, rs2125091, rs10772333, rs9988929, rs34751290, rs4763209
STYK1	11	rs2277410, rs2290717, rs2125087, rs1078437, rs2900467
CSDA	10	
TAS2R7	1	
TAS2R8	1	rs2537817
TAS2R9	1	
TAS2R10	1	rs597468
PRR4	4	rs2227296, rs1047699
PRH1	5	rs61928643, rs11557132, rs35304582, rs2597984, ENSSNP10553847, rs11557132
TAS2R13	1	
PRH2	3	rs1049112
TAS2R14	1	rs7138535, rs3741843
TAS2R50	1	
TAS2R49	1	rs1463237, rs4388985, rs7135018
TAS2R48	1	rs12313469
TAS2R44	1	rs12370363, rs10845293, rs10772423, rs34763234, rs10845295
TAS2R46	1	rs2708381
TAS2R43	1	
TAS2R47	1	
TAS2R42	1	rs34736072, rs1650019, rs1451772, rs1669412, rs1669411, rs1650017, rs1669413
PRB3	5	rs59152757
PRB4	4	
PRB2	4	
PRB1	4	
LOC440084	4	rs11609202
ETV6	8	rs2724601, rs1058028

BCL2L14	10	rs1641728, rs1797647
LRP6	23	rs10219768, c.56-65G>C, rs7979485, rs1012672, rs12313200
MANSC1	4	rs3741800, rs3825260, rs4763282, rs1861676
LOH12CR1	4	rs10772552, rs9412
DUSP16	7	c.-489G>A
CREBL2	4	
GPR19	1	
CDKN1B	3	
APOLD1	3	
DDX47	12	rs1051374, rs12425168
GPRC5A	4	c.-614A>G, rs2075288
GPRC5D	4	rs1291345, rs1291346
HEBP1	4	rs850918
KIAA1467	13	rs1386005
GSG1	8	rs2291396, rs1872626
EMP1	5	
C12orf36	3	rs11609202, c.G122A (p.R41Q) → RefSeq was now permanently suppressed for this gene, because it is now thought that this gene does not encode a protein
GRIN2B	13	rs1806201
ATF7IP	16	rs4479040, rs10624410
FLJ22662	6	rs10846023, rs11056018, rs1345531, rs3983700, rs10846013, rs1600
GUCY2C	27	rs58911033, rs1420635, rs7314345, rs7313027, rs10772800
HIST4H4	1	
H2AFJ	1	rs1047137
WBP11	12	
C12orf69	2	
C12orf60	2	
ART4	3	rs1861698, rs3088189, rs11276, rs3088190
MGP	4	rs4236
ERP27	7	
ARHGDI1B	6	
PDE6H	4	rs11056264, rs12228166, rs7315802
RERG	5	
PTPRO	27	rs4764197, rs4764199, rs1050646, rs2302688, rs960666, rs6488782, rs7134888, rs7132826, rs5796639, rs1024843, rs1558787
EPS8	21	c.986C>T (p.L329P) very recently listed as rs79739141, rs4763427, rs4237955
STRAP	10	
DERA	9	rs2290978
MGST1	4	rs2975152
LMO3	6	
FLJ22655	6	
PIK3C2G	33	rs35277916, rs11044004
PLCZ1	16	rs12306752, rs10841080, rs12300257, c.C606T (p.D202D), rs56185424, rs10523511, rs11044253, rs2306798
CAPZA3	1	rs1075421
PLEKHA5	30	rs6486945, rs7316780

**Supplementary Table 1.** All 77 annotated genes within the critical region which are sequenced.

**References**

1. Forge A, Schacht J. Aminoglycoside antibiotics. *Audiol Neurootol*. 2000;5:3-22.
2. Brummett RE, Morrison RB. The incidence of aminoglycoside antibiotic-induced hearing loss. *Arch Otolaryngol Head Neck Surg*. 1990;116:406-410.
3. Davis BD. Mechanism of bactericidal action of aminoglycosides. *Microbiol Rev*. 1987;51:341-350.
4. Estivill X, Govea N, Barcelo E, et al. Familial progressive sensorineural deafness is mainly due to the mtDNA A1555G mutation and is enhanced by treatment of aminoglycosides. *Am J Hum Genet*. 1998;62:27-35.
5. Warchol ME. Cellular mechanisms of aminoglycoside ototoxicity. *Curr Opin Otolaryngol Head Neck Surg*. 2010;18:454-458.
6. Matoskova B, Wong WT, Salcini AE, et al. Constitutive phosphorylation of eps8 in tumor cell lines: relevance to malignant transformation. *Mol Cell Biol*. 1995;15:3805-3812.
7. Disanza A, Mantoani S, Hertzog M, et al. Regulation of cell shape by Cdc42 is mediated by the synergic actin-bundling activity of the Eps8-IRSp53 complex. *Nat Cell Biol*. 2006;8:1337-1347.
8. Innocenti M, Frittoli E, Ponzanelli I, et al. Phosphoinositide 3-kinase activates Rac by entering in a complex with Eps8, Abi1, and Sos-1. *J Cell Biol*. 2003;160:17-23.
9. Scita G, Nordstrom J, Carbone R, et al. EPS8 and E3B1 transduce signals from Ras to Rac. *Nature*. 1999;401:290-293.
10. Scita G, Tenca P, Areces LB, et al. An effector region in Eps8 is responsible for the activation of the Rac-specific GEF activity of Sos-1 and for the proper localization of the Rac-based actin-polymerizing machine. *J Cell Biol*. 2001;154:1031-1044.
11. Croce A, Cassata G, Disanza A, et al. A novel actin barbed-end-capping activity in EPS-8 regulates apical morphogenesis in intestinal cells of *Caenorhabditis elegans*. *Nat Cell Biol*. 2004;6:1173-1179.
12. Offenhauser N, Borgonovo A, Disanza A, et al. The eps8 family of proteins links growth factor stimulation to actin reorganization generating functional redundancy in the Ras/Rac pathway. *Mol Biol Cell*. 2004;15:91-98.
13. Kishan KV, Scita G, Wong WT, et al. The SH3 domain of Eps8 exists as a novel intertwined dimer. *Nat Struct Biol*. 1997;4:739-743.
14. Tocchetti A, Soppo CB, Zani F, et al. Loss of the actin remodeler Eps8 causes intestinal defects and improved metabolic status in mice. *PLoS One*. 2010;5:e9468.
15. Holme RH, Kiernan BW, Brown SD, et al. Elongation of hair cell stereocilia is defective in the mouse mutant whirler. *J Comp Neurol*. 2002;450:94-102.
16. Mburu P, Mustapha M, Varela A, et al. Defects in whirlin, a PDZ domain molecule involved in stereocilia elongation, cause deafness in the whirler mouse and families with DFNB31. *Nat Genet*. 2003;34:421-428.
17. Rzadzinska AK, Schneider ME, Davies C, et al. An actin molecular treadmill and myosins maintain stereocilia functional architecture and self-renewal. *J Cell Biol*. 2004;164:887-897.

18. Michalski N, Michel V, Bahloul A, et al. Molecular characterization of the ankle-link complex in cochlear hair cells and its role in the hair bundle functioning. *J Neurosci*. 2007;27:6478-6488.
19. Belyantseva IA, Boger ET, Naz S, et al. Myosin-XVa is required for tip localization of whirlin and differential elongation of hair-cell stereocilia. *Nat Cell Biol*. 2005;7:148-156.
20. Mburu P, Romero MR, Hilton H, et al. Gelsolin plays a role in the actin polymerization complex of hair cell stereocilia. *PLoS One*. 2010;5:e11627.
21. Jiang H, Sha SH, Schacht J. Rac/Rho pathway regulates actin depolymerization induced by aminoglycoside antibiotics. *J Neurosci Res*. 2006;83:1544-1551.
22. Khanday FA, Yamamori T, Mattagajasingh I, et al. Rac1 leads to phosphorylation-dependent increase in stability of the p66shc adaptor protein: role in Rac1-induced oxidative stress. *Mol Biol Cell*. 2006;17:122-129.



# Chapter 4

---

## **Usher syndrome and Leber congenital amaurosis are molecularly linked via a novel isoform of the centrosomal ninein-like protein**

Erwin van Wijk<sup>1,2,5</sup>, Ferry F.J. Kersten<sup>1-5</sup>, Aileen Kartono<sup>1,4</sup>, Dorus A. Mans<sup>1</sup>, Kim Brandwijk<sup>1</sup>, Stef J.F. Letteboer<sup>1</sup>, Theo A. Peters<sup>2,5</sup>, Tina Märker<sup>6</sup>, Xiumin Yan<sup>7</sup>, Cor W.R.J. Cremers<sup>2,5</sup>, Frans P.M. Cremers<sup>1,4</sup>, Uwe Wolfrum<sup>6</sup>, Ronald Roepman<sup>1,4,#</sup> and Hannie Kremer<sup>2,4,5,#</sup>

# These authors contributed equally to this work

<sup>1</sup>Department of Human Genetics, <sup>2</sup>Department of Otorhinolaryngology, Head and Neck Surgery and <sup>3</sup>Department of Ophthalmology, Radboud University Nijmegen Medical Centre, Nijmegen, The Netherlands, <sup>4</sup>Nijmegen Centre for Molecular Life Sciences, and <sup>5</sup>Donders Institute for Brain, Cognition and Behaviour, Radboud University Nijmegen, Nijmegen, The Netherlands, <sup>6</sup>Department of Cell and Matrix Biology, Institute of Zoology, Johannes Gutenberg University of Mainz, Mainz, Germany, <sup>7</sup>Department of Cell Biology, Max-Planck Institute of Biochemistry, Martinsried, Germany.

---

*Human Molecular Genetics* 2009; 18 (1): 51-64

---





## **Abstract**

Usher syndrome (USH) and Leber congenital amaurosis (LCA) are autosomal recessive disorders resulting in syndromic and nonsyndromic forms of blindness. In order to gain insight into the pathogenic mechanisms underlying retinal degeneration, we searched for interacting proteins of USH2A isoform B (USH2A<sup>isoB</sup>) and the *LCA5*-encoded protein lebercilin. We identified a novel isoform of the centrosomal ninein-like protein, hereby named Nlp isoform B (Nlp<sup>isoB</sup>), as a common interactor. Although we identified the capacity of this protein to bind calcium with one of its three EF hand domains, the interaction with USH2A<sup>isoB</sup> did not depend on this. Upon expression in ARPE-19 cells, recombinant Nlp<sup>isoB</sup>, lebercilin, and USH2A<sup>isoB</sup> were all found to co-localize at the centrosomes. Staining of retinal sections with specific antibodies against all three proteins revealed their co-localization at the basal bodies of the photoreceptor connecting cilia. Based on this subcellular localization and the nature of their previously identified binding partners, we hypothesize that the pathogenic mechanisms for LCA and USH show significant overlap and involve defects in ciliogenesis, cilia maintenance, and intraflagellar and/or microtubule-based transport. The direct association of Nlp<sup>isoB</sup> with USH2A<sup>isoB</sup> and lebercilin indicates that *Nlp* can be considered as a novel candidate gene for USH, LCA and allied retinal ciliopathies.



## Introduction

Usher syndrome (USH) is the most common cause of combined deaf-blindness with a prevalence of about 1 in 20,000 in the Caucasian population <sup>1-3</sup>. It is a clinically and genetically heterogeneous disorder, for which three different types can be distinguished based on the severity and progression of the hearing loss, the presence or absence of vestibular symptoms and the age of onset of retinitis pigmentosa (RP) <sup>4</sup>. To date, six different genetic loci have been identified for USH type I (USH1), three loci for USH type II (USH2) and one locus for USH type III (USH3) (reviewed in <sup>5</sup>). Mutations have been identified in the genes encoding myosin VIIa, harmonin, cadherin 23, protocadherin 15, and SANS as the underlying defect in USH1b, -c, -d, -f and -g, respectively <sup>5-11</sup>. Defects in USH2A, GPR98 (VLGR1) and whirlin are causative for USH2a, -c and -d, respectively <sup>12-15</sup>. USH3 is caused by mutations in the clarin-1 encoding *USH3A* gene <sup>16</sup>.

Recently, we and others have shown that all known USH1 and USH2 proteins are present in a protein network, the Usher interactome, in which harmonin and whirlin play the role of key organisers that interconnect the other USH proteins <sup>17-22</sup>. Localization studies in rodents revealed that this interactome is present in the stereocilia and the synaptic region of hair cells in the cochlea, and in the synaptic region of photoreceptor cells. Except for harmonin, all known USH1 and USH2 proteins are also present at the region of the connecting cilium of photoreceptor cells, a microtubule-based structure which separates the outer segments from the inner segments <sup>21</sup>. This region encompasses the connecting cilium, its basal body and centriole as well as the periciliary region surrounding the connecting cilium. In the region of the connecting cilium, the Usher interactome may be recruited via PDZ (postsynaptic density 95, PSD-95; discs large, Dlg; zonula occludens-1, ZO-1) domain based interactions with whirlin <sup>20,21,23</sup>. Based on the localization of the Usher protein network to the region of the connecting cilium and the identification of ciliary abnormalities in photoreceptor cells and sperm cells of several patients with USH <sup>24</sup>, the syndrome can be considered as a (retinal) ciliopathy <sup>25</sup>. Recent phenotypic data of patients with different Usher subtypes (USH1b, -1f, -2a or -2c) also suggests that the primary pathogenic insult does not take place at the photoreceptor synapse <sup>26</sup>.

Leber congenital amaurosis (LCA) is another clinically and genetically heterogeneous recessive disorder which has been described as a severe form of retinitis pigmentosa presenting before the age of one year with the absence of photoreceptor function<sup>27</sup>. Patients present with profound visual loss, nystagmus, poorly reactive pupils and a markedly diminished or non-detectable electro-retinogram<sup>27,28</sup>. Defects in the centrosomal and cilia-associated proteins RPGRIP1, CEP290 and lebercilin (encoded by *LCA5*) have been identified to be associated with LCA<sup>29-31</sup>, implicating a role of these proteins in ciliary processes.

At the moment, mutations in several different genes have been described to be the underlying cause of USH and LCA, but the molecular basis of the pathogenic defects of these syndromes still remains largely elusive. Based on similarities in clinical manifestations and the subcellular localization of proteins involved in USH and a number of proteins involved in LCA, the pathogenic mechanisms underlying both disorders might significantly overlap. In order to gain a better insight into the molecular basis of USH and LCA we searched for novel interacting partners of the recently identified lebercilin (*LCA5*) and the intracellular region of USH2A<sup>isoB</sup> by using yeast two-hybrid screening.

In this study we show that both lebercilin and the intracellular region of USH2A<sup>isoB</sup>, directly interact with a novel isoform of the second member of the ninein-family, the centrosomal ninein-like protein (Nlp<sup>isoB</sup>), encoded by the *Nlp* (*KIAA0980*) gene. Nlp<sup>isoB</sup> is a novel component of the Usher interactome, connecting USH and LCA at the molecular level, and the *Nlp* gene can therefore be considered as a novel candidate for USH, LCA, and related disorders.

## Results

### **A novel isoform, isoform B, of the centrosome associated Ninein-like protein interacts with USH2A and lebercilin**

Yeast two-hybrid screens of an oligo d(T) primed human retina cDNA library were performed to identify proteins interacting with lebercilin or with the intracellular region of USH2A<sup>isoB</sup>. Analysis of positive clones that activated all reporter genes, revealed a common interactor for

both bait proteins. In total, eleven overlapping clones of a novel splice-variant of the centrosomal ninein-like protein (Nlp), hereby named Nlp isoform B (Nlp<sup>isoB</sup>), were identified. By using the intracellular region of USH2A<sup>isoB</sup> as a bait, two clones for Nlp<sup>isoB</sup> were identified. These encode amino acids 598-1033 and 658-1033, respectively. For lebercilin, four Nlp clones encoding amino acids 598-1033 and five clones encoding amino acids 658-1033 were identified. The transcript encoding Nlp<sup>isoB</sup> lacks exon 17 from the originally described *Nlp* gene, resulting in in-frame skipping of 349 amino acids after residue 734. The specificity of the interaction in the yeast two-hybrid assay was determined by co-transforming pAD-Nlp<sup>isoB</sup> (aa 658-1033) with the pBD-Gal4 vector expressing the non-related p63 protein. No interaction was observed performing this control experiment (data not shown).

Bioinformatic analysis of the Nlp<sup>isoB</sup> protein (SMART database; <http://smart.embl-heidelberg.de/>) identified three regions that are predicted to form EF hand domains, potentially Ca<sup>2+</sup>-binding, which are known to be involved in the interaction with  $\gamma$ -tubulin<sup>32</sup>. In addition, the C-terminal region was predicted to form an intermediate filament (IF) domain (aa 656-925), likely to be involved in protein-protein interactions (Pfam Home Page; <http://pfam.sanger.ac.uk/>) (Fig. 1A).

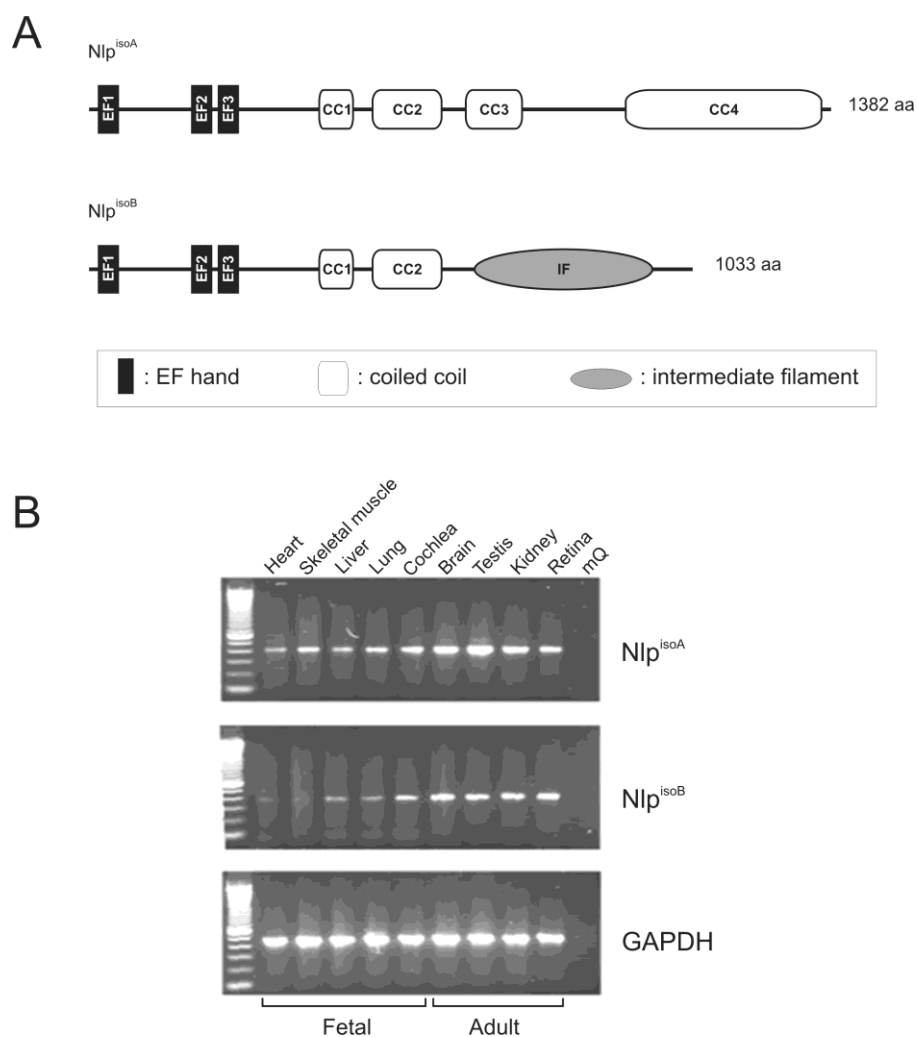


**Figure 1.** Schematic representation of the protein structure of Nlp<sup>isoA</sup> and Nlp<sup>isoB</sup>. **(A)** The predicted EF hands (EF) 1, 2 and 3 are formed by amino acids 11-39, 200-228 and 237-265, respectively. Coiled-coil domains (CC) 1, 2, 3 and 4 are formed by amino acids 384-425, 470-579, 621-699 and 1046-1375, respectively, and the predicted intermediate filament domain (IF) is formed by amino acids 656-925. **(B)** Semi-quantitative RT-PCR for transcripts encoding Nlp<sup>isoA</sup> and Nlp<sup>isoB</sup> in human fetal and adult tissues. Shown are the samples that were taken after 35 cycles. The results are representative for the samples taken after 25 and 30 cycles. As a control, RT-PCR analysis of the household gene *GAPDH* was performed. The transcripts for Nlp<sup>isoA</sup> and Nlp<sup>isoB</sup> show a similar distribution with the strongest expression in fetal cochlea and adult brain, testis and kidney.

The intermediate filament domain, however, was predicted with low significance (E-value:  $5.2 \times 10^{-1}$ ). We analyzed the spatial and temporal expression pattern of transcripts encoding Nlp<sup>isoA</sup> and Nlp<sup>isoB</sup> by semi-quantitative RT-PCR, using several human fetal and adult tissues. No major differences in expression were observed for isoforms A and B, indicating that both isoforms function in the same tissues (Fig. 1B). However, differences at the cellular level cannot be excluded.

Deletion constructs were made of the intracellular region of USH2A<sup>isoB</sup> and Nlp<sup>isoB</sup> and tested in yeast two-hybrid analysis to determine the regions that are involved in the interaction. By using these deletion constructs we were able to show that in USH2A, the interacting region is located in the fragment containing amino acids 5124-5196 and in Nlp<sup>isoB</sup> in the fragment containing the predicted intermediate filament domain (aa 656-925) (Fig. 2A). In order to further pinpoint the domains involved in the interaction between Nlp<sup>isoB</sup> and lebercilin, parts of the lebercilin protein comprising the amino acids 1-95, 96-305, 306-490 and 491-697 were tested in a yeast two-hybrid assay with different parts of Nlp<sup>isoB</sup>. This revealed that the predicted intermediate filament domain of Nlp<sup>isoB</sup> specifically interacts with the fragment encompassing the first two coiled-coil domains of lebercilin (aa 96-305) (Fig. 2B). To test whether the interactions of USH2A<sup>isoB</sup> and lebercilin with Nlp are isoform-specific, a liquid  $\beta$ -galactosidase assay was performed using both Nlp<sup>isoA</sup> and Nlp<sup>isoB</sup> together with lebercilin and the intracellular region of USH2A<sup>isoB</sup>. A specific interaction was observed between both proteins and Nlp<sup>isoB</sup>, whereas no interaction with Nlp<sup>isoA</sup> could be detected (Fig. 2C and D).

Co-immunoprecipitations were performed to confirm the interaction between USH2A and Nlp<sup>isoB</sup>. For this purpose, COS-1 cells were co-transfected with constructs encoding HA-tagged Nlp<sup>isoB</sup> and the flag-tagged intracellular region of USH2A (USH2A<sub>tail</sub>). From the COS-1 cell lysates we were able to co-immunoprecipitate HA-tagged Nlp<sup>isoB</sup> and flag-tagged USH2A with antibodies against the flag-tag. As a negative control, unrelated flag-tagged STRAD was co-expressed with HA-tagged Nlp<sup>isoB</sup>. As expected, HA-tagged Nlp<sup>isoB</sup> and flag-tagged STRAD did not co-immunoprecipitate (Fig. 3A).

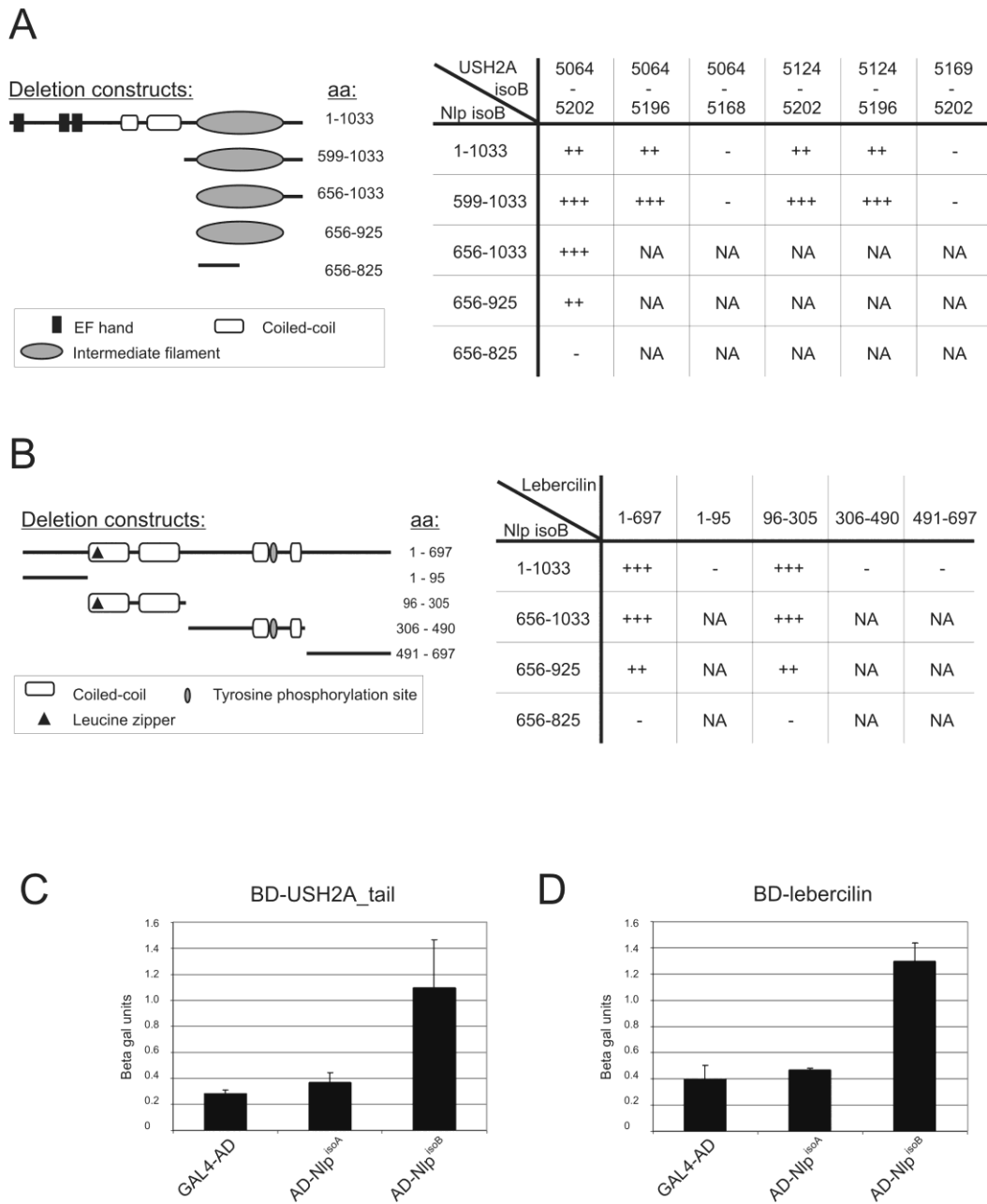


**Figure 2.** Protein-protein interaction studies. **(A)** The schematic protein structure of Nlp<sup>isoB</sup> and protein fragments encoded by deletion constructs with the corresponding amino acids are depicted. Yeast two-hybrid analysis showed a specific interaction between the fragment of the intracellular region of USH2A<sup>isoB</sup> encompassing aa 5124-5196 and the predicted intermediate filament domain (aa 656-925) of Nlp<sup>isoB</sup>. **(B)** Schematic representation of the protein structure of lebercilin and protein fragments encoded by deletion constructs with the corresponding amino acids. Yeast two-hybrid analysis revealed a specific interaction between the lebercilin domain containing the two N-terminal coiled-coil domains (aa 96-305) and the predicted intermediate filament domain of Nlp<sup>isoB</sup> (aa 656-925). A liquid beta-galactosidase assay revealed a specific interaction between Nlp<sup>isoB</sup> and the USH2A<sub>tail</sub> **(C)** and Nlp<sup>isoB</sup> and lebercilin **(D)**. No interaction was observed between USH2A and Nlp<sup>isoA</sup> **(C)**, and lebercilin and Nlp<sup>isoA</sup> **(D)**. aa: amino acids; NA: not assayed.

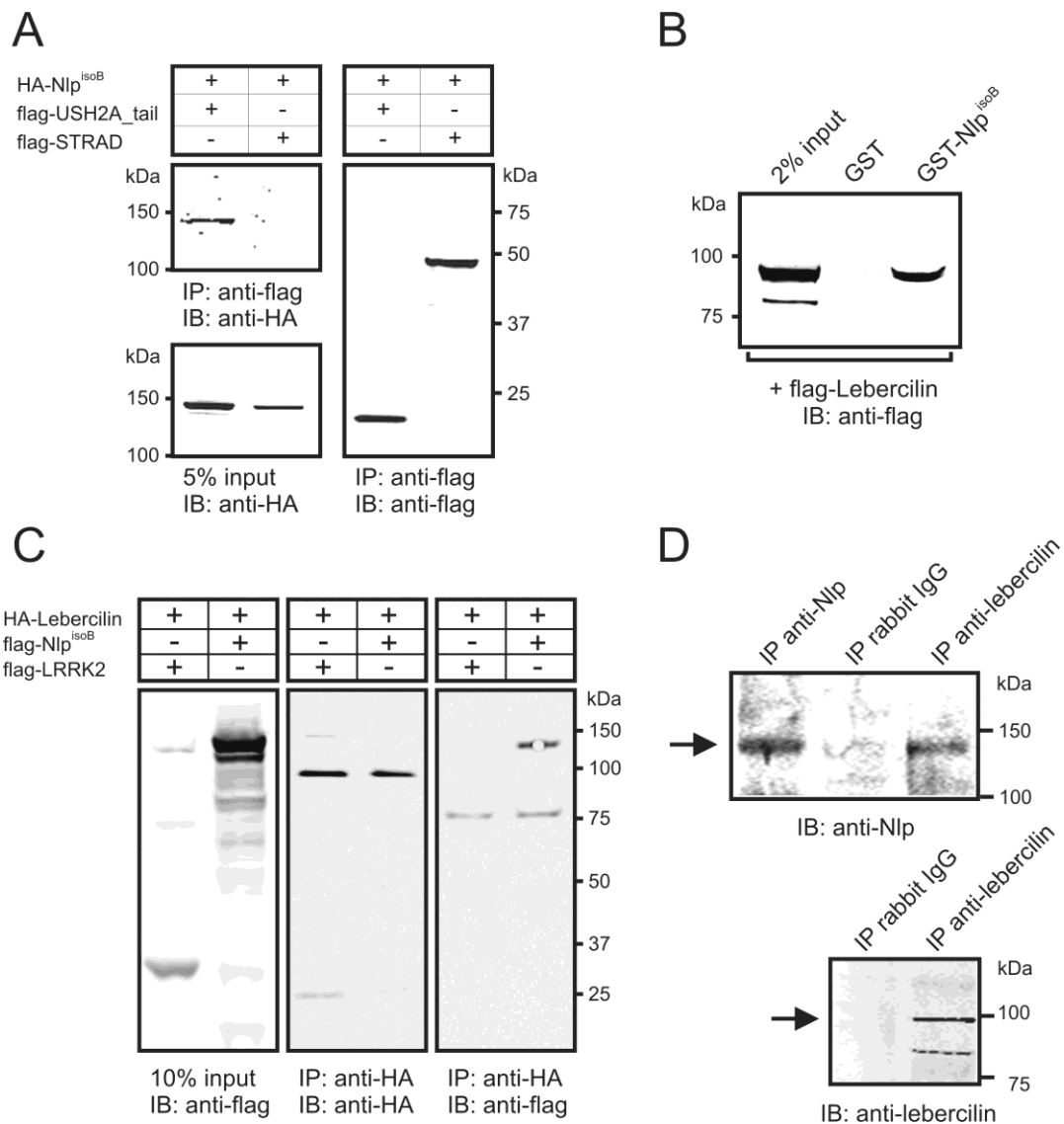


**Figure 3.** Co-immunoprecipitation of Nlp<sup>isoB</sup> with the intracellular region of USH2A<sup>isoB</sup> (USH2A<sub>tail</sub>), but not with STRAD. **(A)** The immunoblot (IB) in the left upper panel shows that HA-Nlp<sup>isoB</sup> (lane 1) co-immunoprecipitated with flag-USH2A<sub>tail</sub>, but not with the unrelated protein flag-STRAD (lane 2). Protein input is shown in the left lower panel; the anti-flag immunoprecipitates are shown in the right panel. **(B)** GST-pull down assays showing that flag-tagged lebercilin was efficiently pulled down by GST-fused Nlp<sup>isoB</sup>, but not by GST alone. The left lane shows 2% input of the protein lysate. **(C)** Co-immunoprecipitation of lebercilin with Nlp<sup>isoB</sup>, but not with LRRK2. The immunoblot (IB) in the right panel shows that flag-Nlp<sup>isoB</sup> (right lane) co-immunoprecipitated with HA-lebercilin, whereas the unrelated protein flag-LRRK2 (left lane) did not. Protein input is shown in the left panel; the anti-HA immunoprecipitates are shown in the middle panel. **(D)** Co-immunoprecipitation of endogenous Nlp with lebercilin from bovine retinal extracts, but not with rabbit IgGs. The top panel shows that Nlp was co-immunoprecipitated with lebercilin, indicated by an arrow, whereas it was not with rabbit IgGs. The bottom panel shows that lebercilin was immunoprecipitated with lebercilin-specific antibodies, as indicated by an arrow, but not with rabbit IgGs.

The interaction between lebercilin and Nlp<sup>isoB</sup> could be confirmed in a GST pull-down experiment and in co-immunoprecipitation assays. We were able to pull down flag-tagged lebercilin from a COS-1 cell lysate with GST-fused Nlp<sup>isoB</sup> but not with GST alone (Fig. 3B). In addition, we were able to co-immunoprecipitate flag-tagged Nlp<sup>isoB</sup> and HA-tagged lebercilin with antibodies against the HA-tag. As a negative control, unrelated flag-tagged LRRK2 was co-expressed with HA-tagged lebercilin. No LRRK2 was co-immunoprecipitated with lebercilin (Fig. 3C). Also, co-immunoprecipitation assays of endogenous proteins were performed from bovine retinal extracts by using antibodies against lebercilin and Nlp. We were able to co-immunoprecipitate Nlp with an antibody against lebercilin. As a negative control, rabbit IgGs were used (Fig. 3D).

### **The interaction between USH2A and Nlp is calcium-independent**

Because of the predicted presence of three EF-hand domains in the N-terminal half of Nlp, we hypothesized that the interaction between USH2A<sup>isoB</sup> and Nlp<sup>isoB</sup> might be dependent on the binding of Ca<sup>2+</sup> ions to these EF-hands, as was shown for the interaction between the EF-hand domain containing proteins centrin and transducin<sup>33</sup>. Therefore, we first determined the Ca<sup>2+</sup>-binding capacity of Nlp. At residue twelve of EF-hand domains, an invariant Glu or Asp provides two oxygens for liganding Ca<sup>2+</sup> (bidentate ligand)<sup>34</sup>. Based on this, only EF-hand 3 would be able to efficiently bind Ca<sup>2+</sup> (Fig. 4A). To test this hypothesis, GST fusion proteins were made of the three predicted EF hands of Nlp. As a positive control, the GST-fused calmodulin 28K subunit was used. We indeed were able to show binding of Ca<sup>2+</sup> to Nlp EF hand 3 and not to EF hands 1 and 2 (Fig. 4B). Subsequently, we performed GST pull-down assays in the presence or absence of 2 mM CaCl<sub>2</sub> in which HA-tagged full length Nlp isoform B was pulled down from a COS-1 cell lysate with GST-USH2A<sub>tail</sub> but not with GST alone. Also, no HA-tagged Nlp<sup>isoB</sup> was pulled-down with GST-fused NBC3<sub>tail</sub>. NBC3 was used as an additional negative control, and is a previously described member of the Usher interactome<sup>17</sup>. Similar results were obtained for pull-down experiments performed in the presence or absence of calcium and therefore there are no indications for calcium-dependence of the interaction (Fig. 4C).



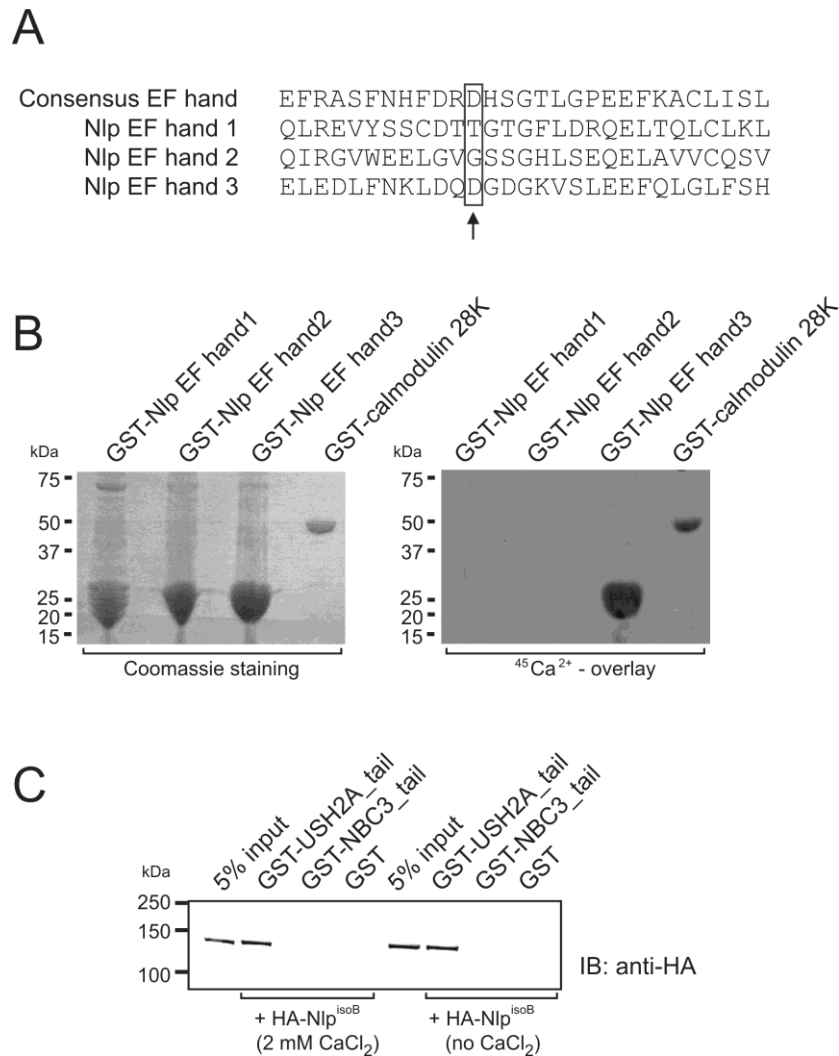


**Figure 4.** Analysis of  $\text{Ca}^{2+}$ -binding properties of Nlp. **(A)** Multiple protein alignment of the predicted EF hand domains in Nlp and the consensus sequence for EF hand domains (SMART database). The invariable D or E at position 12 is boxed and indicated by an arrow and is only present in EF hand 3. **(B)** A calcium-binding assay showing the specific calcium-binding capacities of Nlp EF hand 3. The 28K subunit of calmodulin was used as a positive control. **(C)** GST-pull down analysis showing that HA-tagged Nlp<sup>isoB</sup> was efficiently pulled down by GST-fused USH2A<sub>tail</sub> in the presence and absence of calcium, but not by GST-NBC3<sub>tail</sub> and GST alone. Lanes 1 and 5 show 5% of the input protein lysate.

### Nlp co-localizes with USH2A<sup>isoB</sup> and lebercilin at the photoreceptor cell basal body and centriole

We performed immunohistochemistry for Nlp and USH2A<sup>isoB</sup> to determine whether both proteins co-localize in the retina. Monoclonal anti-*pan*-centrin antibodies (20H5) were used as a marker for the basal body and connecting cilium. With affinity purified antibodies against Nlp, the presence of Nlp was detected in the inner segment and at the basal body, shown as a

partial co-localization with centrin (Fig. 5B). On retinal cryosections Nlp and USH2A<sup>isoB</sup> co-localized in the inner segments and at the region of the connecting cilium (Fig. 5A). In addition, USH2A<sup>isoB</sup> localized to the outer plexiform layer as was already described<sup>17,20</sup>.

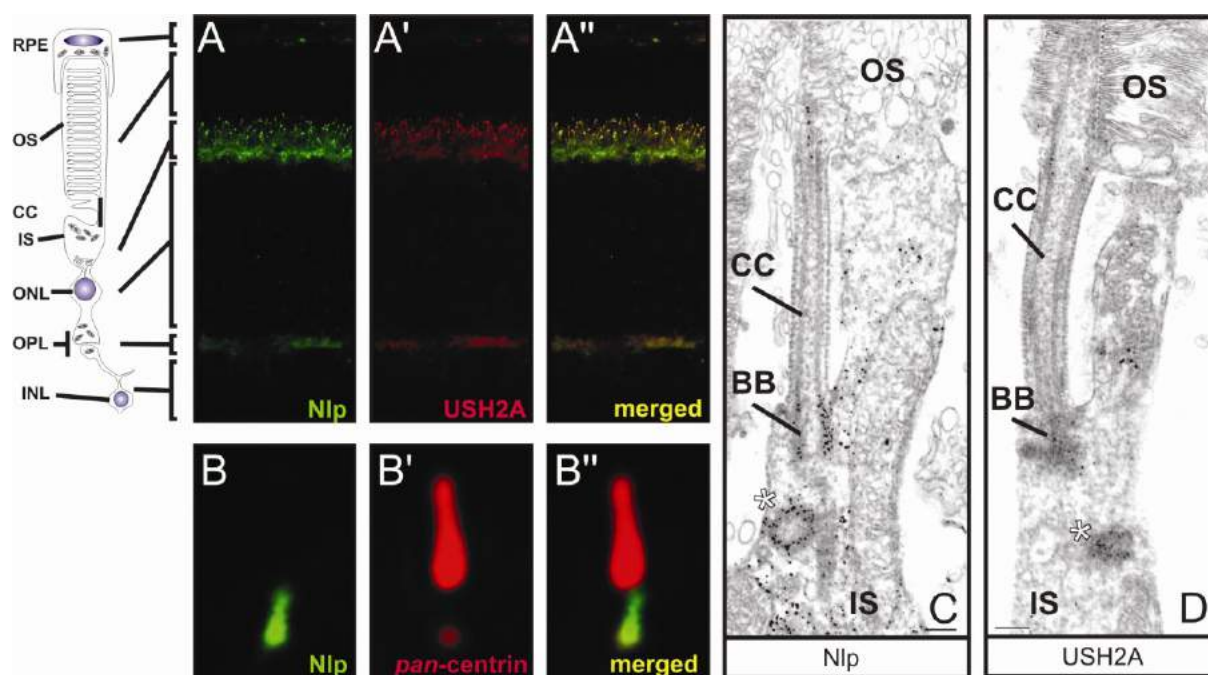


**Figure 5.** Co-localization of Nlp and USH2A in the retina. (A-A'') Co-immunostaining of USH2A and Nlp in radial cryosections of adult (P20) rat retina by using anti-Nlp antibodies (green signal; A) and anti-USH2A antibodies (red signal; A') showing co-localization (yellow signal; A'') in the inner segment (IS) and in the region of the connecting cilium (CC). (B) High magnification fluorescence microscopy analysis of double immunofluorescence with anti-Nlp (green) and anti-*pan-centrin* antibodies (red; marker for the ciliary apparatus: connecting cilium, centriole and basal body) in cryosections through the ciliary part of rat photoreceptor cells. Merged images indicate partial co-localization of Nlp with centrin in the centriole and basal body (yellow signal). Pre-embedding immunolabelings of the ciliary region of mouse photoreceptors by antibodies against Nlp (C) and USH2A<sup>isoB</sup> (D) show a clear staining of the (apical part of) inner segment (IS), the centriole (indicated by an asterisk) and the basal body (BB).

To determine the exact subcellular localization of Nlp in the retina, immunoelectron microscopy was performed. We detected Nlp in the basal body and the centriole of the photoreceptor connecting cilium as well as in periciliary region of the apical inner segments of mouse photoreceptor cells (Fig. 5C). Immunoelectron microscopy for USH2A<sup>isoB</sup> on the retina showed the presence of USH2A<sup>isoB</sup> in the periciliary region, the connecting cilium, basal body and the centriole of photoreceptor cells (Fig. 5D)<sup>21</sup>. Immunohistochemistry on

mouse retinal cryosections revealed lebercilin as a component of the photoreceptor connecting cilium and basal body<sup>29</sup>. Thus, our results indicate that Nlp co-localizes with USH2A<sup>isoB</sup> and also with lebercilin at the photoreceptor cell basal body.

### **Nlp, lebercilin and USH2A co-localize at the centrosome of ARPE-19 cells**

Cashenghi and coworkers have shown that Nlp localizes at the mother centriole of the centrosome in cells during interphase<sup>32</sup>. In order to visualize the interaction between the intracellular domain of USH2A and Nlp<sup>isoB</sup>, we fused these proteins at their N-terminus to enhanced cyan fluorescent protein (eCFP) and monomeric red fluorescent protein (mRFP), respectively. In single transfected human retinal pigment epithelium cells (ARPE-19) expressing Nlp<sup>isoB</sup>, this protein shows a centrosomal localization specifically at one centriole, most probably the mother centriole (Fig. 6A). In mitotic cells a punctate localization in the cell periphery was observed for Nlp<sup>isoB</sup> (data not shown). In single transfected cells a nuclear localization (data not shown)<sup>17,20</sup>, or a centrosomal localization was observed for eCFP-USH2A (Fig. 6B). In cells co-expressing Nlp<sup>isoB</sup> and USH2A, co-localization was observed at both the mother and the daughter centriole of the cell (Fig. 6D-D’’). In addition, overexpression assays in ARPE-19 cells were performed by co-expressing N-terminally fused mRFP-Nlp<sup>isoB</sup> and C-terminally fused lebercilin-eYFP. In single transfected cells, lebercilin-eYFP was localized to the centrosome and microtubule network of the cell, as previously described<sup>29</sup> (Fig. 6C). In cells co-expressing Nlp<sup>isoB</sup> and lebercilin-eYFP, co-localization at the centrosome and non-centrosomal microtubule organization centres (MTOC’s) was observed (Fig. 6E-E’’).

To determine the subcellular localization of endogenous Nlp and lebercilin, ARPE-19 cells were induced to form primary cilia by serum starvation and subsequently used for immunohistochemical stainings with antibodies directed against Nlp and lebercilin. Both proteins could be detected at the base of the cilium, most probably the basal body (Fig. 7A,B). Interestingly, we detected both lebercilin and Nlp at the midbody during cytokinesis (Fig. 7C,D). After telophase, the mother centrioles which are present at the midbody develop into the basal bodies of the newly formed cells<sup>35</sup>. No endogenous USH2A was detected in ARPE-19 cells.

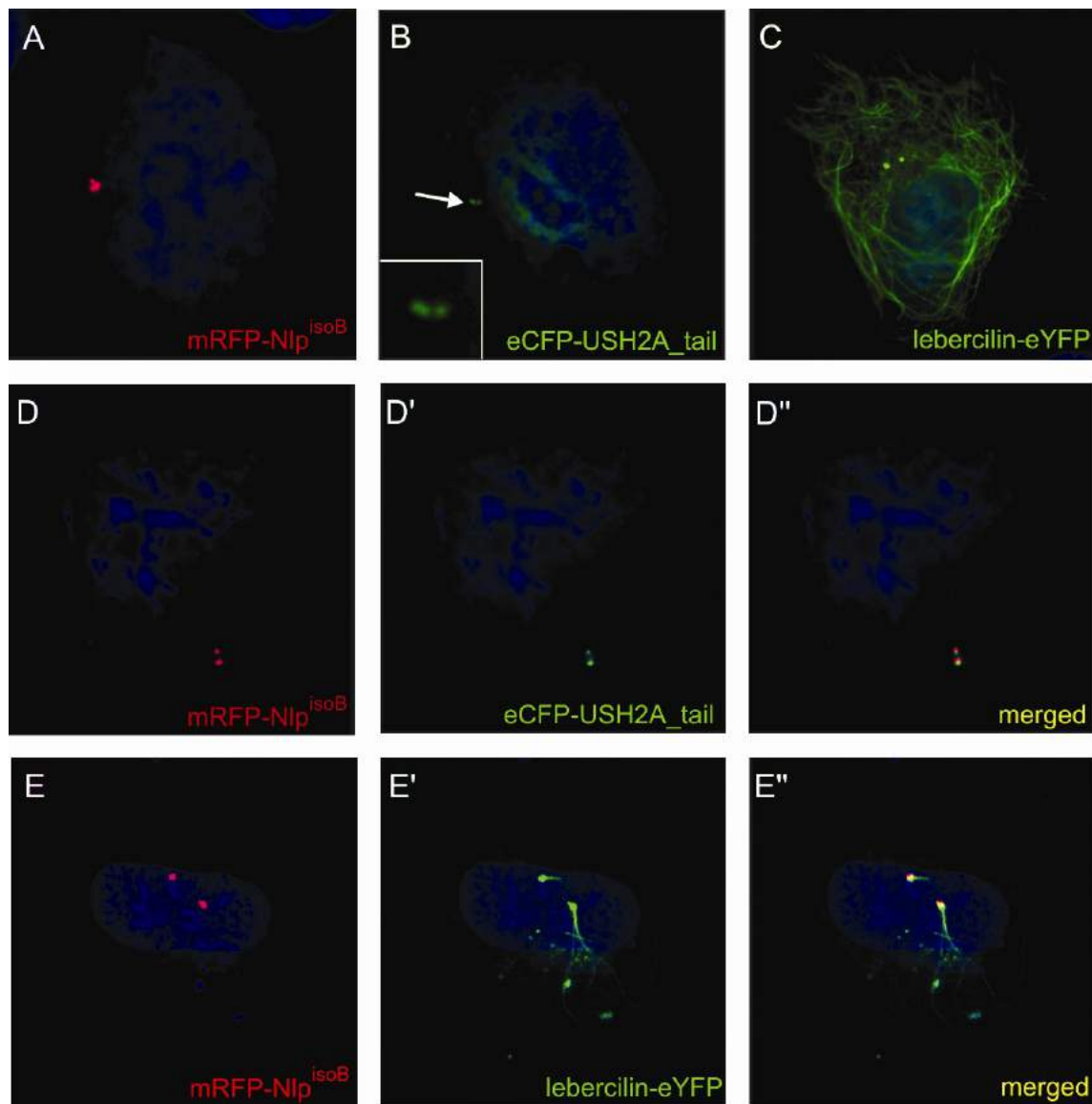


**Figure 6.** Centrosomal localization of Nlp<sup>isoB</sup>, USH2A\_tail and lebercilin in ARPE-19 cells. When expressed alone, mRFP-Nlp<sup>isoB</sup> (red signal) was localized to the mother centriole of the centrosome (A), eCFP-USH2A\_tail (green signal) was localized to the nucleus and the centrosome (indicated by an arrow and in the inlay) (B), whereas eYFP-lebercilin (green signal) was localized at the centrosome and microtubule network of the cell (C). After co-expression of Nlp<sup>isoB</sup> and USH2A both proteins were localized at the mother and daughter centriole of the centrosome, confirming the interaction between both proteins (D-D''). Co-expression of Nlp<sup>isoB</sup> and lebercilin showed co-localization of both proteins at the centrosome and non-centrosomal MTOC's (yellow signal; E''). Lebercilin in addition partly localized at the microtubule network (E-E''). Nuclei were stained with DAPI (blue signal).

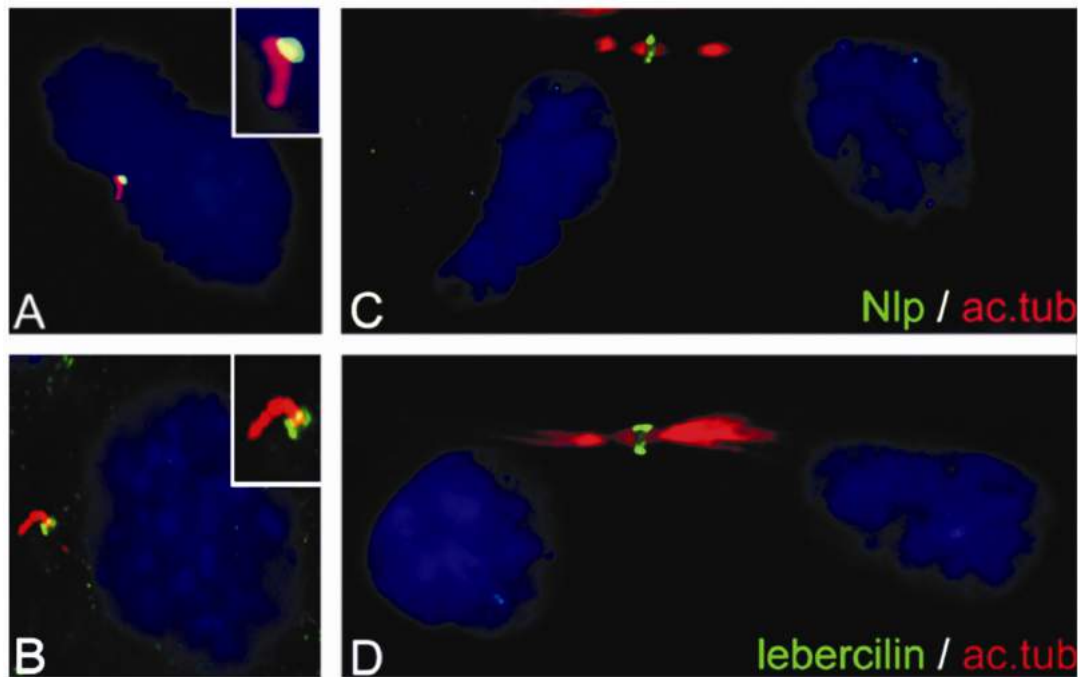


**Figure 7.** Localization of endogenously expressed Nlp and lebercilin in ARPE-19 cells by immunocytochemistry using the anti-Nlp and anti-lebercilin antibodies (green signals) and anti-acetylated tubulin antibodies as an axoneme and microtubule marker (red signal). Nlp (A) and lebercilin (B) were present at the basal body of primary cilia and both proteins were found at the midbody region of ARPE-19 cells during telophase (C and D). Nuclei were stained with DAPI (blue signal).

### Lebercilin mutations affect the interaction with Nlp<sup>isoB</sup>

Recently, we have identified truncating lebercilin mutations in LCA patients<sup>29</sup>. We addressed the biologic relevance of the interaction between lebercilin and Nlp<sup>isoB</sup> by testing the effect of two of these mutations, p.Q279X and p.P493TfsX1, on the association with Nlp<sup>isoB</sup>. In a quantitative yeast two-hybrid interaction assay the p.Q279X mutation significantly enhanced the interaction. The interaction of Nlp<sup>isoB</sup> and the p.P493TfsX1 mutant was found to be completely abolished (Fig. 8A). The subcellular localization of the lebercilin mutants was studied upon expression in ciliated ARPE-19 cells. When expressed alone, mRFP-tagged lebercilin localizes to the basal body, the primary cilium and the microtubule network of the cell (Fig. 8B)<sup>29</sup>. The mRFP-lebercilin<sup>Q279X</sup> mutant does not associate with the microtubule network any longer but is present in the primary cilium and its basal body (Fig. 8C). In contrast, mRFP-lebercilin<sup>P493TfsX1</sup> only localizes to the microtubule network in the cell periphery but no longer to the cilium and basal body (Fig. 8D).

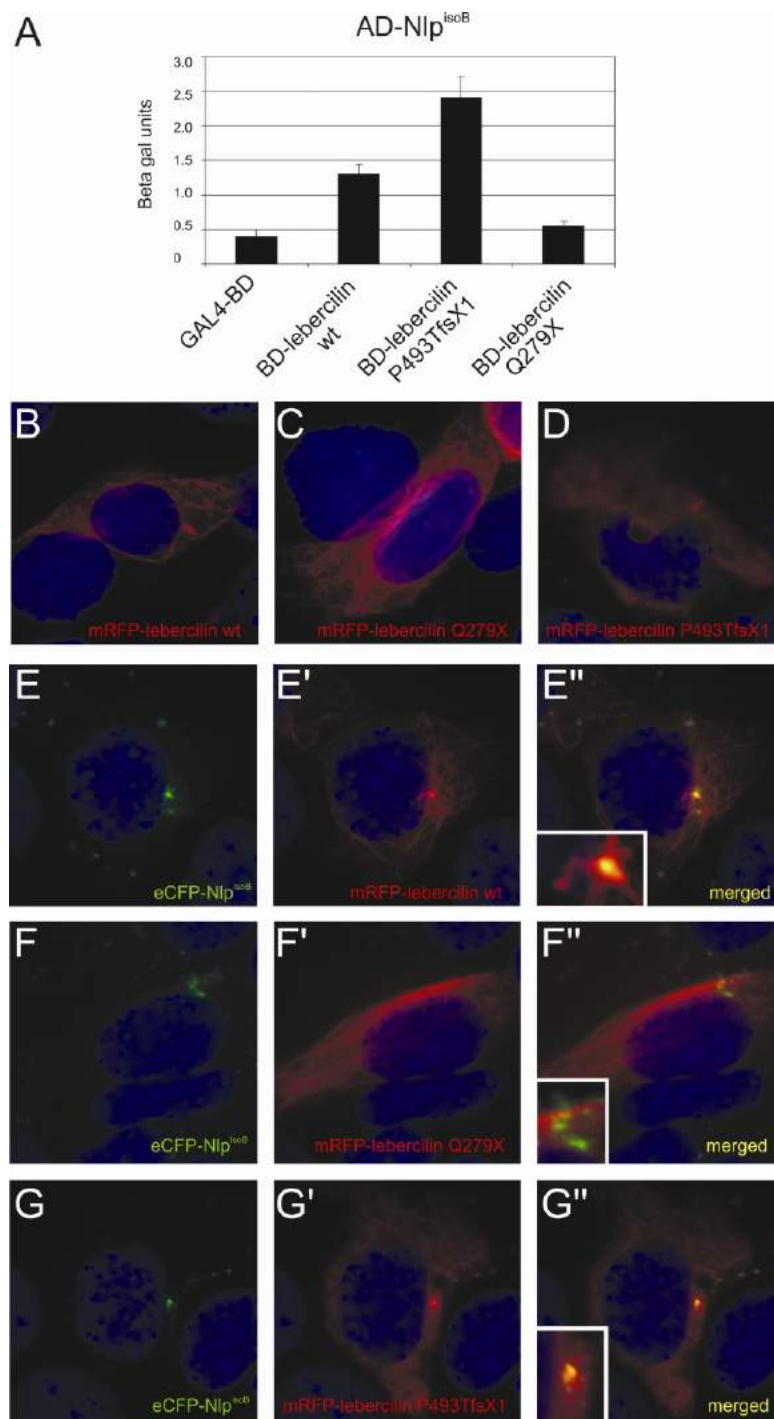


**Figure 8.** Mutations in lebercilin affect the interaction with Nlp<sup>isoB</sup>. A quantitative liquid beta-galactosidase assay shows an enhanced interaction of Nlp<sup>isoB</sup> and lebercilin<sup>Q279X</sup> as compared to wild-type lebercilin, and a reduced interaction of Nlp<sup>isoB</sup> and lebercilin<sup>P493TfsX1</sup> (A). When expressed alone in ARPE-19 cells, mRFP-lebercilin wild-type (red signal) was localized to the basal body, the primary cilium and microtubule network of the cell (B), mRFP-lebercilin<sup>Q279X</sup> was localized to the basal body and primary cilium (C) and mRFP-lebercilin<sup>P493TfsX1</sup> was localized to the microtubule network of the cell (D). Co-expression of Nlp<sup>isoB</sup> and lebercilin showed co-localization of both proteins at the basal body (yellow signal; E'', inset). In addition,



lebercilin localized to the primary cilium and the microtubule network in the cell periphery (red signal; **E'-E''**, inset). Upon co-expression of Nlp<sup>isoB</sup> and lebercilin<sup>Q279X</sup>, both proteins co-localize at the basal body (yellow signal; **F''**, inset). The mutant lebercilin was not found in the primary cilium (**F'-F''**, inset). After co-expression of Nlp<sup>isoB</sup> and lebercilin<sup>P493TfsX1</sup> no co-localization of these proteins was observed (**G-G''**, inset). Nuclei were stained with DAPI (blue signal).

Co-expression of Nlp<sup>isoB</sup> and lebercilin showed a clear co-localization, specifically at the basal body (Fig. 8E-E''). In the primary cilium and the microtubule network, only lebercilin was present. As indicated by the yeast two-hybrid assay, the interaction between Nlp<sup>isoB</sup> and lebercilin<sup>Q279X</sup> is enhanced. When co-expressed with Nlp<sup>isoB</sup>, lebercilin<sup>Q279X</sup> is recruited to the basal body, but is no longer observed in the primary cilium (Fig. 8F-F''). Upon co-expression of Nlp<sup>isoB</sup> and lebercilin<sup>P493TfsX1</sup> no co-localization was observed, confirming the loss of interaction between the two proteins (Fig. 8G-G''). These data indicate that truncating mutations in lebercilin severely affect the association with Nlp at the basal body. However, downregulation of both endogenous *Nlp* and *LCA5* by RNAi in ciliated ARPE-19 cells does not result in altered protein localization of Nlp or lebercilin (Supplementary Fig. 2), suggesting that additional binding partners are involved in their localization at the basal body.

### Discussion

In this study, we demonstrate that a novel isoform of the centrosome-associated ninein-like protein, Nlp<sup>isoB</sup>, specifically interacts with lebercilin and the cytoplasmic region of USH2A, thereby linking Usher syndrome and Leber congenital amaurosis at the molecular level. Previous analysis of *Xenopus laevis* Nlp already suggested the presence of two Nlp isoforms, which correspond with human Nlp<sup>isoA</sup> and Nlp<sup>isoB</sup><sup>36</sup>. Nlp is the second member of the ninein protein family and has a 37 % sequence identity with ninein<sup>32</sup>. Nlp is predominantly present in the mother centriole of the centrosome and in the basal body of primary cilia in cultured cells, and is involved in microtubule nucleation, anchoring and outgrowth<sup>32,36,37</sup>. However, it remains to be elucidated which isoform of Nlp is present and functions at these subcellular structures. The interaction between USH2A<sup>isoB</sup>, lebercilin and Nlp<sup>isoB</sup> and their co-localization in the basal bodies, the centrioles and the periciliary compartments of photoreceptor cells shows that at least Nlp<sup>isoB</sup> molecules are present there.

Basal bodies and associated centrioles are found at the base of cilia and serve as a nucleation site for the axonemal and cytoplasmic microtubules, respectively<sup>38,39</sup>. The photoreceptor cell outer segment is regarded as a highly specialized cilium corresponding to the ciliary shaft of a prototypic cilium<sup>38,39</sup>. The connecting cilium then correlates with the short junction between the basal body and axoneme of a prototypic cilium, the transition zone<sup>38</sup>. The presence of Nlp at the basal bodies and centrioles of the ciliary apparatus of photoreceptor cells matches with the previously determined localization of Nlp in the basal body of ciliated cells<sup>36</sup>. Based on the knowledge on Nlp function in mitotic cells<sup>32,36,37</sup>, we propose that Nlp functions in the development and maintenance of the connecting cilium and outer segment and in the establishment of a microtubule network in (the apical part of) the inner segment in differentiated photoreceptor cells.

In addition to the physical interaction of both USH2A<sup>isoB</sup> and lebercilin with Nlp<sup>isoB</sup>, similarities in clinical manifestations between USH and LCA suggest a significant overlap in the pathogenic mechanisms underlying both disorders. Based on the subcellular localization and the current knowledge on USH2A<sup>isoB</sup> and lebercilin, these pathogenic mechanisms are likely to include ciliary dysfunction. Post-mortem observation of connecting cilium defects in the retina and the identification of sperm abnormalities in some USH patients (reviewed in<sup>40</sup>), as well as the involvement of other cilia-associated proteins in non-syndromic forms of retinal degeneration and USH, contribute to this hypothesis<sup>20,24,29,31,41,42</sup>. Two proteins involved in (non-)syndromic retinitis pigmentosa, RPGR and RP1, and even the LCA-associated proteins RPGRIP1 and CEP290, have been shown to localize to the connecting cilia of photoreceptor cells, emphasizing the role of impaired cilia function in the pathogenesis of retinal degeneration<sup>31,43-46</sup>.

The connecting cilium of photoreceptor cells connects the inner and outer segments. Within the outer segments the actual phototransduction takes place. Since protein synthesis does not occur in the outer segments, the proteins essential for phototransduction and assembly and maintenance of the axonemal and outer segment structure are transported through the connecting cilium between the inner segment and the outer segment, analogous to the intraflagellar transport (IFT)<sup>47,48</sup>. In cilia and flagella, IFT complexes are assembled near the basal body and transported along the axoneme by the heterotrimeric kinesin II



(KIF3A/3B/KAP3) and the homodimeric KIF17 in an anterograde direction and back to the basal body region by cytoplasmic dynein 2/1b<sup>49-52</sup>. In photoreceptor cells, IFT20, IFT52, IFT57 and IFT88 molecules and both kinesin motors are thought to be present in an anterograde transport complex<sup>53-55</sup>. Dysfunction of the components of the IFT transport complex lead to mislocalization of structural proteins and proteins involved in the phototransduction and subsequently lead to retinal degeneration<sup>53,56</sup>. This is corroborated by the development of both polycystic kidney disease in addition to retinal degeneration in mice after the introduction of a hypermorphic mutation in IFT88<sup>53,57</sup>. Also, photoreceptor-specific silencing of KIF3A leads to mislocalization of opsin and arrestin, proteins involved in phototransduction<sup>56</sup>. Similar defects were observed in mice lacking *BBS4*, a gene involved in Bardet-Biedl syndrome<sup>58</sup>. *BBS4* is a member of the recently discovered BBSome, which is required for ciliogenesis and is hypothesized to function in IFT and vesicular transport to the cilium<sup>59</sup>. The evaluation of the cellular function of USH proteins in photoreceptors suggests the participation of these proteins in the transport through the connecting cilium<sup>21,48,60,61</sup>. Also, there is growing evidence that BBS molecules, IFT proteins and USH proteins participate in microtubule-based vesicular transport through the cytoplasm<sup>21,53,59,62</sup>. The molecular links of Nlp<sup>isoB</sup> with the USH2A<sup>isoB</sup> and lebercilin proteins qualified these as common denominators in the associated retinal protein network, suggesting that common molecular processes are disrupted in the retinas of USH2A and LCA5 patients. We indeed were able to determine that protein truncating mutations in lebercilin affect the interaction with Nlp, but as downregulation of expression of any of these proteins by RNAi had no effect on the localization of the interacting partner, the physiological defect is more complex and remains to be identified. The USH2A-associated protein network, the lebercilin interactome<sup>29</sup> and the Nlp interactors p150<sup>glued</sup> and Plk1<sup>32,36,37</sup> provide multiple links with centrosomal and ciliary processes and pathways that are now potentially connected through Nlp.

Recently, we and others showed the presence of the Usher protein network in a periciliary collar-like structure at the apical part of the photoreceptor inner segments, analogous to the periciliary ridge complex of *Xenopus* photoreceptor cells, and the Usher proteins were hypothesized to function in transport and docking of vesicles containing proteins for the outer segment<sup>21,23,63</sup>. These cargo vesicles originate from the trans-Golgi network of the photoreceptor cells and are thought to be transported along microtubules by cytoplasmic

dynein through the inner segment to the apical membrane<sup>21,64</sup>. Nlp might function in this vesicular transport by the direct association with the dynactin p150<sup>glued</sup> subunit of the dynein-dynactin motor complex<sup>37</sup>, explaining the presence of Nlp in the inner segments of photoreceptor cells. The periciliary region and also the basal body and centriole are thought to serve as a docking site from where ciliary proteins (e.g. IFT proteins and proteins involved in signalling) are further distributed<sup>65</sup>. In such a model, Nlp would function as the molecular switch between intracellular and IFT transport. The effect of mutations in lebercilin on its interaction with Nlp<sup>isoB</sup> and on its localization in the cilium are in line with this model.

Interestingly, Nlp is known to be phosphorylated by Polo-like kinase 1 (Plk1)<sup>32,36,37</sup>, which is a key regulator in centrosome function. Plk1 also phosphorylates nucleophosmin<sup>66</sup>, a centrosome-associated protein that acts in nucleocytoplasmic shuttling<sup>67</sup> and is a member of the previously identified lebercilin-interactome<sup>29</sup>. In addition, nucleophosmin associates with RPGR-ORF15, a protein involved in X-linked retinal degeneration<sup>68</sup>. The Nlp-interacting protein p150<sup>glued</sup><sup>37</sup> was found in a protein complex with RPGR-ORF15 and with lebercilin<sup>29,69</sup>. The direct or indirect association of Nlp with several protein complexes in the region of the photoreceptor connecting cilium, stresses the importance of this protein in photoreceptor cell function.

In conclusion, our data show that USH and LCA are molecularly linked by the direct association of USH2A<sup>isoB</sup> and lebercilin with a novel isoform of Nlp, Nlp<sup>isoB</sup>. Co-localization of these proteins at the basal body of photoreceptor cells and the current knowledge on the function of the existing Usher protein network(s) point towards an interdependent function for Nlp<sup>isoB</sup>, USH2A<sup>isoB</sup> and lebercilin, possibly in cytoplasmic trafficking and ciliary transport of proteins involved in photoreception. We propose that at the basal body, Nlp<sup>isoB</sup> could function as a molecular hinge connecting cytoplasmic transport mechanisms to the IFT transport machinery, suggesting an important role for Nlp in photoreceptor cell function. The central position of Nlp in the protein network indicates that *Nlp* can be considered as an excellent candidate gene for Usher syndrome, LCA or other (retinal) ciliopathies. However, no pathogenic mutations have been identified so far.

## **Acknowledgements**

The authors would like to thank Jaap Oostrik and Saskia van der Velde-Visser and Elisabeth Sehn for technical assistance, Dr. Pascal Duijf for providing us with the pBD-*p63* vector and Dr. Erich Nigg for providing us with the antibody against Nlp. This work was supported by grants from the British Retinitis Pigmentosa Society (to H.K. and R.R.), the DFG (to U.W.), Forschung contra Blindheit - Initiative Usher Syndrom (to H.K., T.M. and U.W.), ProRetina Deutschland (to U.W. and R.R.), the FAUN-Stiftung, Nürnberg (U.W.), the Heinsius Houbolt Foundation (to H.K.), the Netherlands Organisation for Scientific Research (VIDI 917.86.396, to R.R.), the European Commission IP “EVI-GenoRet” LSHG-CT-2005-512036, the Foundation for Retinal Research, the Algemene Nederlandse Vereniging ter Voorkoming van Blindheid, the Stichting Blindenhulp, the Stichting OOG, and the Rotterdamse Vereniging Blindenbelangen (to F.P.M.C. and R.R.).

## **Material and methods**

### **Animals and tissues**

In this study mature Wistar rats and C57BL/6J mice housed in standard cages and receiving water and food *ad libitum*, were used. Animal experiments were conducted in accordance with international and institutional guidelines. Bovine retinas were dissected from eye balls obtained from the local slaughterhouse<sup>21</sup>.

### **Plasmids and antibodies**

Affinity purified polyclonal antibodies directed against Nlp were described before<sup>32</sup>. Monoclonal antibodies recognizing centrin 1-4 (20H5), polyclonal antibodies directed against the cytoplasmic region of USH2A, and affinity purified polyclonal antibodies directed against lebercilin were previously described<sup>17,20,29</sup>. The immunohistochemical stainings of Nlp and USH2A were specific. No staining was observed after pre-adsorption of the primary antibodies with the corresponding peptide epitope. In addition, primary Nlp antibodies did not recognize GFP-tagged ninein after Western blot analysis (Supplementary Figure 1). Anti-flag, anti-HA, anti-acetylated tubulin and anti-gamma tubulin antibodies were purchased from Sigma (Germany). Anti-HA beads were purchased from Roche (Germany). Secondary antibodies for immunohistochemistry and western blot analysis were purchased from Molecular Probes-Invitrogen (USA), Rockland (USA), and Jackson ImmunoResearch Laboratories (USA). cDNA encoding (parts of) the cytoplasmic region of human USH2A (Genbank NP\_996816) (aa 5064-5202, 5064-5168, 5064-5196, 5124-5196, 5124-5202 and 5169-5202) were cloned in the pDONR201 vector using the Gateway cloning system (Invitrogen, USA) according to manufacturer's instructions. cDNA fragments of the human *Nlp* gene were amplified by using IMAGE clone IRATp970C1131D (RZPD, Germany) as a template. By using Gateway technology (Invitrogen, USA), cDNAs encoding human full length Nlp<sup>isoB</sup> (aa 1-1033) (Genbank EU718622), Nlp<sup>isoA</sup> (aa 1-1382) (Genbank

NM\_025176), the predicted EF hand domains (aa 11-39, 200-228 and 237-265), the predicted intermediate filament domain (aa 656-925) of Nlp<sup>isoB</sup> and deletion constructs for Nlp<sup>isoB</sup> encoding aa 599-1033, aa 656-1033 and aa 656-825, were cloned in the pDONR201 vector. Lebercilin fragments (Genbank NP\_859065) encoding aa 1-95, 96-305, 306-490 and 491-697 were amplified by PCR, using pDONR201-lebercilin<sup>fl</sup> as a template, and cloned in pDONR201<sup>29</sup>.

### Yeast two-hybrid analysis

A GAL4-based yeast two-hybrid system (HybriZAP, Stratagene, USA) was used to identify proteins that interact with the cytoplasmic region of USH2A<sup>isoB</sup> (aa 5064-5202) and proteins that interact with lebercilin (aa 1-697), using methods previously described<sup>70</sup> with minor variations. Yeast strain PJ69-4 $\alpha$ <sup>71</sup> was used as a host, which carried the *HIS3* (histidine), *ADE2* (adenine), *MEL1* ( $\alpha$ -galactosidase) and *LacZ* ( $\beta$ -galactosidase) reporter genes. The DNA-binding domain fused to the human USH2A cytoplasmic region (pBD-USH2A<sub>tail</sub>) and fused to full length lebercilin (pBD-lebercilin<sup>fl</sup>) were used as a bait for screening a human oligo-d(T) primed retina cDNA library containing  $1.9 \times 10^6$  primary clones fused to the activation domain (pAD). In total,  $1.1 \times 10^7$  clones (USH2A) and  $5.0 \times 10^7$  clones (lebercilin) were plated on amino acid dropout plates lacking Trp, Leu and His (SD -WLH plates), containing 1 mM 3-aminotriazol (3-AT), and selected for growth. Clones were then patched on medium additionally lacking adenine (SD -WLHA plates), and selected for growth and  $\alpha$ -galactosidase activity by the activation of the *MEL1* reporter gene. The latter was done using 20  $\mu$ g/ml of the chromogenic substrate 5-Bromo-4-Chloro-3-indolyl  $\alpha$ -D-galactopyranoside (*X*- $\alpha$ -Gal) in the dropout plates, and selecting the yeast cells that developed a blue-green colour due to hydrolysis of *X*- $\alpha$ -Gal by the secreted  $\alpha$ -galactosidase enzyme. Further selection of positive clones was based on  $\beta$ -galactosidase activity by the activation of the *LacZ* reporter gene, that was detected by a filter lift assay, as previously described<sup>70</sup>.

### Liquid $\beta$ -galactosidase assay

Three independent clones of PJ69-4 $\alpha$  yeast cells co-transformed with pAD-Nlp<sup>isoA</sup> full length or Nlp<sup>isoB</sup> full length and pBD-USH2A<sub>tail</sub> or pBD-lebercilin full length were cultured in selective medium lacking Trp and Leu (SD-WL). After two overnight incubation steps at 30°C, the optical density of the cultures was determined at a wavelength of 600 nm. Cell lysis and subsequent colorimetric reactions were performed by using the Yeast  $\beta$ -galactosidase assay kit (Pierce, USA) according to manufacturer's instructions. Absorbance was measured at a wavelength of 420 nm.

### Expression analysis

The expression of Nlp<sup>isoA</sup> and Nlp<sup>isoB</sup> was examined by performing semi-quantitative RT-PCR analysis on RNA from human fetal and adult tissues as described before<sup>72</sup>. Primers used for the detection of the transcripts encoding Nlp<sup>isoA</sup> are 5'- GAGGGGGAGACCAAAATAGC -3' and 5'- TCTGAATGGTCACACGATGC -3'. For detection of Nlp<sup>isoB</sup> the following primers were used: 5'- ACCTGCAGCAGATCAGACTG -3' and 5'- TGATTTGGTCACTCTGCTG -3'. Samples were taken after 25, 30 and 35 cycles.

### Calcium binding assay

GST-fusion proteins of the predicted Nlp EF hands 1 (aa 11-39), 2 (aa 200-228) and 3 (aa 237-265) were produced by transforming BL21-DE3 cells with pDEST15-Nlp EF hand 1, 2 and 3. Precleared lysates were separated on precasted 4-12% NuPage gradient gels (Invitrogen, USA) and subsequently blotted onto nitrocellulose membranes. The membranes were incubated for 10 minutes at room temperature with 10-20  $\mu\text{Ci/l}$   $^{59}\text{CaCl}_2$  (New England Nuclear, USA) in 10 mM imidazole, pH 6.8, and 60 mM KCl. The blots were washed twice for 5 minutes with 50% ethanol, dried and subsequently exposed to a radiation sensitive film (Kodak, Germany) <sup>73</sup>.

### GST pull-down assay

In order to produce GST (glutathion S-transferase) fusion proteins, BL21-DE3 cells were transformed with pDEST15-USH2A\_tail (aa 5064-5202), pDEST15-NBC3\_tail (aa 1119-1214) and pDEST15-Nlp<sup>isoB</sup> (aa 1-1033). Cells were induced at 30°C for 4 hours with 0.5 mM IPTG and subsequently lysed with STE buffer (1% Sarkosyl, 1% Triton-X-100) supplemented with protease inhibitor cocktail (Roche, Germany). Lysates were precleared and incubated at 4°C for 16 hours with glutathione Sepharose 4B beads (Amersham Biosciences, USA). Beads with bound fusion proteins were washed twice with lysis buffer and three times with TBSTD (TBS with 1% Triton-X-100 and 2 mM DTT). During each washing step, samples were incubated on a rotating wheel at 4°C for 5 minutes. The amount of bound GST-fusion protein was verified on a 10% SDS-PAGE gel stained with Gelcode Blue Stain Reagent (Pierce, USA). HA-tagged Nlp<sup>isoB</sup>, 3xflag-tagged lebercilin, 3xflag-tagged USH2A\_tail and 3xflag-tagged NBC3\_tail were produced by transfecting COS-1 cells with, respectively, pcDNA3-HA-Nlp<sup>isoB</sup>, p3xflag-lebercilin, p3xflag-USH2A\_tail and p3xflag-NBC3\_tail using Nucleofector kit V (Amaxa, USA), program A-24 according to manufacturer's instructions. The precleared supernatants were incubated overnight at 4°C in the presence or absence of 2 mM  $\text{CaCl}_2$  with equal amounts of blocked beads with GST, or beads with GST-fusion proteins. After three washes with lysis buffer, the beads were boiled in 1xSDS loading buffer. Protein complexes were resolved on 4-12% NuPage gradient gels (Invitrogen, USA). For Western blot analysis, proteins were electrophoretically transferred onto nitrocellulose membranes, blocked with 5% non-fat dry milk (Biorad, Germany) in PBST (0.1% Tween) and analyzed with the appropriate primary and secondary antibodies in 0.5% milk in PBST. Bands were visualized using the Odyssey Infrared Imaging System (LI-COR, USA). Tagged molecules were detected by anti-HA or anti-flag mono- or polyclonal antibodies. As secondary antibodies IRDye800 goat-anti-mouse IgG (Rockland, USA) and Alexa Fluor 680 goat-anti-rabbit IgG were used (Molecular Probes, USA).

### Co-immunoprecipitation from COS-1 cells

HA-tagged Nlp<sup>isoB</sup> and HA-tagged lebercilin were expressed by using the mammalian expression vector pcDNA3-HA/DEST. Flag-tagged intracellular region of USH2A, flag-tagged Nlp<sup>isoB</sup> and flag-tagged LRRK2 were expressed by using p3xflag-CMV/DEST from the Gateway cloning system (Invitrogen, USA). Both plasmids contain a CMV promoter. COS-1 cells were (co-)transfected by using Effectene (Qiagen, Germany) according to manufacturer's instructions. Thirty hours after transfection, cells were washed with PBS and

subsequently lysed on ice in lysis buffer (50 mM TRIS-HCl pH 7.5, 150 mM NaCl, 0.5% Triton X-100) supplemented with complete protease inhibitor cocktail (Roche, Germany). HA-tagged Nlp<sup>isoB</sup> and lebercilin were immunoprecipitated from cleared lysates overnight at 4°C by using rat monoclonal anti-HA beads (Roche, Germany) whereas flag-tagged USH2A<sub>tail</sub>, Nlp<sup>isoB</sup> and LRRK2 were immunoprecipitated by using polyclonal anti-flag antibodies (Sigma, Germany) and Protein A/G PLUS-sepharose (Santa Cruz Biotechnology, USA). After 4 washes in lysis buffer, the protein complexes were resolved on 4-12% NuPage gradient gels (Invitrogen, USA) and subsequently analyzed on immunoblots as described for the GST pull-down assay. Bands were visualized by using the Odyssey Infrared Imaging System (LI-COR, USA). Tagged molecules were detected by anti-HA or anti-flag mono- or polyclonal antibodies. As secondary antibodies IRDye800 goat-anti-mouse IgG (Rockland, USA) and Alexa Fluor 680 goat-anti-rabbit IgG were used (Molecular Probes, USA).

#### **Co-immunoprecipitations from bovine retinal extracts**

For immunoprecipitations, bovine retinas from a local slaughterhouse were used. Retinas were lysed by sonification (2 times 30 seconds) in lysisbuffer (50 mM Tris-HCl pH 7.4, 150 mM NaCl, 0.5% Nonidet-P40, 1 mM Natrium-orthovanadate) supplemented with complete protease inhibitor cocktail (Roche, Germany). Lysates were precleared and incubated for 16 hours at 4°C with mouse monoclonal anti-rabbit IgGs, rabbit polyclonal Nlp antibodies or polyclonal rabbit lebercilin antibodies. Protein-antibody complexes were coupled to Protein A/G PLUS-sepharose beads (Santa Cruz, USA) for 2 hours at 4°C After incubations, the beads were pelleted and washed three times with lysis buffer. Beads were boiled and proteins were resolved on 4-12% NuPage gradient gels (Invitrogen, USA) and subsequently analyzed on immunoblots as described for GST pull-down. Bands were visualized using the Odyssey Infrared Imaging System (LI-COR, USA).

#### **Co-localization analyses in ARPE-19 cells**

To determine the cellular localization of the cytoplasmic region of human USH2A, full length lebercilin and full length Nlp<sup>isoB</sup> in ARPE-19 cells, cDNAs encoding the region of USH2A in pDEST501 were cloned by using the Gateway cloning technology (Invitrogen, USA), resulting in N-terminally fused eCFP-USH2A. Nlp was cloned in pDEST733, resulting in N-terminally fused mRFP-Nlp<sup>isoB</sup>. Lebercilin was cloned in pDEST504, resulting in C-terminally fused lebercilin-eYFP. ARPE-19 cells were cotransfected with pDEST733- Nlp<sup>isoB</sup> and pDEST501-USH2A<sub>tail</sub> or pDEST504-lebercilin by using Effectene (Qiagen, Germany) according to manufacturer's instructions. Twenty hours after transfection, cells were washed with PBS, fixed with 4% paraformaldehyde and mounted with Vectashield containing DAPI (Vector Laboratories, Inc., UK). Images were taken with an Axioplan2 Imaging fluorescence microscope (Zeiss, Germany) equipped with a DC350FX camera (Zeiss, Germany) and processed using Adobe Photoshop (Adobe Systems, USA).

#### **Double immunofluorescence labelling of rat retinas**

Unfixed eyes of 20 day old (P20) Wistar rats were isolated and frozen in melting isopentane. Cryosections were made at a thickness of 7 µm and treated with 0.01% Tween-20 in PBS followed by a blocking step with blocking solution (0.1% ovalbumin, 0.5% fish gelatin in PBS). Antibodies diluted in blocking solution were incubated overnight at 4°C. Secondary antibodies were also diluted in blocking solution and incubated in the dark for 1

hour. Sections were embedded with Prolong Gold Anti-fade (Molecular Probes, USA). Pictures were made with an Axioskop2 Mot plus fluorescence microscope (Zeiss, Germany) equipped with an AxioCam MRC5 camera (Zeiss, Germany). Images were processed using Axiovision 4.3 (Zeiss, Germany) and Adobe Photoshop (Adobe Systems, USA).

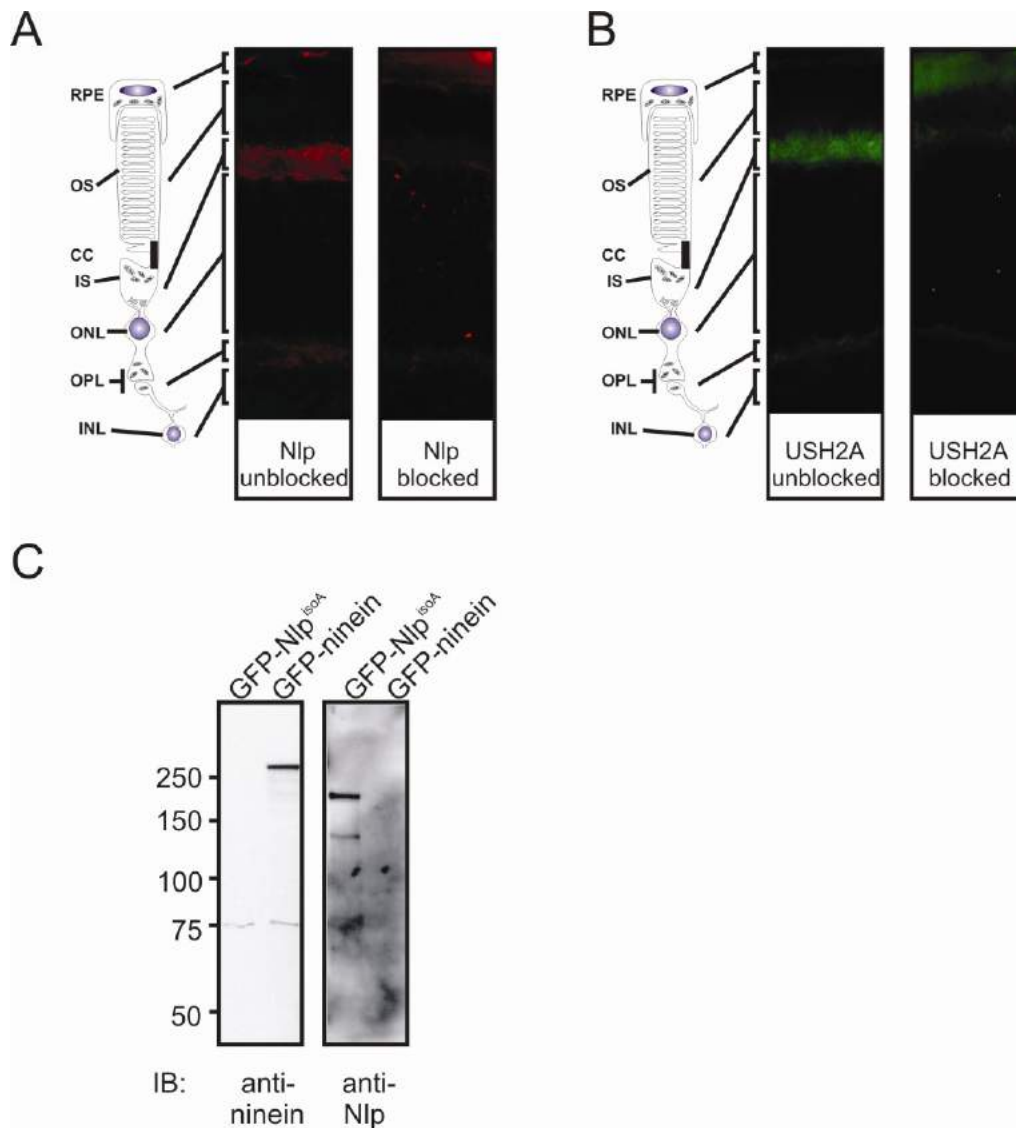
### **Pre-embedding immunoelectron microscopy**

Immunoelectron microscopy was performed on isolated mouse eyes as previously described <sup>21</sup>. In short, vibratome sections through mouse retina were stained by primary antibodies against *Nlp* and visualized by appropriate secondary antibodies (Vectastain ABC-Kit, Vector, UK). After fixation with 0.5% OsO<sub>4</sub> specimens were embedded in araldite and ultrathin sections were analyzed with a FEI Tecnai 12 Biotwin transmission electron microscope (FEI, The Netherlands).

### **Knockdown of *Nlp* in cultured ARPE-19 cells by RNAi**

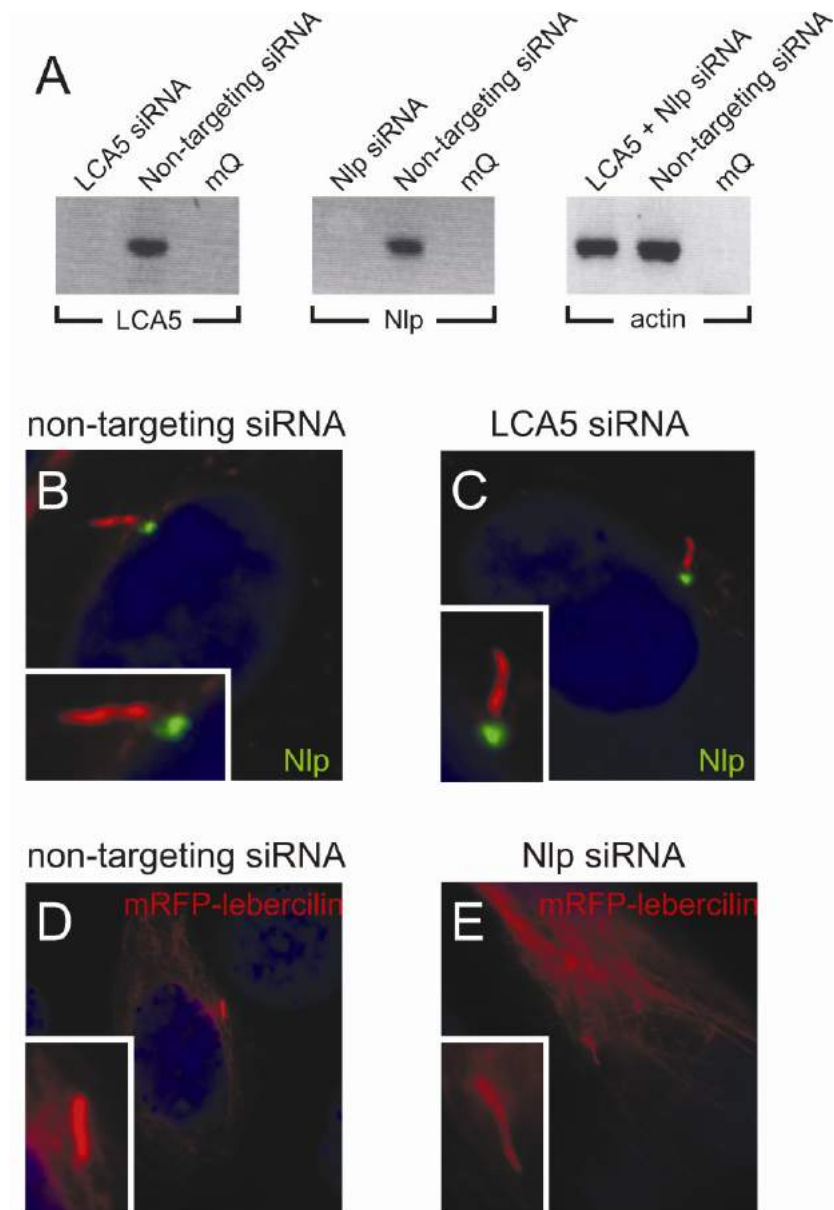
Human ON-TARGET-PLUS siRNA SMART-POOL (Dharmacon, Inc.) was used to knockdown *Nlp* in ARPE-19 cells. As a negative control, the non-targeting siRNA SMART-POOL (Dharmacon, Inc.) was used. Cells were transfected in duplo with siRNA pools (20 nM) by using HiPerFect transfection reagent in complete DMEM medium containing 10% FCS, according to manufacturers instruction (Qiagen). Three days after the initial transfection, cells were transfected for the second time in low-serum containing DMEM medium (0.5% FCS) and cultured for an additional two days. To test the efficiency of the knockdown, RNA was isolated from one well by using RNA-Bee (Tel-Test, Inc.), followed by a semi-quantitative RT-PCR using *Nlp* and *LCA5* specific primers. The second well of cells were fixed with methanol at -20 °C, and subsequently used for immunohistochemistry. Cells were mounted with Vectashield containing DAPI (Vector Laboratories, Inc., UK). Images were taken with an AxioPlan2 Imaging fluorescence microscope (Zeiss) equipped with a DC350FX camera (Zeiss).

**Supplementary material**



**Supplementary Figure 1.** Specificity of anti-Nlp and anti-USH2A antibodies. Immunohistochemical stainings of rat retina (P20) with (pre-adsorped) anti-Nlp antibodies (**A**) and anti-USH2A antibodies (**B**). Upon pre-adsorption, no signals were detected. (**C**) Western blot analysis with anti-Nlp antibodies. Anti-Nlp antibodies detect GFP-tagged Nlp<sup>isoA</sup> but not GFP-tagged ninein, indicating the specificity of the antibodies.





**Supplementary Figure 2.** Silencing of *Nlp* and *LCA5* does not lead to a disruption of lebercilin and Nlp localization, respectively. RT-PCR analysis (30 cycles) on cells silenced with non-targeting, *LCA5*, or *Nlp* siRNAs with primers against *LCA5* (left panel), *Nlp* (middle panel) or *actin* (right panel) (A), indicating the efficiency and specificity of the knockdown. Nlp localization at the basal body (B) is independent of the presence of lebercilin (C). In addition, mRFP-lebercilin localization at the microtubule network, the basal body and the cilium (D) is independent of the presence of Nlp (E).

## References

1. Marazita ML, Ploughman LM, Rawlings B, et al. Genetic epidemiological studies of early-onset deafness in the U.S. school-age population. *Am J Med Genet.* 1993;46:486-491.
2. Spandau UH, Rohrschneider K. Prevalence and geographical distribution of Usher syndrome in Germany. *Graefes Arch Clin Exp Ophthalmol.* 2002;240:495-498.
3. Rosenberg T, Haim M, Hauch AM, et al. The prevalence of Usher syndrome and other retinal dystrophy-hearing impairment associations. *Clin Genet.* 1997;51:314-321.
4. Smith RJ, Berlin CI, Hejtmancik JF, et al. Clinical diagnosis of the Usher syndromes. Usher Syndrome Consortium. *Am J Med Genet.* 1994;50:32-38.
5. Kremer H, van Wijk E, Marker T, et al. Usher syndrome: molecular links of pathogenesis, proteins and pathways. *Hum Mol Genet.* 2006;15 Spec No 2:R262-R270.
6. Weil D, Blanchard S, Kaplan J, et al. Defective myosin VIIA gene responsible for Usher syndrome type 1B. *Nature.* 1995;374:60-61.
7. Weil D, El Amraoui A, Masmoudi S, et al. Usher syndrome type I G (USH1G) is caused by mutations in the gene encoding SANS, a protein that associates with the USH1C protein, harmonin. *Hum Mol Genet.* 2003;12:463-471.
8. Verpy E, Leibovici M, Zwaenepoel I, et al. A defect in harmonin, a PDZ domain-containing protein expressed in the inner ear sensory hair cells, underlies Usher syndrome type 1C. *Nat Genet.* 2000;26:51-55.
9. Bolz H, von Brederlow B, Ramirez A, et al. Mutation of CDH23, encoding a new member of the cadherin gene family, causes Usher syndrome type 1D. *Nat Genet.* 2001;27:108-112.
10. Bork JM, Peters LM, Riazuddin S, et al. Usher syndrome 1D and nonsyndromic autosomal recessive deafness DFNB12 are caused by allelic mutations of the novel cadherin-like gene CDH23. *Am J Hum Genet.* 2001;68:26-37.
11. Ahmed ZM, Riazuddin S, Bernstein SL, et al. Mutations of the protocadherin gene PCDH15 cause Usher syndrome type 1F. *Am J Hum Genet.* 2001;69:25-34.
12. van Wijk E, Pennings RJ, te Brinke H, et al. Identification of 51 novel exons of the Usher syndrome type 2A (USH2A) gene that encode multiple conserved functional domains and that are mutated in patients with Usher syndrome type II. *Am J Hum Genet.* 2004;74:738-744.
13. Eudy JD, Weston MD, Yao S, et al. Mutation of a gene encoding a protein with extracellular matrix motifs in Usher syndrome type IIa. *Science.* 1998;280:1753-1757.
14. Weston MD, Luijendijk MW, Humphrey KD, et al. Mutations in the VLGR1 gene implicate G-protein signaling in the pathogenesis of Usher syndrome type II. *Am J Hum Genet.* 2004;74:357-366.
15. Ebermann I, Scholl HP, Charbel IP, et al. A novel gene for Usher syndrome type 2: mutations in the long isoform of whirlin are associated with retinitis pigmentosa and sensorineural hearing loss. *Hum Genet.* 2007;121:203-211.
16. Joensuu T, Hamalainen R, Yuan B, et al. Mutations in a novel gene with transmembrane domains underlie Usher syndrome type 3. *Am J Hum Genet.* 2001;69:673-684.

17. Reiners J, van Wijk E, Maerker T, et al. Scaffold protein harmonin (USH1C) provides molecular links between Usher syndrome type 1 and type 2. *Hum Mol Genet.* 2005;14:3933-3943.
18. Boeda B, El Amraoui A, Bahloul A, et al. Myosin VIIa, harmonin and cadherin 23, three Usher I gene products that cooperate to shape the sensory hair cell bundle. *EMBO J.* 2002;21:6689-6699.
19. Adato A, Michel V, Kikkawa Y, et al. Interactions in the network of Usher syndrome type 1 proteins. *Hum Mol Genet.* 2005;14:347-356.
20. van Wijk E, van der Zwaag B, Peters TA, et al. The DFNB31 gene product whirlin connects to the Usher protein network in the cochlea and retina by direct association with USH2A and VLGR1. *Hum Mol Genet.* 2006;15:751-765.
21. Maerker T, van Wijk E, Overlack N, et al. A novel Usher protein network at the periciliary reloading point between molecular transport machineries in vertebrate photoreceptor cells. *Hum Mol Genet.* 2008;17:71-86.
22. Adato A, Lefevre G, Delprat B, et al. Usherin, the defective protein in Usher syndrome type IIA, is likely to be a component of interstereocilia ankle links in the inner ear sensory cells. *Hum Mol Genet.* 2005;14:3921-3932.
23. Liu X, Bulgakov OV, Darrow KN, et al. Usherin is required for maintenance of retinal photoreceptors and normal development of cochlear hair cells. *Proc Natl Acad Sci U S A.* 2007;104:4413-4418.
24. Hunter DG, Fishman GA, Mehta RS, et al. Abnormal sperm and photoreceptor axonemes in Usher's syndrome. *Arch Ophthalmol.* 1986;104:385-389.
25. Adams NA, Awadein A, Toma HS. The retinal ciliopathies. *Ophthalmic Genet.* 2007;28:113-125.
26. Jacobson SG, Cideciyan AV, Aleman TS, et al. Usher syndromes due to MYO7A, PCDH15, USH2A or GPR98 mutations share retinal disease mechanism. *Hum Mol Genet.* 2008;17:2405-2415.
27. Leber T. Uber retinitis pigmentosa und angebore amaurose. *Graefes Arch Clin Exp Ophthalmol.* 1869;15:1-25.
28. Franceschetti A, Dieterle P. Diagnostic and prognostic importance of the electroretinogram in tapetoretinal degeneration with reduction of the visual field and hemeralopia. *Confin Neurol.* 1954;14:184-186.
29. den Hollander AI, Koenekoop RK, Mohamed MD, et al. Mutations in LCA5, encoding the ciliary protein lebercilin, cause Leber congenital amaurosis. *Nat Genet.* 2007;39:889-895.
30. Arts HH, Cremers FPM, Knoers NVAM, et al. Focus on Molecules: RPGRIP1. *Exp Eye Res.* 2008;88:332-333.
31. den Hollander AI, Koenekoop RK, Yzer S, et al. Mutations in the CEP290 (NPHP6) gene are a frequent cause of Leber congenital amaurosis. *Am J Hum Genet.* 2006;79:556-561.
32. Casenghi M, Meraldi P, Weinhard U, et al. Polo-like kinase 1 regulates Nlp, a centrosome protein involved in microtubule nucleation. *Dev Cell.* 2003;5:113-125.
33. Trojan P, Krauss N, Choe HW, et al. Centriins in retinal photoreceptor cells: Regulators in the connecting cilium. *Prog Retin Eye Res.* 2008;27:237-259.

34. Grabarek Z. Structure of a trapped intermediate of calmodulin: calcium regulation of EF-hand proteins from a new perspective. *J Mol Biol.* 2005;346:1351-1366.
35. Cohen E, Binet S, Meininger V. Ciliogenesis and centriole formation in the mouse embryonic nervous system. An ultrastructural analysis. *Biol Cell.* 1988;62:165-169.
36. Rapley J, Baxter JE, Blot J, et al. Coordinate regulation of the mother centriole component nlp by nek2 and plk1 protein kinases. *Mol Cell Biol.* 2005;25:1309-1324.
37. Casenghi M, Barr FA, Nigg EA. Phosphorylation of Nlp by Plk1 negatively regulates its dynein-dynactin-dependent targeting to the centrosome. *J Cell Sci.* 2005;118:5101-5108.
38. Roepman R, Wolfrum U. Protein networks and complexes in photoreceptor cilia. *Subcell Biochem.* 2007;43:209-235.
39. Besharse JC, Horst CJ. Ciliary and Flagellar Membranes. In: In Bloodgood RA (ed) New York: Plenum; 2005:389-417.
40. Reiners J, Nagel-Wolfrum K, Jurgens K, et al. Molecular basis of human Usher syndrome: deciphering the meshes of the Usher protein network provides insights into the pathomechanisms of the Usher disease. *Exp Eye Res.* 2006;83:97-119.
41. Barrong SD, Chaitin MH, Fliesler SJ, et al. Ultrastructure of connecting cilia in different forms of retinitis pigmentosa. *Arch Ophthalmol.* 1992;110:706-710.
42. Dryja TP, Adams SM, Grimsby JL, et al. Null RPGRIP1 alleles in patients with Leber congenital amaurosis. *Am J Hum Genet.* 2001;68:1295-1298.
43. Liu Q, Zhou J, Daiger SP, et al. Identification and subcellular localization of the RP1 protein in human and mouse photoreceptors. *Invest Ophthalmol Vis Sci.* 2002;43:22-32.
44. Liu Q, Zuo J, Pierce EA. The retinitis pigmentosa 1 protein is a photoreceptor microtubule-associated protein. *J Neurosci.* 2004;24:6427-6436.
45. Iannaccone A, Breuer DK, Wang XF, et al. Clinical and immunohistochemical evidence for an X linked retinitis pigmentosa syndrome with recurrent infections and hearing loss in association with an RPGR mutation. *J Med Genet.* 2003;40:e118.
46. Hong DH, Yue G, Adamian M, Li T. Retinitis pigmentosa GTPase regulator (RPGR)-interacting protein is stably associated with the photoreceptor ciliary axoneme and anchors RPGR to the connecting cilium. *J Biol Chem.* 2001;276:12091-12099.
47. Rosenbaum JL, Witman GB. Intraflagellar transport. *Nat Rev Mol Cell Biol.* 2002;3:813-825.
48. Wolfrum U, Schmitt A. Rhodopsin transport in the membrane of the connecting cilium of mammalian photoreceptor cells. *Cell Motil Cytoskeleton.* 2000;46:95-107.
49. Pazour GJ, Dickert BL, Witman GB. The DHC1b (DHC2) isoform of cytoplasmic dynein is required for flagellar assembly. *J Cell Biol.* 1999;144:473-481.
50. Pedersen LB, Miller MS, Geimer S, et al. Chlamydomonas IFT172 is encoded by FLA11, interacts with CrEB1, and regulates IFT at the flagellar tip. *Curr Biol.* 2005;15:262-266.
51. Kozminski KG, Beech PL, Rosenbaum JL. The Chlamydomonas kinesin-like protein FLA10 is involved in motility associated with the flagellar membrane. *J Cell Biol.* 1995;131:1517-1527.

52. Evans JE, Snow JJ, Gunnarson AL, et al. Functional modulation of IFT kinesins extends the sensory repertoire of ciliated neurons in *Caenorhabditis elegans*. *J Cell Biol.* 2006;172:663-669.
53. Pazour GJ, Baker SA, Deane JA, et al. The intraflagellar transport protein, IFT88, is essential for vertebrate photoreceptor assembly and maintenance. *J Cell Biol.* 2002;157:103-113.
54. Baker SA, Freeman K, Luby-Phelps K, et al. IFT20 links kinesin II with a mammalian intraflagellar transport complex that is conserved in motile flagella and sensory cilia. *J Biol Chem.* 2003;278:34211-34218.
55. Insinna C, Pathak N, Perkins B, et al. The homodimeric kinesin, Kif17, is essential for vertebrate photoreceptor sensory outer segment development. *Dev Biol.* 2008;316:160-170.
56. Marszalek JR, Liu X, Roberts EA, et al. Genetic evidence for selective transport of opsin and arrestin by kinesin-II in mammalian photoreceptors. *Cell.* 2000;102:175-187.
57. Pazour GJ, Dickert BL, Vucica Y, et al. Chlamydomonas IFT88 and its mouse homologue, polycystic kidney disease gene *tg737*, are required for assembly of cilia and flagella. *J Cell Biol.* 2000;151:709-718.
58. Abd-El-Barr MM, Sykoudis K, Andrabi S, et al. Impaired photoreceptor protein transport and synaptic transmission in a mouse model of Bardet-Biedl syndrome. *Vision Res.* 2007;47:3394-3407.
59. Nachury MV, Loktev AV, Zhang Q, et al. A core complex of BBS proteins cooperates with the GTPase Rab8 to promote ciliary membrane biogenesis. *Cell.* 2007;129:1201-1213.
60. Overlack N, Maerker T, Latz M, et al. SANS (USH1G) expression in developing and mature mammalian retina. *Vision Res.* 2008;48:400-412.
61. Liu X, Udovichenko IP, Brown SD, et al. Myosin VIIa participates in opsin transport through the photoreceptor cilium. *J Neurosci.* 1999;19:6267-6274.
62. Follit JA, Tuft RA, Fogarty KE, et al. The intraflagellar transport protein IFT20 is associated with the Golgi complex and is required for cilia assembly. *Mol Biol Cell.* 2006;17:3781-3792.
63. Papermaster DS. The birth and death of photoreceptors: the Friedenwald Lecture. *Invest Ophthalmol Vis Sci.* 2002;43:1300-1309.
64. Tai AW, Chuang JZ, Bode C, et al. Rhodopsin's carboxy-terminal cytoplasmic tail acts as a membrane receptor for cytoplasmic dynein by binding to the dynein light chain Tctex-1. *Cell.* 1999;97:877-887.
65. Reiter JF, Mostov K. Vesicle transport, cilium formation, and membrane specialization: the origins of a sensory organelle. *Proc Natl Acad Sci U S A.* 2006;103:18383-18384.
66. Zhang H, Shi X, Paddon H, et al. B23/nucleophosmin serine 4 phosphorylation mediates mitotic functions of polo-like kinase 1. *J Biol Chem.* 2004;279:35726-35734.
67. Shinmura K, Tarapore P, Tokuyama Y, et al. Characterization of centrosomal association of nucleophosmin/B23 linked to Crm1 activity. *FEBS Lett.* 2005;579:6621-6634.
68. Shu X, Fry AM, Tulloch B, et al. RPGR ORF15 isoform co-localizes with RPGRIP1 at centrioles and basal bodies and interacts with nucleophosmin. *Hum Mol Genet.* 2005;14:1183-1197.
69. Khanna H, Hurd TW, Lillo C, et al. RPGR-ORF15, which is mutated in retinitis pigmentosa, associates with SMC1, SMC3, and microtubule transport proteins. *J Biol Chem.* 2005;280:33580-33587.

70. Roepman R, Schick D, Ferreira PA. Isolation of retinal proteins that interact with retinitis pigmentosa GTPase regulator by interaction trap screen in yeast. *Methods Enzymol.* 2000;316:688-704.
71. James P, Halladay J, Craig EA. Genomic libraries and a host strain designed for highly efficient two-hybrid selection in yeast. *Genetics.* 1996;144:1425-1436.
72. Lujendijk MWJ, van de Pol TJ, van Duijnhoven G, et al. Cloning, characterization, and mRNA expression analysis of novel human fetal cochlear cDNAs. *Genomics.* 2003;82:480-490.
73. Maruyama K, Mikawa T, Ebashi S. Detection of calcium binding proteins by <sup>45</sup>Ca autoradiography on nitrocellulose membrane after sodium dodecyl sulfate gel electrophoresis. *J Biochem (Tokyo).* 1984;95:511-519.



# Chapter 5

---

## **The mitotic spindle protein SPAG5/Astrin connects to the Usher protein network postmitotically**

Ferry F.J. Kersten<sup>1-5</sup>, Erwin van Wijk<sup>1,2,4,5</sup>, Lisette Hetterschijt<sup>1</sup>, Katharina Bauß<sup>6</sup>, Theo A. Peters<sup>2,4,5</sup>, Mariam G. Aslanyan<sup>1,4</sup>, Bert van der Zwaag<sup>7</sup>, Uwe Wolfrum<sup>6</sup>, Jan E.E. Keunen<sup>3</sup>, Ronald Roepman<sup>1,4,#</sup> and Hannie Kremer<sup>1,2,4,5,#</sup>

# These authors contributed equally to this work

<sup>1</sup>Department of Human Genetics, <sup>2</sup>Department of Otorhinolaryngology, Head and Neck Surgery and <sup>3</sup>Department of Ophthalmology, Radboud University Nijmegen Medical Centre, Nijmegen, The Netherlands, <sup>4</sup>Nijmegen Centre for Molecular Life Sciences, and <sup>5</sup>Donders Institute for Brain, Cognition and Behaviour, Radboud University Nijmegen, Nijmegen, The Netherlands, <sup>6</sup>Department of Cell and Matrix Biology, Institute of Zoology, Johannes Gutenberg University of Mainz, Mainz, Germany, <sup>7</sup>Department of Neuroscience and Pharmacology, Rudolf Magnus Institute of Neuroscience, University Medical Centre Utrecht, Utrecht, The Netherlands.

---

*Cilia* 2011; in press

---







## **Abstract**

Mutations in *USH2A* are causative for non-syndromic retinitis pigmentosa and Usher syndrome that is the most common cause of combined deaf-blindness. To gain insight into the molecular pathology underlying USH2A-associated retinal degeneration, we set out to identify interacting proteins of USH2A isoform B (USH2A<sup>isoB</sup>) in the retina. As a result the centrosomal and microtubule-associated protein SPAG5 was identified. SPAG5 was also found to interact with another previously described USH2A<sup>isoB</sup> interaction partner: the centrosomal ninein-like protein NINL<sup>isoB</sup>. *In situ* hybridization demonstrated that *Spag5* was widely expressed during murine embryonic development, with prominent signals in the eye, cochlea, brain, kidney and liver. *SPAG5* expression in adult human tissues was detected by quantitative PCR in the retina, brain, intestine, kidney and testis. In the retina, *Spag5*, *Ush2a*<sup>isoB</sup> and *Ninl*<sup>isoB</sup> were present at several subcellular structures of photoreceptor cells, and co-localized at the basal bodies. Based on this and on the suggested roles for USH proteins in vesicle transport and providing structural support to both the inner ear and the retina, we hypothesize that SPAG5, USH2A<sup>isoB</sup> and NINL<sup>isoB</sup> may function together in microtubule-based cytoplasmic trafficking of proteins that are essential for cilium formation, maintenance and/or function.

## Introduction

Mutations in *USH2A* are causative for non-syndromic recessive retinitis pigmentosa (RP)<sup>1-4</sup> and for Usher syndrome type II (USH2), a recessive disease characterized by congenital moderate to severe, stable hearing loss and RP that often leads to blindness<sup>5</sup>. Mutations in this gene likely account for 8-20% of the autosomal recessive RP cases<sup>3,6</sup> and are suggested to be the most common cause of RP in the USA<sup>3</sup>. It is estimated that up to 85% of USH2 patients and about half of all Usher syndrome cases have mutations in *USH2A*<sup>7</sup>. All proteins encoded by genes associated with USH1 and USH2 are present in hair cells and photoreceptor cells, and are interconnected in a network of interacting proteins<sup>8-12</sup>. To gain insight into the molecular pathology of retinal degeneration resulting from *USH2A* mutations, we have set out to determine the retinal repertoire of USH2A<sup>isoB</sup>-interacting proteins. By using the intracellular domain of USH2A<sup>isoB</sup> as a bait in an interaction trap screen of a retinal cDNA library expressed in yeast (yeast two-hybrid screening), we recently identified the centrosomal protein NINL<sup>isoB</sup>, previously known as Nlp (ninein-like protein). Ninl<sup>isoB</sup> co-localized with Ush2a<sup>isoB</sup> at centrioles, basal bodies and in the periciliary regions of photoreceptor cells<sup>13</sup>. We hypothesized that NINL<sup>isoB</sup> functions in handing over cargo vesicles from the transport system of the inner segment to the intraflagellar transport (IFT) machinery that is involved in transport through the connecting cilium<sup>13,14</sup>. Thereby, NINL<sup>isoB</sup> may function in the development and maintenance of the connecting cilium and outer segment<sup>13</sup>. Besides NINL<sup>isoB</sup>, another centrosomal and microtubule-associated protein was identified in the yeast two-hybrid screen, namely SPAG5, also called astrin. SPAG5 was originally identified as a microtubule-associated protein with a dual localization to both centrosomes and kinetochores and is required for mitotic spindle formation and chromosome segregation<sup>15,16</sup>. Targeting of SPAG5 to the centrosome during the S and G2 phases of the cell cycle is mediated by ninein and the SPAG5-ninein interaction is required for the maintenance of centrosome/spindle pole integrity<sup>17</sup>. Interestingly, ninein is a paralog of NINL which prompted us to investigate the interaction between SPAG5 and NINL<sup>isoB</sup>. In this study, we describe the specific interaction between SPAG5 and both USH2A<sup>isoB</sup> and NINL<sup>isoB</sup> and their (partial) co-localization in photoreceptor cells. Our results suggest that these proteins function directly or indirectly in microtubule-based vesicle transport that is essential for the long-term maintenance and/or function of photoreceptor cells.

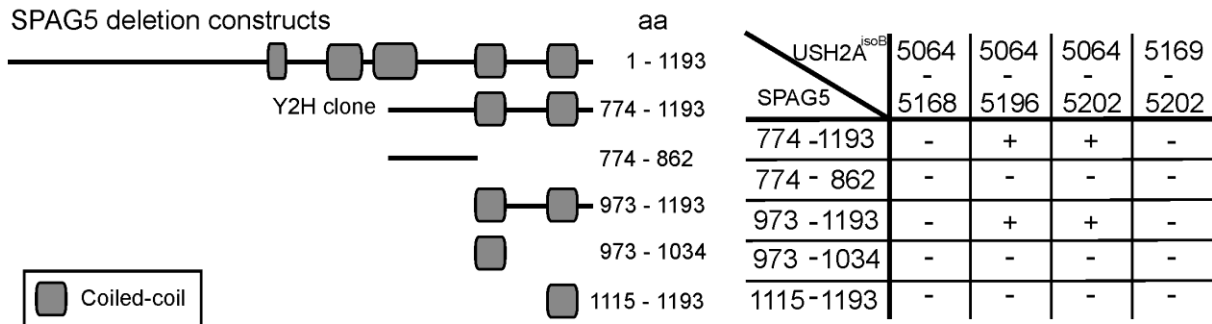
## Results

### Interaction of SPAG5 with USH2A<sup>isoB</sup> and NINL<sup>isoB</sup>

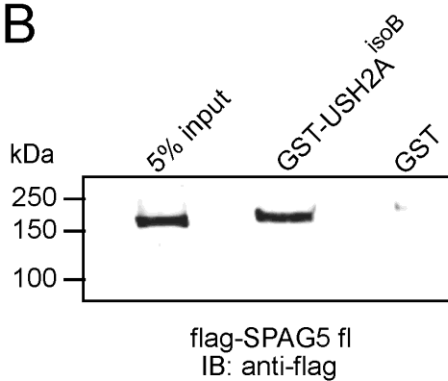
A yeast two-hybrid (Y2H) screen of an oligo-d(T) primed human retinal cDNA library was performed to identify interaction partners of USH2A<sup>isoB</sup> by using its intracellular domain (icd; USH2A<sup>isoB</sup>icd) as a bait. Two identical clones, encoding SPAG5 amino acid (aa) 774-1193 were identified among the clones that activated all four reporter genes (Fig. 1A). The interaction between USH2A<sup>isoB</sup> and SPAG5 was confirmed by a glutathione *S*-transferase (GST) pull-down assay as full-length (fl) flag-tagged SPAG5 was efficiently pulled down from COS-1 cell lysates by GST-fused USH2A<sup>isoB</sup>icd, and not by GST alone (Fig. 1B). To determine the interacting epitopes of the proteins, we performed a Y2H analysis using constructs encoding fragments of USH2A<sup>isoB</sup>icd (aa 5064-5202) and the SPAG5 Y2H clone. The USH2A<sup>isoB</sup> peptide containing aa 5064-5196 was determined to interact with the SPAG5 fragment containing aa 973-1193 (Fig. 1A). To further validate the interaction, we performed a co-immunoprecipitation assay from COS-1 cells. This assay showed that HA-tagged SPAG5 aa 973-1193 specifically co-immunoprecipitated with the GFP-tagged USH2A<sup>isoB</sup>icd peptide (Fig. 1C).

In the described Y2H screen with the USH2A<sup>isoB</sup>icd peptide as a bait, also NINL<sup>isoB</sup> was identified as an interaction partner<sup>13</sup>. Interestingly, Cheng and coworkers previously demonstrated that SPAG5 also interacts with ninein<sup>17</sup> which is a paralog of NINL. We therefore assessed the interaction between SPAG5 and NINL<sup>isoB</sup> as well. In a liquid beta-galactosidase assay, both NINL<sup>isoB</sup> fl and the predicted NINL<sup>isoB</sup> intermediate filament domain (IF; aa 656-925) were found to interact with SPAG5 aa 973-1193 (Fig. 2A). The interaction strength between SPAG5 aa 973-1193 and NINL<sup>isoA</sup> fl was significantly weaker (data not shown). The interaction between SPAG5 and NINL<sup>isoB</sup> was confirmed in a GST pull-down assay, as well as by co-immunoprecipitation. Flag-tagged NINL<sup>isoB</sup> fl was efficiently pulled down from COS-1 lysates by GST-fused SPAG5 aa: 973-1193 (Fig. 2B). Besides that it co-immunoprecipitated with HA-tagged SPAG5 fl (Fig. 2C). From these experiments we can conclude that SPAG5 interacts with both USH2A<sup>isoB</sup> and NINL<sup>isoB</sup>.

A



B



C

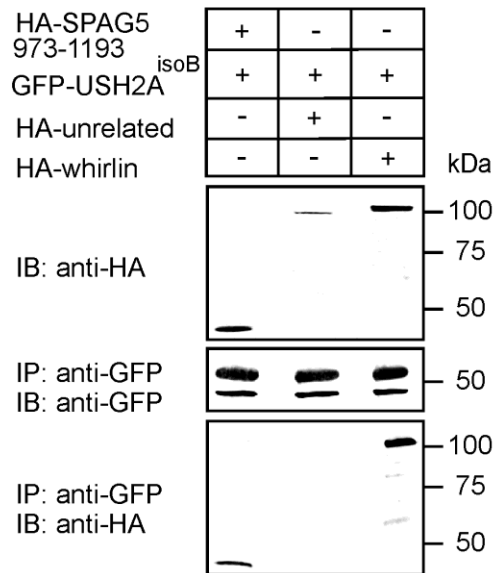
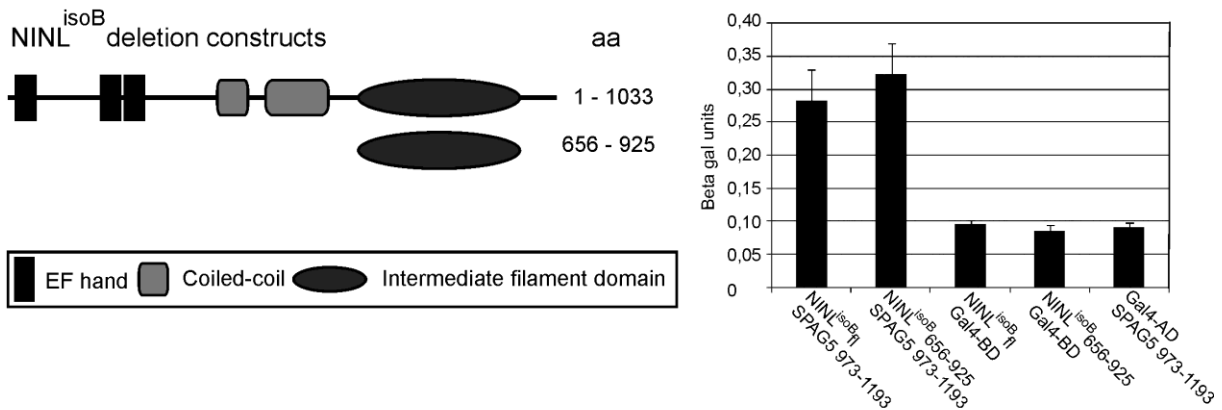
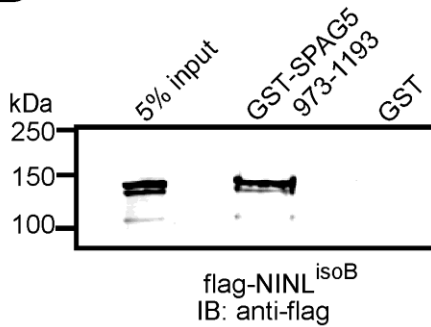


**Figure 1.** SPAG5 and U<sup>isoB</sup> interact. (A) Depicted are the schematic protein structures of SPAG5 and the peptides encoded by deletion constructs. Numbers represent amino acids (aa; NP\_006452). Protein fragments encoded by deletion constructs of *SPAG5* and the intracellular domain (icd) of U<sup>isoB</sup> were used in a yeast two-hybrid analysis. This demonstrates a specific interaction between U<sup>isoB</sup> (aa 5064-5196) and the c-terminal two coiled-coil domains (aa 973-1193) of SPAG5. (B) GST pull-down assays showing that flag-tagged SPAG5 is efficiently pulled down by GST-U<sup>isoB</sup>icd, but not by GST alone, as detected by an anti-flag antibody. The first lane shows 5% of the input of COS-1 cell lysate. (C) HA-SPAG5 aa 973-1193 from COS-1 lysates co-immunoprecipitates with GFP-fused U<sup>isoB</sup>icd, but not with an unrelated HA-tagged protein (EPS8). As a positive control, HA-whirlin is shown to co-immunoprecipitate with GFP-fused U<sup>isoB</sup>icd. The upper protein band in the middle blot represents the heavy chain of the anti-GFP antibody.

A



B



C

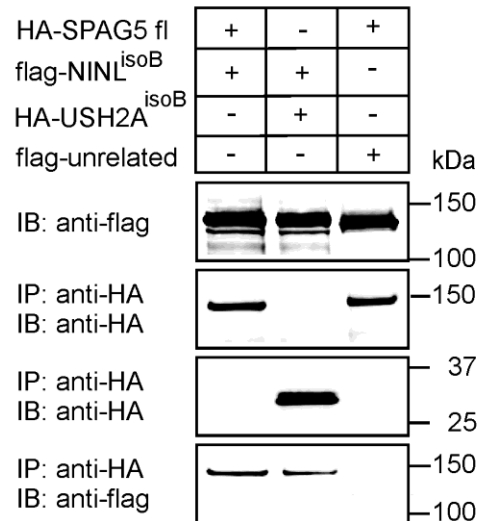


**Figure 2.** Validation of the SPAG5 – NINL<sup>isoB</sup> interaction. (A) The schematic protein structure of NINL<sup>isoB</sup> and the predicted intermediate filament domain (IF; aa 656-925), encoded by a deletion construct. A liquid beta-galactosidase assay revealed a specific interaction between SPAG5 (aa 973-1193) and the IF domain of NINL<sup>isoB</sup>. (B) GST pull-down assay showing that flag-tagged NINL<sup>isoB</sup> was efficiently pulled down by GST-SPAG5 (aa 973-1193), but not by GST alone, as detected by an anti-flag antibody. The first lane shows 5% of the protein input. (C) Flag-NINL<sup>isoB</sup> co-immunoprecipitated with HA-SPAG5 fl and the positive control HA-USH2A<sup>isoB</sup> icd, but not with the HA-tagged unrelated protein MDA5.

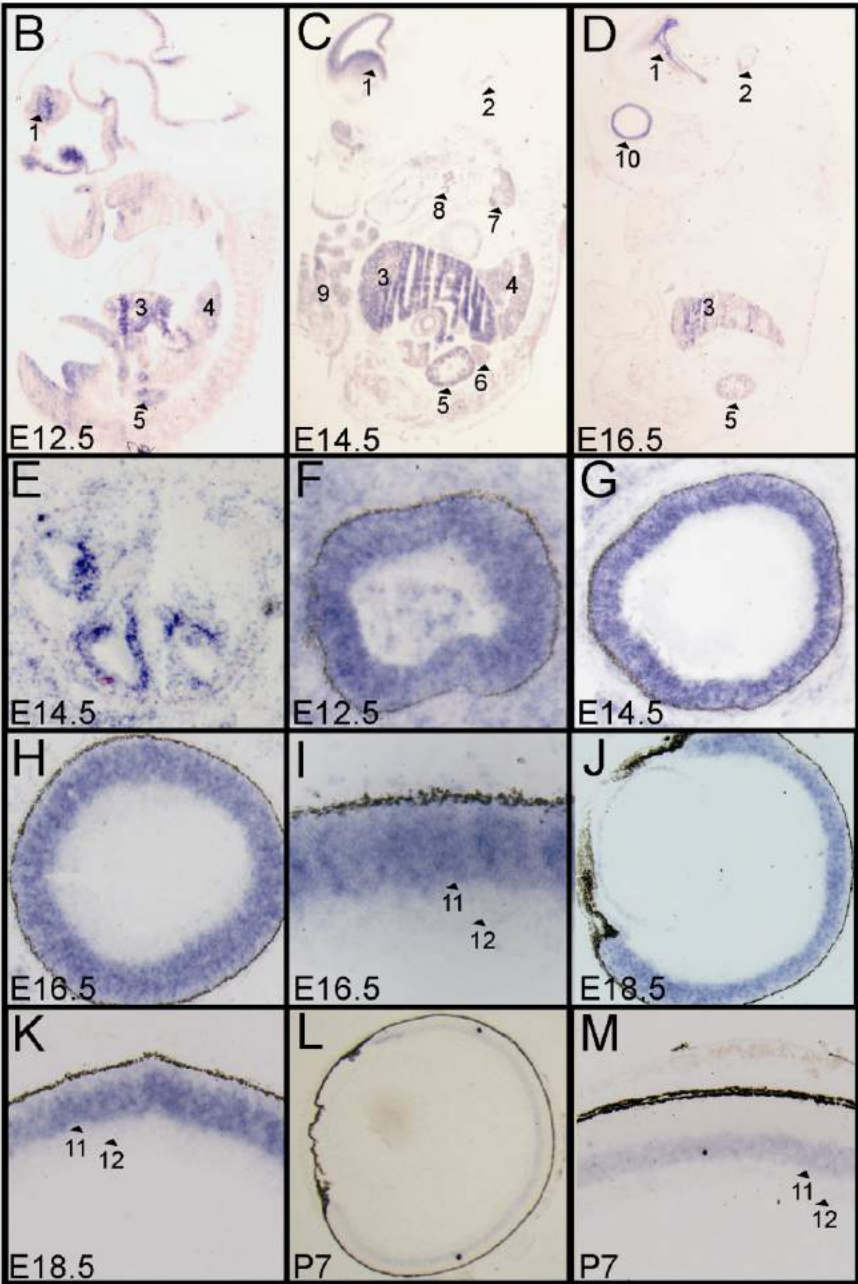
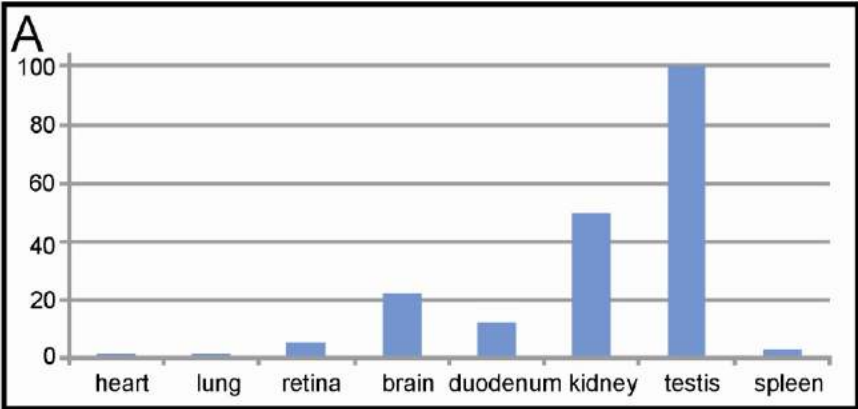


**Figure 3.** *SPAG5* expression in human adult tissues and *Spag5* expression during murine development. (A) By using quantitative PCR, *SPAG5* expression was detected in the human retina, brain, duodenum, kidney and testis. (B-M). RNA *in situ* hybridization of *Spag5* mRNA in mouse embryos at day E12.5-E18.5 and eyes of mice at postnatal day 7 (P7). *Spag5* was widely expressed during murine development (E12.5-E16.5; B-D), with most intense signals, in the following structures indicated by numbers and *arrowheads*: ventricular zone of forebrain (1), and midbrain (2), liver (3), lung (4), kidney (5), adrenal gland (6), thymus gland (7), submandibular salivary gland (8), limbs (9), eye (10). Expression was also observed in the cochlea (E), primordial of follicles of vibrissae, upper and lower jaw, intestine, heart, olfactory epithelium and in the testis (data not shown). From E16.5 onwards, expression was mainly detected in the eye, brain, kidney, lung, thymus, primordial of follicles of vibrissae and in the liver (D; and data not shown). A strong signal for *Spag5* was observed in the eye during embryonic development E12.5-E18.5 in the neuroblastic layer of the retina (F-K). At E16.5 (I) and E18.5 (K), *Spag5* expression was present in the developing inner nuclear layer (INL; 11) and, although much weaker, in the ganglion cell layer (GCL; 12) and maintained at postnatal day 7 (L-M).

### ***SPAG5* expression in human adult tissues and during murine development**

*SPAG5* is known to play a role in cell proliferation and therefore an important function during development could be expected. To examine this, we determined the expression pattern of *SPAG5* in human adult tissues by quantitative PCR (qPCR), using primers in exon 12 and 13. Of the examined human adult tissues, expression of *SPAG5* was mainly detected in the retina, brain, duodenum, kidney and testis (Fig. 3A).

We used RNA *in situ* hybridization (ISH) to determine the expression of *Spag5* during development. ISH was performed using mouse embryos of gestational day 12.5-18.5 (E12.5-E18.5) and eyes of mice at postnatal day 7 (P7). *Spag5* was found to be widely transcribed during murine embryonic development. At E12.5 and E14.5, transcripts were detected in the eye, cochlea, fore- and midbrain, kidney, liver, lung, adrenal gland, thymus, submandibular (salivary) glands, primordial of follicles of vibrissae, limbs, upper and lower jaws, intestine, heart, olfactory epithelium, and in the testis (Figs. 3B-C, E-G and data not shown). From E16.5 onwards, *Spag5* transcripts were mainly observed in the eye, the brain, the kidney, the lung, the thymus, the primordial of follicles of vibrissae and in the liver (Figs. 3D, H-K and data not shown). From E12.5 to E18.5, *Spag5* transcripts were observed in the neuroblastic layer of the retina (Figs. 3F-K) and at E16.5 (Fig. 3I) and E18.5 (Fig. 3K) these transcripts were detected more specifically at the (developing) inner nuclear layer (INL) and in low amounts in the ganglion cell layer (GCL). This pattern is maintained at P7 (Fig. 3L-M).



Hybridizations with a sense cRNA probe revealed no signals indicating the specificity of the assay (data not shown).

### ***Spag5 localization in the retina***

As SPAG5 was identified from a retinal cDNA library and *Spag5* mRNA was expressed in the developing and the adult retina, we set out to determine its retinal subcellular localization. For this purpose, rat cryosections (P20) were co-stained with affinity purified anti-SPAG5 antibodies (green; Figs. 4A-Aii) and monoclonal anti-*pan*-centrin antibodies (20H5, red; Figs. 4B-Bii) as a marker for the basal body, the connecting cilium, the accessory centriole of photoreceptor cells, and the centrioles in both the inner nuclear layer (INL) and the ganglion cell layer (GCL) <sup>18</sup>. *Spag5* was predominantly detected at the basal body (BB) of photoreceptor cells and at one of the two centrosomal centrioles in both the INL and GCL, as shown by a partial co-localization with centrin that mark these structures (yellow; Figs. 4C-Cii and data not shown). In addition, *Spag5* immunostaining was weakly detected at the distal part of the connecting cilium (CC), in the accessory centriole, at the outer limiting membrane (OLM; *filled arrowhead*) and at the outer plexiform layer (OPL) (Fig. 4A-Ai).

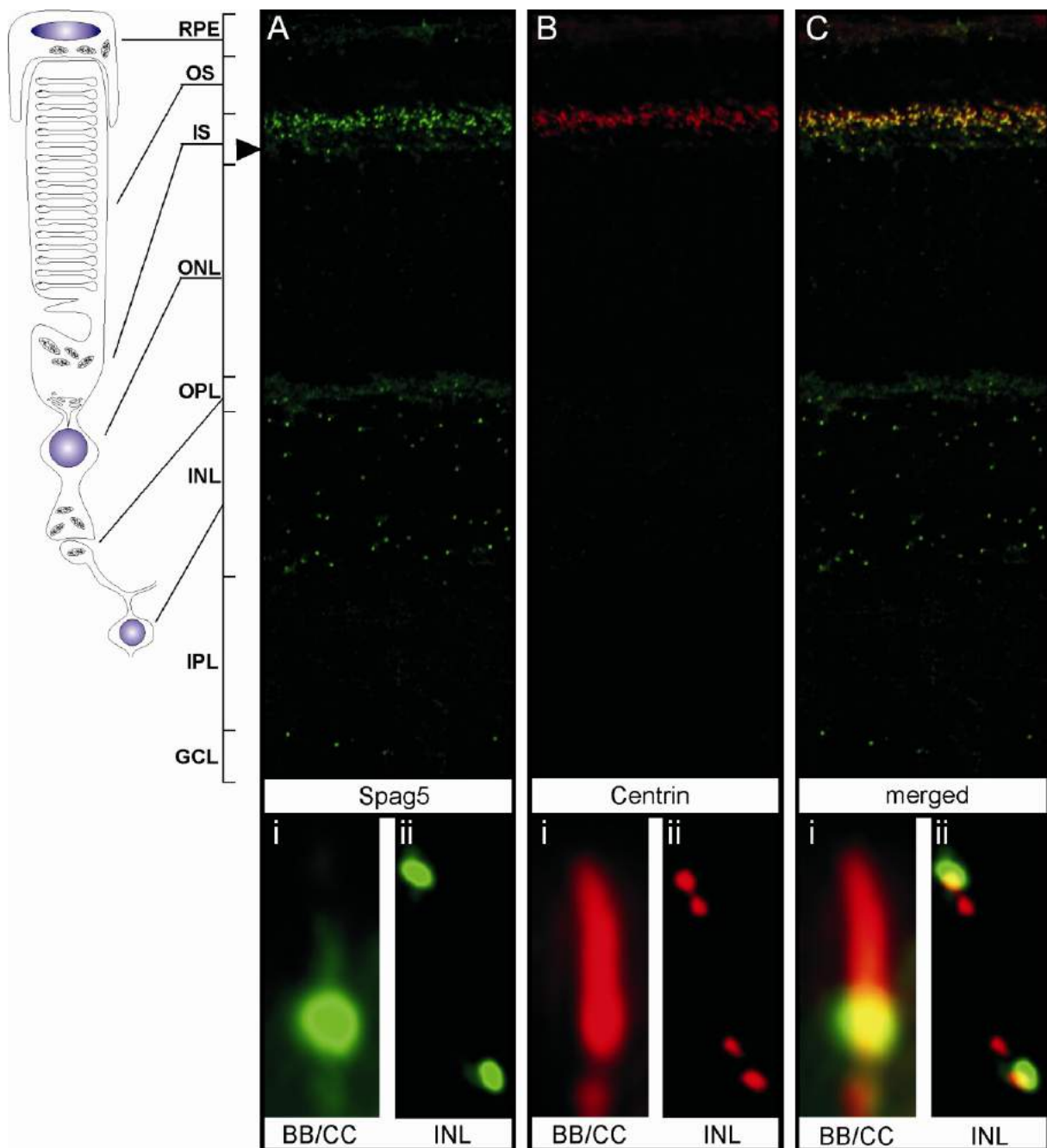


**Figure 4.** Subcellular localization of Spag5 in retina cryosections of adult (P20) rats. (A-C) Co-immunostaining using anti-SPAG5 antibodies (A; green) and anti-pan-centrin antibodies (B; red, a marker for the connecting cilium, basal body and centrioles). Co-localization (C; yellow) was detected at the basal body (BB; Ci) and in one of the two centrioles of the inner nuclear layer (INL; Cii). Centriole staining is also visible in the ganglion cell layer (GCL; A, C). In addition, weaker Spag5 labeling was detected at the outer limiting membrane (OLM; filled arrowhead), the outer plexiform layer (OPL), at the distal part of the connecting cilium (CC) and at the accessory centriole. (ABCi-ii). High magnification fluorescence microscopy of the BB/CC region and the INL.

To determine the Spag5 distribution in the photoreceptor cells in more detail, we used immunoelectron microscopy. Spag5 was detected around the basal body (BB; Figs. 5A-B) and at the collar-like extension of the apical inner segment (CE; Figs. 5A-C). In some photoreceptors labelling was detected in the region of the rootlet (R; Figs. 5A). Recently, immunoelectron microscopy studies demonstrated the subcellular localization of Ush2a<sup>isoB</sup> and Ninl<sup>isoB</sup> at these structures as well, although both proteins were detected directly at the basal body<sup>10,13</sup> and Spag5 was mainly located around it.

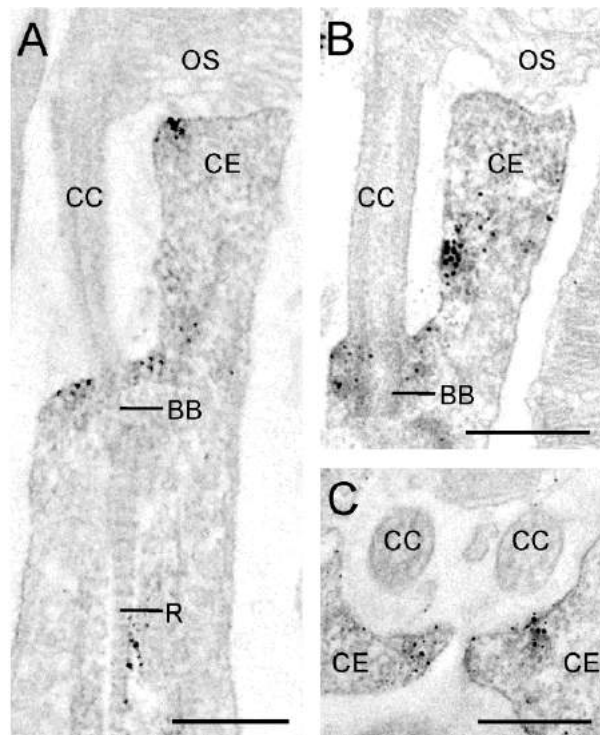


**Figure 5.** Localization of Spag5 by immunoelectron microscopy. Electron micrographs of pre-embedded anti-SPAG5 labeling in longitudinal (A-B) and cross (C) sections of mouse rod photoreceptor cells. Spag5 was detected around the basal body (BB; A-B), in the collar-like extension of the apical inner segment (CE; A-C), in some photoreceptors at the region of the rootlet (R; A). Connecting cilium (CC), Outer segment (OS), Inner segment (IS), Scale bars: 0.5  $\mu$ m.

### Spag5 co-localization with Ush2a<sup>isoB</sup> and Ninl<sup>isoB</sup> in photoreceptor cells

To investigate whether Spag5 and Ush2a<sup>isoB</sup> co-localize in the retina, we performed immunostainings on retinal cryosections using affinity-purified antibodies against SPAG5 (red; Fig. 6A) and USH2A<sup>isoB</sup> (green; Fig. 6B). This revealed partial co-localization of these proteins at the basal body (yellow; Fig. 6C). The same analysis was performed for SPAG5

and NINL<sup>isoB</sup>. By using affinity-purified antibodies against SPAG5 (green; Fig. 6D) and NINL<sup>isoB</sup> (red; Fig. 6E), a partial co-localization was detected at the basal body/centriole in the region of the connecting cilium and in the INL (yellow; Fig. 6F and data not shown). Although weak for anti-SPAG5, both antibodies also stained the ciliary rootlets (Figs. 6Di-Ei). The rootlet localization of SPAG5 was confirmed indirectly by a co-immunostaining (yellow; Fig. 6I) using antibodies against NINL<sup>isoB</sup> (green; Fig. 6G) and rootletin (red; Fig. 6H).

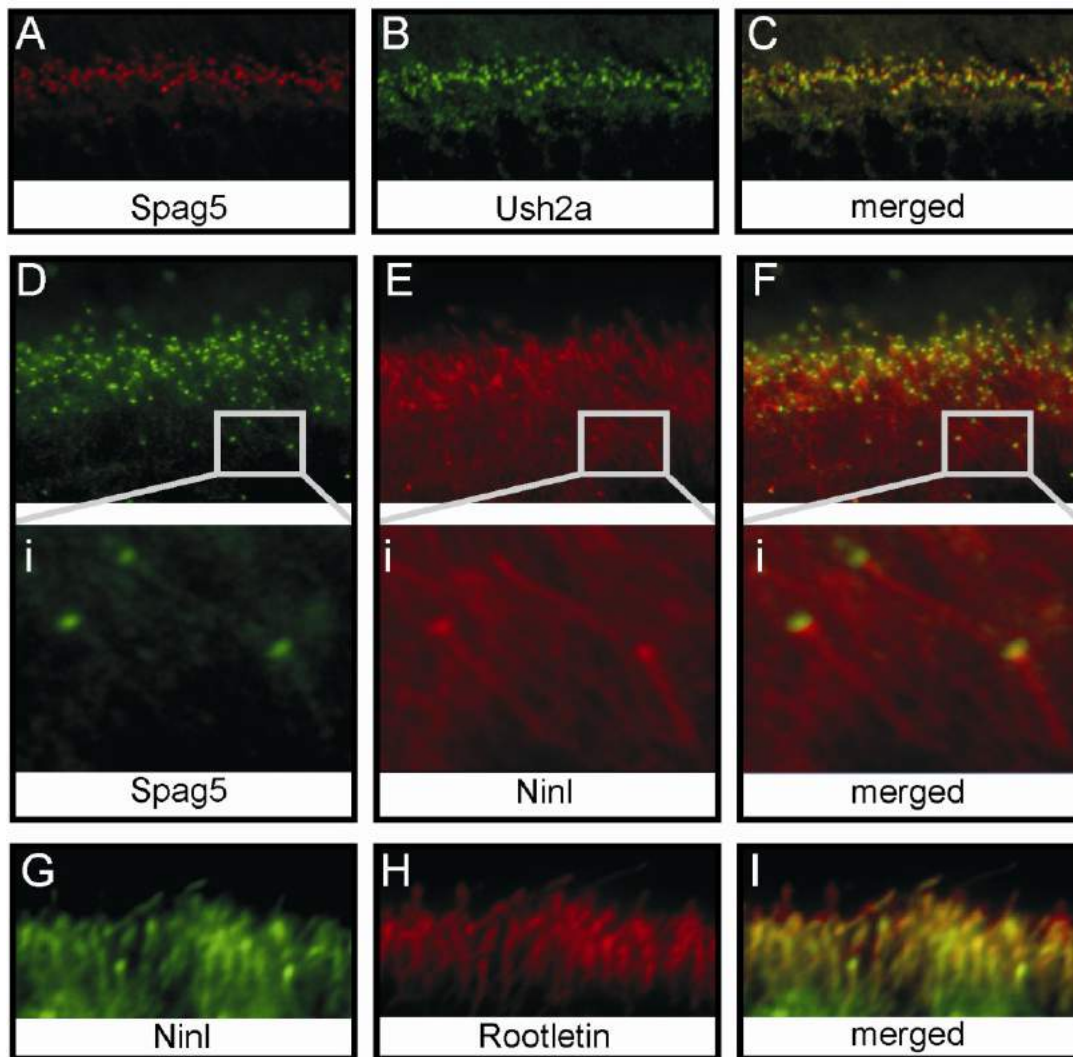


**Figure 6.** Co-localization of Spag5 and Ush2a<sup>isoB</sup>, and Ninl<sup>isoB</sup> in the retina of young adult (P20) rat. Co-immunostaining of Spag5 and Ush2a<sup>isoB</sup> in retinal cryosections using anti-SPAG5 antibodies (A; red) and anti-USH2A<sup>isoB</sup> antibodies (B; green) show partial co-localization (C; yellow) at the basal body. Co-immunostaining using anti-SPAG5 antibodies (D; green) and anti-NINL<sup>isoB</sup> antibodies (E; red). A partial co-localization (F; yellow) was detected at the basal body. In addition, both antibodies label the ciliary rootlets (Di,Ei), which was confirmed by a co-staining (I; yellow) using anti-NINL<sup>isoB</sup> (G; green) and anti-rootletin (H; red) antibodies.

**Discussion**

In this study, we identified SPAG5 as a novel member of the Usher protein network via its interaction with both USH2A<sup>isoB</sup> and NINL<sup>isoB</sup>. SPAG5 is a non-motor microtubule-associated protein that is essential for progression through mitosis<sup>15,16,19,20</sup>. We show that *Spag5* is widely expressed during mouse development which meets its function in cell proliferation. However, we also detected Spag5 in photoreceptor cells, indicating that Spag5 also plays a postmitotic role in differentiated ciliated cells.

During mitosis, SPAG5 localizes to centrosomes and spindle- and kinetochore microtubules and is required for correct mitotic spindle formation, sister chromatid cohesion and centrosome integrity<sup>15,16,19-21</sup>. In contrast, SPAG5's interaction partner NINL<sup>isoB</sup> mainly fulfills a role during interphase where it is involved in microtubule organization and nucleation<sup>22-24</sup>. However, during cytokinesis at the end-stage of mitosis, SPAG5 and NINL were detected at the midzone microtubules<sup>15,21</sup> and the midbody,<sup>13,25</sup> respectively. Depletion of SPAG5 results in cellular growth arrest with disorganized multipolar spindles, which ultimately leads to (p53-dependent) apoptosis<sup>16,20,26</sup>. NINL is required for proper centrosome maturation and spindle assembly and NINL abnormalities may contribute to genomic instability and tumorigenesis<sup>22,27,28</sup>. In conclusion, both SPAG5 and NINL are essential for proper cell proliferation.

After exit from the cell cycle, a primary cilium develops which essentially is a microtubule-based antenna-like structure that protrudes from the (apical) surface of many cell types. Cilia are involved in a wide variety of sensory functions, such as chemical, mechanical and photo-sensation, hedgehog signaling and the control of cell growth<sup>29,30</sup>. Cilia assembly and disassembly are tightly coupled to the cell cycle<sup>31</sup>. Therefore, it is not surprising that similar protein complexes play a role in both cell cycle regulation and cilia assembly and function. Indeed, Smith and co-workers recently found that the proteomes of the midbody and of the cilia/basal body significantly overlap<sup>32</sup>. Furthermore, they demonstrated the presence of a number of central spindle/midbody proteins, which control cytokinesis during mitosis, at the basal body/rootlet of ciliated cells, where they were suggested to control cilia morphogenesis and function<sup>32</sup>.

The outer segment of the postmitotic photoreceptor cell is a highly specialized sensory cilium with the connecting cilium as the ciliary transition zone<sup>33,34</sup>. Proteins involved in the formation and maintenance of the outer segments as well as proteins involved in the visual cycle are synthesized in the inner segment and actively transported to the outer segment involving the intraflagellar transport (IFT) machinery<sup>14,35</sup>. A significant part of protein transport towards the basal body is via trans-Golgi derived vesicles that migrate along microtubules. These vesicles are thought to dock in the region of the basal body and at the membrane of the apical inner segment that surrounds the connecting cilium as a collar<sup>10,14,36,37</sup>. At the central spindle and midbody, a protein network, including proteins that are also present at the basal body, organizes the microtubule bundles and vesicle recruitment for cell abscission<sup>32</sup>. Based on this and on the (co-)localization of Spag5 and Ninl<sup>isoB</sup> at the basal body, the rootlet, and the collar-like apical inner segment of photoreceptor cells (Figs. 5, 6)<sup>13</sup>, we propose that both proteins function in the development and/or function of the photoreceptor cilium by a direct involvement in vesicle transport towards the basal body and possibly the rootlet, or by an indirect role in microtubule organization. More specifically, Ninl<sup>isoB</sup> might function as an adapter protein in this retrograde transport by its association with the dynactin p50-dynamitin and p150<sup>Glued</sup> subunits of the dynein-dynactin motor complex<sup>13,23</sup>. This complex also transports kinetochore-components from kinetochores to spindle poles during mitosis<sup>38</sup>. As Spag5 is present at kinetochores and spindle poles during mitosis<sup>15,16</sup> it may serve as cargo of this complex. Therefore, Spag5 may be transported towards the basal body by the dynein-dynactin motor complex via its interaction with Ninl<sup>isoB</sup>, analogous to the targeting of Spag5 to the centrosome by Ninl's paralog ninein during the cell cycle<sup>17</sup>. At the basal body, Spag5 may have a structural and organizational role by bundling microtubules or cross-linking them to other components, similar to its role during mitosis<sup>15,16</sup>. Since both SPAG5 and NINL<sup>isoB</sup> associate with the cytoplasmic region of USH2A<sup>isoB</sup>, these proteins may well be involved in microtubule-based transport of USH2A<sup>isoB</sup>-containing vesicles towards the membrane of the apical inner segment of photoreceptor cells. Indeed, Zallocchi and co-workers provided evidence for the existence of USH protein complexes in vesicles of tracheal epithelium and their results implied that the ectodomain of Ush2a<sup>isoB</sup> is facing the lumen of vesicles and its cytoplasmic domain towards the cytosol<sup>39</sup>.

The association of SPAG5 with both USH2A<sup>isoB</sup> and NINL<sup>isoB</sup> and its localization in photoreceptor cells pinpoints *SPAG5* as a functional candidate gene for retinal ciliopathies. This hypothesis is supported by the observed expression of *Spag5* in tissues that are often affected in ciliopathies *e.g.* retina, kidney, brain, and testis. Two *Spag5* animal models have been reported. *Spag5*-null mice were viable and fertile and did not display a clear phenotype<sup>40</sup>. Defects may have been missed, as this model is probably phenotyped with a focus on spermatogenesis and fertility anomalies. The rat model is characterized by male sterility, reduced female fertility, hypogonadism, progressive renal insufficiency and body growth retardation as a consequence of hypogenesis that might result from defective cell proliferation<sup>41,42</sup>. The renal phenotype is similar to oligomeganephronia<sup>43,44</sup>, the most common form of human congenital renal hypoplasia which in a few cases is found to be associated with retinitis pigmentosa, hearing impairment and stunted growth<sup>45</sup>. *SPAG5* is a candidate gene to be associated with the clinical features in the patient described by Janin-Mercier and co-workers<sup>45</sup>. No retinal dysfunction has been reported in the *Spag5* animal models. Thus a detailed retinal examination is needed to exclude defects in visual function. Unfortunately, the models were not available anymore for this analysis.

In conclusion, our studies demonstrate that SPAG5 associates with both USH2A<sup>isoB</sup> and NINL<sup>isoB</sup>. Therefore, it seems likely that besides its known function in cell proliferation, SPAG5 has a role in differentiated cells *e.g.* photoreceptor cells. Our data suggest that SPAG5 and NINL<sup>isoB</sup> functions directly or indirectly in the microtubule-based transport and docking of (USH2A<sup>isoB</sup>-containing) vesicles to the apical inner segment and basal body of photoreceptor cells, which is essential for their long-term maintenance and/or function. In continuation with its expression pattern this indicates that *SPAG5* can be regarded as an excellent candidate gene for (retinal) ciliopathies.

## **Acknowledgements**

This research was supported by the Radboud University Nijmegen Medical Centre, Nijmegen, The Netherlands, The British Retinitis Pigmentosa Society (GR552, to RR and HK), the Heinsius Houbolt Foundation (to HK), The ‘Landelijke Stichting voor Blinden en Slechtzienenden’ (RR and HK), the ‘Stichting Blindenhulp’ (to JK and HK), the Netherlands Organization for Scientific Research (NWO Vidi-91786396; to RR), and the European Community’s Seventh Framework Programme FP7/2009 under grant agreement No 241955, SYSCILIA (to RR and HK).

## **Material and methods**

### **Animals**

The Wistar rats and C57BL6 J0laHsD mice (Harlan, Horst, The Netherlands) used in this study were housed in standard cages and received water and food *ad libitum*. All experiments were conducted according to international and institutional guidelines.

### **Plasmids and antibodies**

The human image clone IRAUp969C082D (ImaGenes.GmbH, Berlin, Germany) was used as a template to amplify full length SPAG5. The amino acid (aa) numbers are according to the following GenBank entries: SPAG5 NP\_006452, USH2A NP\_996816, (<https://www.ncbi.nlm.nih.gov/protein>; provided in the public domain by the National Center for Biotechnology Information, Bethesda, MD) All constructs were generated using commercial cloning technology (Gateway; Invitrogen, Carlsbad, CA), according to the manufacturer’s instructions.

Antibodies against the C-terminal region of SPAG5 were used which were raised in guinea pigs against a GST-fusion protein encoding a peptide consisting of aa 1063-1187. The cDNA encoding this peptide was amplified by using 5’- GGCGAGCTCATAAGCCTTAG -3’ as a forward primer and 5’- TCCCTGTAGTTCTTTGC -3’ as a reversed primer. The affinity purified SPAG5 antibodies neither revealed immunohistochemical staining nor did detect SPAG5 on Western blot after pre-adsorption of the primary antibodies with the antigen. (Suppl Fig. S1). Antibodies against rootletin (Novus Biologicals, Cambridge, UK), are used in 1:1000 dilution. The monoclonal antibodies directed against centrin and the polyclonal antibodies directed against NINL and the cytoplasmic region of USH2A<sup>isoB</sup> were previously described<sup>12, 13, 46</sup> and used in 1:250 dilution. Anti-HA and anti-flag were derived from Sigma-Aldrich (Munich, Germany) and employed in a 1:1000 dilution. As secondary antibodies the goat-anti-guinea pig Alexa Fluor 488 and Alexa Fluor 568, the goat-anti-rabbit Alexa Fluor 568, the goat-anti-human Alexa Fluor 568, the IRDye800 goat-anti-guinea pig IgG, the IRDye800 goat-anti-mouse and the IRDye800 goat-anti-rabbit were used in a 1:500 dilution (all from Molecular Probes-Invitrogen Carlsbad, USA).



### **Yeast two-hybrid analysis**

A GAL4-based yeast two-hybrid system (HybriZAP, Stratagene, La Jolla, CA) to identify proteins that interact with the cytoplasmic region of USH2A<sup>isoB</sup> (aa 5064-5202; NP\_996816) was used according to methods previously described<sup>13,47</sup>.

### **GST Pull-Down**

The GST-fusion proteins were produced by transforming *Escherichia coli* BL21-DE3 with plasmids pDEST15-USH2A<sub>icd</sub> (aa 5064-5202) or pDEST15-SPAG5 (aa 973-1193) respectively, according to methods previously described<sup>12</sup>. Flag-tagged SPAG5 or flag-tagged NINL<sup>isoB</sup> were produced by transfecting COS-1 cells with plasmids encoding p3xflag-SPAG5 or NINL<sup>isoB</sup> respectively using a Effectene (QIAGEN, Hildene, Germany) according the manufacturer's instruction. The GST pull-down assay was performed as described elsewhere<sup>12</sup>.

### **Immunohistochemistry in Rat Retina**

Unfixed eyes of 20-day-old (P20) Wistar rats were isolated and frozen in melting isopentane. Seven-micrometer-thick cryosections were treated and immunolabeled as described previously<sup>12</sup>. Immunofluorescence was visualized by using the Zeiss Axio Imager Z1 fluorescent microscope (Zeiss, Switzerland) equipped with an AxioCam MRm camera (Zeiss). Images were processed using Axiovision Rel.4.6 and Adobe Photoshop (Adobe Systems, San Jose, CA).

### **Expression by real-time qPCR**

Total RNA was used from several human adult tissues (Agilent Technologies, Santa Clara, CA) and cDNA was generated using reverse transcriptase according the manufacturer's instructions (iScript; Bio-rad laboratories, Hercules, CA). cDNA primers were designed using Primer3 and validated for SPAG5 and the reference gene GUSB: SPAG5 exon 12-13 F 5'- ACTCTGCCAGCTTACCCAG -3' and SPAG5 R 5'- CAGTTCTGCCTGCATGTG -3', GUSB F 5' -AGAGTGGTGCTGAGGATTGG -3' and GUSB R 5'- CCCTCATGCTCTAGCGTGTC -3'. qPCR was performed using adult human cDNA as a template and the SYBR Green PCR master mix (Applied Biosystems, Life technologies, USA). PCR program: 10 min. at 95 °C, 95 °C for 15 sec. and 60 °C for 30 sec. during 40 cycles, 1 min. at 95 °C, 1 min. at 65 °C using the Applied Biosystems 7500 Fast Real-Time PCR System. The data was analyzed using the 7500 fast system SDS software version 1.4.0.25.

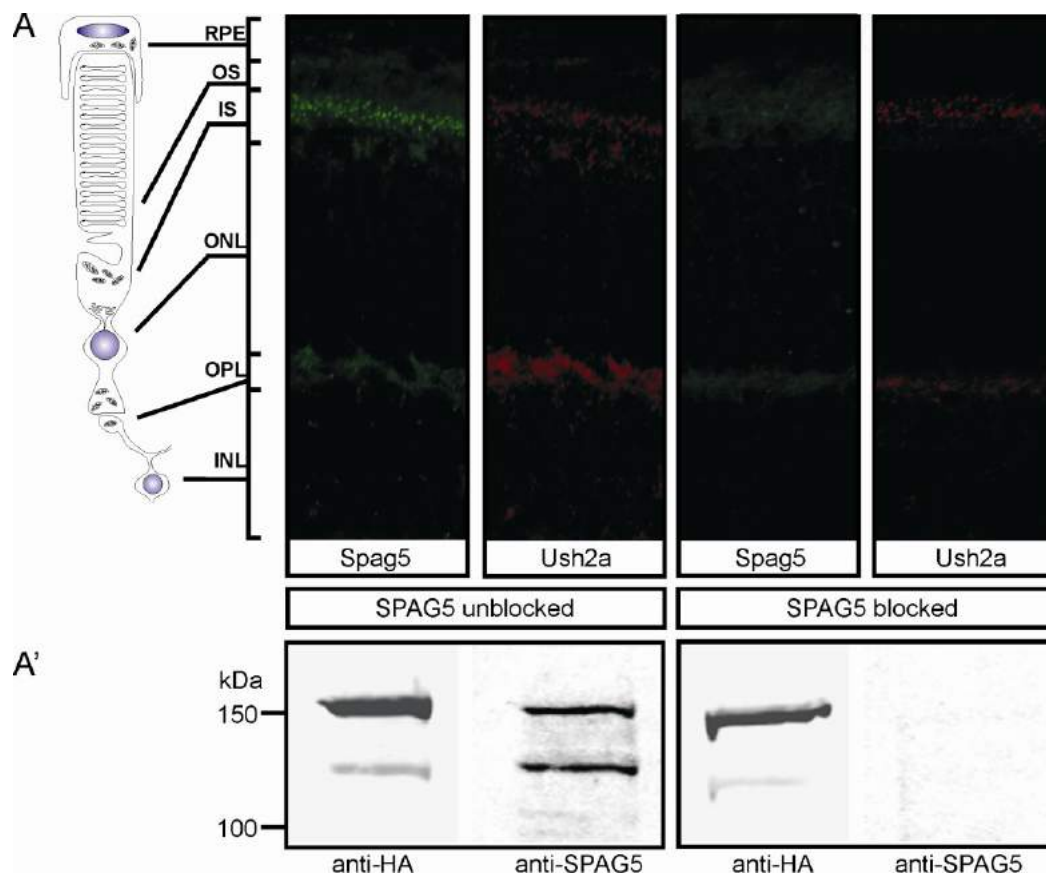
### **Mouse RNA probes *In Situ* Hybridization**

A probe corresponding to nucleotides 2698-3757 (GenBank NM\_017407), which recognizes mouse *Spag5* transcripts was generated from mouse retina cDNA (Marathon; Clontech, USA) with 5'- ATACCTGTGCAGGCTGGAG -3' as a forward primer and 5'- GTTCTCTCCAAGTCGTGTC -3' as a reversed primer. The digoxigenin labeling was performed as previously described<sup>12</sup>. C57Bl6 J1co mouse embryos were collected at various embryonic stages (E12.5 to E18.5), as well as postnatal day 7 (P7) mouse eyes. RNA *in situ* hybridization was performed as previously described<sup>12</sup>.

**Pre-Embedding Immunoelectron Microscopy**

Vibratome sections of mouse retina were incubated with a 100x diluted antibody against SPAG5 and visualized by a secondary antibody (Vectastain ABC-Kit, Vector laboratories, Peterborough, UK). After fixation with 0.5% OsO<sub>4</sub> the specimens were embedded in araldite, and ultrathin sections were analyzed with a transmission electron microscope (Tecnai 12; FEI, Hillsboro, OR). The procedure is described elsewhere<sup>10</sup>.

## Supplementary material



**Supplementary Figure 1.** Specificity of the anti-SPAG5 antibodies. **(A)** Co-immunostainings of SPAG5 (*green*) and USH2A (*red*) in retina cryosections of adult (P20) rat using anti-USH2A and anti-SPAG5 antibodies. Both antibodies were blocked together with the SPAG5 antigen and after pre-absorption no specific SPAG5 signals were detected in contrast to the normal USH2A staining. **(A')** Western blot analysis of HA-tagged SPAG5 using (pre-absorbed) anti-HA and anti-SPAG5 antibodies. After pre-absorption of the antibodies with the SPAG5 antigen, HA-SPAG5 could only be detected by anti-HA antibodies and not by the blocked anti-SPAG5 antibodies, indicating the specificity of the antibodies.

## References

1. Kaiserman N, Obolensky A, Banin E, et al. Novel USH2A mutations in Israeli patients with retinitis pigmentosa and Usher syndrome type 2. *Arch Ophthalmol.* 2007;125:219-224.
2. Liu X, Tang Z, Li C, et al. Novel USH2A compound heterozygous mutations cause RP/USH2 in a Chinese family. *Mol Vis.* 2010;16:454-461.
3. McGee TL, Seyedahmadi BJ, Sweeney MO, et al. Novel mutations in the long isoform of the USH2A gene in patients with Usher syndrome type II or non-syndromic retinitis pigmentosa. *J Med Genet.* 2010;47:499-506.
4. Rivolta C, Sweklo EA, Berson EL, et al. Missense mutation in the USH2A gene: association with recessive retinitis pigmentosa without hearing loss. *Am J Hum Genet.* 2000;66:1975-1978.
5. Smith RJ, Berlin CI, Hejtmancik JF, et al. Clinical diagnosis of the Usher syndromes. Usher Syndrome Consortium. *Am J Med Genet.* 1994;50:32-38.
6. Hartong DT, Berson EL, Dryja TP. Retinitis pigmentosa. *Lancet.* 2006;368:1795-1809.
7. Cohen M, Bitner-Glindzicz M, Luxon L. The changing face of Usher syndrome: clinical implications. *Int J Audiol.* 2007;46:82-93.
8. Adato A, Michel V, Kikkawa Y, et al. Interactions in the network of Usher syndrome type 1 proteins. *Hum Mol Genet.* 2005;14:347-356.
9. Kremer H, van Wijk E, Marker T, et al. Usher syndrome: molecular links of pathogenesis, proteins and pathways. *Hum Mol Genet.* 2006;15 Spec No 2:R262-R270.
10. Maerker T, van Wijk E, Overlack N, et al. A novel Usher protein network at the periciliary reloading point between molecular transport machineries in vertebrate photoreceptor cells. *Hum Mol Genet.* 2008;17:71-86.
11. Reiners J, van Wijk E, Maerker T, et al. Scaffold protein harmonin (USH1C) provides molecular links between Usher syndrome type 1 and type 2. *Hum Mol Genet.* 2005;14:3933-3943.
12. van Wijk E, van der Zwaag B, Peters TA, et al. The DFNB31 gene product whirlin connects to the Usher protein network in the cochlea and retina by direct association with USH2A and VLGR1. *Hum Mol Genet.* 2006;15:751-765.
13. Van Wijk E, Kersten FFJ, Kartono A, et al. Usher syndrome and Leber congenital amaurosis are molecularly linked via a novel isoform of the centrosomal ninein-like protein. *Hum Mol Genet.* 2009;18:51-64.
14. Sedmak T, Wolfrum U. Intraflagellar transport molecules in ciliary and nonciliary cells of the retina. *J Cell Biol.* 2010;189:171-186.
15. Mack GJ, Compton DA. Analysis of mitotic microtubule-associated proteins using mass spectrometry identifies astrin, a spindle-associated protein. *Proc Natl Acad Sci U S A.* 2001;98:14434-14439.
16. Thein KH, Kleylein-Sohn J, Nigg EA, et al. Astrin is required for the maintenance of sister chromatid cohesion and centrosome integrity. *J Cell Biol.* 2007;178:345-354.
17. Cheng TS, Hsiao YL, Lin CC, et al. hNinein is required for targeting spindle-associated protein Astrin to the centrosome during the S and G2 phases. *Exp Cell Res.* 2007;313:1710-1721.

18. Wolfrum U, Salisbury JL. Expression of centrin isoforms in the mammalian retina. *Exp Cell Res.* 1998;242:10-17.
19. Chang MS, Huang CJ, Chen ML, et al. Cloning and characterization of hMAP126, a new member of mitotic spindle-associated proteins. *Biochem Biophys Res Commun.* 2001;287:116-121.
20. Gruber J, Harborth J, Schnabel J, et al. The mitotic-spindle-associated protein astrin is essential for progression through mitosis. *J Cell Sci.* 2002;115:4053-4059.
21. Du J, Jablonski S, Yen TJ, et al. Astrin regulates Aurora-A localization. *Biochem Biophys Res Commun.* 2008;370:213-219.
22. Casenghi M, Meraldi P, Weinhart U, et al. Polo-like kinase 1 regulates Nlp, a centrosome protein involved in microtubule nucleation. *Dev Cell.* 2003;5:113-125.
23. Casenghi M, Barr FA, Nigg EA. Phosphorylation of Nlp by Plk1 negatively regulates its dynein-dynactin-dependent targeting to the centrosome. *J Cell Sci.* 2005;118:5101-5108.
24. Rapley J, Baxter JE, Blot J, et al. Coordinate regulation of the mother centriole component nlp by nek2 and plk1 protein kinases. *Mol Cell Biol.* 2005;25:1309-1324.
25. Yan J, Jin S, Li J, et al. Aurora B Interaction of Centrosomal Nlp Regulates Cytokinesis. *J Biol Chem.* 2010;285:40230-40239.
26. Yang YC, Hsu YT, Wu CC, et al. Silencing of astrin induces the p53-dependent apoptosis by suppression of HPV18 E6 expression and sensitizes cells to paclitaxel treatment in HeLa cells. *Biochem Biophys Res Commun.* 2006;343:428-434.
27. Shao S, Liu R, Wang Y, et al. Centrosomal Nlp is an oncogenic protein that is gene-amplified in human tumors and causes spontaneous tumorigenesis in transgenic mice. *J Clin Invest.* 2010;120:498-507.
28. Wang Y, Zhan Q. Cell cycle-dependent expression of centrosomal ninein-like protein in human cells is regulated by the anaphase-promoting complex. *J Biol Chem.* 2007;282:17712-17719.
29. Christensen ST, Pedersen LB, Schneider L, et al. Sensory cilia and integration of signal transduction in human health and disease. *Traffic.* 2007;8:97-109.
30. Singla V, Reiter JF. The primary cilium as the cell's antenna: signaling at a sensory organelle. *Science.* 2006;313:629-633.
31. Quarmby LM, Parker JD. Cilia and the cell cycle? *J Cell Biol.* 2005;169:707-710.
32. Smith KR, Kieserman EK, Wang PI, et al. A role for central spindle proteins in cilia structure and function. *Cytoskeleton (Hoboken).* 2011;68:112-124.
33. Liu Q, Tan G, Levenkova N, et al. The proteome of the mouse photoreceptor sensory cilium complex. *Mol Cell Proteomics.* 2007;6:1299-1317.
34. Roepman R, Wolfrum U. Protein networks and complexes in photoreceptor cilia. *Subcell Biochem.* 2007;43:209-235.
35. Wolfrum U, Schmitt A. Rhodopsin transport in the membrane of the connecting cilium of mammalian photoreceptor cells. *Cell Motil Cytoskeleton.* 2000;46:95-107.
36. Liu X, Bulgakov OV, Darrow KN, et al. Usherin is required for maintenance of retinal photoreceptors and normal development of cochlear hair cells. *Proc Natl Acad Sci U S A.* 2007;104:4413-4418.

37. Papermaster DS. The birth and death of photoreceptors: the Friedenwald Lecture. *Invest Ophthalmol Vis Sci.* 2002;43:1300-1309.
38. Famulski JK, Vos LJ, Rattner JB, et al. Dynein/Dynactin-mediated transport of kinetochore components off kinetochores and onto spindle poles induced by nordihydroguaiaretic acid. *PLoS One.* 2011;6:e16494.
39. Zallocchi M, Sisson JH, Cosgrove D. Biochemical characterization of native Usher protein complexes from a vesicular subfraction of tracheal epithelial cells. *Biochemistry.* 2010;49:1236-1247.
40. Xue J, Tarnasky HA, Rancourt DE, et al. Targeted disruption of the testicular SPAG5/deepest protein does not affect spermatogenesis or fertility. *Mol Cell Biol.* 2002;22:1993-1997.
41. Suzuki H, Yagi M, Suzuki K. Duplicated insertion mutation in the microtubule-associated protein Spag5 (astrin/MAP126) and defective proliferation of immature Sertoli cells in rat hypogonadic (hgn/hgn) testes. *Reproduction.* 2006;132:79-93.
42. Suzuki H, Yagi M, Saito K, et al. Embryonic pathogenesis of hypogonadism and renal hypoplasia in hgn/hgn rats characterized by male sterility, reduced female fertility and progressive renal insufficiency. *Congenit Anom (Kyoto).* 2007;47:34-44.
43. Suzuki H, Tokuriki T, Saito K, et al. Glomerular hyperfiltration and hypertrophy in the rat hypoplastic kidney as a model of oligomeganephronic disease. *Nephrol Dial Transplant.* 2005;20:1362-1369.
44. Suzuki H, Tokuriki T, Kamita H, et al. Age-related pathophysiological changes in rat oligomeganephronic hypoplastic kidney. *Pediatr Nephrol.* 2006;21:637-642.
45. Janin-Mercier A, Palcoux JB, Gubler MC, et al. Oligomeganephronic renal hypoplasia with tapetoretinal degeneration. Report of one case with ultrastructural study of the renal biopsy. *Virchows Arch A Pathol Anat Histopathol.* 1985;407:477-483.
46. Reiners J, Nagel-Wolfrum K, Jurgens K, et al. Molecular basis of human Usher syndrome: deciphering the meshes of the Usher protein network provides insights into the pathomechanisms of the Usher disease. *Exp Eye Res.* 2006;83:97-119.
47. Roepman R, Schick D, Ferreira PA. Isolation of retinal proteins that interact with retinitis pigmentosa GTPase regulator by interaction trap screen in yeast. *Methods Enzymol.* 2000;316:688-704.



# Chapter

---

# 6

## ***CLRN1* mutations cause non-syndromic retinitis pigmentosa**

Muhammad Imran Khan<sup>1,2,#</sup>, Ferry F.J. Kersten<sup>2-6,#</sup>, Maleeha Azam<sup>1,2</sup>, Rob W.J. Collin<sup>2,4,5</sup>, Alamdar Hussain<sup>1</sup>, Syed Tahir-A. Shah<sup>1</sup>, Jan E.E. Keunen<sup>4</sup>, Hannie Kremer<sup>3,5,6</sup>, Frans P. M. Cremers<sup>1,2,5</sup>, Raheel Qamar<sup>1,7</sup>, Anneke I. den Hollander<sup>2,4,5</sup>

# These authors contributed equally to this work

<sup>1</sup>Department of Biosciences, COMSATS Institute of Information Technology, Islamabad, Pakistan; <sup>2</sup>Department of Human Genetics, <sup>3</sup>Department of Otorhinolaryngology, Head and Neck Surgery, <sup>4</sup>Department of Ophthalmology, <sup>5</sup>Nijmegen Centre for Molecular Life Sciences, and <sup>6</sup>Donders Institute for Brain, Cognition and Behaviour, Centre for Neuroscience, Radboud University Nijmegen Medical Centre, Nijmegen, The Netherlands; <sup>7</sup>Shifa College of Medicine, Islamabad, Pakistan.

---

*Ophthalmology* 2011; 118 (7): 1444-1448

---







## **Abstract**

Patients of two consanguineous Pakistani families diagnosed with autosomal recessive retinitis pigmentosa (arRP) were genotyped with single-nucleotide polymorphism microarrays for genome-wide linkage analysis. The search for potential candidate genes within the 8 Mb overlapping homozygous region in these families revealed the presence of *CLRN1*, a gene previously known to cause Usher syndrome type III (USH3). Audiometric assessment revealed no hearing impairment, thereby excluding Usher syndrome. Sequencing of *CLRN1* revealed two novel missense mutations (p.Pro31Leu and p.Leu154Trp) segregating in two families. Subcellular localization studies demonstrated the retention of the mutant proteins in the endoplasmic reticulum, whereas the wild-type protein was mainly present at the cell membrane.

The RP-associated mutations p.Pro31Leu and p.Leu154Trp may represent hypomorphic mutations, because the substituted amino acids located in the transmembrane domains remain polar, while more severe changes have been detected in patients with USH3. These data indicate that mutations in *CLRN1* are associated not only with USH3, but also with non-syndromic arRP.

**Introduction**

Retinitis pigmentosa (RP, MIM#268000) consists of a group of photoreceptor degenerative disorders, initially characterized by impairment of night vision and mid-peripheral visual field loss. A hallmark feature of RP is the formation of pigmentary deposits in the retina, commonly known as bone spicules, along with mild to severe loss of rod function gauged by electroretinography (ERG) <sup>1-3</sup>.

RP is clinically and genetically a very heterogeneous disease. Several syndromic forms of RP exist where individuals suffer from other disease such as deafness in Usher syndrome, and obesity and renal abnormalities in Bardet-Biedl syndrome. Genetically, RP exhibits multiple modes of inheritance, and to date 48 genes and 8 loci have been described. Autosomal recessive RP (arRP) accounts for approximately 20% to 25% of the cases; approximately 45% are isolated cases, which for the majority likely also represent autosomal recessive cases. The percentage of autosomal recessive cases has been found to be as high as 87% in the Pakistani population (Azam et al., unpublished data). Twenty-six genes have been identified for arRP, and they explain the etiology of 50% to 60% of all recessive cases <sup>3</sup>. These genes encode proteins that exert diverse functions in the retina including phototransduction, vitamin A metabolism, and ciliary transport <sup>3</sup>. Mutations in the *USH2A* gene have been reported to cause both Usher syndrome type II (USH2), and non-syndromic arRP <sup>4-7</sup>.

In the current study, we describe two Pakistani families with arRP caused by two different missense mutations in the *CLRN1* gene. Mutations in this gene have previously only been associated with Usher syndrome type III (USH3), which is characterized by progressive post-lingual hearing loss, in addition to RP of variable onset and severity <sup>8,9</sup>. USH3 patients may also have normal or mildly reduced vestibular responses <sup>9</sup>. This study demonstrates that mutations in the *CLRN1* gene can also cause non-syndromic RP without hearing loss. Functional analysis of the missense mutations in transfected cultured cells indicates that the mutant proteins are not targeted to the plasma membrane, and support pathogenicity of both variants.

## Results

### Linkage and mutation analyses

Linkage analysis in the consanguineous Pakistani family RP06 revealed 5 regions with a log of odds score of  $>3.0$ , on chromosomes 1, 3, 5 and 11 (Table 1). The region on chromosome 3 with a log of odds score of 3.32 between rs1009621 and rs1563436 was the only interval that was homozygous in all affected individuals, and encompassed the *CLRNI* gene. Mutations in this gene have previously been associated with USH3, which is characterized by progressive post-lingual hearing loss, RP, and normal or mildly reduced vestibular responses. Sequence analysis of all coding and non-coding exons of *CLRNI* revealed a novel missense mutation (c.461T>G; p.Leu154Trp) in exon 3 (Fig. 1C). Sequence analysis in all available family members revealed that the mutation segregates with the disease in family RP06 (Fig. 1A). Amplification refractory mutation system-polymerase chain reaction analysis of a panel of 81 Pakistani RP patients and 90 ethnically matched controls yielded no carriers of this mutation.

Linkage analysis in the other consanguineous Pakistani family, RP18, yielded two regions with a maximum log of odds score of 2.40 (Table 1). The largest homozygous region spans about 15 Mb on chromosome 3 between rs724016 and rs718142. Sequence analysis of the *CLRNI* gene which resides in the interval also revealed a missense mutation (c.92C>T; p.Pro31Leu) in exon 1 of *CLRNI* (Fig. 1D). The mutation also segregated with the disease (Fig.1B) and was found neither in 81 unrelated Pakistani RP patients, nor in 90 ethnically matched controls from the Pakistani population.

Family	Chr.	LOD	Flanking SNP	hg18 position (Mb)	SNPs #	Stretch hom. SNPs
RP06	1	3.20	rs1526480; rs10785852	90,98-104,41	22	4
	3	3.32	rs1009621; rs1563436	149,67-173,26	40	30
	3	3.30	rs7628308; rs1515504	179,31-191,13	30	4
	5	3.18	rs1989154; rs906678	147,83-150,76	6	1
	11	3.30	rs892336; rs961746	5,56-20,18	22	3
RP18	3	2.40	rs724016; rs718142	142,59-158,95	57	51
	8	2.40	rs1816371; rs1356763	98,35-129,87	124	38

# Total SNPs (single-nucleotide polymorphisms) in regions with indicated LOD (Log of odds) score

**Table 1.** Linkage analysis of the families RP06 and RP18

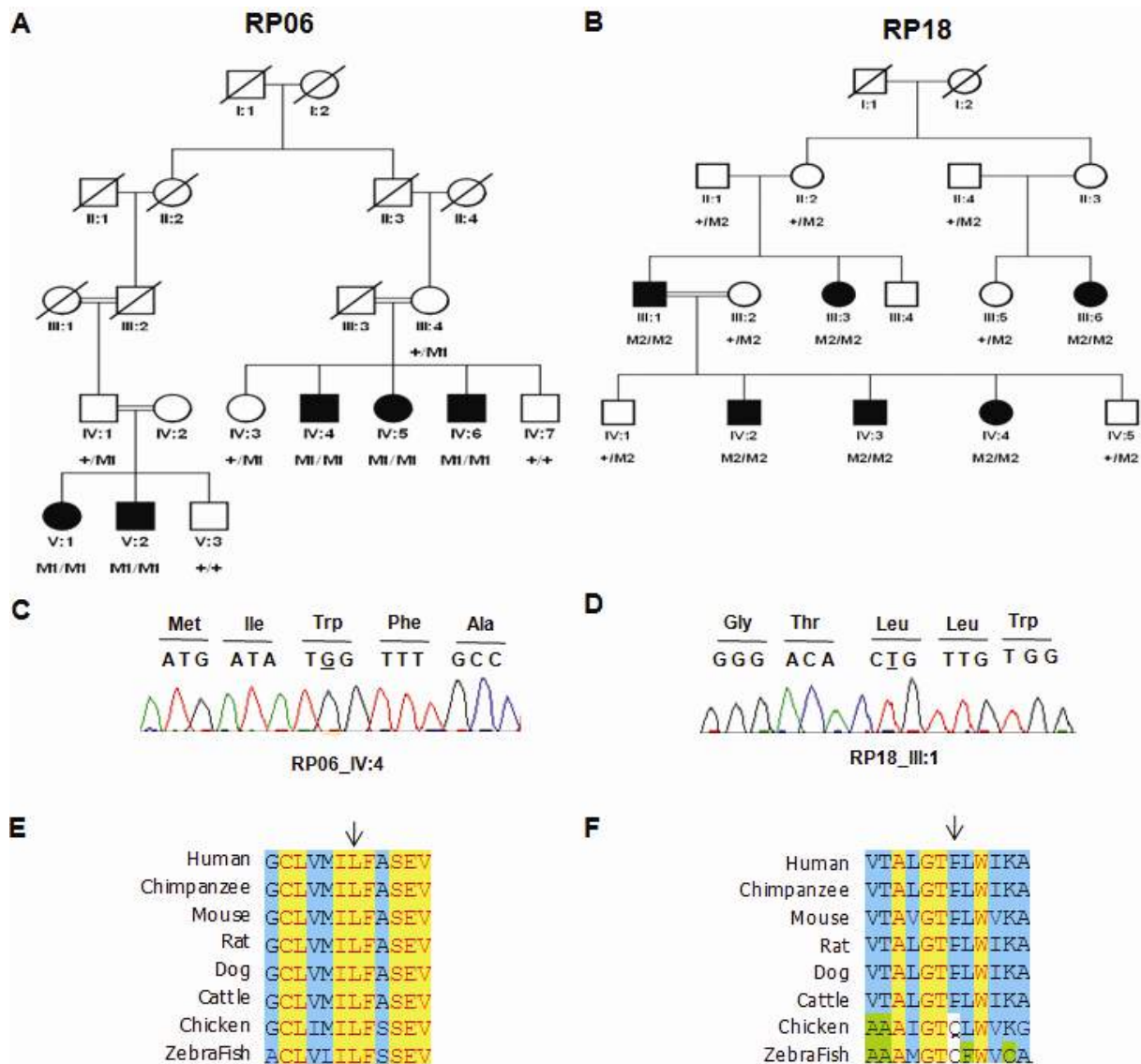


**Figure 1.** Identification of *CLRN1* mutations in two consanguineous Pakistani families. (A,B) Pedigrees and segregation analysis of *CLRN1* mutations in families RP06 and RP18. M1 represents c.461T>G; p.Leu154Trp and M2 represents c.92C>T; p.Pro31Leu. (C,D) Sequence chromatograms of *CLRN1* mutations in affected individuals of families RP06 and RP18; the substituted nucleotides are underlined. (E,F) Sequence alignments of *CLRN1* orthologues. The arrows indicate the mutated amino acids, which are completely conserved throughout vertebrate evolution (p.Leu154) or completely conserved in mammals (p.Pro31).

### Clinical evaluations

Both families were recruited because the affected individuals suffered from RP. The identified mutations in *CLRN1*, a gene known to be involved in Usher syndrome, warranted further clinical assessment to rule out hearing impairment. Therefore, detailed clinical analyses were performed during a follow-up visit, which included fundoscopy, ERG, and audiometry. Analysis of the fundus of the affected individuals of both families indicated attenuation of the retinal vessels, waxy appearance of the optic disc and bone spicule pigmentation in the periphery of the retina (Figs. 2A-C). The ERG analyses revealed that the scotopic responses, which are indicative of the activity of the rod photoreceptors, were more severely diminished than the photopic responses (Table 2).

The patients reported no hearing problems. To completely rule out any hearing impairment, selected patients of both families underwent audiometric assessment. Two out of five affected individuals (IV:4 and IV:6) and one unaffected individual (III:1) of family RP06 and one affected individual (III:1) of family RP18 underwent pure tone audiometry. The audiograms of all examined individuals were found to be within the normal range (Fig. 2D) and no hearing impairment was observed. In contrast, *USH3* patients generally suffer from severe hearing loss at this age <sup>9</sup>.

	<b>RP06:IV:6 (age 39y)</b>	<b>RP18:III:1 (age 37y)</b>	<b>Normal values (age 40y)</b>
Scotopic 25 dB b-wave amplitude ( $\mu$ V)	23.4	31.1	>141
Scotopic 0 dB b-wave amplitude ( $\mu$ V)	70.9	68.7	>387
Photopic 0 dB b-wave amplitude ( $\mu$ V)	60.9	59.7	>82
Photopic 0 dB 30Hz Flicker amplitude ( $\mu$ V)	4.3	3.8	>56

**Table 2.** Electroretinography response of affected individuals from families RP06 and RP18

### In-silico analysis of mutations

Alignment of the clarin-1 protein sequences of various orthologs shows that the two substituted amino acids in both families were highly conserved in other species (Figs 1E and F). The pathologic potential of both substitutions evaluated with PolyPhen predicted that both substitutions were probably damaging, and SIFT analysis revealed that both are not tolerated. Both mutations affect residues that are located in transmembrane domains of clarin-1, which is a member of the tetraspanin family (Fig. 3). The p.Pro31Leu mutation identified in family RP18 is located at the extracellular end of the first transmembrane domain, whereas the p.Leu154Trp mutation identified in family RP06 is located at the end of the third transmembrane domain.

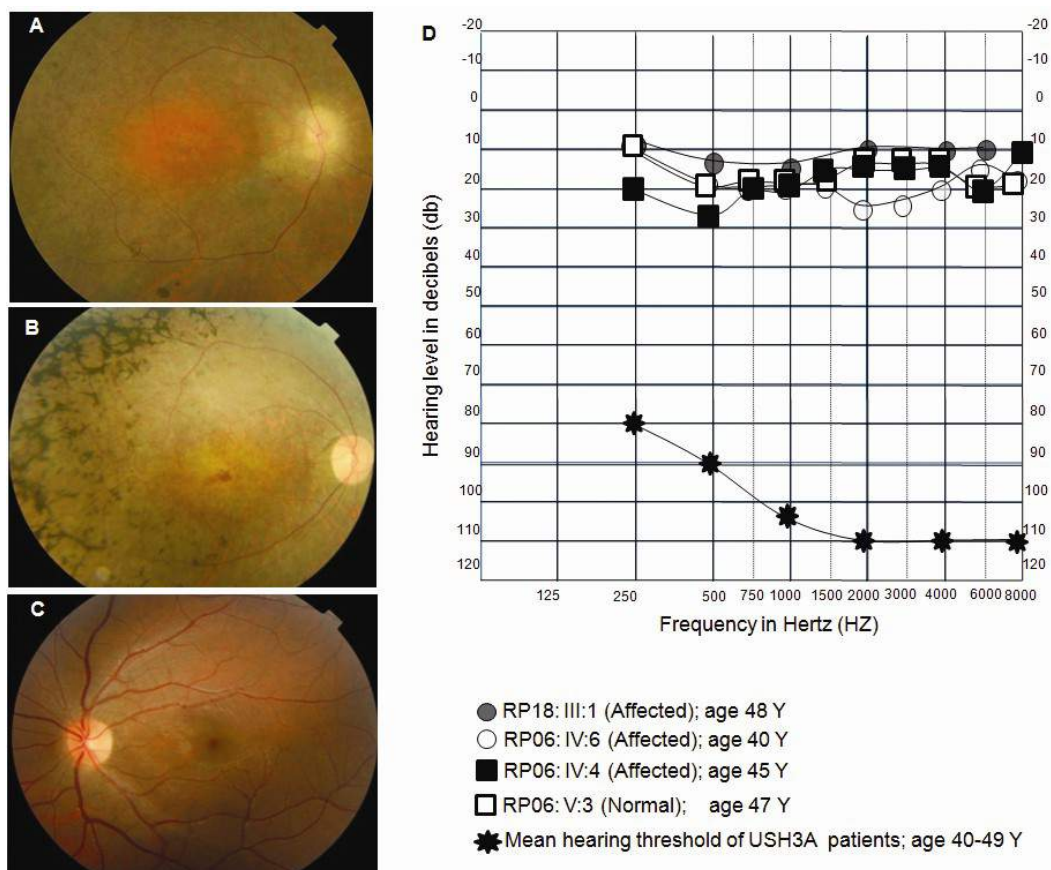


**Figure 2.** Clinical features of families RP06 and RP18. (A-C) Fundus photographs of two affected individuals (RP06 (IV:6), B; RP18 (III:1)) and one unaffected individual (C: RP18 (IV:1)). (D) Audiograms of three affected individuals and one unaffected individual of families RP06 and RP18. Mean hearing threshold was calculated of 27 Usher syndrome type III (USH3) patients with 5 different *CLRN1* mutations <sup>9</sup>, demonstrating severe hearing loss in USH3 patients whereas hearing in affected individuals of families RP06 and RP18 is normal.

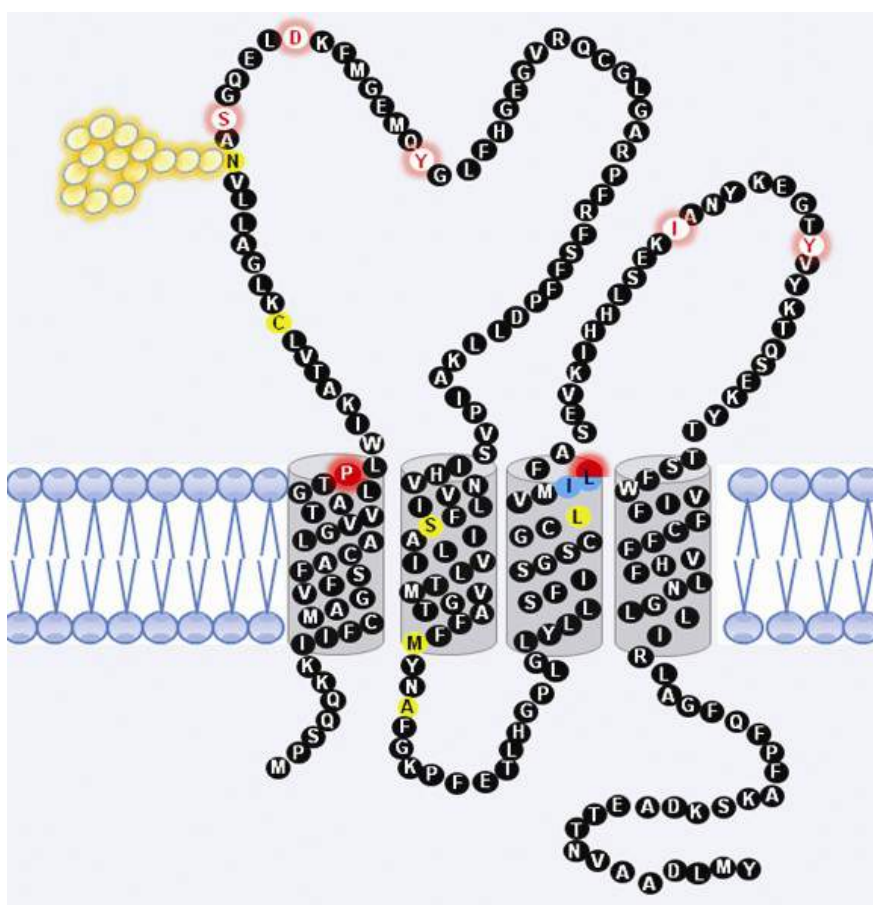


**Figure 3.** The clarin-1 protein and position of mutations identified in Usher syndrome type III (USH3) and autosomal recessive RP (arRP) patients. Nonsense and frameshift mutations identified in USH3 patients are indicated in white, missense mutations identified in USH3 patients are indicated in yellow, and an in-frame insertion-deletion mutation identified in USH3 is marked in blue. Missense mutations identified in arRP families in this study are filled red.

### Subcellular localization of wild-type and mutant clarin-1 proteins

To determine the subcellular localization of wild-type clarin-1 and the two mutant proteins, full-length wild-type and mutant *CLRN1* constructs were transfected in hTERT\_RPE1 cells. Because clarin-1 is normally expressed at the plasma membrane<sup>10,11</sup>, a construct encoding a palmitoylation-myristoylation-cyan fluorescent protein fused to the intracellular domain of USH2A (palmyr-USH2A) was used as a marker of the plasma membrane<sup>12</sup>. Wild-type clarin-1 was found to be present throughout the cell and at the plasma membrane as demonstrated by colocalization of the protein with palmyr-USH2A (Fig. 4A). The mutant clarin-1 proteins carrying the missense mutations p.Pro31Leu and p.Leu154Trp were detected



throughout the cell, but not at the membrane (Figs. 4B and C). The mutant clarin-1 proteins were almost exclusively observed within the endoplasmic reticulum (ER), as shown by colocalization with an ER marker (protein disulfide isomerase), whereas only a partial colocalization was observed with the wild-type clarin-1 protein (data not shown). Together, these data indicate that the two mutant clarin-1 proteins are not properly targeted to the plasma membrane, but rather retained at the ER.

### **Discussion**

For the present study, we have described two Pakistani arRP families with novel missense mutations in the *CLRNI* gene that segregate with the disease. The p.Pro31Leu mutation identified in family RP18 is located at the extracellular end of the first transmembrane domain, whereas the p.Leu154Trp mutation identified in family RP06 is located at the end of the third transmembrane domain. The patients from both families suffered from progressive night blindness accompanied by loss of peripheral visual field. Clinically, the patients of both families presented typical features of RP, including arterial attenuation, bone spicule deposition, and a waxy appearance of the optic disc. None of the affected members of either family had any apparent auditory abnormality, which was confirmed by audiometry.

Mutations in the *CLRNI* gene have previously been associated with USH3, which accounts for a small proportion of all Usher syndrome cases<sup>13,14</sup>. Interestingly, mutations in *CLRNI* have only been reported in patients of European ancestry, mostly Finnish and Ashkenazi Jewish<sup>11,14,15</sup>. Five of the twelve *CLRNI* mutations detected in USH3 patients create premature stop codons and hence may lead to translational termination and/or nonsense-mediated decay of the mRNA. Six of the mutations identified in USH3 patients are amino acid substitutions (p.Cys40Gly, p.Asn48Lys, p.Ser105Pro, p.Met120Lys, p.Ala123Asp and p.Leu150Pro) and one mutation leads to an in-frame insertion-deletion (p.Ile153\_Leu154delinsMet). Recently, it was shown that mutant clarin-1 proteins carrying one of the missense mutations identified in USH3 patients (p.Asn48Lys, p.Met120Lys, p.Ala123Asp and p.Leu150Pro) or the p.Ile153\_Leu154delinsMet mutation, are retained in the ER and are not inserted into the plasma membrane<sup>13</sup>.

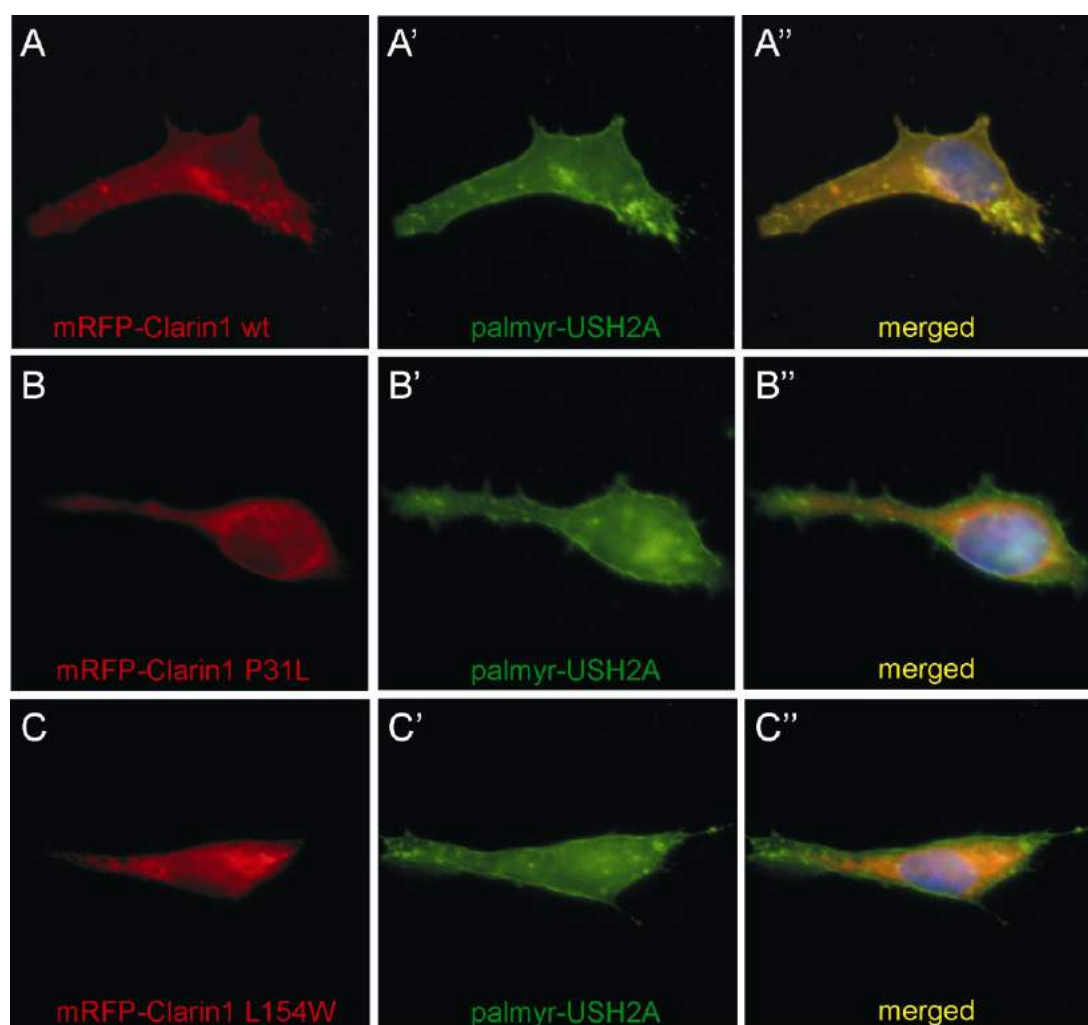


**Figure 4.** Subcellular localization of wildtype and mutant clarin-1 proteins in hTERT-RPE1 cells. hTERT-RPE1 cells were cotransfected with constructs encoding mRFP-clarin-1 fusion proteins (*red* in **A**, **B** and **C**) and a marker for the plasma membrane (palmitoylated-myristoylated-CFP fused to the intracellular domain of Usher syndrome type II A (USH2A); *green* in **A'**, **B'** and **C'**). Subcellular localization studies were performed for (**A**) wildtype mRFP-clarin-1, (**B**) mutant mRFP-clarin-1 carrying the missense mutation p.Pro31Leu, and (**C**) mutant mRFP-clarin-1 carrying the missense mutation p.Leu154Trp. Overlay demonstrates colocalization of wildtype mRFP-clarin-1 with the plasma membrane (*yellow* in **A''**), while the mutant mRFP-clarin-1 proteins were detected throughout the cell, but not at the plasma membrane (**B''** and **C''**).

Our results, and those of others<sup>10,11,13-16</sup>, demonstrate that wild-type clarin-1 protein is localized at the plasma membrane and also found in the ER, indicating that clarin-1 is processed through the ER to the plasma membrane. We demonstrate in our current study that the clarin-1 mutant proteins carrying the RP-associated mutations p.Pro31Leu and p.Leu154Trp are only detected in the ER, suggesting that these proteins are also retained in the ER and are not properly transported to the plasma membrane.

The residues affected by the mutations identified in this study in families with autosomal recessive RP (p.Pro31Leu and p.Leu154Trp) are located in the transmembrane domains (Fig. 4). Three of the missense mutations identified in USH3 patients affect residues in the extracellular and intracellular loops, which could have a more damaging effect compared with mutations in the transmembrane domains. The p.Asn48Lys mutation in the extracellular loop affects a glycosylation site, and lack of glycosylation has been shown to lead to misfolding, mislocalization and degradation of the protein<sup>10</sup>. The p.Cys40Gly mutation affects a cysteine residue in the first extracellular loop, which might be involved in the formation of disulfide bonds and/or protein interactions. Three other missense mutations (p.Ser105Pro, p.Met120Lys and p.Leu150Pro) and the in-frame insertion-deletion mutation (p.Ile153\_Leu154delinsMet) found in USH3 patients affect residues, which are located in the transmembrane domains. Two (p.Met120Lys and p.Leu150Pro) were found in compound heterozygous state with a nonsense mutation (p.Tyr176X) and a missense mutation (p.Asn48Lys) in the extracellular loop which affects glycosylation<sup>15,17</sup>, respectively, and therefore probably cause a more severe phenotype. The p.Ile153\_Leu154delinsMet mutation found in USH3 patients inserts a methionine residue and removes two amino acids<sup>18</sup>, including the Leu154 residue which was found to be mutated in family RP06 in this study. Because this mutation leads to an in-frame amino acid deletion in the transmembrane domain, it could potentially have a more severe effect than a missense mutation. The p.Ser105Pro missense mutation found in USH3 is located in the middle of the second transmembrane domain and changes a polar to a non-polar residue<sup>9</sup>, whereas the missense mutations p.Pro31Leu and p.Leu154Trp, described in autosomal recessive RP in this study, are located at the boundaries of the first and third transmembrane domain, respectively, and in both cases the substituted amino acid remains nonpolar. Perhaps the position of the substituted amino acids in the transmembrane domains, and the side chain polarity of the substituted amino acids may explain the differences in phenotypes. The RP-associated mutations p.Pro31Leu and p.Leu154Trp may represent hypomorphic mutations, which would suggest that the retina may be more vulnerable to impaired clarin-1 function than the inner ear.

The findings presented here show that mutations in the *CLRN1* gene, besides USH3, can also cause non-syndromic arRP. Similar findings have been reported for mutations in the *USH2A* gene, which can cause Usher syndrome type II and non-syndromic arRP<sup>4-7</sup>. Functional

analysis of the missense mutations in transfected cultured cells indicates that the mutant proteins are not targeted to the plasma membrane, and support pathogenicity of both variants. This study adds *CLRN1* to the growing list of genes which can cause syndromic and non-syndromic forms of retinal degeneration<sup>4-7,19-23</sup>.

## **Acknowledgements**

Financial Support: this work was supported by grant no. 530 awarded (to R.Q.) by the Higher Education Commission of Pakistan and a core grant from the Shifa College of Medicine. This study was also supported by the Foundation Fighting Blindness USA (BR-GE-0507-0381-RAD to A.I.d.H.), Stichting Nederlands Oogheelkundig Onderzoek, the Stichting Nelly Reef Fund, and the Stichting ter Verbetering van het Lot der Blinden (to F.P.M.C).

## **Material and methods**

### **Subjects**

Two families, RP06 and RP18 (Figures 1 A and B), consisting of 5 and 6 affected individuals, respectively, were recruited from central Punjab, Pakistan. The affected individuals of these families were characterized to suffer from RP based upon loss of night vision and progressive visual field loss. Blood samples were collected from all available affected and normal individuals after obtaining an informed consent in accordance to the declaration of Helsinki. This study was approved by the Shifa College of Medicine/Shifa International Hospital Ethics Committee and Institutional Review Board.

### **Linkage analysis**

DNA was isolated using a standard organic extraction method<sup>24</sup>. DNA samples of all five affected individuals (IV:4, IV:5, IV:6, V:1 and V:2) of family RP06 were analyzed with 6K Illumina arrays (Illumina, Inc, San Diego, CA) containing 6090 single-nucleotide polymorphism markers. DNA samples of five affected individuals (III:1, III:3, III:6, IV:2 and IV:4) of family RP18 were analyzed for 11555 single-nucleotide polymorphisms using the Affymetrix 10K array (Affymetrix, Santa Clara, CA). Multipoint linkage analysis was performed with the Genehunter program (version 2.1r5) in the easyLinkage Plus software package (version 5.08)<sup>25</sup> using the Asian single-nucleotide polymorphism allele frequencies.

### **Mutation analysis**

Potential candidate genes in the identified linkage intervals were sequenced to identify the causative variants, using dye termination chemistry (BigDye Terminator, version 1.1 on a 3730 DNA analyzer; Applied Biosystems Inc, Foster City, CA). Segregation analysis was performed by sequence analysis, and additional RP cases and

ethnically matched control individuals were screened with an amplification refractory mutation system-polymerase chain reaction<sup>26</sup>.

### **Clinical Evaluation**

Clinical investigations included pure tone audiometry, funduscopy, and ERG in accordance to the guidelines of the International Society for Clinical Electrophysiology of Vision<sup>27</sup> using a monopolar contact lens electrode (LKC Inc., Gaithersburg, MD).

### **Bioinformatic evaluation of the mutations**

To assess the conservation of the mutated amino acids of the clarin-1 protein at the substitution positions, the amino acid sequences of various orthologs were obtained from the NCBI protein database (available at: <http://www.ncbi.nlm.nih.gov/protein/>; accessed June 10, 2010) and aligned with the human sequence (NP\_777367.1) using Align software in Vector NTI program, version 11 (Invitrogen, Carlsbad, CA). Web-based servers including PolyPhen (available at: <http://genetics.bwh.harvard.edu/pph/>; accessed July 5 2010) and SIFT (available at: <http://sift.jcvi.org>; accessed July 5, 2010) were used to assess the pathogenic potential of the mutations. The SMART database (available at: <http://smart.embl-heidelberg.de/>; accessed July 5, 2010) was used to identify the positions of the functional domains of the clarin-1 protein.

### **Functional analysis of the mutations**

To determine the subcellular localization of wild-type clarin-1, and the two mutant proteins, full-length cDNA constructs were generated using commercially available Gateway cloning technology (Invitrogen), according to the manufacturer's instructions. Human testis cDNA (Marathon; Clontech Laboratories, Inc., Palo Alto, CA) was used as a template to amplify the full-length clarin-1 cDNA (*CLRNI*; NM\_174878; available at: <http://www.ncbi.nlm.nih.gov/Genbank>; NCBI, Bethesda, MD) using the forward primer 5'- atg cca agc caa cag aag aaa atc -3' and the reverse primer 5'- tca gta cat tag atc tgc agc -3'. Mutant constructs carrying the missense mutations p.Pro31Leu and p.Leu154Trp were generated using site-directed mutagenesis of the wild-type clarin-1 plasmid with phusion DNA polymerase (Finnzymes, Espoo, Finland). The expression vector pDest733 was used, which generates a fusion protein with monomeric red fluorescent protein (mRFP) at the N-terminus (Invitrogen). The subcellular localizations of the wild-type and mutant clarin-1 proteins in hTERT-RPE1 cells (Clontech Laboratories, Inc.) were determined by transfecting these cells with pDEST733-clarin-1 wild-type, p.Pro31Leu, and p.Leu154Trp constructs using the Effectene transfection reagent (Qiagen, Hilden, Germany) according to the manufacturer's instructions, resulting in clarin-1 proteins fused to mRFP at the N-terminus.

A construct encoding a palmitoylation-myristoylation-cyan fluorescent protein fused with the intracellular domain (icd) of USH2A was cotransfected with the pDEST733-clarin-1 constructs, resulting in plasma membrane-anchored-USH2A\_icd, which was used as a marker for the plasma membrane<sup>12</sup>. Twenty-four hours after transfection, the cells were washed with PBS and fixed with methanol. A mouse monoclonal antibody to protein disulphide isomerase was used as an endoplasmic reticulum (ER) marker (Abcam, Cambridge, UK). A goat-anti-mouse secondary antibody (Alexa Fluor 488, Molecular Probes-Invitrogen) was used for visualization and the cells were embedded with Vectashield containing DAPI (Vector Laboratories, Peterborough, UK).

---

*CLRN1* mutations cause non-syndromic retinitis pigmentosa

Photographic images of the cells were obtained with an Axio imagerZ1 fluorescence microscope (Zeiss, Jena, Germany) equipped with an AxioCam MRm camera (Zeiss). Images were processed using Axiovision Rel.4.6 and Adobe Photoshop (Adobe Systems, San Jose, CA).

**References**

1. Koenekoop RK. Why do cone photoreceptors die in rod-specific forms of retinal degenerations? *Ophthalmic Genet.* 2009;30:152-154.
2. Wang DY, Chan WM, Tam PO, et al. Genetic markers for retinitis pigmentosa. *Hong Kong Med J.* 2005;11:281-288.
3. Hartong DT, Berson EL, Dryja TP. Retinitis pigmentosa. *Lancet.* 2006;368:1795-1809.
4. Liu X, Tang Z, Li C, et al. Novel USH2A compound heterozygous mutations cause RP/USH2 in a Chinese family. *Mol Vis.* 2010;16:454-461.
5. Rivolta C, Sweklo EA, Berson EL, et al. Missense mutation in the USH2A gene: association with recessive retinitis pigmentosa without hearing loss. *Am J Hum Genet.* 2000;66:1975-1978.
6. Kaiserman N, Obolensky A, Banin E, et al. Novel USH2A mutations in Israeli patients with retinitis pigmentosa and Usher syndrome type 2. *Arch Ophthalmol.* 2007;125:219-224.
7. Seyedahmadi BJ, Rivolta C, Keene JA, et al. Comprehensive screening of the USH2A gene in Usher syndrome type II and non-syndromic recessive retinitis pigmentosa. *Exp Eye Res.* 2004;79:167-173.
8. Ebermann I, Wilke R, Lauhoff T, et al. Two truncating USH3A mutations, including one novel, in a German family with Usher syndrome. *Mol Vis.* 2007;13:1539-1547.
9. Sadeghi M, Cohn ES, Kimberling WJ, et al. Audiological and vestibular features in affected subjects with USH3: a genotype/phenotype correlation. *Int J Audiol.* 2005;44:307-316.
10. Tian G, Zhou Y, Hajkova D, et al. Clarin-1, encoded by the Usher Syndrome III causative gene, forms a membranous microdomain: possible role of clarin-1 in organizing the actin cytoskeleton. *J Biol Chem.* 2009;284:18980-18993.
11. Zallocchi M, Meehan DT, Delimont D, et al. Localization and expression of clarin-1, the Clrn1 gene product, in auditory hair cells and photoreceptors. *Hear Res.* 2009;255:109-120.
12. Violin JD, Zhang J, Tsien RY, et al. A genetically encoded fluorescent reporter reveals oscillatory phosphorylation by protein kinase C. *J Cell Biol.* 2003;161:899-909.
13. Isosomppi J, Vastinsalo H, Geller SF, et al. Disease-causing mutations in the CLRN1 gene alter normal CLRN1 protein trafficking to the plasma membrane. *Mol Vis.* 2009;15:1806-1818.
14. Jaijo T, Aller E, Garcia-Garcia G, et al. Microarray-based mutation analysis of 183 Spanish families with Usher syndrome. *Invest Ophthalmol Vis Sci.* 2010;51:1311-1317.
15. Ness SL, Ben-Yosef T, Bar-Lev A, et al. Genetic homogeneity and phenotypic variability among Ashkenazi Jews with Usher syndrome type III. *J Med Genet.* 2003;40:767-772.
16. Cohen M, Bitner-Glindzicz M, Luxon L. The changing face of Usher syndrome: clinical implications. *Int J Audiol.* 2007;46:82-93.
17. Fields RR, Zhou G, Huang D, et al. Usher syndrome type III: revised genomic structure of the USH3 gene and identification of novel mutations. *Am J Hum Genet.* 2002;71:607-617.
18. Joensuu T, Hamalainen R, Yuan B, et al. Mutations in a novel gene with transmembrane domains underlie Usher syndrome type 3. *Am J Hum Genet.* 2001;69:673-684.

19. den Hollander AI, Koenekoop RK, Yzer S, et al. Mutations in the CEP290 (NPHP6) gene are a frequent cause of Leber congenital amaurosis. *Am J Hum Genet.* 2006;79:556-561.
20. Aldahmesh MA, Safieh LA, Alkuraya H, et al. Molecular characterization of retinitis pigmentosa in Saudi Arabia. *Mol Vis.* 2009;15:2464-2469.
21. Riazuddin SA, Iqbal M, Wang Y, et al. A splice-site mutation in a retina-specific exon of BBS8 causes nonsyndromic retinitis pigmentosa. *Am J Hum Genet.* 2010;86:805-812.
22. Estrada-Cuzcano A, Koenekoop RK, Coppieters F, et al. IQCB1 mutations in patients with Leber congenital amaurosis. *Invest Ophthalmol Vis Sci.* 2010;52:834-839.
23. Stone EM, Cideciyan AV, Aleman TS, et al. Variations in NPHP5 cause nonsyndromic Leber Congenital Amaurosis (LCA). *ARVO abstract.* 2010;51:6354.
24. Sambrook J, Russel DW. Molecular Cloning: A laboratory Manual. *New York: Cold Spring Harbor Laboratory Press;* 2001;3<sup>rd</sup> ed:3-11.
25. Hoffmann K, Lindner TH. easyLINKAGE-Plus--automated linkage analyses using large-scale SNP data. *Bioinformatics.* 2005;21:3565-3567.
26. little S. Amplification-refractory mutation system (ARMS) analysis of point mutations. *Current protocols in human genetics.* 2001;may Chapter 9: Unit 9.8.
27. Marmor MF, Fulton AB, Holder GE, et al. ISCEV Standard for full-field clinical electroretinography (2008 update). *Doc Ophthalmol.* 2009;118:69-77.





# Chapter



# 7

## General discussion





## 1. The expanding USH protein network

Usher syndrome is a genetically heterogeneous disorder, as so far nine genes have been associated with the disease. The USH proteins that are encoded by these genes, with exception of the USH3 protein clarin-1, can be integrated in a single protein network, organized by the scaffold proteins whirlin and harmonin (Fig. 1) <sup>1-7</sup>. If mutations in different genes, such as the USH genes, can cause an overlapping disease phenotype, these genes are often expressed in the same tissues and the encoded proteins play a role in shared functional modules such as the same biochemical pathway, or closely connected protein complexes that are dependent on each other's function. The physical interaction of proteins is essential for their function <sup>8,9</sup>. Therefore, the identification of interaction partners of USH proteins might well contribute to the understanding of the function of the USH protein complex. In the studies described in this thesis, different approaches have been successfully used to expand the USH protein network (chapters 2, 3, 4 and 5) (Fig. 1).

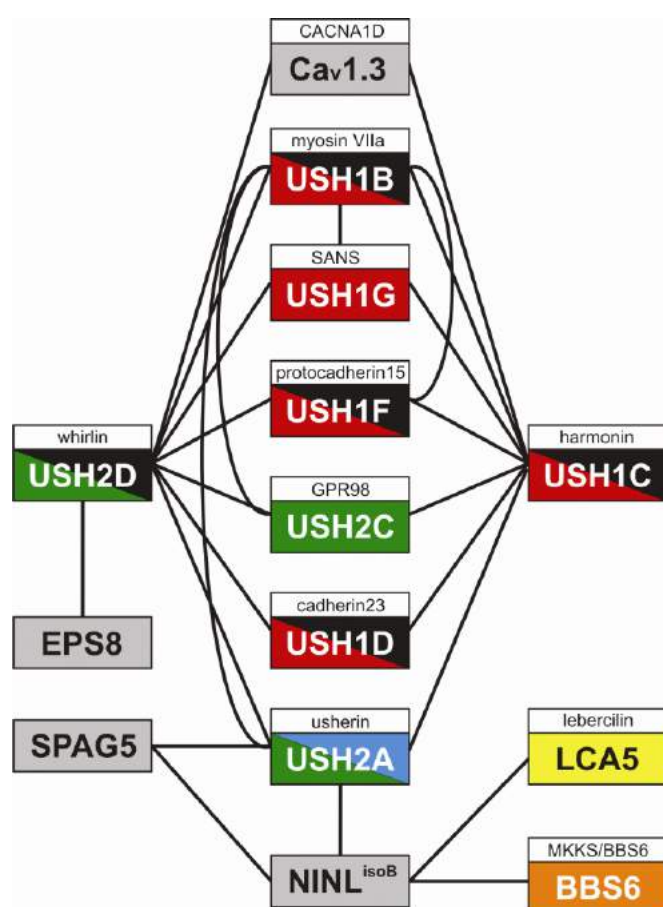


**Figure 1.** Novel members of the USH protein network are part of the USH protein network. Lines indicate protein interactions. Grey indicates novel members of the USH protein network described in this thesis, red indicates association with Usher syndrome type I (USH1), green indicates association with Usher syndrome type II (USH2), blue indicates association with isolated retinitis pigmentosa (RP), black indicates association with isolated deafness, orange indicates association with Bardet-Biedl syndrome (BBS), and yellow indicates association with Leber Congenital amaurosis (LCA).

### 1.1 Identification of novel members of the USH protein network

To identify novel interaction partners, we have used yeast two-hybrid (Y2H) interaction trap screens. Screening of a retinal cDNA library using the intracellular domain of USH2A<sup>isoB</sup> as a bait revealed the novel interaction partners NINL<sup>isoB</sup> ([chapter 4](#)) and SPAG5 ([chapter 5](#)) (Fig. 1). A number of other members of the USH protein network have also been identified by this method such as lebercilin ([chapter 4](#)) (Fig. 1).

Another successful method that we employed was based on bioinformatics. This query yielded eighteen genes including the USH genes *USH2A*, *CDH23* and *PCDH15* ([chapter 2](#)). Ca<sub>v</sub>1.3 was identified to link to the USH protein network via whirlin ([chapter 2](#)) (Fig. 1), indicating the usefulness of this bioinformatic approach to identify interaction partners of the key players of the USH protein network, the PDZ domain-containing scaffold proteins harmonin and whirlin. Novel members of the USH protein network might be identified by testing the interaction between the remaining fourteen candidate proteins and these scaffold proteins as well. The same holds true for the remaining 99 genes which matched all criteria except the inner ear or retina phenotypes of animal models ([chapter 2](#)).

Also, an overlapping cellular phenotype of animal models for two genes in combination with co-localization of the encoded proteins can give a hint for their physical interaction. For example, the morphological abnormalities seen in hair cells of the *Eps8*<sup>-/-</sup> mice resembled those seen in hair cells of *whirler* mice and the encoded proteins are both located at the tips of stereocilia. Indeed, the interaction between EPS8 and whirlin was subsequently found ([chapter 3](#)) (Fig. 1).

### 1.2 Biological relevance of the interactions with novel members

The identification of protein-protein interactions *in vitro* or *ex vivo* does not necessarily mean that these interactions are biologically relevant. The majority of the direct interactions within the USH protein network have been determined by using *in vitro* assays and/or *ex vivo* assays based on overexpression of the proteins of interest. The biological relevance has been proven for a subset of these interactions *e.g.* mislocalization of harmonin-b in the inner ear of mice defective for *SANS* and *myosin VIIa*<sup>10</sup>, abnormal localization of harmonin and myosin VIIa in hair cells of *Cdh23* null mutants<sup>11</sup>, mislocalization of SANS and *Pcdh15* in hair cells of

---

*Ush1c*<sup>-/-</sup> mice<sup>12</sup>, and the restored localization and expression levels of both *Ush2a* and *Gpr98* in the retina of the *whirlin* knockout mouse by transgenic whirlin expression<sup>13</sup>.

For most of the novel interactions described in this thesis additional studies are necessary that provide more clues on the biological role of these interactions. The interaction between EPS8 and whirlin is biologically relevant as demonstrated by aberrant distribution of Eps8 in hair cells of mice with a defective *Whrn* gene and *vice versa* ([chapter 3](#)). Furthermore, the mutations in *EPS8* affect the association with whirlin indicating that the proteins are dependent on each other ([chapter 3](#)). Truncating mutations in lebercilin severely affect the association with NINL<sup>isoB</sup> at the basal body indicating biological relevance ([chapter 4](#)). However, downregulation of both endogenous *Ninl* and *LCA5* by RNAi in ciliated cells does not result in altered protein localization of lebercilin nor *Ninl*, respectively, suggesting the involvement of other binding partners ([chapter 4](#)). Whirlin-Ca<sub>v</sub>1.3 ([chapter 2](#)), USH2A<sup>isoB</sup>-NINL<sup>isoB</sup> ([chapter 4](#)) and SPAG5- NINL<sup>isoB</sup> ([chapter 5](#)) interact and co-localize at subcellular structures suggesting that the proteins function together. However, whether these proteins are dependent on each other for their localization and function together or in the same pathway, indicating biological relevance, remains to be determined. Some of the novel described interactions are indicated to be biologically relevant, whereas for others more studies are necessary to conclude this. These studies may encompass the identification of genetic interactions in animal models to examine whether both proteins function in the same cellular process or pathway, as well as protein localization studies in animal models in which the interaction partner(s) are disrupted.

## **2. Functions of the USH protein network: what do novel members tell?**

The USH protein network is dynamic and the different USH proteins and their direct or indirect interaction partners fulfill several functions in the inner ear and retina ([chapter 1](#))<sup>14-17</sup>. A number of USH proteins have been identified as components of fibrous links that interconnect adjacent stereocilia and the stereocilia and the kinocilium of hair cells and are therefore involved in hair-bundle cohesion. Tip-links connect the tips of stereocilia to the side of their taller neighbors and are thought to gate the mechanotransduction channels. USH proteins are components of these links and are therefore suggested to be involved in hair cell

function<sup>18,19</sup>. Analogous to the links in the hair bundle are the fibrous links that provide the structural support between the membranes of the connecting cilium and the apical inner segment of photoreceptor cells. USH proteins are suggested to be components of these links as well<sup>20,21</sup>. Several other functions of the USH protein complex are described below.

By the studies described in this thesis, four functionally completely different proteins are linked to the USH protein network. The calcium channel subunit Ca<sub>v</sub>1.3 ([chapter 2](#)), the epidermal growth factor receptor substrate EPS8 ([chapter 3](#)), the ninein-like protein (NINL<sup>isoB</sup>) ([chapter 4](#)), and the sperm associated antigen SPAG5 ([chapter 5](#)). This provided more clues about the function of the network.

## 2.1 Organization of ion channels

Presence of USH proteins at the synapse of hair cells and photoreceptor cells suggests a role in synapse formation, maintenance and/or synaptic transmission<sup>5-7,20</sup>. A role in the organization of ion channels or transporters had already been proposed for harmonin and whirlin based on the direct interaction of harmonin with NBC3<sup>5,16</sup>. The identification of the L-type calcium channel subunit Ca<sub>v</sub>1.3 as an interaction partner of both whirlin and harmonin supports this role ([chapter 2](#))<sup>22</sup>. These proteins co-localized at the synaptic regions of photoreceptor cells and hair cells ([chapter 2](#))<sup>23,24</sup>. In synapses of hair cells, the calcium current for Ca<sup>2+</sup> dependent exocytosis is generated by these Ca<sub>v</sub>1.3 channels<sup>23,24</sup> and disturbed Ca<sub>v</sub>1.3 currents and impaired exocytosis has been observed in inner hair cells of *dfcr* mice with a mutation in the *Ush1c* gene<sup>22</sup>. As Ca<sub>v</sub>1.3 is an interaction partner of both harmonin and whirlin, analysis of the calcium currents and exocytosis in the inner hair cells of the *whirler*<sup>25</sup> and *Whrn*<sup>-/-</sup><sup>26</sup> mice will answer the question if these disturbances are also present due to mutations in the *Whrn* gene. These studies indicate that of the USH proteins, at least harmonin and whirlin may have a role in the organization of ion channels at the synapse. Whirlin may also fulfill this role at the periciliary region of photoreceptor cells (see below).

## 2.2 Planar cell polarity

The USH protein complex is essential for the development of the hair bundle including hair bundle orientation<sup>10</sup>. Hair bundles in USH1 mouse models are misoriented by a deviated position of the kinocilium, suggesting the involvement of USH1 proteins in the positioning of

the kinocilium, which is regulated by the planar cell polarity (PCP) pathway<sup>10</sup>. A number of core PCP proteins have been demonstrated to be normally distributed at hair cells of USH1 mice models<sup>10</sup> indicating that USH1 proteins could well be downstream effectors of PCP proteins. Other links between the USH protein network and the PCP pathway have been suggested. The recently identified genetic interaction in zebrafish between *Bbs* genes and the gene encoding *Ninl*, and the direct interaction between *NINL*<sup>isoB</sup> and *BBS6*<sup>27</sup> suggest an indirect link between the USH protein complex and the PCP pathway since PCP is perturbed in Bardet-Biedl syndrome (BBS)<sup>28</sup>. Another association is provided by the genetic interaction of the *Drosophila* gene *crinkled*, a homolog of the USH gene *MYO7A*, with the frizzled/dishevelled cytoskeletal signaling pathway that regulates PCP<sup>29</sup>. Dishevelled controls both docking and planar polarization of basal bodies and is one of the core proteins of the PCP<sup>30,31</sup>. Interestingly, dishevelled also associates with an interaction partner of whirlin, EPS8<sup>32</sup>. Nevertheless, no PCP defects have been observed in the *Eps8*<sup>-/-</sup> mice which have a normal hair bundle orientation (chapter 3). Also no abnormalities in hair bundle orientation have so far been demonstrated in mice with defects in the *Whrn* gene or in the genes *Ush2a* and *Clrn1*. In *Gpr98*<sup>-/-</sup> mice, the hair bundle orientation is abnormal<sup>4,19,21</sup>, but it remains to be conclusively analyzed whether the PCP pathway regulates USH2 and USH3 proteins.

### 2.3 Stereocilia formation and elongation

After the orientation of the hair bundles in the inner ear has been defined by the PCP pathway, the stereocilia begin to elongate differentially, according to their position in the hair bundle. This results in a staircase-like pattern of stereocilia. The complex mechanism involved in this patterning is slowly being elucidated. A number of members of the USH protein network including whirlin, p55/MPP1, EPS8 and myosin XVa function in stereocilia elongation and staircase pattern regulation and its maintenance (chapter 3)<sup>33,34</sup>. The presence of the whirlin-myosin XVa complex at the tips of the stereocilia is essential for their elongation<sup>33</sup>. EPS8 is indicated to be a member of this complex. Myosin XVa is crucial for EPS8 localization at the stereocilia tips and whirlin is essential for the distribution of EPS8 within the bundle (chapter 3). Whirlin also binds to p55/MPP1 that interacts with the actin capping protein gelsolin and these latter two proteins are so far only detected in OHCs<sup>34-36</sup>. Gelsolin was only detected at the tips of rows of shorter stereocilia<sup>36</sup>. The same holds true for twinfilin-2, another actin



capping protein<sup>37</sup> which interacts with myosin VIIA<sup>38</sup>. This suggests an interplay between the whirlin-p55/MPP1 complex and the myosin VIIA-twinfilin-2 complex in staircase patterning of rows with short and middle length stereocilia<sup>36</sup>. Interestingly, we found that EPS8 was enriched at the tips of the longest stereocilia in hair bundles of both IHCs and OHCs ([chapter 3](#)). This suggests that the whirlin-EPS8 complex regulates the staircase patterning in mainly the rows of the longest stereocilia, and the whirlin-p55/MPP1-gelsolin and the myosin VIIA-twinfilin-2 complexes mainly in the shorter stereocilia. Thus, whirlin organizes different sets of proteins to the tip of stereocilia which act to control stereocilia elongation. Further, identification of novel whirlin interaction partners, especially actin regulating molecules may contribute to the elucidation of the complex mechanism of differential stereocilia elongation that leads to staircase patterning.

## 2.4 Vesicle transport

It has been hypothesized that USH proteins play a role in vesicle transport and docking in photoreceptor- and hair cells<sup>16,20,39</sup>. In photoreceptor cells, USH proteins may contribute to the control of vesicle docking at the periciliary region and cargo transfer from the inner segment transport system to that of the cilium<sup>16,20</sup>. Vesicle docking and/or fusion are regulated by influx of Ca<sup>2+</sup> via voltage gated calcium channels. Since whirlin associates with the calcium channel subunit Ca<sub>v</sub>1.3, it is likely to have a role in the transport and/or organization of voltage gated calcium channels and thereby it may contribute to the control of vesicle docking and/or fusion via regulation of the local Ca<sup>2+</sup> concentration ([chapter 2](#)).

At the basal body, cargo vesicles are loaded from the inner segment transport system to the intraflagellar transport (IFT) machinery which is involved in the transport through the connecting cilium to the photoreceptor outer segments<sup>40</sup>. NINL<sup>isoB</sup> may function in this cargo handover ([chapter 4](#)). We also suggested that SPAG5 and NINL<sup>isoB</sup> together play a role in the microtubule-based transport and docking of (USH2A<sup>isoB</sup>-containing) vesicles to the apical inner segment and basal body of photoreceptor cells ([chapter 5](#)). Defects in vesicle docking and transport and/or structural support can lead to shorter photoreceptor outer segments<sup>41-45</sup>. Studying the photoreceptor outer segments during development or adult stage of the recently available *Ninl* knockout mice and *Spag5* mutant rats<sup>46</sup> may demonstrate whether or not NINL and SPAG5 are indeed essential for outer segment development and/or function. Also

downregulation of these genes in zebrafish by morpholinos, and subsequent assessment of photoreceptor development and maintenance may answer this question. Indeed, preliminary data demonstrate shorter photoreceptor outer segments after downregulation of *Ninl* in zebrafish (van Wijk unpublished results).

In hair cells of the inner ear, the pericuticular necklace is a vesicle-rich region surrounding the actin-based cuticular plate that may be equivalent to the photoreceptor apical inner segment<sup>47,48</sup>. The presence of USH proteins and Spag5 at this location suggest also an association with transport vesicles in the inner ear (Figure 6A in [chapter 1, unpublished results](#)). If USH proteins are indeed transported within these vesicles and/or have a role in vesicle transport in the retina and inner ear remains to be determined in more detail. At least in bovine tracheal epithelial cells USH proteins are present in both vesicles and in the cytosol<sup>49</sup>.

The (hypothesized) functions of the identified novel members support several of the previously suggested roles of the USH protein network. However, more detailed studies will be needed to answer the question whether these proteins indeed fulfill these roles.

### **3. Disease association of genes encoding USH proteins and novel members of the protein network**

At the onset of the study described in chapter 6 mutations in the USH genes, with the exception of *SANS*, *GPR98* and *CLRN1*, were known to be causative for Usher syndrome and nonsyndromic deafness or nonsyndromic retinitis pigmentosa (RP). Besides Usher syndrome, mutations in *MYO7A* can cause autosomal dominant deafness (DFNA11)<sup>50-52</sup>. Defects in *MYO7A*, *USH1C*, *CDH23*, *PCDH15* and *DFNB31* can cause autosomal recessive deafness (DFNB2)<sup>53,54</sup>, (DFNB18)<sup>55,56</sup>, (DFNB12)<sup>57</sup>, (DFNB23)<sup>58,59</sup>, (DFNB31)<sup>60</sup>, respectively and mutations in *USH2A* have been associated with autosomal recessive RP<sup>61-63</sup>. A mutation in *SANS* causes atypical Usher syndrome with sensorineural hearing loss, normal vision, mild or late onset RP and normal vestibular function<sup>64</sup>. Therefore, *SANS*, *GPR98*, and *CLRN1* are also candidate genes for nonsyndromic deafness or nonsyndromic RP. Indeed, we identified that mutations in *CLRN1*, besides USH3, can also cause nonsyndromic autosomal recessive RP ([chapter 6](#)).

### 3.1 Clinical variability

The clinical variability in patients with mutations in USH genes may be explained by the fact that mutations might only affect tissue specific exons/isoforms or isoforms with preferential expression in either retina or inner ear. Another explanation may be that certain mutations affect protein domains that are important for function in the retina or cochlea via tissue-specific interaction partners. Also, the combination of a mutation with different other mutations may explain the diversity in phenotypes. Although not proven, the presence of modifiers might also influence the clinical outcome. This is supported by Ebermann and coworkers who identified *PDZD7* as a retinal disease modifier in patients with Usher syndrome <sup>65</sup>.

For some USH genes, the type of mutations and/or their position in the genes can explain the phenotypic differences. Truncating mutations in *CDH23* cause USH1, and missense mutations affecting conserved motifs of the protein cause nonsyndromic deafness (DFNB12) <sup>57,66</sup>. For *USH1C*, Ahmed and coworkers suggested a genotype-phenotype correlation in which hypomorphic alleles cause nonsyndromic deafness, whereas more severe mutations cause USH1 <sup>55</sup>. In addition, mutations in alternatively spliced exons of this gene were only identified in nonsyndromic deafness patients, suggesting inner ear specific expression of these exons <sup>56</sup>. Furthermore, mutations in the 5' part of the *DFNB31/Whrn* gene cause both vision and hearing impairment, <sup>26,67</sup> whereas mutations in the 3' region are associated with more severe deafness without visual problems <sup>25,60</sup>. This suggests a short retina-specific isoform encoded by the 5'-region of the gene. For mutations in *CLRN1* we also suggested a genotype-phenotype correlation. The RP-associated mutations may cause a less severe phenotype due to the positions of the affected amino acids and their substitutions by amino acids of the same class (side chain polarity) ([chapter 6](#)). It is also possible that the RP-associated mutations may represent hypomorphic mutations, which would suggest that the retina may be more vulnerable to impaired clarin-1 function than the inner ear ([chapter 6](#)).

For genetic counseling it is useful to predict the clinical outcome of mutations in USH genes. However, the mutations we identified in *CLRN1* will probably not contribute importantly to genetic counseling, as in USH3 the onset of hearing loss usually precedes the onset of visual loss <sup>68</sup> although visual symptoms can develop before hearing problems <sup>69</sup>. Besides this, USH3

is rare and the frequency is the highest in the Finnish population due to founder mutations<sup>70</sup> while we identified mutations in RP patients from Pakistani origin ([chapter 6](#)).

### 3.2 Disease association of genes encoding novel members of the USH protein network

The identification of interaction partners of the USH proteins not only contributes to the knowledge of the molecular disease mechanisms, but the genes encoding these protein partners are also functional candidates for Usher syndrome and related disorders. For Usher syndrome two additional loci (USH1e, USH1h) are known for which the causative gene has not yet been identified. However, none of the genes encoding novel members of the USH protein network are located in these two loci.

Usher syndrome is recessively inherited and homozygosity mapping is an effective method to identify disease loci in families with a recessive disorder<sup>71-75</sup>. By this method, a candidate locus for RP was identified containing the *SPAG5* gene. A homozygous variation in *SPAG5* (p.A1082V) was detected in all four affected individuals of this family which was not present in 214 control alleles (unpublished results). However, in this family three additional homozygous regions could harbor the disease gene, all with a LOD score of almost 3. To exclude potential other causative variations within the family, the genes in all four homozygous regions were analyzed by exome sequencing. Some of the identified variations need to be evaluated for their potential pathogenicity before it can be concluded that the mutation in *SPAG5* is indeed causative for RP in this family. Preliminary data suggest an effect of the mutation on the interaction of the mutant with USH2A (unpublished results) suggesting that the microtubule-based transport of (USH2A-containing) vesicles in photoreceptor cells is affected which might result in retinal degeneration. The renal phenotype of the *Spag5* rat model is similar to oligomeganephronia<sup>76,77</sup> that is found to be associated with other ailments including RP and deafness<sup>78</sup>. Therefore, it is interesting to screen cohorts of patients suffering from syndromic and nonsyndromic oligomeganephronia for mutations in *SPAG5*.

In our cohorts of Usher syndrome, deafness and RP patients, *CACNAID* encoding Ca<sub>v</sub>1.3 ([chapter 2](#)) was not present in the candidate disease loci using our cut-off values for homozygous regions and therefore it was not analyzed for mutations. The formerly described

USH2b locus which harbored the *CACNAID* gene has been withdrawn<sup>79,80</sup>. Recently, a homozygous mutation (p.403\_404insG) in the alternatively spliced *CACNAID* exon 8B was identified in affected individuals of two families suffering from congenital deafness and bradycardia (slow heart rate)<sup>81</sup>. The absence of a retinal phenotype might be explained by the fact that this inframe-insertion does not affect the PBM of the protein and therefore the interaction with whirlin might not be disturbed. Another explanation might be that the affected splice variant might not be expressed in the retina or that the function is taken over by other isoforms or proteins such as Ca<sub>v</sub>1.4 ([chapter 2](#)).

Mutation analysis of the *NINL* gene, revealed three heterozygous variations p.L873V, p.L12I and p.R451W in one RP patient and in two USH2 patients, respectively which were not present in 192 control alleles<sup>82</sup>. Besides p.L873V, no second mutation has been identified in an arRP gene so far. The p.L12I and p.R451W variations in USH2 patients co-segregate with the heterozygous mutations p.E767fsX56 and p.C419F in *USH2A*, respectively, which might suggest digenic inheritance<sup>82</sup>. This is supported by Zheng and coworkers who identified digenic inheritance with heterozygous mutations in *CDH23* and *PCDH15*<sup>83</sup>. Alternatively, *NINL* might be a modifier gene for *USH2A*, similar to *PDZD7* that is a retinal disease modifier<sup>65</sup>. Modifying variations have also been detected in other ciliopathies; e.g. a mutation in *RPGRIP1L* is a modifier of retinal degeneration in ciliopathies<sup>84</sup> and heterozygous mutations in *BBS1*, *BBS2*, or *BBS6* correlate with a more severe phenotype in BBS patients with mutations at a second locus<sup>85,86</sup>.

It is still unclear whether and which genetic factors are responsible for clinical variability in (retinal) ciliopathies including Usher syndrome. However, techniques such as next generation sequencing will contribute to their identification in the very near future. Sequencing of all (predicted) ciliary genes or even whole exomes in large cohorts of patients with ciliopathies can already be achieved by using this technique. This will contribute to the identification of many known and so far unknown causative mutations<sup>87,88</sup>.

#### **4. Prospects on future research**

The studies described in this thesis contributed to the identification of novel interaction partners of the USH proteins which provided important knowledge on the putative functions of the USH protein complex. However, many questions remain to be addressed for better understanding of the molecular pathology of Usher syndrome.

##### **4.1 Extending the knowledge on the function of the USH protein network**

To obtain more knowledge of the function of the protein network, novel members of the USH proteins network need to be identified and the function of the known and novel members need to be further explored. Y2H screens of retinal and cochlear cDNA libraries are very useful to identify interaction partners of USH proteins ([chapters 4 and 5](#))<sup>89</sup>. Whereas the Y2H method only detects binary protein-protein interactions, the tandem affinity purification (TAP) technology followed by mass-spectrometry analysis can be used for the isolation and identification of protein complexes in (ciliated) cultured cells<sup>90</sup>. The TAP method in HEK293 cells was successfully employed by our group to identify interaction partners of lebercilin which suggested, together with its localization, a link of lebercilin to centrosomal and ciliary functions<sup>72</sup>. In the future, it is also important to identify interaction partners from cell lines that express the USH proteins endogenously (*e.g.* UB/OC-1 derived from cochlea). GST pull-down assays and immunoprecipitations from retinal extracts (*e.g.* bovine or pig eyes that represent close similarities with human eyes) followed by mass-spectrometry analysis are also important techniques to generate protein interaction data which provide further clues for the function of the protein network and the genes encoding these proteins are functional candidates for Usher syndrome and related disorders.

Further strategies to unravel the function of USH proteins and their interaction partners include downregulation of genes by RNAi in cell lines or tissue explants. Also, downregulation of the genes by morpholinos in zebrafish or mutant zebrafish to study eye development will provide more insight in the function of USH proteins, especially in the retina. Also, USH knockout mice and mice that are deficient for novel network members will be useful to study the effect of their deficiencies. Importantly, bioinformatic analysis to dissect molecular pathways, may also provide more insights into the function of the network.

## 4.2 Dynamics of the USH protein complex

USH proteins were found to interact with specific protein domains to a number of other proteins. The first two PDZ domains of whirlin, for example, can interact with multiple USH proteins<sup>7</sup> and with Ca<sub>v</sub>1.3 ([chapter 2](#)). Further, USH2A binds with its intracellular domain to whirlin, harmonin<sup>7</sup>, SPAG5 ([chapter 5](#)) and NINL<sup>isoB</sup> ([chapter 4](#)). The latter also binds with its intermediate filament domain to lebercilin ([chapter 4](#)) and SPAG5 ([chapter 5](#)). It remains to be elucidated how these different interactions are regulated, but likely by spatiotemporal expression patterns and/or posttranslational modifications such as phosphorylation. Understanding the dynamics of the USH protein network is even more complicated because of the existence of a (large) number of different isoforms of most of the USH proteins which vary in their spatiotemporal expression pattern ([chapter 1](#)). Therefore, it would be interesting to perform protein-protein interaction studies using the same baits in different tissues and cell types to investigate the differences in protein composition at diverse locations. Also, isoform-specific antibodies are crucial to study the localization of the different USH protein isoforms in wildtype and USH mutant mouse models during development.

## 4.3 Therapeutic interventions

Understanding the molecular disease mechanisms underlying Usher syndrome and related disorders will eventually contribute to therapeutic strategies. Currently, clinical trials are ongoing for gene augmentation therapy for retinal degeneration. This improved visual function in patients carrying a mutation in *RPE65*, a gene causative for early-onset RP and LCA<sup>91-95</sup>. However, this strategy is not suitable for all genes; for example *USH2A* is too large for the current AAV vectors to express the full-length wildtype replacing gene. However, the identification of USH2A interaction partners may provide targets for therapy. Knowledge on interaction partners of USH proteins is also important to evaluate the effects of the therapy on the molecular level.

A final strategy that holds significant promise is the suppression of nonsense mutations by certain chemicals that in the future may be effective in the treatment of patients with retinal ciliopathies due to these mutations<sup>96-102,103</sup>.

## 5. References

1. Adato A, Lefevre G, Delprat B, et al. Usherin, the defective protein in Usher syndrome type IIA, is likely to be a component of interstereocilia ankle links in the inner ear sensory cells. *Hum Mol Genet.* 2005;14:3921-3932.
2. Adato A, Michel V, Kikkawa Y, et al. Interactions in the network of Usher syndrome type I proteins. *Hum Mol Genet.* 2005;14:347-356.
3. Boeda B, El Amraoui A, Bahloul A, et al. Myosin VIIa, harmonin and cadherin 23, three Usher I gene products that cooperate to shape the sensory hair cell bundle. *EMBO J.* 2002;21:6689-6699.
4. Michalski N, Michel V, Bahloul A, et al. Molecular characterization of the ankle-link complex in cochlear hair cells and its role in the hair bundle functioning. *J Neurosci.* 2007;27:6478-6488.
5. Reiners J, van Wijk E, Maerker T, et al. Scaffold protein harmonin (USH1C) provides molecular links between Usher syndrome type I and type 2. *Hum Mol Genet.* 2005;14:3933-3943.
6. Reiners J, Marker T, Jurgens K, et al. Photoreceptor expression of the Usher syndrome type I protein protocadherin 15 (USH1F) and its interaction with the scaffold protein harmonin (USH1C). *Mol Vis.* 2005;11:347-355.
7. van Wijk E, van der Zwaag B, Peters TA, et al. The DFNB31 gene product whirlin connects to the Usher protein network in the cochlea and retina by direct association with USH2A and VLGR1. *Hum Mol Genet.* 2006;15:751-765.
8. Goh KI, Cusick ME, Valle D, et al. The human disease network. *Proc Natl Acad Sci U S A.* 2007;104:8685-8690.
9. Oti M, Brunner HG. The modular nature of genetic diseases. *Clin Genet.* 2007;71:1-11.
10. Lefevre G, Michel V, Weil D, et al. A core cochlear phenotype in USH1 mouse mutants implicates fibrous links of the hair bundle in its cohesion, orientation and differential growth. *Development.* 2008;135:1427-1437.
11. Bahloul A, Michel V, Hardelin JP, et al. Cadherin-23, myosin VIIa and harmonin, encoded by Usher syndrome type I genes, form a ternary complex and interact with membrane phospholipids. *Hum Mol Genet.* 2010;19:3557-3565.
12. Yan D, Kamiya K, Ouyang XM, et al. Analysis of subcellular localization of Myo7a, Pcdh15 and Sans in Ush1c knockout mice. *Int J Exp Pathol.* 2011;92:66-71.
13. Zou J, Luo L, Shen Z, et al. Whirlin Replacement Restores the Formation of the USH2 Protein Complex in Whirlin Knockout Photoreceptors. *Invest Ophthalmol Vis Sci.* 2011;52:2343-2351.
14. Brown SD, Hardisty-Hughes RE, Mburu P. Quiet as a mouse: dissecting the molecular and genetic basis of hearing. *Nat Rev Genet.* 2008;9:277-290.
15. El Amraoui A, Petit C. Usher I syndrome: unravelling the mechanisms that underlie the cohesion of the growing hair bundle in inner ear sensory cells. *J Cell Sci.* 2005;118:4593-4603.
16. Kremer H, van Wijk E, Marker T, et al. Usher syndrome: molecular links of pathogenesis, proteins and pathways. *Hum Mol Genet.* 2006;15 Spec No 2:R262-R270.



17. Reiners J, Nagel-Wolfrum K, Jurgens K, et al. Molecular basis of human Usher syndrome: deciphering the meshes of the Usher protein network provides insights into the pathomechanisms of the Usher disease. *Exp Eye Res.* 2006;83:97-119.
18. Caberlotto E, Michel V, Foucher I, et al. Usher type 1G protein sans is a critical component of the tip-link complex, a structure controlling actin polymerization in stereocilia. *Proc Natl Acad Sci U S A.* 2011;108:5825-5830.
19. Petit C, Richardson GP. Linking genes underlying deafness to hair-bundle development and function. *Nat Neurosci.* 2009;12:703-710.
20. Maerker T, van Wijk E, Overlack N, et al. A novel Usher protein network at the periciliary reloading point between molecular transport machineries in vertebrate photoreceptor cells. *Hum Mol Genet.* 2008;17:71-86.
21. McGee J, Goodyear RJ, McMillan DR, et al. The very large G-protein-coupled receptor VLGR1: a component of the ankle link complex required for the normal development of auditory hair bundles. *J Neurosci.* 2006;26:6543-6553.
22. Gregory F, Couchoux H, Pangrsic T. A presynaptic role for harmonin in regulating Cav1.3 channels in mouse inner hair cells. *ARO 2010 abstract*;587
23. Brandt A, Striessnig J, Moser T. CaV1.3 channels are essential for development and presynaptic activity of cochlear inner hair cells. *J Neurosci.* 2003;23:10832-10840.
24. Knirsch M, Brandt N, Braig C, et al. Persistence of Ca(v)1.3 Ca<sup>2+</sup> channels in mature outer hair cells supports outer hair cell afferent signaling. *J Neurosci.* 2007;27:6442-6451.
25. Tlili A, Charfedine I, Lahmar I, et al. Identification of a novel frameshift mutation in the DFNB31/WHRN gene in a Tunisian consanguineous family with hereditary non-syndromic recessive hearing loss. *Hum Mutat.* 2005;25:503.
26. Yang J, Liu X, Zhao Y, et al. Ablation of whirlin long isoform disrupts the USH2 protein complex and causes vision and hearing loss. *PLoS Genet.* 2010;6:e1000955
27. Van Wijk E, Kersten FFJ, Zaghloul T, et al. A Centrosomal Protein Molecularly Links Usher Syndrome to Leber Congenital Amaurosis and Bardet-Biedl Syndrome in the Retina. *Invest Ophthalmol Vis Sci.* 2008;abstract 49:4033
28. Ross AJ, May-Simera H, Eichers ER, et al. Disruption of Bardet-Biedl syndrome ciliary proteins perturbs planar cell polarity in vertebrates. *Nat Genet.* 2005;37:1135-1140.
29. Winter CG, Wang B, Ballew A, et al. Drosophila Rho-associated kinase (Drok) links Frizzled-mediated planar cell polarity signaling to the actin cytoskeleton. *Cell.* 2001;105:81-91.
30. Park TJ, Mitchell BJ, Abitua PB, et al. Dishevelled controls apical docking and planar polarization of basal bodies in ciliated epithelial cells. *Nat Genet.* 2008;40:871-879.
31. Vladar EK, Axelrod JD. Dishevelled links basal body docking and orientation in ciliated epithelial cells. *Trends Cell Biol.* 2008;18:517-520.
32. Inobe M, Katsube K, Miyagoe Y, et al. Identification of EPS8 as a Dvl1-associated molecule. *Biochem Biophys Res Commun.* 1999;266:216-221.

33. Kikkawa Y, Mburu P, Morse S, et al. Mutant analysis reveals whirlin as a dynamic organizer in the growing hair cell stereocilium. *Hum Mol Genet.* 2005;14:391-400.
34. Mburu P, Kikkawa Y, Townsend S, et al. Whirlin complexes with p55 at the stereocilia tip during hair cell development. *Proc Natl Acad Sci U S A.* 2006;103:10973-10978.
35. Gosens I, van Wijk E, Kersten FFJ, et al. MPP1 links the Usher protein network and the Crumbs protein complex in the retina. *Hum Mol Genet.* 2007;16:1993-2003.
36. Mburu P, Romero MR, Hilton H, et al. Gelsolin plays a role in the actin polymerization complex of hair cell stereocilia. *PLoS One.* 2010;5:e11627.
37. Peng AW, Belyantseva IA, Hsu PD, et al. Twinfilin 2 regulates actin filament lengths in cochlear stereocilia. *J Neurosci.* 2009;29:15083-15088.
38. Rzadzinska AK, Nevalainen EM, Prosser HM, et al. Myosin VIIa interacts with Twinfilin-2 at the tips of mechanosensory stereocilia in the inner ear. *PLoS One.* 2009;4:e7097.
39. Kersten FFJ, Peters TA, Kremer H, et al. The Usher Interactome Functions in Inner Ear and Retina; Comparative Pathogenesis. In: Ahuja S (ed), *Usher Syndrome: Pathogenesis, Diagnosis and Therapy*; NOVA publishers; 2011.
40. Sedmak T, Wolfrum U. Intraflagellar transport molecules in ciliary and nonciliary cells of the retina. *J Cell Biol.* 2010;189:171-186.
41. Hudak LM, Lunt S, Chang CH, et al. The intraflagellar transport protein ift80 is essential for photoreceptor survival in a zebrafish model of jeune asphyxiating thoracic dystrophy. *Invest Ophthalmol Vis Sci.* 2010;51:3792-3799.
42. Pazour GJ, Baker SA, Deane JA, et al. The intraflagellar transport protein, IFT88, is essential for vertebrate photoreceptor assembly and maintenance. *J Cell Biol.* 2002;157:103-113.
43. Shu X, Zeng Z, Gautier P, et al. Zebrafish Rpgr is required for normal retinal development and plays a role in dynein-based retrograde transport processes. *Hum Mol Genet.* 2010;19:657-670.
44. Sukumaran S, Perkins BD. Early defects in photoreceptor outer segment morphogenesis in zebrafish ift57, ift88 and ift172 Intraflagellar Transport mutants. *Vision Res.* 2009;49:479-489.
45. Westfall JE, Hoyt C, Liu Q, et al. Retinal degeneration and failure of photoreceptor outer segment formation in mice with targeted deletion of the Joubert syndrome gene, Ahi1. *J Neurosci.* 2010;30:8759-8768.
46. Suzuki H, Yagi M, Suzuki K. Duplicated insertion mutation in the microtubule-associated protein Spag5 (astrin/MAP126) and defective proliferation of immature Sertoli cells in rat hypogonadic (hgn/hgn) testes. *Reproduction.* 2006;132:79-93.
47. Dumont RA, Lins U, Filoteo AG, et al. Plasma membrane Ca<sup>2+</sup>-ATPase isoform 2a is the PMCA of hair bundles. *J Neurosci.* 2001;21:5066-5078.
48. Hasson T, Gillespie PG, Garcia JA, et al. Unconventional myosins in inner-ear sensory epithelia. *J Cell Biol.* 1997;137:1287-1307.
49. Zallocchi M, Sisson JH, Cosgrove D. Biochemical characterization of native Usher protein complexes from a vesicular subfraction of tracheal epithelial cells. *Biochemistry.* 2010;49:1236-1247.

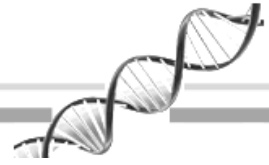
50. Liu XZ, Walsh J, Tamagawa Y, et al. Autosomal dominant non-syndromic deafness caused by a mutation in the myosin VIIA gene. *Nat Genet.* 1997;17:268-269.
51. Luijendijk MW, Van Wijk E, Bischoff AM, et al. Identification and molecular modelling of a mutation in the motor head domain of myosin VIIA in a family with autosomal dominant hearing impairment (DFNA11). *Hum Genet.* 2004;115:149-156.
52. Tamagawa Y, Ishikawa K, Ishikawa K, et al. Phenotype of DFNA11: a nonsyndromic hearing loss caused by a myosin VIIA mutation. *Laryngoscope.* 2002;112:292-297.
53. Liu XZ, Walsh J, Mburu P, et al. Mutations in the myosin VIIA gene cause non-syndromic recessive deafness. *Nat Genet.* 1997;16:188-190.
54. Weil D, Kussel P, Blanchard S, et al. The autosomal recessive isolated deafness, DFNB2, and the Usher 1B syndrome are allelic defects of the myosin-VIIA gene. *Nat Genet.* 1997;16:191-193.
55. Ahmed ZM, Smith TN, Riazuddin S, et al. Nonsyndromic recessive deafness DFNB18 and Usher syndrome type IC are allelic mutations of USH1C. *Hum Genet.* 2002;110:527-531.
56. Ouyang XM, Xia XJ, Verpy E, et al. Mutations in the alternatively spliced exons of USH1C cause non-syndromic recessive deafness. *Hum Genet.* 2002;111:26-30.
57. Bork JM, Peters LM, Riazuddin S, et al. Usher syndrome 1D and nonsyndromic autosomal recessive deafness DFNB12 are caused by allelic mutations of the novel cadherin-like gene CDH23. *Am J Hum Genet.* 2001;68:26-37.
58. Ahmed ZM, Riazuddin S, Ahmad J, et al. PCDH15 is expressed in the neurosensory epithelium of the eye and ear and mutant alleles are responsible for both USH1F and DFNB23. *Hum Mol Genet.* 2003;12:3215-3223.
59. Ahmed ZM, Riazuddin S, Aye S, et al. Gene structure and mutant alleles of PCDH15: nonsyndromic deafness DFNB23 and type 1 Usher syndrome. *Hum Genet.* 2008;124:215-223.
60. Mburu P, Mustapha M, Varela A, et al. Defects in whirlin, a PDZ domain molecule involved in stereocilia elongation, cause deafness in the whirler mouse and families with DFNB31. *Nat Genet.* 2003;34:421-428.
61. McGee TL, Seyedahmadi BJ, Sweeney MO, et al. Novel mutations in the long isoform of the USH2A gene in patients with Usher syndrome type II or non-syndromic retinitis pigmentosa. *J Med Genet.* 2010;47:499-506.
62. Rivolta C, Sweklo EA, Berson EL, et al. Missense mutation in the USH2A gene: association with recessive retinitis pigmentosa without hearing loss. *Am J Hum Genet.* 2000;66:1975-1978.
63. Seyedahmadi BJ, Rivolta C, Keene JA, et al. Comprehensive screening of the USH2A gene in Usher syndrome type II and non-syndromic recessive retinitis pigmentosa. *Exp Eye Res.* 2004;79:167-173.
64. Kalay E, de Brouwer AP, Caylan R, et al. A novel D458V mutation in the SANS PDZ binding motif causes atypical Usher syndrome. *J Mol Med.* 2005;83:1025-1032.
65. Ebermann I, Phillips JB, Liebau MC, et al. PDZD7 is a modifier of retinal disease and a contributor to digenic Usher syndrome. *J Clin Invest.* 2010;120:1812-1823.

66. Becirovic E, Ebermann I, Nagy D, et al. Usher syndrome type 1 due to missense mutations on both CDH23 alleles: investigation of mRNA splicing. *Hum Mutat.* 2008;29:452.
67. Ebermann I, Scholl HP, Charbel IP, et al. A novel gene for Usher syndrome type 2: mutations in the long isoform of whirlin are associated with retinitis pigmentosa and sensorineural hearing loss. *Hum Genet.* 2007;121:203-211.
68. Plantinga RF, Kleemola L, Huygen PL, et al. Serial audiometry and speech recognition findings in Finnish Usher syndrome type III patients. *Audiol Neurootol.* 2005;10:79-89.
69. Grondahl J. Estimation of prognosis and prevalence of retinitis pigmentosa and Usher syndrome in Norway. *Clin Genet.* 1987;31:255-264.
70. Pakarinen L, Tuppurainen K, Laippala P, et al. The ophthalmological course of Usher syndrome type III. *Int Ophthalmol.* 1995;19:307-311.
71. Collin RW, Littink KW, Klevering BJ, et al. Identification of a 2 Mb human ortholog of *Drosophila* eyes shut/spacemaker that is mutated in patients with retinitis pigmentosa. *Am J Hum Genet.* 2008;83:594-603.
72. den Hollander AI, Koenekoop RK, Mohamed MD, et al. Mutations in LCA5, encoding the ciliary protein lebercilin, cause Leber congenital amaurosis. *Nat Genet.* 2007;39:889-895.
73. Fagerheim T, Raeymaekers P, Merren J, et al. Homozygosity mapping to the USH2A locus in two isolated populations. *J Med Genet.* 1999;36:144-147.
74. Schraders M, Lee K, Oostrik J, et al. Homozygosity mapping reveals mutations of GRXCR1 as a cause of autosomal-recessive nonsyndromic hearing impairment. *Am J Hum Genet.* 2010;86:138-147.
75. Thiadens AA, den Hollander AI, Roosing S, et al. Homozygosity mapping reveals PDE6C mutations in patients with early-onset cone photoreceptor disorders. *Am J Hum Genet.* 2009;85:240-247.
76. Suzuki H, Tokuriki T, Saito K, et al. Glomerular hyperfiltration and hypertrophy in the rat hypoplastic kidney as a model of oligomeganephronic disease. *Nephrol Dial Transplant.* 2005;20:1362-1369.
77. Suzuki H, Tokuriki T, Kamita H, et al. Age-related pathophysiological changes in rat oligomeganephronic hypoplastic kidney. *Pediatr Nephrol.* 2006;21:637-642.
78. Janin-Mercier A, Palcoux JB, Gubler MC, et al. Oligomeganephronic renal hypoplasia with tapetoretinal degeneration. Report of one case with ultrastructural study of the renal biopsy. *Virchows Arch A Pathol Anat Histopathol.* 1985;407:477-483.
79. Hmani-Aifa M, Benzina Z, Zulficar F, et al. Identification of two new mutations in the GPR98 and the PDE6B genes segregating in a Tunisian family. *Eur J Hum Genet.* 2009;17:474-482.
80. Hmani M, Ghorbel A, Boulila-Elgaied A, et al. A novel locus for Usher syndrome type II, USH2B, maps to chromosome 3 at p23-24.2. *Eur J Hum Genet.* 1999;7:363-367.
81. Baig SM, Koschak A, Lieb A, et al. Loss of Ca(v)1.3 (CACNA1D) function in a human channelopathy with bradycardia and congenital deafness. *Nat Neurosci.* 2011;14:77-84.
82. Van Wijk E. Dissection of the molecular pathology of Usher syndrome. *Thesis.* 2009.
83. Zheng QY, Yan D, Ouyang XM, et al. Digenic inheritance of deafness caused by mutations in genes encoding cadherin 23 and protocadherin 15 in mice and humans. *Hum Mol Genet.* 2005;14:103-111.

84. Khanna H, Davis EE, Murga-Zamalloa CA, et al. A common allele in RPGRIP1L is a modifier of retinal degeneration in ciliopathies. *Nat Genet.* 2009;41:739-745.
85. Badano JL, Kim JC, Hoskins BE, et al. Heterozygous mutations in BBS1, BBS2 and BBS6 have a potential epistatic effect on Bardet-Biedl patients with two mutations at a second BBS locus. *Hum Mol Genet.* 2003;12:1651-1659.
86. Katsanis N, Ansley SJ, Badano JL, et al. Triallelic inheritance in Bardet-Biedl syndrome, a Mendelian recessive disorder. *Science.* 2001;293:2256-2259.
87. Otto EA, Hurd TW, Airik R, et al. Candidate exome capture identifies mutation of SDCCAG8 as the cause of a retinal-renal ciliopathy. *Nat Genet.* 2010;42:840-850.
88. Otto EA, Ramaswami G, Janssen S, et al. Mutation analysis of 18 nephronophthisis associated ciliopathy disease genes using a DNA pooling and next generation sequencing strategy. *J Med Genet.* 2011;48:105-116.
89. Zheng J, Anderson CT, Miller KK, et al. Identifying components of the hair-cell interactome involved in cochlear amplification. *BMC Genomics.* 2009;10:127.
90. Gloeckner CJ, Boldt K, Schumacher A, et al. A novel tandem affinity purification strategy for the efficient isolation and characterisation of native protein complexes. *Proteomics.* 2007;7:4228-4234.
91. Bainbridge JW, Smith AJ, Barker SS, et al. Effect of gene therapy on visual function in Leber's congenital amaurosis. *N Engl J Med.* 2008;358:2231-2239.
92. Cideciyan AV, Hauswirth WW, Aleman TS, et al. Human RPE65 gene therapy for Leber congenital amaurosis: persistence of early visual improvements and safety at 1 year. *Hum Gene Ther.* 2009;20:999-1004.
93. Hauswirth WW, Aleman TS, Kaushal S, et al. Treatment of leber congenital amaurosis due to RPE65 mutations by ocular subretinal injection of adeno-associated virus gene vector: short-term results of a phase I trial. *Hum Gene Ther.* 2008;19:979-990.
94. Maguire AM, Simonelli F, Pierce EA, et al. Safety and efficacy of gene transfer for Leber's congenital amaurosis. *N Engl J Med.* 2008;358:2240-2248.
95. Maguire AM, High KA, Auricchio A, et al. Age-dependent effects of RPE65 gene therapy for Leber's congenital amaurosis: a phase 1 dose-escalation trial. *Lancet.* 2009;374:1597-1605.
96. Du M, Liu X, Welch EM, et al. PTC124 is an orally bioavailable compound that promotes suppression of the human CFTR-G542X nonsense allele in a CF mouse model. *Proc Natl Acad Sci U S A.* 2008;105:2064-2069.
97. Goldmann T, Rebibo-Sabbah A, Overlack N, et al. Beneficial read-through of a USH1C nonsense mutation by designed aminoglycoside NB30 in the retina. *Invest Ophthalmol Vis Sci.* 2010;51:6671-6680.
98. Hirawat S, Welch EM, Elfring GL, et al. Safety, tolerability, and pharmacokinetics of PTC124, a nonaminoglycoside nonsense mutation suppressor, following single- and multiple-dose administration to healthy male and female adult volunteers. *J Clin Pharmacol.* 2007;47:430-444.

99. Linde L, Kerem B. Introducing sense into nonsense in treatments of human genetic diseases. *Trends Genet.* 2008;24:552-563.
100. Nudelman I, Rebibo-Sabbah A, Cherniavsky M, et al. Development of novel aminoglycoside (NB54) with reduced toxicity and enhanced suppression of disease-causing premature stop mutations. *J Med Chem.* 2009;52:2836-2845.
101. Rebibo-Sabbah A, Nudelman I, Ahmed ZM, et al. In vitro and ex vivo suppression by aminoglycosides of PCDH15 nonsense mutations underlying type 1 Usher syndrome. *Hum Genet.* 2007;122:373-381.
102. Welch EM, Barton ER, Zhuo J, et al. PTC124 targets genetic disorders caused by nonsense mutations. *Nature.* 2007;447:87-91.
103. Goldmann T, Overlack N, Wolfrum U, et al. PTC124-Mediated Translational Readthrough of a Nonsense Mutation Causing Usher Syndrome Type 1C. *Hum Gene Ther.* 2011;22:537-547.





## **Summary / Samenvatting**







## Summary

Usher syndrome is the most common cause of inherited deaf-blindness with a prevalence ranging from about 3 to 6 per 100,000 individuals, and it exhibits a recessive pattern of inheritance. Patients suffering from both hereditary deafness and hereditary blindness were first described by Albrecht von Graefe in 1858, but Usher syndrome was finally eponymously named after the Scottish ophthalmologist Charles H. Usher in 1935.

Three clinical types (USH1-USH3) are distinguished mainly on the basis of the severity and progression of the symptoms. Congenital, stable severe to profound hearing loss is characteristic of USH1 as is the absence of vestibular function. Progressive retinal degeneration by retinitis pigmentosa (RP) is generally diagnosed before puberty. The first symptom of RP is night blindness, that precedes affected daytime vision and further constriction of the visual field (tunnel vision); eventually RP may lead to complete blindness. The genes associated with USH1 are *MYO7A*, *USH1C*, *CDH23*, *PCDH15*, and *USH1G*. For two additional loci the corresponding genes have not yet been identified. Moderate to severe, congenital and stable hearing loss, especially in the high frequencies, is typical for USH2 patients. Vestibular function is within the normal range and RP is usually diagnosed around or after puberty. *USH2A*, *GPR98*, and *DFNB31* are the genes involved in USH2 and there is at least one additional locus for which the causative gene remains to be identified. USH3 is characterized by progressive hearing loss with an onset at variable age. Diagnosis is mostly before the age of 10, but up to the age of 40 in some patients. Also the presence of vestibular dysfunction and the onset of RP is variable between the age of 3 and 51, with an average of 17 years. So far only *CLRN1* is associated with USH3. In a subset of patients, the disease cannot be classified as one of the three types USH1-3 and is, therefore, called atypical.

USH1 and USH2 proteins are part of a dynamic USH protein network and the different USH proteins and their direct or indirect interaction partners fulfill several functions in the hair cells of the inner ear and in the photoreceptor cells of the retina. The structure and function of the inner ear and retina are described in **chapter 1**. The USH protein complex functions in the development of the hair bundle of hair cells. Some of the USH proteins are indicated to be crucial for hair bundle orientation and for stereocilia formation/elongation. USH proteins have been identified as components of fibrous links that interconnect adjacent stereocilia and

stereocilia and the kinocilium of hair cells and are therefore involved in hair-bundle cohesion. USH proteins form tip-links that are gating the mechanotransduction channels and are therefore suggested to be involved in hair cell function. In photoreceptor cells, analogous to the links in the hair bundle, fibrous links are formed by USH proteins which provide structural support between the membranes of the connecting cilium and apical inner segment. USH proteins may also participate in vesicle transport and vesicle docking in the photoreceptor cells. Presence of USH proteins at the synapse of hair cells and photoreceptor cells suggests a role in synapse formation and/or synaptic transmission.

If mutations in different genes, such as the USH genes, can cause an overlapping disease phenotype, these genes are often expressed in the same tissues and the encoded proteins play a role in shared functional modules such as the same biochemical pathway, or closely connected protein complexes that are dependent on each other's function. The physical interaction of proteins is essential for their function. Therefore, the identification of interaction partners of USH proteins might well contribute to the understanding of the function of the USH protein complex (**chapter 1**).

**Chapter 2** describes the connection of the L-type voltage-gated calcium channel subunit  $Ca_v1.3$  to the USH protein network.  $Ca_v1.3$  was identified as a candidate network member by a bioinformatic approach and specifically interacts and co-localizes with whirlin in photoreceptor cells of adult rats and mice. We hypothesize that in the photoreceptor cells whirlin scaffolds  $Ca_v1.3$  and thereby contributes to the organization of calcium channels, which may be important for membrane fusions of vesicles with each other and with the plasma membrane.

A further interaction partner of whirlin is EPS8 as described in **chapter 3**. In a Turkish family, a homozygous mutation in *EPS8* (p.L329P) predisposes to ototoxicity after treatment with antibiotics and this mutation affects the whirlin-EPS8 binding. The association of EPS8 and whirlin is biologically relevant as demonstrated by the aberrant localization of EPS8 and whirlin in mutant mouse models. The EPS8-whirlin interaction is essential for hair cell development, in particular in differential stereocilia elongation to achieve the characteristic hair bundle pattern.

To identify interaction partners which provide handles for the elucidation of the molecular pathology underlying retinal degeneration, yeast two-hybrid screens of human retinal cDNA libraries were performed. By using the intracellular domain of USH2A isoform B (USH2A<sup>isoB</sup>) and the *LCA5*-encoded protein lebercilin as ‘baits’, a novel isoform of the centrosomal ninein-like protein (Nlp/NINL<sup>isoB</sup>) was identified as a common interaction partner. This revealed a molecular link between Usher syndrome and Leber congenital amaurosis. The subcellular localization of the proteins and the function of their previously identified binding partners, suggest that the pathogenic mechanisms for LCA and Usher syndrome show significant overlap and involve defects in ciliogenesis, cilia maintenance, and intraflagellar and/or microtubule-based transport (**chapter 4**).

Besides NINL<sup>isoB</sup> another centrosomal and microtubule-associated protein was identified by the yeast two-hybrid screen using the intracellular domain of USH2A<sup>isoB</sup> as a ‘bait’. **Chapter 5** describes the identification of SPAG5 as a common interaction partner of both USH2A<sup>isoB</sup> and NINL<sup>isoB</sup>. Co-localization of these proteins in the photoreceptor cell and the knowledge of their functions suggest that SPAG5, USH2A<sup>isoB</sup> and NINL<sup>isoB</sup> function in microtubule-based cytoplasmic protein trafficking, ciliary transport and/or structural maintenance of the cilium in photoreceptor cells.

Mutations in several USH genes can underlie nonsyndromic deafness or nonsyndromic RP. **Chapter 6** reports two different mutations (p.Pro31Leu and p.Leu154Trp) in the USH3 gene *CLRN1* which cause nonsyndromic autosomal recessive RP in two Pakistani families. Audiometric assessment revealed no hearing impairment and thereby excluded Usher syndrome. The mutated proteins were retained in the endoplasmic reticulum, whereas the wildtype protein was transported to the plasma membrane.

In conclusion, the studies described in this thesis contributed to the expansion of the USH protein network and further specified its pathogenic relevance. To obtain more knowledge of the function of the protein network, novel members of the USH proteins network need to be identified and the function of the known and novel members need to be further explored. This will eventually lead to a better understanding of the molecular pathology of Usher syndrome and related disorders. (**chapter 7**).



## Samenvatting

Usher syndroom is de belangrijkste oorzaak van erfelijke doofblindheid en ongeveer 3 tot 6 personen per 100.000 hebben deze recessief overervende ziekte. Patiënten met zowel erfelijk gehoorverlies als erfelijke blindheid zijn voor het eerst beschreven door Albrecht von Graefe in 1858, maar Usher syndroom is uiteindelijk vernoemd naar de schotse oogarts Charles H. Usher in 1935. Drie klinische typen (USH1-USH3) kunnen worden onderscheiden op basis van de ernst en de progressie van de symptomen, evenals de leeftijd waarop de symptomen voor het eerst opgemerkt worden. Vanaf de geboorte hebben USH1 patiënten ernstig gehoorverlies en evenwichtsproblemen. Progressieve netvliesdegeneratie in de vorm van retinitis pigmentosa (RP) kan al voor de puberteit worden vastgesteld. De eerste symptomen van RP zijn nachtblindheid, waarna ook het gezichtsvermogen bij daglicht progressief vermindert. Dit leidt tot vernauwing van het gezichtsveld (tunnel-visie) en uiteindelijk kan RP leiden tot blindheid. Voor USH1 zijn er defecten gevonden in de genen *MYO7A*, *USH1C*, *CDH23*, *PCDH15*, en *USH1G*. Daarnaast zijn er ook twee chromosomale loci geïdentificeerd waarvoor het oorzakelijke gen nog gevonden moet worden. Patiënten met USH2 hebben vanaf hun geboorte matig tot ernstig gehoorverlies, met name in de hoge frequenties. Het evenwicht is normaal en RP kan worden vastgesteld tijdens of na de puberteit. *USH2A*, *GPR98*, en *DFNB31* zijn de genen die betrokken zijn bij USH2 en er is ten minste nog één locus waarin het ziekteveroorzakende gen gevonden moet worden. USH3 wordt gekenmerkt door progressief gehoorverlies, maar de leeftijd waarop de diagnose wordt gesteld varieert van vóór de leeftijd van 10 jaar tot zelfs 40 jaar. Er is eveneens variatie in de aanwezigheid van evenwichtsproblemen en in de leeftijd waarop RP wordt vastgesteld die varieert tussen de 3 en 51 jaar, met een gemiddelde van 17 jaar. Tot dusver is alleen *CLRN1* bekend voor USH3. Als het fenotype niet kan worden geklassificeerd als een van de drie typen USH1-3 wordt het atypisch genoemd.

De USH1- en USH2-eiwitten maken deel uit van een dynamisch eiwitnetwerk. De USH-eiwitten hebben verschillende functies in de haarcel van het binnenoor en in de fotoreceptoren van het netvlies. De structuur en functie van het binnenoor en het netvlies zijn beschreven in **hoofdstuk 1**. Het USH-eiwitcomplex heeft een functie in de ontwikkeling van de haarbundel in het binnenoor waarbij USH-eiwitten mogelijk een cruciale rol spelen bij de plaatsing van deze haarbundel op het oppervlak van de haarcel en bij de formatie en elongatie van

stereocilia. USH-eiwitten maken deel uit van verbindingen tussen de stereocilia onderling en tussen stereocilia en het kinocilium van de haarcellen en ook tussen de membranen van het connecting cilium en het apicale binnenste segment van de fotoreceptorcellen. Deze verbindingen zijn waarschijnlijk belangrijk voor de stevigheid. Mogelijk spelen USH-eiwitten ook een rol in het transport van vesicles en in het binden en fuseren van deze vesicles met het membraan in de fotoreceptorcel. De aanwezigheid van USH-eiwitten in of bij de synapsen van haarcellen en fotoreceptorcellen suggereert een rol in de aanleg van synapsen en/of signaaltransmissie door de synapsen.

Indien mutaties in verschillende (USH-) genen kunnen leiden tot een overlappend ziektebeeld komen deze genen vaak tot expressie in dezelfde weefsels en vervullen de gecodeerde eiwitten hun functie gezamenlijk, of zijn aanwezig in gerelateerde eiwitcomplexen die afhankelijk zijn van elkaars functie. Voor deze functie is het dus essentieel dat deze eiwitten fysiek aan elkaar binden. Vandaar dat onderzoek naar eiwit-eiwit interacties erg zinvol is bij het begrijpen van de functie van het USH-eiwitcomplex en bij het indirect identificeren van kandidaat-genen voor Usher syndroom en gerelateerde ziekten (**hoofdstuk 1**).

**Hoofdstuk 2** beschrijft de identificatie van  $Ca_v1.3$ , een subunit van een calciumkanaal, als kandidaat-partner van USH-eiwitten met behulp van bioinformatica.  $Ca_v1.3$  bindt specifiek aan whirlin en de eiwitten colocaliseren in fotoreceptoren. Onze hypothese is dat whirlin het eiwit  $Ca_v1.3$  in het netvlies naar de juiste plaats dirigeert en daardoor bijdraagt aan de organisatie van calciumkanalen in fotoreceptorcellen waarin beide eiwitten mogelijk betrokken zijn bij fusies van membranen van vesicles met elkaar en met de celmembraan.

Een andere nieuwe bindingspartner van whirlin is EPS8 en het onderzoek hiernaar staat beschreven in **hoofdstuk 3**. Bij een Turkse familie zorgt een homozygoot defect in *EPS8* (p.L329P) ervoor dat deze familieleden aanleg hebben voor gehoorbeschadiging door behandeling met antibiotica (ototoxiciteit). Deze mutatie verzwakt de binding tussen EPS8 en whirlin. De associatie tussen deze eiwitten is biologisch relevant, aangezien de lokalisatie van EPS8 en whirlin afwijkt in muismodellen met mutaties in de corresponderende genen. De interactie tussen EPS8 en whirlin is essentieel voor de ontwikkeling van haarcellen, met name in het verlengen van de stereocilia tot het karakteristieke haarbundel patroon.

Om interactiepartners te identificeren en zo handvaten te krijgen voor het ophelderen van de moleculaire pathologie die ten grondslag ligt aan netvliesdegeneratie, zijn er expressiebanken van het cDNA van humane netvliezen gescreend met behulp van een techniek die gebruik maakt van expressie en interactiedetectie in gistcellen, het zogenaamde “yeast two-hybrid” systeem. Met deze techniek zijn eiwitten geïdentificeerd die binden aan de intracellulaire regio van USH2A<sup>isoB</sup> of aan lebercilin dat wordt gecodeerd door het *LCA5*-gen. Een nieuwe isovorm van het centrosomale-eiwit Nlp/NINL is geïdentificeerd als bindingspartner van zowel USH2A<sup>isoB</sup> als lebercilin. Hierdoor is er een moleculaire verbinding tussen Usher syndroom en Leber congenitale amaurosis (LCA) aangetoond. LCA is de meest ernstige vorm van erfelijke retinadegeneratie en de symptomen treden op voor het eerste levensjaar. De lokalisatie van deze eiwitten en de functie van de al eerder geïdentificeerde bindingspartners suggereert dat de pathogene mechanismen van Usher syndroom en LCA overlappen. Defecten in ciliogenese, cilia behoud, en intraflagellar en/of ander microtubuli-geassocieerd transport zou mogelijk beide ziektebeelden kunnen verklaren (**hoofdstuk 4**).

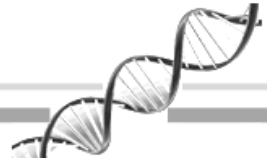
Met de yeast two-hybrid techniek is er behalve NINL<sup>isoB</sup> een ander centrosomaal en microtubuli-geassocieerd eiwit geïdentificeerd dat bindt aan het intracellulaire deel van USH2A<sup>isoB</sup>. **Hoofdstuk 5** beschrijft de identificatie van SPAG5 als een bindingspartner van zowel USH2A<sup>isoB</sup> als NINL<sup>isoB</sup>. De colokalisatie van deze eiwitten in de fotoreceptor en de kennis van hun functie, suggereert dat SPAG5, USH2A<sup>isoB</sup> en NINL<sup>isoB</sup> een functie hebben in het microtubuli-geassocieerde eiwittransport in het cytoplasma, het transport door het cilium en het structurele behoud van het cilium in fotoreceptorcellen.

Mutaties in verschillende USH-genen kunnen ook niet-syndromale doofheid of RP veroorzaken. **Hoofdstuk 6** beschrijft twee mutaties (p.Pro31Leu en p.Leu154Trp) in het USH3-gen *CLRN1* die niet-syndromale recessief overervende RP veroorzaken in twee Pakistaanse families. Gehoormetingen hebben gehoorverlies uitgesloten en daarbij dus ook Usher syndroom. De gemuteerde eiwitten worden vastgehouden in het endoplasmatisch reticulum terwijl het normale eiwit getransporteerd wordt naar het plasmamembraan.

De studies die staan beschreven in dit proefschrift hebben bijgedragen aan het uitbreiden van het USH-eiwitnetwerk en het verder specificeren van de pathogene relevantie. Om de functie van het USH-eiwitnetwerk beter te begrijpen moeten er nieuwe bindingspartners worden



geïdentificeerd en de functie van bekende en nieuwe leden moet verder worden onderzocht. Dit zal uiteindelijk leiden tot het begrijpen van de moleculaire pathologie van Usher syndroom en gerelateerde ziekten (**hoofdstuk 7**).



## **Dankwoord**





## Dankwoord

Promoveren is te vergelijken met het lopen van de Nijmeegse vierdaagse. Vooraf heb je er ontzettend veel zin in; tijdens vraag je jezelf wel eens af waaraan je bent begonnen; eenmaal voltooid ben je enorm trots. Het is dus zover; mijn proefschrift is af. Dit proefschrift is het resultaat van de inzet van velen in zowel mijn werk- als privé-omgeving. Daarom wil ik iedereen bedanken die op enige wijze hierbij betrokken is geweest. Voor sommige mensen wil ik mijn dank graag persoonlijk toelichten.

Ten eerste wil ik mijn beide promotoren Prof. dr. Jan Keunen en Prof. dr. Hannie Kremer en mijn copromotor Dr. ir. Ronald Roepman hartelijk bedanken. Jullie hebben gezamenlijk de aanvraag geschreven om mijn promotieproject te financieren en ieder heeft op eigen wijze enorm bijgedragen aan de totstandkoming van dit proefschrift waar we allen trots op mogen zijn. Jan, heel hartelijk dank voor jouw vertrouwen, jouw enthousiasme bij het doorspreken van mijn data en de snelle beoordeling van de manuscripten. Hannie, jij bent het meest direct bij mijn werk betrokken geweest. Toen Heleen wegging heb ik haar plaats ingenomen om als analist te werken aan het Usher-project en werd ik al snel omgedoopt tot een van jouw “Usher-boys”. Een jaar later kwam er een positie vrij als OIO en jij en Ronald hadden het vertrouwen in mij om deze positie te vervullen. Daarvoor ben ik jullie erg dankbaar. Jouw betrokkenheid, jouw manier van kritiek geven en jouw prettige manier van begeleiden hebben bijgedragen aan dit mooie proefschrift. Ronald, mede door jouw enthousiasme, optimisme, wetenschappelijke kennis, en de door jou geïntroduceerde “proteomics-studies” is dit boekje er gekomen. Ik heb met veel genoegen met jullie samengewerkt.

Natuurlijk wil ik Erwin van Wijk en Lisette Hetterschijt in het bijzonder danken voor hun bijdrage aan dit project en ik ben er dan ook trots op dat jullie mijn paranimfen zijn. Erwin, we hebben meer dan 5 jaar samengewerkt aan het Usher-project “yeah”, waarvan ik het eerste jaar als analist heb gewerkt aan jouw project. Je hebt gedurende deze periode voor mij meerdere functies vervuld. Naast een fijne collega en een soort van mentor/coach ben je bovenal een hele goede vriend geworden. We hebben samen een paar mooie wetenschappelijke doorbraken geforceerd die onder andere beschreven staan in dit proefschrift. Ook gingen we regelmatig een balletje meppen, maar ons sportieve hoogtepunt was toch wel het ongetraind uitlopen van de Nijmeegse vierdaagse. Lisette, in het laatste jaar

van mijn promotie kwam jij het team versterken. Het project was soms erg lastig, maar door je enthousiasme, nauwkeurigheid en enorme inzet zijn er toch een paar mooie resultaten uit gekomen. Daarnaast konden we gezellig ouwehoeren en hadden we onze pipetballon-duels. Ook heb ik genoten van het delen van onze culinaire ervaringen en dat moeten we zeker blijven voortzetten. Het “eiwitlab” mag enorm blij zijn dat jij de groep bent komen versterken. Erwin en Lisette, het doet me goed dat jullie beiden op de grote dag aan mijn zijde staan.

Hartelijk dank aan alle andere (oud) collega’s van Antropogenetica (P5) voor de open werksfeer op de afdeling. Ik heb erg genoten van de gezelligheid en van alle leuke dingen die er werden georganiseerd zoals squash toernooien, feestjes, samen stappen, samen voetbal kijken, pokeravonden, kerstdiners, en nog veel meer. Een speciale dank aan de mensen van het “eiwitlab”: Sylvia, Jeroen, Dorus, Karlien, Heleen, Stef, en Theo; jij bent toch eigenlijk ook een van “ons”. Door jullie was er een relaxte en goede werksfeer en ook de gezamenlijke “acties” hebben zeker bijgedragen aan de totstandkoming van dit boekje. Ik wil de studenten die ik gedurende mijn promotie (mede) heb mogen begeleiden, Edwin Lamers, Judith Bergboer en Mariam Aslanyan, bedanken voor hun inzet en enthousiasme. En natuurlijk dank aan mijn Antropo-(fiets)-vrienden voor de nodige ont- / inspanning. Na meer dan 7 jaar met veel plezier bij Antropogenetica te hebben gewerkt vind ik het dan ook erg jammer om afscheid te moeten nemen.

I would also like to thank our (inter) national collaborators from the Netherlands, Germany, Pakistan, Turkey, Italy, Spain, UK and the USA who contributed to the chapters in this thesis and other publications. Special thanks to Dr. Eric Pierce’s lab (F.M. Kirby Center for Molecular Ophthalmology, University of Pennsylvania School of Medicine, Philadelphia, USA); Eric Pierce, Qin Liu, Qi zhang, Yun Liu, Suzanne Pavluk, Donna Garland, Alexei Saveliev, John Graziotto and Mike Farkas. Thank you all for giving me the opportunity to visit your lab for two months and for all the work and help. I had a great time!

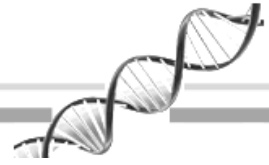
Ook dank aan Dr. Hendriks. Beste Wiljan, bedankt voor je rol als mentor gedurende mijn promotieproject.

Nu ik de mensen in mijn werkomgeving heb bedankt is het tijd om mijn vrienden en familie te bedanken. Vrienden, naast mijn werk heb ik samen met jullie de nodige ontspanning gezocht door uit te gaan, films te kijken, samen te koken, te sporten en gewoon gezellig bij elkaar te zijn. Zeker door de drukte van de laatste maanden heeft dit op een wat lager pitje gestaan, maar gelukkig hadden jullie alle begrip. Bedankt hiervoor en nu komt er weer meer tijd voor gezelligheid.

Lieve Ma en Toon; Dennis, Ingrid, Julian en Philip; Anco, Hermien en Suzan; Arnold en Gerrit; Joke en Gert, bedankt voor jullie interesse in mijn onderzoek, alle onvoorwaardelijke steun en gezelligheid. Een speciaal woord van dank aan mijn moeder. Mam, je hebt er heel wat jaren alleen voor gestaan en het was niet altijd even gemakkelijk. Ik ben er enorm trots op hoe je het allemaal hebt gedaan. Zonder jouw steun en liefde was dit boekje er nooit gekomen.

Lieve Aline, Ik wil jou ontzettend bedanken voor al je steun en begrip als ik 's avonds of in het weekend weer eens achter mijn laptop zat of als ik iets minder goed gehumeurd was. Ook had je alle vertrouwen in mij en wist je dat het allemaal goed zou komen. Tevens maakte je me ervan bewust dat de nodige ontspanning tot een veel hogere productiviteit leidt dan constant doorwerken. Ik ben heel erg blij dat ik je heb leren kennen en dat we volgend jaar gaan trouwen. Ik hou van je.





**Curriculum vitae /  
List of publications**







## **Curriculum Vitae**

Ferry (Fredericus Johannes) Kersten werd op 3 november 1979 geboren te Arnhem en groeide op in het naburige Huissen. Zijn HAVO opleiding volgde hij aan het Olympus College te Arnhem, waar hij in 1997 zijn diploma behaalde. Datzelfde jaar begon hij aan de Hogere Laboratorium Opleiding aan de Hogeschool van Arnhem en Nijmegen, met als afstudeerrichting Biochemie. Zijn afstudeerstage deed hij bij de afdeling Celfysiologie in het Nijmegen Centre for Molecular Life Sciences (NCMLS) te Nijmegen, onder begeleiding van Dr. Dominique Müller, Prof. dr. Joost Hoenderop en Prof. dr. René Bindels. Het onderzoek omvatte de identificatie en karakterisering van het epitheliaal calcium kanaal (ECAC1), tegenwoordig TRPV5. Na zijn afstuderen in 2001, werkte hij nog twee jaar als research analist binnen deze afdeling. Het eerste jaar werkte hij aan de Na-K-2Cl co-transporter (NKCC2) waarin mutaties in het gen resulteren in Bartter syndrome en het tweede jaar was hij betrokken bij het bestuderen van de TRPV5 knock-out muis.

Vanaf augustus 2003 is hij gaan werken bij de afdeling Antropogenetica van het UMC St. Radboud te Nijmegen, onder supervisie van Dr. Anneke den Hollander en Prof. dr. Frans Cremers. Het doel was om de genetische oorzaak van bepaalde vormen van erfelijke blindheid te achterhalen. Na drie jaar is hij binnen de afdeling naar de onderzoeksgroep van Prof. dr. Hannie Kremer gegaan om te werken aan het ontrafelen van de moleculaire pathologie van Usher syndrome. Op 1 augustus 2006 startte hij als Onderzoeker in Opleiding (OIO) bij deze afdeling met het in dit proefschrift beschreven promotieonderzoek, onder begeleiding van Prof. dr. Jan Keunen, Prof. dr. Hannie Kremer en Dr. ir. Ronald Roepman. Van eind januari tot en met eind maart 2009 is hij als onderzoeker werkzaam geweest bij het F.M. Kirby Center for Molecular Ophthalmology te Philadelphia, USA, onder supervisie van Dr. Eric Pierce. In 2010 ontving hij een travel award for young investigators van de Foundation Forschung contra Blindheit (FcB).



## List of publications

Starremans PG, **Kersten FFJ**, Knoers NV, Van Den Heuvel LP, Bindels RJ. Mutations in the human Na-K-2Cl cotransporter (NKCC2) identified in Bartter syndrome type I consistently result in nonfunctional transporters.

*J Am Soc Nephrol.* 2003;14:1419-1426.

Starremans PG, **Kersten FFJ**, Van Den Heuvel LP, Knoers NV, Bindels RJ. Dimeric architecture of the human bumetanide-sensitive Na-K-Cl Co-transporter.

*J Am Soc Nephrol.* 2003;14:3039-3046.

Hoenderop JG, van Leeuwen JP, van der Eerden BC, **Kersten FFJ**, van der Kemp AW, Mérillat AM, Waarsing JH, Rossier BC, Vallon V, Hummler E, Bindels RJ. Renal Ca<sup>2+</sup> wasting, hyperabsorption, and reduced bone thickness in mice lacking TRPV5.

*J Clin Invest.* 2003;112:1906-1914.

den Hollander AI, van Lith-Verhoeven JJ, **Kersten FFJ**, Heister JG, de Kovel CG, Deutman AF, Hoyng CB, Cremers FP. Identification of novel locus for autosomal dominant butterfly shaped macular dystrophy on 5q21.2-q33.2.

*J Med Genet.* 2004;41:699-702.

van Wijk E, van der Zwaag B, Peters T, Zimmermann U, te Brinke H, **Kersten FFJ**, Märker T, Aller E, Hoefsloot LH, Cremers CW, Cremers FP, Wolfrum U, Knipper M, Roepman R #, Kremer H #. The DFNB31 gene product whirlin connects to the Usher protein network in the cochlea and retina by direct association with USH2A and VLGR1.

(#: authors contributed equally to the work)

*Hum Mol Genet.* 2006;15:751-765.

Kalay E, Li Y, Uzumcu A, Uyguner O, Collin RW, Caylan R, Ulubil-Emiroglu M, **Kersten FFJ**, Hafiz G, van Wijk E, Kayserili H, Rohmann E, Wagenstaller J, Hoefsloot LH, Strom TM, Nürnberg G, Baserer N, den Hollander AI, Cremers FP, Cremers CW, Becker C, Brunner HG, Nürnberg P, Karaguzel A, Basaran S, Kubisch C, Kremer H, Wollnik B. Mutations in the lipoma HMGIC fusion partner-like 5 (LHFPL5) gene cause autosomal recessive nonsyndromic hearing loss.

*Hum Mutat.* 2006;27:633-639.

den Hollander AI #, Koenekoop RK #, Mohamed MD #, Arts HH #, Boldt K, Towns KV, Sedmak T, Beer M, Nagel-Wolfrum K, McKibbin M, Dharmaraj S, Lopez I, Ivings L, Williams GA, Springell K, Woods CG, Jafri H, Rashid Y, Strom TM, van der Zwaag B, Gosens I, **Kersten FFJ**, van Wijk E, Veltman JA, Zonneveld MN, van Beersum SE, Maumenee IH, Wolfrum U, Cheetham ME, Ueffing M, Cremers FP #, Inglehearn CF #, Roepman R #. Mutations in LCA5, encoding the ciliary protein lebercilin, cause Leber congenital amaurosis.

(#: authors contributed equally to the work)

*Nat Genet.* 2007;39:889-895.

Gosens I, van Wijk E, **Kersten FFJ**, Krieger E, van der Zwaag B, Märker T, Letteboer SJ, Dusseljee S, Peters T, Spierenburg HA, Punte IM, Wolfrum U, Cremers FP, Kremer H #, Roepman R #. MPP1 links the Usher protein network and the Crumbs protein complex in the retina.

(#: authors contributed equally to the work)

*Hum Mol Genet.* 2007;16:1993-2003.

Maerker T, van Wijk E, Overlack N, **Kersten FFJ**, McGee J, Goldmann T, Seh E, Roepman R, Walsh EJ, Kremer H, Wolfrum U. A novel Usher protein network at the periciliary reloading point between molecular transport machineries in vertebrate photoreceptor cells.

*Hum Mol Genet.* 2008;17:71-86.

van Wijk E, **Kersten FFJ**, Kartono A, Mans DA, Brandwijk K, Letteboer SJ, Peters TA, Märker T, Yan X, Cremers CW, Cremers FP, Wolfrum U, Roepman R #, Kremer H #. Usher syndrome and Leber congenital amaurosis are molecularly linked via a novel isoform of the centrosomal ninein-like protein.

(#: authors contributed equally to the work)

*Hum Mol Genet.* 2009;18:51-64.

**Kersten FFJ**, van Wijk E, van Reeuwijk J, van der Zwaag B, Märker T, Peters TA, Katsanis N, Wolfrum U, Keunen JE, Roepman R #, Kremer H #. Association of whirlin with Cav1.3 (alpha1D) channels in photoreceptors, defining a novel member of the usher protein network.

(#: authors contributed equally to the work)

*Invest Ophthalmol Vis Sci.* 2010;51:2338-2346.

Aller E #, Jaijo T #, van Wijk E, Ebermann I, **Kersten FFJ**, Garcia-Garcia G, Voesenek K, Aparisi MJ, Hoefsloot L, Cremers C, Diaz-Llopis M, Pennings R, Bolz HJ, Kremer H, Millán JM. Sequence variants of the DFNB31 gene among Usher syndrome patients of diverse origin.

(#: authors contributed equally to the work)

*Mol Vis.* 2010;16:495-500.

Khan MI #, **Kersten FFJ** #, Azam M, Collin RW, Hussain A, Shah ST, Keunen JE, Kremer H, Cremers FP, Qamar R, den Hollander AI . CLRN1 Mutations Cause Nonsyndromic Retinitis Pigmentosa.

(#: authors contributed equally to the work)

*Ophthalmology.* 2011;118:1444-1448.

**Kersten FFJ**, Peters TA, Kremer H, Van Wijk E. The Usher Interactome Functions in Inner Ear and Retina; Comparative Pathogenesis. In: Ahuja S (ed), *Usher Syndrome: Pathogenesis, Diagnosis and Therapy*:

NOVA publishers 2011.

**Kersten FFJ**, van Wijk E, Hetterschijt L, Bauß K, Peters TA, Aslanyan MG, van der Zwaag B, Wolfrum U, Keunen JEE, Roepman R #, Kremer H #. The mitotic spindle protein SPAG5/Astrin connects to the Usher protein network postmitotically.

(#: authors contributed equally to the work)

*Cilia*. 2011; in press

Van Wijk E, Zaghoul NA, Bachmann R, **Kersten FFJ**, Gerdes JM, Mans DA, Peters TA, Arts HH, Rooijen EMHC, van Beersum SEC, Davis EE, Leitch CC, May-Simera H, Cremers CWRJ, Cremers FPM, Beales PL, Doherty D, Moens CB, Roepman R #, Katsanis N #, Kremer H #. Nlnl functions in ciliogenesis and upstream of mkks/bbs6 in establishing planar cell polarity during zebrafish development

(#: authors contributed equally to the work)

*J Clin Invest*. 2011; submitted

Üzümcü A #, Offenhäuser N #, **Kersten FFJ** #, Li Y #, Rzadzinska AK #, Uyguner O, Pohl E, Blanche Ekalle Soppo C, Strenzke N, Yigit G, Nürnberg G, Emiroglu M, Hafiz G, Kayserili H, Becker C, Karaman B, del Castillo I, Basaran S, Yüksel Apak M, Nürnberg P, Moser T, Kubisch C, Steel KP, Di Fiore PP, Kremer H, Wollnik B. A hypofunctional EPS8 variant predisposes to ototoxicity.

(#: authors contributed equally to the work)

*Nat Genet*. 2011; submitted





